Biennial Report

Zweijahresbericht
2016 / 2017

Leibniz
Association

TROPOS

Leibniz Institute for
Tropospheric Research

TROPOS

Leibniz Institute for
Tropospheric Research

Table of contents

Table of contents

Introduction

Since 1992 the Leibniz Institute for Tropospheric Research (TROPOS) is located in the "Research Park Leipzig/Permoserstraße" close to the Helmholtz Centre for Environmental Research, the Leibniz-Institute for Surface Modification and other research establishments and related businesses. Its name identifies TROPOS as a member of the Leibniz Asso-

Fig. / Abb. 1: TROPOS main building. / TROPOS-Hauptgebäude. (Photo: Patric Seifert / TROPOS)

ciation. The institute was founded for the investigation of physical and chemical processes in the polluted troposphere.

Over the years a well-defined and globally unique research profile of TROPOS emerged. Today, the focus is on the physical and chemical interactions between atmospheric small airborne particles (aerosol particles) and cloud particles. Despite their minute absolute amount, aerosol and cloud particles are essential parts of the atmosphere because they control the budgets of energy, water and trace substances of the Earth System. Human activities can change these highly disperse systems and thus directly as well as indirectly feedback on human beings. This occurs for example via health effects

Fig. / Abb. 2: The new TROPOS chemistry laboratory. / Des neue TROPOS-Chemielaborgebäudes. (Photo: Tilo Arnhold / TROPOS)

Einleitung

Im Wissenschaftspark Leipzig/Permoserstraße befindet sich seit 1992 das Leibniz-Institut für Troposphärenforschung e. V. (TROPOS) in Nachbarschaft zum Helmholtz-Zentrum für Umweltforschung, zum Leibniz-Institut für Oberflächenmodifizierung sowie weiteren Einrichtungen. Sein Name weist es als Mitglied der Wissenschaftsgemeinschaft Gottfried Wilhelm Leibniz aus. Gegründet wurde es zur Erforschung physikalischer und chemischer Prozesse in der belasteten Troposphäre.

Das TROPOS hat über die Jahre ein klares und weltweit einzigartiges Forschungsprofil herausgebildet, in dessen Mittelpunkt heute die physikalischen und chemischen Wechselwirkungen zwischen atmosphärischen Schwebeteilchen (Aerosolpartikeln) und Wolkenpartikeln stehen. Trotz geringster absoluter Mengen sind diese Partikel wesentliche Bestandteile der Atmosphäre, weil sie den Energie-, Wasser- und Spurenstoffhaushalt des Erdsystems beeinflussen. Menschliche Aktivitäten können die Eigenschaften dieser hochdispersen Systeme verändern und damit sowohl direkt als auch indirekt auf den Menschen

Fig. / Abb. 3: TROPOS cloud laboratory. / TROPOS-Wolkenlabor. (Photo: Tilo Arnhold / TROPOS)

zurückwirken. Beispielhaft seien hier die gesundheitliche Wirkung eingeatmeter Partikel und Nebeltröpfchen und die regionalen und globalen Klimaänderungen genannt.

Trotz dieser wichtigen Beziehungen zwischen Mensch auf der einen und Aerosol/Wolken auf der anderen Seite müssen die physiko-chemischen Prozesse von Aerosol- und Wolkenbildung und die Wechselwirkungen mit Gesundheit und Klima zu einem großen Teil noch erforscht werden. Gründe dafür sind Schwierigkeiten bei der Analyse der beteiligten kleinsten Stoffmengen und das komplexe Verhalten atmosphärischer Mehrphasensysteme, deren Einzelprozesse in der Atmosphäre nicht klar getrennt beobachtet werden können. Im

Introduction / Einleitung

Fig. / Abb. 4: Measurements of the LACROS instrument suite in Limassol, Cyprus which were conducted in the frame of the CyCARE project. / Im Rahmen des CyCARE Projektes durchgeführte Messungen von LACROS in Limassol, Zypern. (Photo: Patric Seifert / TROPOS)

caused by inhaled particles and fog droplets and through regional and global climate change.

Despite these strong connections between human beings, aerosols, and clouds, the important physico-chemical processes of aerosol and cloud formation and the relationships with climate and health still need to be investigated to a large extent. This is mainly due to difficulties with analysing the very small samples and because of the complex behaviour of tropospheric multiphase systems, in which individual processes seldom can clearly be distinguished. In climate research this limitation is reflected in much larger uncertainties in predicted anthropogenic aerosol and cloud effects in comparison to the greenhouse effects of gases.

To gain rapid advances in our process understanding of the tropospheric multiphase system and to improve the application of this process understanding in the prediction of human impacts in this system field studies, laboratory and model studies are developed and performed. These three approaches for the investigation of aerosols and clouds are closely coordinated and constitute an overall process understanding of atmospheric multiphase systems.

The long-term measurements, to a large extend initiated by TROPOS, increasingly enable the identification of trends in regional and large-scale aerosol distribution.

Field experiments and process studies

Field experiments elucidate the atmospheric life cycle and related processes of aerosol and cloud particles. The complexity of this system is reflected in the fact that atmospheric aerosols and cloud particle exist with diameter from nano- to micrometer

gegenwärtigen Sachstand zum globalen Klimawandel spiegelt sich diese Komplexität in den sehr viel größeren Unsicherheiten in allen zu Aerosol- und Wolkenwirkung veröffentlichten Zahlen im Vergleich zu den Treibhauseffekten der Gase wieder.

Um raschen Zuwachs im Prozessverständnis troposphärischer Mehrphasenprozesse zu erreichen und dessen Anwendung auf die Vorhersage der Folgen menschlicher Eingriffe zu verbessern, werden am TROPOS aufeinander abgestimmte Feld-, Labor und Modellstudien zur Untersuchung von Aerosolpartikeln und Wolken entwickelt und durchgeführt und bilden so den Rahmen für ein umfassendes Prozessverständnis atmosphärischer Multiphasensysteme. Die vom TROPOS maßgeblich initiierten Langzeitmessungen erlauben mehr und mehr auch die Erfassung von Trends in der regionalen und großräumigen Aerosolverteilung.

Feldexperimente und Prozessstudien

Die Feldexperimente des Instituts dienen der Aufklärung des atmosphärischen Kreislaufs der Aerosol- und Wolkenpartikel und der damit verbundenen Prozesse. Die Komplexität dieses Systems wird dabei unter anderem dadurch bestimmt, dass in der Atmosphäre Partikel und Tropfen auftreten, deren Durchmesser sich vom Nano- bis zum Mikrometerbereich um mehr als sechs Größenordnungen unterscheiden. Außerdem kann man in den Aerosolpartikeln viele der kondensationsfähigen Stoffe des Erdsystems finden, von denen wiederum eine große Zahl Einfluss auf das Klima und die Biosphäre haben kann. Als Folge dieser Vielfalt und der mengenbedingten analytischen Schwierigkeiten

Fig. / Abb. 5: Test of a Balloon ascent in preparation of the Arctic-Experiment at the TROPOS Observatory Melpitz (February 2017). / Test eines Ballonaufstieges vor dem Arktis-Experiment an der TROPOS-Forschungsstation Melpitz (Februar 2017). (Photo: Gerald Spindler / TROPOS)

spanning more than six orders of magnitude. Furthermore, many of the condensable substances of the Earth system can be found in the aerosol and a large number of them in turn effect climate and biosphere. As a result of this diversity and mass-related analytical difficulties, essential global aerosol and cloud properties are still known to a small extend only.

This uncertainty already begins with particle sources, which are research efforts of TROPOS as well. The combustion of fossil and renewable fuels is a significant aerosol source. Measurements of the institute at many urban and rural background stations show that emissions of particles and their precursor gases are followed by strong physical and chemical transformations that need to be investigated with high-resolution sensors in order to identify the underlying processes. Despite extensive legal measures air pollution still exists in Germany and Europe with its consequences for morbidity and mortality of the respective population.

Also the conurbation Leipzig and the background station Melpitz is in the focus of investigations on air pollution with emphasis on aerosol particles, often conducted in collaboration with the Saxon State Agency for Environment and Geology (LfULG). The Melpitz research station is more and more applied to specific measurement campaigns with national and international partners. Hereby the high-resolution physical-chemical characterization on the ground is combined with other in-situ and remote sensing measurements of the entire column ("Melpitz-Column").

Even the strongest polluted regions over North America, Europe, Asia with priority on China, Africa, the Indian subcontinent, and South America are far from being sufficiently characterized in terms of

Fig. / Abb. 7: Stopover during the Antarctic Circumnavigation Experiment (ACE) close to the Antarctic volcano Mt. Siple (3110 m asl). / Zwischenstopp beim Antarctic Circumnavigation Experiment (ACE) in der Nähe des antarktischen Vulkans Siple (3110 m ü.d.M.). (Photo: Silvia Henning / TROPOS)

sind wesentliche globale Aerosol- und Wolkeneigenschaften noch wenig bekannt.

Diese Unsicherheit beginnt schon bei den Partikelquellen, die ebenfalls Forschungsgegenstand am TROPOS sind. Die Verbrennung fossiler und nachwachsender Brennstoffe zur Energieerzeugung und im Verkehr ist eine maßgebliche Aerosolquelle. Messungen des Instituts an vielen urbanen Messstellen und kontinentalen Hintergrundstationen zeigen, dass den Emissionen von Partikeln und deren Vorläufern enorme physikalische und chemische Umwandlungen folgen, die mit hoher zeitlicher Auflösung analysiert werden müssen, um die beteiligten Prozesse aufzuklären.

Auch der Ballungsraum Leipzig mit der Hintergrundstation Melpitz steht hier immer wieder im Interesse für Untersuchungen zur Luftverschmutzung mit dem Schwerpunkt auf Partikeln, die oft in Kooperationen mit dem Sächsischen Landesamt für Umwelt und Geologie (LfULG) durchgeführt werden. Trotz sehr weitgehender gesetzlicher Regelungen existiert in Deutschland und Europa immer noch Luftverschmutzung mit ihren Folgen für Morbidität und Mortalität in der betroffenen Bevölkerung. Die Forschungsstation Melpitz wird zunehmend für fokussierte Messkampagnen mit nationalen und internationalen Partnern genutzt, auch um die physikalisch-chemisch hoch aufgelöste in-situ Charakterisierung am Boden mit in-situ- und Fernerkundungsmessungen der gesamten Säule zu kombinieren ("Melpitz-Säule").

Die am höchsten belasteten Regionen über Nordamerika, Europa, Asien mit dem Schwerpunkt China, Afrika, über dem indischen Subkontinent und Südamerika sind bei weitem noch nicht hinreichend bezüglich ihrer Aerosolbelastungen und den

Fig. / Abb. 6: The catamaran "MarParCat" running during the field campaign MarParCloud/MARSU in September/October 2017 on the Cap Verde Islands. / Der Katamaran „MarParCat" im Einsatz bei der Feldkampagne MarParCloud/MARSU im September/Oktober 2017 auf den kapverdischen Inseln. (Photo: Manuela van Pinxteren / TROPOS)

Introduction / Einleitung

Fig. / Abb. 8: Coal power plant Tušimice near Kadan/Kaaden, Czech Republic (CZ). / Braunkohlenkraftwerk Tušimice bei Kadan/Kaaden, Tschechische Republik (CZ). (Photo: Tilo Arnhold / TROPOS)

aerosol burdens and ensuing climate effects. Subsequently the institute focuses its participation in international field campaigns and dedicated long-term studies in Asia, South America and the Mediterranean area. But also the marine troposphere over the clean southern and the polluted northern Atlantic is observed by long-term measurements for a better understanding aerosol cloud interactions.

Investigations on mineral dust and marine aerosol particles and its impact on the radiation budget, cloud formation processes and the atmospheric ice nucleation remain a core component of the institute's research. To this end, investigations in the Central Asian and the Mediterranean region will be intensified.

In the framework of the European infrastructure IAGOS the aerosol distribution in the upper

Fig. / Abb. 9: During the Long Night of the Sciences in Leipzig 2016: Leipzigers examine the air quality in Leipzig's city center live on a tour with a backpack-based measuring device. / LeipzigerInnen untersuchen live auf einer Tour per Rucksack-getragenem Messgerät die Luftqualität in Leipzigs Innenstadt, Lange Nacht der Wissenschaften in Leipzig 2016. (Photo: Tilo Arnhold / TROPOS)

daraus resultierenden Klimawirkungen untersucht. Auf diese Regionen konzentrieren sich daher in internationaler Zusammenarbeit die Feldexperimente des TROPOS, u. a. in Form von Messkampagnen und Langzeitmessungen in Asien, Südamerika und dem mediterranen Bereich. Aber auch die maritime Troposphäre über dem sauberen südlichen und dem belasteten nördlichen Atlantik wird langfristig vermessen, um Aerosol-Wolken-Wechselwirkungen besser zu verstehen. Untersuchungen zum Mineralstaub und marinen Aerosolpartikeln und deren Wirkungen auf den Strahlungshaushalt, die Wolkenbildung und die atmosphärische Eisbildung bleiben ein Kernbestandteil der Arbeiten am TROPOS. Hierzu werden vermehrt Untersuchungen im zentralasiatischen und mediterranem Raum vorgenommen. Durch Nutzung eines kommerziellen Verkehrsflugzeuges der Lufthansa werden im Rahmen der Europäischen Forschungsinfrastruktur IAGOS auch Aerosolverteilungen in der oberen Troposphäre auf regelmäßig beflogenen interkontinentalen Routen gemessen und analysiert.

Am TROPOS werden verschiedene bodengebundene Fernerkundungsverfahren gekoppelt, um so zu einem synergetischen Bild der vertikalen Verteilung von Aerosolen und Hydrometeoren sowie deren Prozessierung zu gelangen. Das hierzu entwickelte Leipzig Aerosol and Cloud Remote Observation System (LACROS) wird darüberhinaus zu einem Prototyp-Instrument eines europäischen Messnetzes erweitert.

Auf kleineren Skalen werden Untersuchungen zur Partikelbildung und Wechselwirkung zwischen Aerosolpartikeln und Wolken und der Einfluss turbulenter Mischungsprozesse auf die Wolkenentwicklung mit Hilfe der hubschraubergetragenen Messplattform ACTOS durchgeführt. Zusätzlich werden

Fig. / Abb. 10: German research vessel "Polarstern" and the TROPOS tethered balloon during the "PASCAL" expedition (PS106), works on the ice floe. / Das deutsche Forschungsschiff „Polarstern" und der TROPOS-Fesselballon während der Expedition „PASCAL" (PS106), Arbeiten auf der Eisscholle. (Photo: PS 106-Team)

troposphere is measured and analysed using a commercial Lufthansa aircraft operated on frequent intercontinental routes.

At TROPOS different ground-based remote sensing methods are coupled in order to achieve a synergetic picture of the vertical distribution of clouds and aerosols as well as their processing. The Leipzig Aerosol and Cloud Remote Observation System (LACROS), that has been developed to this end, will be further extended towards a European network prototype instrument.

On smaller scales, investigations concerning new particle formation, the interactions between aerosol particles and clouds, and the influences of turbulent mixing processes on cloud development are carried out with help of the helicopter-borne measurement platform ACTOS. In addition, process studies are conducted at suitable locations such as mountain observatories to investigate particle nucleation, particle processing through clouds, and the influence of aerosols particles on the development and freezing of clouds.

TROPOS leads several regional, national and European measurement networks to monitor atmospheric aerosols and cloudiness. In the framework of the Global Atmospheric Watch (GAW) programme of the WMO TROPOS hosts the World Calibration Centre for physical in-situ aerosol measurement (WCCAP) to assure high quality standards at national and international observatories.

Further on TROPOS is primary responsible for the development and operation of the European and national measurement network for the observation of aerosols, clouds and trace gases (ACTRIS) to ensure, besides process understanding, a basis for the long-term characterisation of short-lifed climate components.

Bergstationen zu Prozessstudien genutzt, die sich dem Verständnis von Einzelprozessen, wie der Partikelneubildung, der physiko-chemischen Veränderung der Aerosolpartikel beim Wolkendurchgang und dem Einfluss von Aerosolpartikeln auf die Entwicklung und das Gefrieren von Wolken widmen.

TROPOS ist maßgeblich an regionalen, nationalen und Europäischen Messnetzen zur Erfassung des atmosphärischen Aerosols und der Bewölkung beteiligt. Das Institut betreibt im Rahmen des Global Atmospheric Watch (GAW) Programmes der WMO das Weltkalibrierzentrum für physikalische Aerosolmessungen (WCCAP) mit dem Ziel der Qualitätssicherung von in-situ Messungen an nationalen und internationalen Messstationen.

TROPOS ist weiterhin federführend an der Entwicklung und dem Betrieb des europäischen und
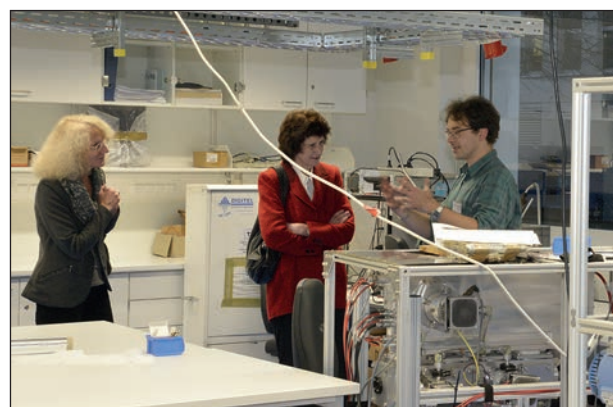
*Fig. / Abb. 11: Dr. Laurent Poulain (right) explains Dr Eva-Maria Stange (Saxon Minister of State for Science and Art) and RORin Cathrin Liebner (SMWK, left) his work in the new chemistry lab building. / Dr. Laurent Poulain (rechts) erklärt Dr. Eva-Maria Stange (Sächsische Staatsministerin für Wissenschaft und Kunst) und RORin Cathrin Liebner (SMWK, links) seine Arbeit im neuen Chemielabor-Gebäude. (Photo: Tilo Arnhold / TROPOS)*

Introduction / Einleitung
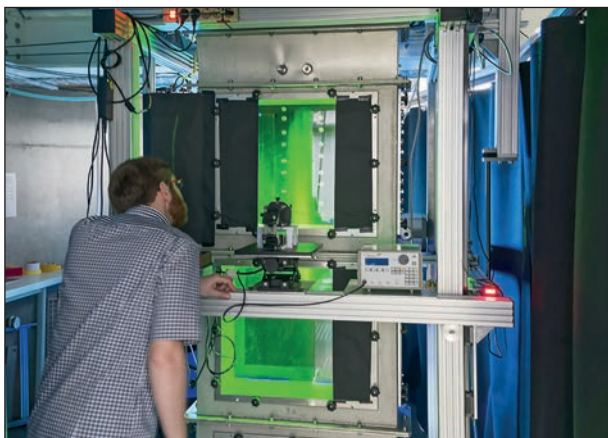
Fig. / Abb. 12: The turbulent wind tunnel "LACIS-T" allows the investigation cloud formation and freezing processes under turbulent flow conditions with previously unattainable precision and reproducibility. / Der turbulenten Windkanal „LACIS-T" erlaubt die Untersuchung von z.B. Wolkenbildungs- und Gefrierprozessen unter turbulenten Strömungsbedingungen mit bisher nicht erreichbarer Genauig- und Reproduzierbarkeit. (Photo: Tilo Arnhold / TROPOS)

Field campaigns are supported and complemented by analyses based on meteorological satellites. In particular satellite products provide the spatio-temporal development of clouds and their interaction with radiation, as well as transport paths of aerosols. Especially the geostationary European weather satellite Meteosat is applied to this end.

Laboratory experiments

In atmospheric research, physico-chemical models for the description of the most relevant process are continuously developed. These models are based on process parameters that need to be determined in laboratory experiments under controlled environmental conditions.

Laboratory experiments cover the development of a large number of methods to characterize atmospheric particles in ground-based or airborne field measurement campaigns. This work includes for example the improvement of aerosol size spectrometers as well as collection systems for the physical and chemical characterization of cloud droplets and the interstitial aerosol that means those aerosol particles that are suspended in the gas phase inside the cloud along with the cloud particles.

Optical measurement techniques are developed and applied to determine the extinction coefficient of aerosol particles. Multi-wavelength lidar systems and a wind lidar are further developed in the laboratory and applied in the field to determine aerosol properties, aerosol fluxes and meteorological parameters such as temperature, relative humidity and wind. The amount of black carbon and mineral aerosol

nationalen Messnetzes zur Erfassung von Aerosolen, Wolken und Spurengasen (ACTRIS) beteiligt, um neben Prozessverständnis auch die Basis für eine langfristige Charakterisierung der kurzlebigen Klimabestandteile zu liefern.

Feldexperimente werden durch Analysen, basierend auf meteorologischen Satelliten, unterstützt und erweitert. Insbesondere werden mit Satellitenprodukten die raumzeitliche Entwicklung von Wolken und deren Strahlungsantrieb untersucht, ebenso wie die Transportwege von Aerosolen.

Laborexperimente

In der Atmosphärenforschung werden kontinuierlich physikalisch-chemische Modelle zur Beschreibung der wesentlichen Prozesse entwickelt. Grundlage derartiger Modelle sind stets Prozessparameter, die in Laborexperimenten unter bekannten Umgebungsbedingungen ermittelt werden.

In Laborexperimenten werden zahlreiche Messmethoden entwickelt, die zur Partikelcharakterisierung in boden- und luftgestützten Feldmesskampagnen eingesetzt werden. Diese Arbeiten beinhalten z. B. die Weiterentwicklung von Aerosolgrößenspektrometern sowie Sammelsysteme zur physikalischen und chemischen Charakterisierung von Wolkentröpfchen und dem interstitiellen Aerosol, also denjenigen Aerosolpartikeln, die innerhalb von Wolken neben den Wolkenpartikeln selbst in der Gasphase suspendiert sind.

Optische Messmethoden werden zur Bestimmung des Extinktionskoeffizienten von Partikeln entwickelt und angewendet. Mehrwellenlängenlidare
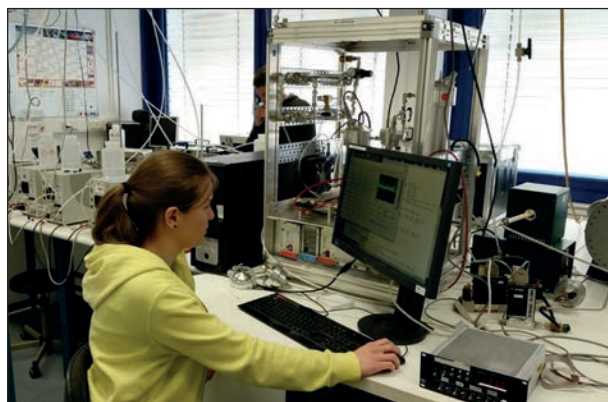
Fig. / Abb. 13: Inter comparison measurements of condensation particle counters for quality insurance of particle mobility size spectrometer measurements in one of the TROPOS WCCAP laboratories (World Calibration Center for Aerosol Physics). / Vergleichsmessungen von Kondensationspartikelzählern zur Qualitätssicherung von Partikelgrößenspektrometer-Messungen in einem der Labore des Weltkalibrierzentrums für Aerosolphysik (WCCAP) des TROPOS. (Photo: Kay Weinhold / TROPOS)

components in the aerosol samples are quantified with spectral absorption measurements.

Research at the Leipzig Aerosol Cloud Simulator LACIS addresses the activation of cloud droplets and primarily the heterogeneous formation of ice under realistic surrounding conditions. These investigations aim at a better understanding of the underlying fundamental processes, the identification of critical and controlling parameters, and the development of parameterizations to characterize droplet and ice formation processes for applications in dynamical models.

Gas phase reactions of various radicals are being investigated in flow reactors and in the Leipzig Aerosol Chamber (LEAK). These reactions are important for ozone and particle formation caused by anthropogenic or biogenic volatile hydrocarbons. The generated particles are also investigated with regard to hygroscopic growth and cloud droplet activation behaviour. In single drop experiments, investigations on phase transfer parameters of trace gases and radicals are being conducted. The determination of phase transfer parameters and reactive uptake coefficients hereby is being extended to previously not considered chemical species and complex surfaces.

In the field of liquid phase mechanisms reactions of primarily radical oxidants are investigated with time-resolved optical detection techniques. These reactions proceed within haze particles, fog and cloud droplets as well as in deliquescent aerosol particles.

For the understanding of the oxidation of organic trace gases in the tropospheric multiphase system, a large number of reactions with various radicals are

Fig. / Abb. 15: In the Chemistry laboratory of TROPOS in Leipzig, the chemical reactions could be detected in a experiment. Laboratory assistant Kornelia Pielok on the laminar flow-tube. / Im Labor des TROPOS in Leipzig konnten die chemischen Reaktionen in einem Freistrahlexperiment nachgewiesen werden. Laborantin Kornelia Pielok am Experimentaufbau.. (Photo: Tilo Arnhold / TROPOS)

und ein Windlidar werden zur Bestimmung von Aerosoleigenschaften, Aerosolflüssen und meteorologischen Parametern wie Temperatur, Feuchte und Wind im Labor weiterentwickelt und im Feld eingesetzt. Die Anteile „schwarzen Kohlenstoffs" und mineralischer Aerosolkomponenten in Aerosolproben werden durch spektrale Absorptionsmessungen bestimmt.

Die Arbeiten am Strömungsreaktor LACIS betreffen die Aktivierung von Wolkentröpfchen und schwerpunktmäßig die heterogene Eisbildung unter realistischen Umgebungsbedingungen. Ziele dieser Untersuchungen sind die Erlangung eines besseren Prozessverständnisses auf fundamentaler Ebene, die Identifikation kritischer und kontrollierender Parameter und die Entwicklung geeigneter Parametrisierungen zur Beschreibung von Tröpfchen- und Eisbildung in dynamischen Modellen.

Gasphasenreaktionen verschiedener Radikale werden in Strömungsreaktoren und der Leipziger Aerosolkammer (LEAK) untersucht. Diese Reaktionen sind von Interesse für die Ozon- und Partikelbildung, verursacht durch anthropogene oder biogene flüchtige Kohlenwasserstoffe. Die erzeugten Partikel werden auch hinsichtlich ihres Feuchtewachstums- und Aktivierungsverhaltens untersucht.

In Einzeltropfenexperimenten werden Untersuchungen bzgl. der Phasentransferparameter für Spurengase und Radikale durchgeführt. Die Bestimmung von Phasentransferparametern und reaktiven Aufnahmekoeffizienten wird dabei auf bisher nicht betrachtete chemische Spezies und komplexe Oberflächen ausgeweitet.

Im Bereich von Flüssigphasenmechanismen werden Reaktionen von vorwiegend radikalischen Oxidantien mit zeitaufgelösten optischen

Fig. / Abb. 14: The samples of the surface film are collected for the ensuing laboratory investigations (Polarstern expedition PS106, 2017, in the Arctic). / Probenahme des Oberflächenfilms für anschließende Laboruntersuchungen (Polarstern-Expedition PS106, 2017 in der Arktis). (Photo: Marcel Nicolaus / AWI)

being studied as well as reactions of halogenated oxidants. The latter species are of interest for the emission of reactive halogen compounds from sea salt particles, the so-called halogen activation.

The liquid phase laboratory for the investigation of tropospheric liquid phase processes is an important centre for these research activities. The process studies result in the improvement of chemical mechanisms, which can be applied to the self-developed model mechanism CAPRAM.

In the field of analytic measurement technology laboratory experiments are dedicated to improve and test methods for the chemical characterization of organic aerosol components. These methods are mostly based on mass spectrometric processes, which are deployed in various coupling techniques.

In the field of sampling techniques the "Atmospheric Chemistry Department" closely collaborates with the "Experimental Aerosol and Cloud Microphysics Department" on the development of the specific segregation of aerosol particles of a distinct size and their chemical analysis and also on the development of inlet systems and reactors.

Modeling

For the description of complex atmospheric processes, model systems of varying dimensions, complexity, and scales are developed, tested and

Fig. / Abb. 16: Burden of atmospheric Black Carbon over the Arctic as simulated with ECHAM-HAM using the ECLIPSE emission inventory, averaged over the years 2008 to 2012. / Rußbeladung der arktischen Atmosphäre aus ECHAM-HAM Simulationen unter Benutzung des ECLIPSE Emissionskatasters als Mittel über die Jahre 2008 bis 2012.

Nachweistechniken untersucht. Diese Reaktionen laufen in den Tröpfchen von Wolken, Regen und Nebel sowie in wässrigen Aerosolpartikeln ab. Hier werden zum Verständnis der Oxidation organischer Spurengase im troposphärischen Mehrphasensystem eine Vielzahl von Reaktionen verschiedener Radikale sowie Reaktionen von halogenhaltigen Oxidantien untersucht. Letztere Spezies sind von Interesse bei der Freisetzung von Halogenverbindungen aus maritimen Seesalzpartikeln, der so genannten Halogenaktivierung.

Das Flüssigphasen-Laserlabor zur Untersuchung der troposphärischen Flüssigphasenprozesse ist ein wichtiges Zentrum dieses Forschungsbereiches. Aus den Prozessuntersuchungen resultieren Verbesserungen chemischer Mechanismen, die in der Modellierung mit dem eigenen Mechanismus CAPRAM angewendet werden.

In der analytischen Messtechnik werden in Laborexperimenten Verfahren zur besseren chemischen Charakterisierung der organischen Bestandteile von Aerosolpartikeln entwickelt und getestet. Diese Techniken beruhen zumeist auf massenspektrometrischen Verfahren, die in verschiedenen Kopplungstechniken eingesetzt werden. Im Bereich der Probenahmetechniken gibt es auch hier eine enge Kooperation mit der Abteilung „Experimentelle Aerosol- und Wolkenmikrophysik" zur Entwicklung einer gezielten Abscheidung von Partikeln bestimmter Größe und deren chemischer Analyse aber auch zur Entwicklung von Einlasssystemen und Reaktoren.

Modellierung

Zur Beschreibung der komplexen atmosphärischen Vorgänge werden Modellsysteme verschiedener Dimension, Komplexität und Skalenbereiche entwickelt, überprüft und angewendet, auch in Kombination mit Daten aus Feldmessungen und aus satellitengestützten Fernerkundungen.

Ein Forschungsschwerpunkt ist die Beschreibung von Kreisläufen, Wechselwirkungen und Phasenübergängen zwischen Aerosolpartikeln, Gasen und Wolken, um so unser Verständnis klimarelevanter Prozesse in troposphärischen Mehrphasensystemen zu verbessern.

Chemie-Transportmodellierung wird durch das am TROPOS entwickelte 3D-Modellsystem COSMO-MUSCAT realisiert. Seine Eignung zur Simulation des Ausbreitungsverhaltens von Partikeln und Gasen auf regionaler Skala wurde in mehreren internationalen Modellvergleichen und bei der Bearbeitung von Fragen zur Luftqualität gezeigt. In mehreren Projekten wird die Dynamik primärer und sekundärer Aerosolpartikel simuliert und deren Wechelwirkung mit
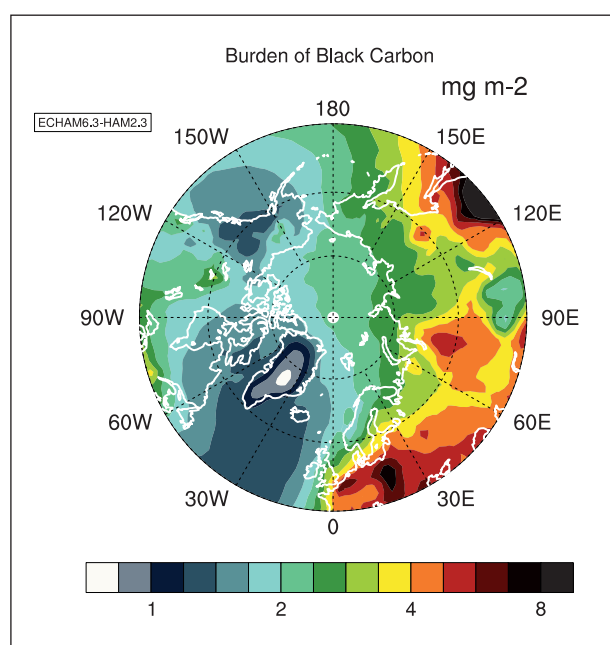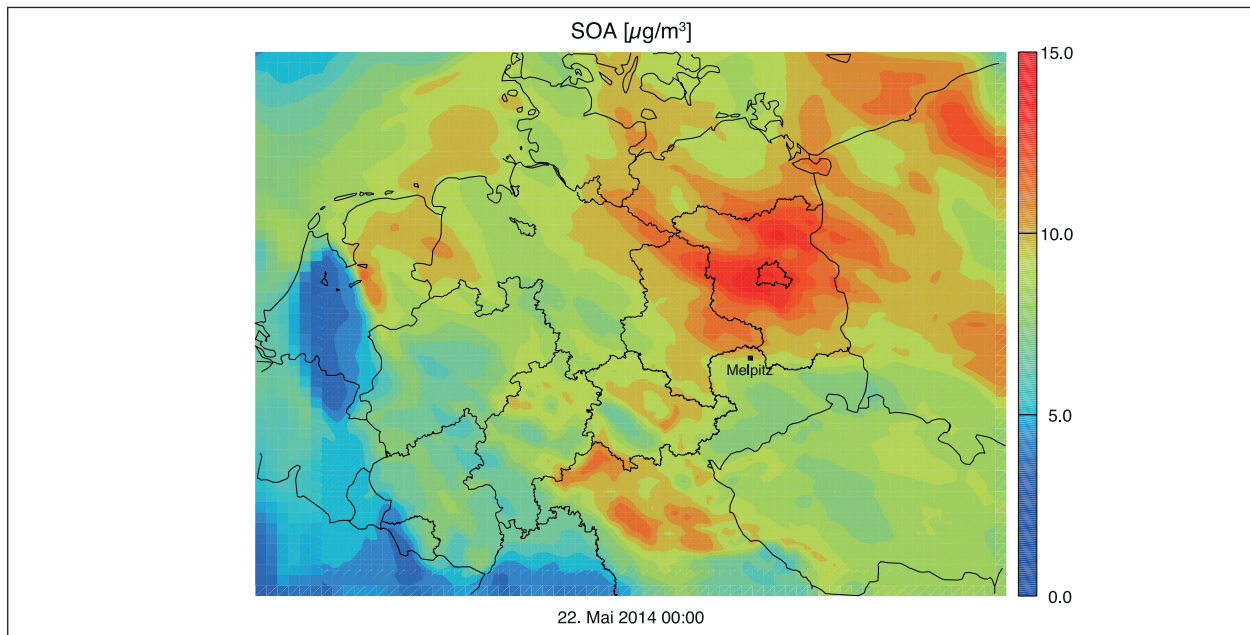
Fig. / Abb. 17: SOA mass for 22 May 2014 (0 UTC) considering HOMs. / SOA-Massenkonzentration für den 22. Mai 2014 (0 UTC) unter Berücksichtigung von HOMs.

applied, also in combination with data from field and satellite measurements.

One focus of research is the description of cycles, interactions and phase transfer between aerosol particles, gases and clouds. The aim is an improvement in understanding of climate-relevant processes in the tropospheric multiphase system.

Chemistry-transport modelling is realized with the three-dimensional modelling system COSMO-MUSCAT that has been developed at TROPOS. Its appropriateness for the simulation of particle and gas distribution on regional scale was demonstrated in international model-intercomparison studies and in applications on air quality issues.

Several projects investigate the dynamics of primary and secondary particles and their interaction with radiation and clouds. For further studies an additional "urbanized" version of COSMO-MUSCAT is being developed using a horizontal grid resolution up to a few 100 m. It will be applied for studies of the influence of regional climate variability on the budgets of trace elements.

The model ASAM (All Scale Atmospheric Model) indicates future developments, applicable from the micro to the global scale. It realizes cut cells in a Cartesian grid for the description of orography and obstacles. Currently it is mainly used for simulations of boundary layer processes on the Large Eddy scale.

Besides this, one- and two-dimensional process models were also developed and will be developed further. SPECS (SPECtral bin cloud microphysicS) can be used for the investigation of cloud processes

Strahlung und Wolken untersucht. Für weitere Anwendungsmöglichkeiten wird zusätzlich eine „urbanisierte" Version von COSMO-MUSCAT entwickelt, die eine horizontale Gitterauflösung bis zu wenigen 100 m nutzt. Damit werden auch Untersuchungen zum Einfluss der regionalen Klimavariabilität auf Spurenstoffhaushalte durchgeführt.

Mit ASAM (All Scale Atmospheric Model) steht ein noch in der Weiterentwicklung befindliches Modell zur Verfügung, dessen dynamischer Kern für Anwendungen vom mikroskaligen bis zum globalen Maßstab eingesetzt werden kann. In einem kartesischen Gitter wird die Darstellung von Orographie und Hindernissen mit angeschnittenen Zellen realisiert. Das Modell wird gegenwärtig für die Untersuchung von Grenzschichtprozessen auf der Large-Eddy-Skala genutzt.

Daneben wurden und werden ein- und zweidimensionale Prozessmodelle entwickelt bzw. weiterentwickelt. SPECS (SPECtral bin cloud microphysicS) dient zur Beschreibung von Wolkenprozessen. Es erlaubt eine explizite und sehr genaue Berechnung der Prozesse Kondensation, Kollision oder Gefrieren. SPACCIM (SPectral Aerosol Cloud Chemistry Interaction Model) ist ein Paketmodell zur gekoppelten größenaufgelösten Beschreibung von Mikrophysik und Mehrphasenchemie. Beide Module können sowohl als Boxmodell zur Prozessmodellierung als auch gekoppelt an das mesoskalige COSMO-Modell zur Untersuchung von realen Situationen verwendet werden. Die Prozessmodellierungen werden im Zusammenhang mit Feldstudien sowie mit Laborexperimenten durchgeführt.

Introduction / Einleitung

with a detailed description of condensation, collision or freezing. SPACCIM (SPectral Aerosol Cloud Chemistry Interaction Model) is a parcel model, which combines the size-resolved description of microphysics with a complex multiphase chemistry. Both modules can be applied for process modelling as one-dimensional box model version as well as coupled with the mesoscale-model COSMO for the investigation of real situations. The process modelling studies are realized in connection with field studies and laboratory experiments.

The model simulation of the complex atmospheric systems is numerically highly demanding. The models need to be sufficiently accurate and numerically efficient to be used productively on existing computer systems. Following the improvement of the numerical methods and parallelisation strategies is also a part of the scientific works.

Besides the dynamic/microphysical/chemical modelling at TROPOS also radiation transport models are developed and applied. These models are used to generate remote sensing algorithms for the improved understanding of the solar and thermal radiation effect of aerosols and clouds.
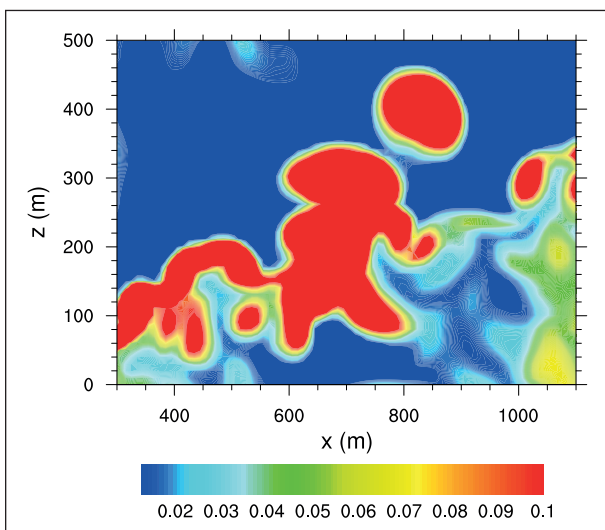
Fig. / Abb. 18: Large-Eddy modelling of fire impacts on near-surface wind pattern to investigate the dust emission potential of wildfires. Wildfires are related to strongly enhanced turbulence, lead to a frequent occurrence of high wind gusts close to the surface, and, sometimes, produce their own firefighter; here expressed in fields of the turbulent kinetic energy (TKE). / Large-Eddy-Simulationen der Auswirkungen von natürlichen und anthropogenen Feuern auf die bodennahen Windmuster, zwecks Abschätzung möglicher feuer-induzierter Emissionen von Mineralstaub. Wie hier anhand der turbulenten kinetischen Energie (TKE) dargestellt ist, sind solche Feuer mit stark erhöhter Turbulenz verbunden, führen häufig zum Auftreten starker Windböen in Bodennähe und produzieren manchmal auch ihren eigenen Feuerwehrmann.

Die modelltechnische Behandlung des komplexen atmosphärischen Systems ist numerisch sehr aufwändig. Die zu entwickelnden Modelle müssen hinreichend genau sein und numerisch sehr effizient den jeweils zur Verfügung stehenden Rechnerarchitekturen angepasst werden. Die Optimierung der verwendeten numerischen Verfahren und Parallelisierungsstrategien ist daher ebenfalls ein Teil der wissenschaftlichen Arbeiten.

Neben der dynamischen/mikrophyskalischen/chemischen Modellierung werden am TROPOS auch Strahlungstransportmodelle entwickelt und betrieben, um Fernerkundungsalgorithmen zu entwerfen und den solaren und thermischen Strahlungseffekt von Aerosolen und Wolken besser zu verstehen.

Overview of the individual contributions / Übersicht der Einzelbeiträge

Overview of the individual contributions

The biannual report presented here introduces selected works at TROPOS by means of five extended and 20 short contributions for the time period 2016 to 2017. Both years were characterised by the preparation and performance of numerous mostly international measurement campaigns reaching from the Antarctic, through the Subtropics, the Mediterranean and Central Asia to the Central Arctic.

The integrative detection of the physical and chemical aerosol cloud system under the involvement of all departments becomes more and more common praxis.

Also directly here in Leipzig, in eastern Germany, and in urban regions worldwide, the expertise of TROPOS is increasingly used to analyse air quality in connection with its causes and developments.

Method development in numerical simulation, in laboratory experiments, and in the synergetic use of different remote sensing sensors continuously expands the horizon of tropospheric multisystem observation possibilities.

Expanded contributions

Due to the fact that aerosol particle transport is crossing boarders, the general question arises, to which extend regional aerosol particle concentrations depend on regional emission sources or on sources from remote locations.

Especially in eastern German states the transport of ultrafine particles from east European regions can significantly contribute to the local air pollution. This is investigated at TROPOS by means of process studies and long-term trend analyses in collaboration with the environmental authorities. The results of a comprehensive meteorological and statistic/chemical study of the winter period 2016/2017 by **Van Pinxteren et al**. could proof that 50% of the high air pollution in central Germany derives from eastern European sources („increment east"), which can be allocated mainly to wood and coal combustion as well as to SO_2 emissions and subsequent particle formation processes. Interestingly, backward trajectories indicate, that this sources are not only situated near borders, but have their origin rather in remote eastern parts of central and south central Europe.

Long-range transports also play an important role in the deposition of mineral dust, especially transport from the world's largest source of mineral dust – the Sahara dessert. Mineral dust with a growing anthropogenic percentage and multiple effects on the radiation budget, cloud and ice formation processes,

Übersicht der Einzelbeiträge

Der vorliegende Zweijahresbericht stellt in fünf längeren und 20 Kurzbeiträgen ausgewählte Arbeiten des TROPOS im Zeitraum 2016 bis 2017 vor. Beide Jahre waren sehr durch Vorbereitung und Durchführung zahlreicher und zumeist internationaler Messkampagnen geprägt, von der Antarktis über die Subtropen, dem mediterranem Bereich, Zentralasien bis in die zentrale Arktis. Hierbei setzt sich mehr und mehr die integrative Erfassung des physikalischen und chemischen Aerosol-Wolken-Systems unter Beteiligung aller Abteilungen des Instituts durch. Auch vor Ort in Leipzig, im ostdeutschen Raum und in urbanen Regionen weltweit wird die TROPOS-Expertise zunehmend genutzt, um Luftqualität und deren Ursachen und Entwicklung zu erfassen. Methodenentwicklung in der numerischen Simulation, der Labormessung und der Synergie verschiedener Fernerkundungssensoren erweitert kontinuierlich den Horizont der Erfassung des troposphärischen Multiphasensystems.

Langbeiträge

Da Aerosoltransporte nicht vor Ländergrenzen halt machen, stellt sich generell die Frage, in welchem Maße regionale Aerosolkonzentrationen von regionalen und von fernen Quellen abhängen. Insbesondere für die ostdeutschen Bundesländer kann der Feinstaubtransport aus dem osteuropäischen Raum erheblich zur lokalen Luftbelastung beitragen. In Zusammenarbeit mit Umweltbehörden wird dies am TROPOS sowohl in Prozess-Studien als auch in Trendanalysen langfristig untersucht. **Van Pinxteren et al**. konnten nun mittels einer gesamtmeteorologischen und statistisch/chemisch genaueren Betrachtung eindeutiger als bisher für den Zeitraum Winter 2016/2017 nachweisen, dass hohe Luftverschmutzung in Mitteldeutschland zu 50% aus osteuropäischen Quellen (Stichwort „Inkrement Ost") stammt und das diese Quellen zumeist Holz- und Kohleverbrennung sowie SO_2-Emissionen und anschließender Partikelbildung zuzuordnen sind. Interessanterweise weisen Rückwärtstrajektorien darauf hin, dass diese Quellen nicht ausschließlich grenznah sind, sondern insgesamt mehr im entfernteren östlichen Teil von Zentralsowie in Südosteuropa liegen.

Ferntransporte spielen auch eine entscheidende Rolle in der großräumigen Verteilung des Mineralstaubs, insbesondere der Transport aus der weltweit größten Staub-Quelle, der Sahara. Mineralstaub mit seinem zunehmend anthropogenen Anteil und vielfachen Auswirkungen auf die Strahlungsbilanz, Wolken- und Eisbildung, biogeochemische Prozesse sowie

Overview of the individual contributions / Übersicht der Einzelbeiträge

biochemical processes as well as different risks for health and traffic remains a central focus at TRO-POS. In their article **Schepanski et al.** indicate the significance of dust sources and of various emission processes on the micro-physical composition of the global dust distribution and the related interactions in the coupled Earth system. An interesting example in this context is dust emission caused by pyroconvection, which forms a new research topic in the field of modelling and mineral dust remote sensing. In contrast to the continental and anthropogenic influenced northern hemisphere, sources and pollutions in the maritime southern hemisphere are significantly lower and maybe even comparable with the situation in the pre-industrial northern hemisphere. TROPOS scientists had the opportunity to participate in the unique expedition of the research vessel „Academic Tryoshnikov". This three-month cruise around Antarctica provided the opportunity for extensive aerosol characterisation over the southern Atlantic. **Henning et al.** investigated the deposit, physical properties, and the sources (for example organic marine, long-range transport) of cloud condensation nuclei (CCN) and ice nucleating particles (INP) in the surrounding area of the Antarctic continent. During the entire cruise the CNN concentration was unexpectedly constant. High values were especially found near the Antarctic continent. INP concentrations mostly were very low, which may explain the dominance of liquid water clouds in this region. This work significantly contributes to a characterisation/climatology of CCN/INP in the southern ocean, which has not been exhaustively sampled until now.

After the Antarctic circumnavigation during the southern hemisphere summer TROPOS was a leading member of the Arctic expedition PS106 of the German research icebreaker „Polarstern". Here the extensive remote sensing and aerosol characterisation devices, which already have been used for nearly 10 years during Atlantic transects of "Polarstern", could be deployed under Arctic conditions for the first time. **Macke et al**. describe the variety of measurements and first results of the Arctic atmosphere vertical profiling, and the related energy fluxes in the boundary layer and on the ground. In the same time, in situ physical and chemical aerosol particle characterisations as well as measurements on the deposit and properties of Arctic CNN and INP were carried out. The work aims at a better understanding of how the atmosphere influences the globally most extreme warming in the Arctic („Arctic amplification"). Most of these studies belong to the collaborative research center SFB/Transregio TR172 "Arctic Amplification". As for the Antarctic data, also the Arctic measurements show very low concentration of INP. Among other

diversen Risiken für Gesundheit und Verkehr, bleibt ein zentraler Fokus am TROPOS. **Schepanski et al.** weisen in ihrem Artikel auf die Bedeutung der Staubquellen und unterschiedlichen Emissionsprozesse auf die mikrophysikalische Zusammensetzung der globalen Staubverteilung und die damit verbundenen Wechselwirkungen im gekoppelten Erdsystem hin. Ein interessantes Beispiel in diesem Zusammenhang ist die Staubemission aufgrund von Pyrokonvektion, die ein neues Forschungsfeld im Bereich Modellierung und Fernerkundung des Mineralstaubes eröffnet.

Im Gegensatz zur kontinental und anthropogen geprägten Nordhemisphäre sind Quellen und Belastungen in der maritimen Südhemisphäre deutlich geringer und vielleicht vergleichbar mit der Situation der vorindustriellen Nordhemisphäre. TROPOS konnte an der bislang beispiellosen Schiffsexpedition ACE-SPACE auf dem russischen Forschungsschiff „Akademik Tryoshnikov" teilnehmen, die in über drei Monaten die Antarktis umrundete und so Gelegenheit zu einer umfangreichen Aerosolcharakterisierung über dem Südlichen Atlantik gab. **Henning et al.** untersuchten das Vorkommen, die physikalischen Eigenschaften, und die Quellen (z.B. organisch marin, Ferntransport) von Wolkenkondensationskernen (CCN) und eisnukleierenden Partikeln (INP) in der Umgebung des antarktischen Kontinents. Die CCN-Konzentration war über dem gesamten Fahrtverlauf überraschend konstant. Extreme Werte wurden insbesondere in der Nähe des antarktischen Kontinents gefunden. INP-Konzentrationen waren in der Regel sehr gering, was die Dominanz von Flüssigwolken in dieser Region erklären kann. Diese Arbeiten tragen maßgeblich zu einer CCN/INP-Charakterisierung/ Klimatologie im bislang wenig beprobten Südlichen Ozean bei.

Nach der Antarktis-Umrundung im südhemisphärischen Sommer war TROPOS federführend an der Arktis-Expedition PS106 des deutschen Forschungseisbrechers „Polarstern" beteiligt. Hier wurde die umfangreiche Fernerkundung und Aerosolcharakterisierung, die schon seit fast 10 Jahren auf den atlantischen Überfahrten der Polarstern genutzt wurde, erstmalig unter arktischen Bedingungen eingesetzt. **Macke et al**. berichten über die Vielzahl der Messungen und zeigen erste Ergebnisse zur Vertikalprofilierung der arktischen Atmosphäre und den zugehörigen Energieflüssen in der Grenzschicht und am Boden. Ebenso wurden in-situ physikalische und chemische Aerosol-Charakterisierungen sowie Messungen zum Vorkommen und zu den Eigenschaften arktischer CCN und INP vorgenommen. Ziel der Arbeiten ist es, den Einfluss der Atmosphäre auf die global extremste Klimaerwärmung in der Arktis („Arktische Verstärkung") besser zu verstehen. Die Arbeiten

Overview of the individual contributions / Übersicht der Einzelbeiträge

analyses, the compliance of the INP measurement data with the ice particle frequency in the Arctic boundary layer is currently investigated, for instance, to what extent the local marine biogenic sources can explain the INP concentrations. These marine biogenic sources were characterised by separate surface micro-layer measurements (SML).

A major benefit of ground-based remote sensing – as also deployed on board Polarstern – is the continuous detection of the vertical aerosol and cloud distribution. This helps to clarify the sensitivity of cloud and precipitation processes on varying aerosol properties. **Seifert et al**. summarize the synergetic remote sensing works at TROPOS and depict, how this works contribute to an almost complete characterisation of microphysical interaction processes in the medium term. A new method allows collecting vertical profiles of CCN and INP concentrations from backscattered lidar information. All necessary devices for these measurements are comprised in the mobile measurement station LACROS, consisting of the TROPOS developed lidar system "Polly^{XT}", of a 35-GHz cloud radar, a Doppler lidar as well as devices for passive remote sensing, like microwave radiometer and sun photometer. On this basis new methods of aerosol typing for the determination of cloud microphysical properties, for the derivation of temperature-dependency on freezing and precipitation as well as for the separation of particle fall velocity and vertical winds inside of clouds and precipitation have been developed, in order to analyse the sensitivity of cloud and precipitation processes on varying aerosol properties in meteorological/climatic characteristic regions.

Short contributions

The above-described remote sensing synergy platform was specifically applied in the framework of the CyCARE measurement campaign in Limassol, Cyprus, in conjunction with additional in-situ airborne measurements performed by the German research aircraft Falcon. Exemplarily with CyCARE, **Bühl et al.** show to what extent various aerosol sources from Africa, the Middle East and the European continent influence the Mediterranean region.

An analogous combination of ground-based remote sensing and airborne measurements was already performed during the long-range transport project SALTRACE 2013 and 2014 at Barbados. In the corresponding article **Haarig et al.** can among others detect Saharan dust 12.000 km away from source regions as well as the long-range transport of the ultrafine particle mode nearly without any losses.

Ground-based remote sensing also basically serves to validate atmospheric models. On the basis

sind größtenteils im SFB/Transregio TR172 „Arctic Amplification" angesiedelt. Analog zu den Antarktismessungen wurden auch in der Arktis sehr geringe INP-Konzentrationen ermittelt. Aktuelle Auswertungen untersuchen unter anderem, inwieweit die INP-Messungen mit der Häufigkeit von Eispartikeln in der arktischen Grenzschicht im Einklang sind und inwieweit lokale marine biogene Quellen, die in eigenen Oberflächenfilm-Messungen (SML) charakterisiert wurden, die INP-Konzentrationen erklären können.

Ein großer Vorteil der bodengebundenen Fernerkundung - wie sie auch auf Polarstern eingesetzt wird - ist die kontinuierliche Erfassung der vertikalen Aerosol- und Wolkenverteilung, aus der die Sensitivität von Wolken und Niederschlagsprozessen auf eine Variation der Aerosoleigenschaften erschlossen werden kann. **Seifert et al**. fassen die synergetischen Arbeiten der Fernerkundung am TROPOS zusammen und zeigen, wie diese mittelfristig zu einer nahezu vollständigen Charakterisierung von mikrophysikalischen Wechselwirkungsprozessen beitragen können. Eine neue Methode ermöglicht es, aus der zurückgestreuten Lidarinformation Vertikalprofile von CCN- und INP-Konzentrationen zu erhalten. Die für die Messungen nötigen Geräte sind in der mobilen LACROS Messstation zusammengefasst und umfassen unter anderem das am TROPOS entwickelte Lidarsystem Polly^{XT}, ein 35-GHz Wolkenradar, ein Dopplerlidar sowie passive Fernerkundung mittels Mikrowellenradiometer und Sonnenphotometer. Auf deren Basis wurden neue Methoden zur Aerosol-Typisierung, zur Bestimmung von wolkenmikrophysikalischen Eigenschaften, zur Ableitung der Temperaturabhängigkeit von Eisbildung und Niederschlag sowie zur Trennung von Partikelfallgeschwindigkeit und Vertikalwinden innerhalb von Wolken- und Niederschlag entwickelt, um so die Sensitivität von Wolken und Niederschlagsprozessen auf eine Variation der Aerosoleigenschaften in meteorologisch/klimatisch charakteristischen Regionen untersuchen zu können

Kurzbeiträge

Eine konkrete Anwendung der oben genannten Fernerkundungssynergie fand im Rahmen der CyCARE-Kampagne in Limassol, Zypern, statt, bei der zusätzlich in-situ Flugzeugmessungen des deutschen Forschungsflugzeuges Falcon eingebunden waren. **Bühl et al.** zeigen am Beispiel von CyCARE, wie sehr der mediterrane Raum von unterschiedlichsten Aerosolquellen aus Afrika, dem mittleren Osten und dem europäischen Kontinent beeinflusst ist. Eine analoge Kombination aus bodengebundener Fernerkundung und Flugzeugmessungen fand bereits 2013 und 2014 im Rahmen des Ferntransport-Projektes

Overview of the individual contributions / Übersicht der Einzelbeiträge

of the transect of the research vessel "METEOR" alongside a trans-Atlantic dust transport event over nearly four weeks, **Ansmann et al.** could proof that dust transport models are able to provide acceptable results up to a distance of 2000 km from the dust source and that the dry deposition of dust is generally too strong in models.

Besides mineral dust, biomass aerosol particles or smoke from the African continent respectively, determine the aerosol distribution over large areas of the Atlantic. By means of satellite data, **Merk et al.** show to what extend this highly absorbent smoke modifies the radiation budget, especially over bright clouds, and also how it can induce cloud remote sensing errors. Especially the geostationary satellite "Meteosat" allows a comparison with highly resolved model calculations thanks to the high temporary and (partially) spatial resolution. With the help of a complex spatio-temporal correlation analyses **Bley et al.** indicate, to what extend model/data comparison is possible and feasible.

In the area of physical aerosol and cloud observation numerous field and laboratory studies took place within the reporting period. One interesting and yet poorly understood aspect is the formation of aerosol particles or clouds in single or multiple layers. **Siebert et al.** discuss the hereby-occurring complex interplay of thermodynamics, turbulence and microphysics on the example of a field experiment in the Azores. Here, the helicopter-borne measurement platform ACTOS, which was developed at TROPOS, plays an important role in the simultaneous detection of all relevant parameters.

Another successful development of TROPOS is the mobile measurement backpack for the high-resolution detection of ultrafine particles in heterogeneous urban regions. **Alas et al.** propose to combine mobile and stationary measurements, which seeks to minimise uncertainties of measurement in terms of the spatial observation of air quality and has been exemplarily tested in the city of Rome. Taking into account, that today humans spent a large part of their time indoor rooms it is reasonable to apply TROPOS expertise in in-situ aerosol observation also for indoor analyses. **Zhao et al.** demonstrate in their „Indoor/Outdoor" measurement study to which extend especially health relevant ultrafine indoor particles stem from indoor or outdoor sources, depending on different everyday life activities. Anthropogenic particles, that influence the air quality, potentially can also have relevance for cloud and ice formation. Fly ash, emitted in large amounts by power plants is one example for this. **Grawe et al**. provide evidence that dry emitted fly ash can indeed contribute to ice formation in the atmosphere and that this ice nucleation

SALTRACE auf Barbados statt. Hierbei können **Haarig et al.** u.a. Saharastaub in 12.000 km Abstand von den Quellregionen sowie den nahezu verlustfreien Ferntransport des Feinstaubanteils nachweisen. Bodengebundene Fernerkundung dient grundsätzlich auch der Validierung von atmosphärischen Modellen. Auf der Basis des Transits des Forschungsschiffes METEOR entlang eines transatlantischen Saharastaubtransportereignisses über nahezu vier Wochen konnten **Ansmann et al.** u.a. nachweisen, dass Staubtransportmodelle bis zu einer Entfernung von 2000 km vom Staubursprung akzeptable Ergebnisse liefern und dass generell in Modellen die Trockendeposition des Staubes zu stark ist. Neben Mineralstaub bestimmt Biomasse-Aerosol bzw. Rauch vom afrikanischen Kontinent wesentlich die Aerosolverteilung über weite Teile des Atlantiks. **Merk et al.** zeigen anhand von Satellitendaten, wie stark der stark absorbierende Rauch speziell über hellen Wolken die Strahlungsbilanz modifiziert, aber auch zu Fehlern in der Wolkenfernerkundung führen kann. Insbesondere der geostationäre Meteosat-Satellit ermöglicht dank der hohen zeitlichen und (partiell) hohen räumlichen Auflösung einen Vergleich mit hochaufgelösten Modellrechnungen. **Bley et al.** zeigen mittels aufwändiger raumzeitlicher Korrelationsanalyse, bis zu welchem Grad Modell-Satellit-Vergleiche sinnvoll möglich sind.

Im Bereich der physikalischen Aerosol- und Wolkenerfassung fanden ebenfalls zahlreiche Feld- und Laborstudien statt. Ein interessanter und dennoch kaum verstandener Aspekt ist die Organisation von Aerosol und Wolken in einzelne oder multiple Schichten. Das hierbei komplexe Wechselspiel von Thermodynamik, Turbulenz und Mikrophysik diskutieren **Siebert et al.** am Beispiel eines Feldexperiments auf den Azoren, bei dem die am TROPOS entwickelte hubschraubergetragene Schleppsonde ACTOS eine zentrale Rolle in der gleichzeitigen Erfassung aller relevanten Parameter spielt. Eine weitere erfolgreiche Entwicklung am TROPOS ist der mobile Messrucksack zur hochaufgelösten Feinstaubmessung in heterogenen urbanen Regionen. **Alas et al.** schlagen eine Kombination von mobilen und stationären Messungen vor, die eine Minimierung der Messunsicherheiten bzgl. der räumlichen Erfassung der Luftqualität bewirken sollen und am Beispiel der Stadt Rom getestet wurde. Da heutzutage Menschen einen großen Teil ihrer Zeit in geschlossenen Räumen verbringen, liegt es nahe, die TROPOS-Expertise in der in-situ-Aerosol-Erfassung auch für Innenraumstudien anzuwenden. **Zhao et al.** zeigen in einer umfangreichen „Indoor/Outdoor" Messstudie, in welchem Maße insbesondere die gesundheitlich relevanten ultrafeinen Innenraum-Partikel aufgrund

Overview of the individual contributions / Übersicht der Einzelbeiträge

capability can be considerably reduced by previous suspension in water.

With the help of the newly developed turbulent wind channel LACIS-T **Niedermeyer et al.** are going to investigate how turbulent processes influence cloud and ice formation in the atmosphere. After the successful installation and initial operation in 2017 first results are presented.

As a substantial simplification most models use a constant reservoir of cloud condensation nuclei (CCN) and ice nucleating particles (INP). In the framework of a model comparison by means of the spectral (high resolution) model COSMO-SPECS **Simmel et al.** demonstrate the consequences of a prognostic handling of INP, applied in the characterisation of Arctic stratus clouds. It turns out that an a-priori specification of ice crystal size distribution can lead to errors in the ice particle lifetime due to wrong sedimentation rates.

Also aerosol particles itself can influence the energy balance in the Arctic by direct radiation effects and by alterations of the ground albedo. This especially occurs with strongly absorbing soot aerosol from anthropogenic sources. As a first step **Schacht et al.** show the uncertainties in current transport models caused by different emission data.

In a similar study as Simmel et al., **Heinold et al.** simulate a specific Saharan transport towards the European area using the regional model COSMO-MUSCAT. Thanks to the interacting aerosol-cloud microphysics the event's impacts on water, mixed and ice clouds becomes obvious here. As expected, the ice phase is always extremely underestimated in comparison to control runs without aerosol cloud interactions. This also affects the prediction skill of atmospheric models.

The chemistry transport model MUSCAT, developed at TROPOS, allows decided studies on particle formation processes. **Gatzsche et al.** extend the gas phase mechanism in MUSCAT to account for the recently discovered highly oxidised organic oxidation products (HOMs) and the correspondingly higher formation of organic aerosol in comparison to previous models. For solving these and other complex chemical problems in spatio-temporal high-resolution atmospheric models, adapted numerical methods need to be developed and applied. **Schimmel et al.** present AtCSol, a simulation environment permitting consideration of very large and complex multi-phase processes in a comparatively short time as well as testing of new numerical methods in the field of atmospheric chemistry.

unterschiedlicher Alltagsaktivitäten aus Innen- oder Außenquellen stammen können. Anthropogene Partikel, die die Luftqualität beeinflussen, können potentiell auch für Wolken- und Eisbildung relevant sein. Ein Beispiel hierfür ist Flugasche, die insbesondere in großem Maße aus Kraftwerken emittiert wird. **Grawe et al**. können nachweisen, dass trocken emittierte Flugasche tatsächlich zur Eisbildung in der Atmosphäre beiträgt und dass diese Eiskeimfähigkeit durch vorherige Suspension in Wasser beträchtlich reduziert werden kann. In welchem Maße turbulente Prozesse Wolken- und Eisbildung in der Atmosphäre beeinflussen, wollen **Niedermeyer et al.** mit Hilfe des neu entwickelten turbulenten Windkanals LACIS-T erforschen. Nach erfolgreichem Aufbau und Inbetriebnahme in 2017 werden Messkonzept und erste Ergebnisse vorgestellt.

Eine maßgebliche Vereinfachung in den meisten Modellen ist die Nutzung eines konstanten Reservoirs an Wolkenkondensationskernen (CCN) und Eiskeimen (INP). Im Rahmen einer Modellvergleiches zeigen **Simmel et al**. anhand des spektralen (größenauflösenden) Modells COSMO-SPECS, welche Auswirkungen eine prognostische Handhabung von INP in der Beschreibung arktischer Stratuswolken hat und dass eine Vorgabe der Eiskristallgrößenverteilung zu Fehlern in der Lebensdauer von Eispartikeln aufgrund falscher Sedimentationsraten führen kann. Auch Aerosol selbst kann die Energiebilanz in der Arktis durch direkte Strahlungseffekte und durch Veränderung der Bodenalbedo beeinflussen. Dies ist insbesondere der Fall für stark absorbierendes Ruß-Aerosol aus anthropogenen Quellen. In einem ersten Schritt zeigen **Schacht et al.** wie groß die Unsicherheiten in den aktuellen Transportmodellen aufgrund unterschiedlicher Emissionsdaten sind. In einer ähnlichen Studie wie Simmel et al. simulieren **Heinold et al.** mit dem Regionalmodell COSMO-MUSCAT einen konkreten Saharastaubtransport in den europäischen Raum und dank der interaktiven Aerosol-Wolken Mikrophysik dessen Auswirkungen auf Wasser-, Misch- und Eiswolken. Erwartungsgemäß wird die Eisphase in Vergleichsläufen ohne Aerosol-Wechselwirkung massiv unterschätzt, was auch Auswirkungen auf die Vorhersagegüte von Atmosphärenmodellen hat. Das am TROPOS entwickelte Chemietransportmodul MUSCAT erlaubt dezidierte Studien zu Partikelbildungsprozessen. **Gatzsche et al.** erweiterten den Gasphasenmechanismus in MUSCAT um die kürzlich entdeckten hochoxidierten, organischen Oxidationsprodukte (HOMs) und die damit verbundene stärkere Bildung von organischem Aerosol im Vergleich zu früheren Modellen. Um diese und andere komplexe chemische Systeme in raum-

Overview of the individual contributions / Übersicht der Einzelbeiträge

Organic carbon is one of the main components of atmospheric aerosol particles. But the exact composition is widely unidentified. For a better characterisation a fractionation method by means of 2D liquid chromatography was developed by **Spranger et al.** and they detected, that the composition of organic compounds shows differences between summer and winter as well as various airflows.

Criegee Intermediate (CIs) is formed through the gas phase ozonolysis of alkenes and constitutes an oxidizer in the atmosphere, which needs to be investigated more precisely. A method for the essentially needed CI verification was detected for the first time by **Berndt et al.** by means of mass spectroscopy allowing CI-detection from 10^4 - 10^5 molecules per cm^{-3}.

Dihydroxycarbonyle, 3,4-Dihydroxy-2-butanon (DHBO), and 2,3-Dihydroxy-2-methylpropanal (DHMP) are potential precursors of secondary organic aerosol in the liquid phase (aqSOA). **Otto et al.** investigated the reaction kinetics as well as the product distribution of radical oxidation with OH-radicals in the liquid phase. They could proof and quantify a fast degradation of booth compounds in the liquid phase. Besides oxidations through radical oxidants also oxidation reactions through non-radical oxidants like O_3 and H_2O_2 can be relevant. **Tilgner et al.** provide evidence for this on the basis of a newly developed complex multi phase chemistry module. Model simulations for continental environmental conditions show that liquid phase ozonolysis reactions of unsaturated organic compounds and reactions of H_2O_2 especially with substituted organic acids can contribute substantially to oxidation.

Although chemical processing with and without photochemistry (daytime chemistry versus nighttime chemistry) in the atmosphere is fundamentally different, both are also closely interconnected, because products of the night-time chemistry are further chemically processed through the subsequent daytime chemistry and vice versa. In the framework of the project Dark Knight **Mutzel et al.** illustrate, that the interplay of day- and night-time chemistry strongly influences the partitioning behaviour of oxidation products and following the formation of SOA.

zeitlich hochaufgelösten Atmosphärenmodellen effizient zu lösen, müssen angepasste numerische Verfahren entwickelt und verwendet werden. **Schimmel et al.** stellen die Simulationsumgebung AtCSol vor, die es erlaubt, sehr große und komplexe Multiphasenprozesse in vergleichbar kurzer Zeit zu berücksichtigen sowie neue numerische Verfahren im Bereich der Atmosphärenchemie zu testen.

Organischer Kohlenstoff ist eine der Hauptkomponenten von atmosphärischen Aerosolpartikeln. Die genaue Zusammensetzung ist jedoch weitgehend unbekannt. Um diese besser zu charakterisieren, haben **Spranger et al.** eine Fraktionierungsmethode mittels 2D-Flüssigchromatografie entwickelt und damit für die Messstation Melpitz deutliche Unterschiede in der Zusammensetzung der organischen Verbindungen zwischen Sommer und Winter sowie verschiedenen Luftströmungen festgestellt. Criegee Intermediate (CIs) werden über die Gasphasenozonolyse von Alkenen gebildet werden und stellen ein noch genauer zu untersuchendes Oxidationsmittel in der Atmosphäre dar. Für den dringend benötigten direkten CI-Nachweis haben **Berndt et al**. erstmalig eine Methode mittels Massenspektrometrie entdeckt, welche den CI-Nachweis von 10^4 - 10^5 Molekülen cm^{-3} erlaubt. Die Dihydroxycarbonyle, 3,4-Dihydroxy-2-butanon (DHBO) und 2,3-Dihydroxy-2-methylpropanal (DHMP) sind potentielle Vorläuferverbindungen sekundärer organischer Aerosole in der Flüssigphase (aqSOA). **Otto et al**. haben u.a. die Reaktionskinetik sowie die Produktverteilung der radikalischen Oxidation mit OH-Radikalen in wässriger Phase untersucht und einen raschen Abbau beider Verbindungen in der wässrigen Phase nachgewiesen und quantifiziert. Neben Oxidationen durch radikalische Oxidantien können auch Oxidationsreaktionen von nicht-radikalischen Oxidantien wie O_3 und H_2O_2 von Bedeutung sein. Den Nachwies hierzu liefern **Tilgner et al**. auf Basis eines neu entwickelten komplexen Multiphasenchemiemoduls. Modellsimulationen für kontinentale Umweltbedingungen zeigen, dass Ozonolysen in der Flüssigphase für oxidierte ungesättigte organische Verbindungen und Reaktionen von H_2O_2 insbesondere für substituierte organische Säuren substantiell zur Oxidation beitragen können. Obwohl die chemische Prozessierung in der Atmosphäre mit und ohne Photochemie (Tag- versus Nachtchemie) grundverschieden ist, sind beide auch eng miteinander verbunden, da die Produkte der Nachtchemie durch die darauffolgende Tagchemie weiterprozessiert werden und umgekehrt. **Mutzel et al.** zeigen im Rahmen des Projektes Dark Knight, dass durch das Wechselspiel von Tag- und Nachtchemie das Partitionierungsverhalten von Oxidationsprodukten und somit die SOA-Bildung stark beeinflusst werden.

Transfer in science and society – overview

Knowledge transfer and public visibility

TROPOS research for the expert public. On account of the application oriented fundamental research of the Institute its scientific knowledge is mainly transferred through scientific publications and conference contributions (see list, p. 149).

Among the worldwide most influential scientists in the area of geosciences a researcher of the Leibniz Institute for Tropospheric Research (TROPOS) was ranked 2016 and 2017. Prof. Alfred Wiedensohler is one of only 11 scientists in Germany listed in the current citations ranking "Highly Cited Researchers" by Thomson Reuters. Therefore scientific publications from 2005 to 2017 were evaluated and the number of citations was collected.

During the reporting period the following conferences with TROPOS organisation or co-organisation should be highlighted: The German-speaking SETAC Annual Conference (September 05-08, 2016, Tübingen) with 220 participants as well as the 3rd VDI Expert Forum for Atmospheric Chemistry (EFAC 3) (December 2016, Frankfurt/Main) with 60 participants were co-organised by Prof. Herrmann as chairperson of the GDCh Working Group on Atmospheric Chemistry. Also the TROPOS organised "Dust Days" 2016 and 2017 are worth emphasizing, where current research topics and questions in the research area mineral dust were presented to show the variety of disciplines in this field and to work out new collaborations. TROPOS also organised a session on "Asian Dust" at the 2nd international Conference on Atmospheric Dust (June, 2016, Catellaneta Marina, Italy). At the international level the "Sino European School on Atmospheric Chemistry" also has to be mentioned. This training school was conducted already for the third time to provide and transfer multidisciplinary knowledge to 60 selected Chinese and European doctoral candidates (SESAC3, November 21-30, 2017, Shandong, China).

TROPOS plays a leading role in managing the European infrastructure ACTRIS (Aerosols, Clouds, and Trace gases Research InfraStructure Network). In cooperation with 12 other German institutions TROPOS prepared the proposal "ACTRIS-D", the inclusion of ACTRIS in the German National Roadmap for infrastructures. In the year 2017 the proposal received a very good evaluation result from the Science Council and the final decision of inclusion will be communicated within the next months.

Results from TROPOS research contributes to policy advice in the environmental sector. For example

Transfer in Wissenschaft und Gesellschaft – Überblick

Wissenstransfer und Außenwirkung

TROPOS-Forschung für Fachpublikum. Auf Grund der Ausrichtung des Institutes als anwendungsorientiertes Grundlagenforschungsinstitut erfolgt die Verwertung hauptsächlich in Fachpublikationen und Konferenzbeiträgen (siehe Liste, S. 149). Unter den weltweit einflussreichsten Wissenschaftlern im Bereich der Geowissenschaften rangierte 2016 und 2017 ein Forscher des Leibniz-Institutes für Troposphärenforschung (TROPOS). Prof. Alfred Wiedensohler ist einer von lediglich elf Forschenden aus Deutschland, die im aktuellen Zitations-Ranking „Highly Cited Researchers" von Thomson Reuters aufgelistet wurden. Dazu wurden wissenschaftliche Publikationen aus den Jahren 2005 bis 2015 ausgewertet und wie oft diese in anderen Publikationen zitiert wurden.

Von den wissenschaftlichen Tagungen, an deren Organisation TROPOS beteiligt war, stechen im Berichtszeitraum folgende heraus: Die deutschsprachige SETAC-Jahrestagung (05.-08.09.2016, Tübingen) mit 220 Teilnehmenden sowie das 3. VDI-Expertenforum zur Atmosphärenchemie (EFAC 3) (Dezember 2016, Frankfurt am Main) mit 60 Teilnehmenden wurde von Prof. Hartmut Herrmann als Vorsitzendem des GDCh-Arbeitskreises „Atmosphärenchemie" mitorganisiert.

Herauszuheben sind ebenfalls die vom TROPOS organisierten „Leipziger Staubtage" 2016 und 2017, an denen aktuelle Forschungsthemen und Fragestellungen zum Thema Wüstenstaub vorgestellt wurden, um die Vielfalt der Fachbereiche zum Forschungsbereich zu zeigen und neue Verbindungen zu knüpfen. TROPOS organisierte zu diesem Forschungsthema auch eine „Asian Dust" Session auf der „2nd International Conference on Atmospheric Dust" (Juni 2016, Castellaneta Marina, Italien). Ebenfalls auf internationaler Ebene zu erwähnen ist die „Sino-European School on Atmospheric Chemistry", die bereits zum dritten Mal stattfand und 60 ausgewählten chinesischen und europäischen Promovierenden multidisziplinäre Kenntnisse vermittelte (SESAC3, 21.-30.11.2017, Shandong, China).

TROPOS spielt eine führende Rolle im Netzwerk der europäischen Forschungsinfrastruktur ACTRIS (Aerosols, Clouds, and Trace gases Research InfraStructure Network) und stellte zusammen mit 12 weiteren deutschen Institutionen den Antrag zur Aufnahme von „ACTRIS-D" auf die Nationale Roadmap für Forschungsinfrastrukturen. Der Antrag hat in diesem Jahr vom Wissenschaftsrat eine sehr

for the Land of Saxony and the Federal Environmental Agency (UBA) practise oriented investigations regarding the behaviour and the future development of air pollutants are conducted. In the framework of projects in collaboration with the Environmental Agency and the Saxon State Office for the Environment, Agriculture and Geology (LfULG) measurement data of fine and ultrafine particles are collected, evaluated and provided for further interpretation of the concentration and chemical composition of these particles.

In the field of clean-air policy-advice TROPOS also contributes with its own studies, which are used for air directive discussions and the implementation of clean-air strategies. This includes for example the engagement in respective advisory boards and events on the topic of air quality, like the meeting of the Joint Committee "Particulate Matter" (December, 14, 2017, Frankfurt/Main), the DECHEMA special colloquium "Stickstoffdioxid: Ist der Diesel noch zu retten?" (Nitrogen dioxide: is there still hope for diesel?) (December 5, 2017, Frankfurt/Main), presentations on the 4th LfULG status colloquium "Luft" (air) (December 6, 2017), and the final meeting of the project "PM Ost" in cooperation with environmental agencies of the Federal Government, Berlin, Brandenburg, Mecklenburg-Western Pomerania, and Saxony. In addition, the institute uses national forums for the presentation of research results.

TROPOS research results for the public at large. TROPOS seeks dialogue with the public using print media, radio and TV. The disseminations of press releases maintained 2016/2017 at a continuous high level with 22 press releases and additional 10 short notice press releases. During the current reporting period every month one press release could be published. Subsequently, 137 publications in 2016 and 230 publications in 2017 were registered. A special highlight in this respect is the output of the media cooperation "Eiszeit" (ice age) with "Sächsische Zeitung" (Saxonian Newspaper), which resulted in a series of print and online articles. The articles were created before, during, and after the expedition PS106 of the German research icebreaker "Polarstern". A broad audience gained insight into cloud and climate research and the understanding, that the Arctic warming can also have an influence on weather in Saxony.

Besides traditionally written reports the science editor Stephan Schön used his possibility to take part in the expedition also for fresh formats, like a multimedia essay or a 3D edition of the newspaper, which became one of the biggest projects of the publishing

gute wissenschaftliche Bewertung erhalten. Die endgültige Entscheidung zur Aufnahme fällt voraussichtlich in den nächsten Monaten.

Die Forschungsergebnisse des TROPOS dienen auch als ein Beitrag zur Politikberatung im Umweltbereich. So werden für das Land Sachsen und das Umweltbundesamt (UBA) praxisrelevante Untersuchungen zum Verhalten und zur künftigen Entwicklung von Schadstoffen in der Atmosphäre durchgeführt. Außerdem werden im Rahmen von Auftragsprojekten für das UBA und das Sächsische Landesamt für Umwelt und Geologie (LfULG) über längere Zeiträume Messdaten zu den Konzentrationen feiner und ultrafeiner Aerosolpartikel sowie zur chemischen Partikelzusammensetzung in der Atmosphäre erhoben, ausgewertet und diesen Institutionen zur weiteren Nutzung zur Verfügung gestellt.

Im Bereich der Luftreinhaltung trägt TROPOS zur Politikberatung auch durch eigene Forschungsergebnisse bei, die in der Richtliniendiskussion und bei der Erstellung von Luftreinhalteplänen verwendet werden. Dazu zählt unter anderem das Engagement in entsprechenden Gremien und Veranstaltungen zum Thema Luftqualität wie die Sitzung des Gemeinschaftsausschusses „Feinstäube" (14.12.2017, Frankfurt am Main), das DECHEMA-Sonderkolloquium „Stickstoffdioxid: Ist der Diesel noch zu retten?" (05.12.17, Frankfurt am Main), Vorträge auf dem 4. LfULG-Statuskolloquium Luft (06.12.2017, Dresden) oder die Abschlussveranstaltung des Projektes „PM-Ost" zusammen mit den Umweltbehörden von Bund, Berlin, Brandenburg, Mecklenburg-Vorpommern und Sachsen.

Fig. / Abb. 1: Expert Forum on urban air quality at the "Week of the Environment", Schloss Bellevue, Berlin (Dr. Dominik van Pinxteren, Prof. Dr. Alfred Wiedensohler (TROPOS), Marion Wichmann-Fiebig (UBA), Martin Lutz (Berliner Senatsverwaltung f. Stadtentwicklung). / Fachforum zu urbaner Luftqualität auf der „Woche der Umwelt", Schloss Bellevue, Berlin. (Photo: Tilo Arnhold / TROPOS)

company in 2017. The author's categorisation of the "Polarstern expedition" PS106 under the supervision of Prof. Macke as a "Highlight of research in Saxony 2017" summarises the profit for both partners.

The 2013 launched website was further enhanced and addresses research partners as well as the public at large. The section "Discover" aims at presenting TROPOS research for the interested public.

On the occasion of the WMO "World Meteorological Day" 2017 for example an overview of the cloud research centre Leipzig was given on this website. To illustrate scientific work on www.tropos.de increasingly scientists perform picture reports from their work around the world. For this purpose the section "Measurement campaigns" was installed under the menu point "Current issues", where impressions and reports from measurement campaigns, like "Azores 2017", the Arctic Expedition PS106, the Antarctic circumnavigation "ACE 2016/2017" or the "Central Asian Dust Experiment" in Tajikistan are available.

The twitter channel "@TROPOS_de" now also connects the institute to social media. Nearly 300 persons and institutions are following the channel. On monthly average the tweets are visited about 20.000 times ("impressions"). During the Polarstern expedition the visitor numbers have doubled.

Together with 60 other institutions TROPOS participated in the "Science Night" on 27 June, 2016, when laboratories, lecture halls, institutes, clinics, repositories, and archives gave an insight into their work. On the occasion of the "Leibniz Year" all three Leibniz institutes located in Leipzig presented a joint exhibition booth and a programme of short lectures and activities in the centre of Leipzig, in

Fig. / Abb. 2: "Sächsische Zeitung" journalist Stephan Schön reported from the Arctic expedition PS106 in the framework of the media cooperation "Eiszeit" with TROPOS. / Stephan Schön, Redakteur der „Sächsischen Zeitung", erstattete Bericht von der Arktis-Expedition PS106 im Rahmen der TROPOS-Medienkooperation „Eiszeit". (Photo: Sächsische Zeitung)

Das Institut nutzt zusätzlich nationale Innovations- und Forschungsforen für die Präsentation und Darstellung seiner Forschung.

TROPOS-Forschung für die breite Öffentlichkeit. TROPOS sucht den Dialog mit der Öffentlichkeit auch über Printmedien sowie Hör- und Fernsehfunk. Die Veröffentlichung von Mitteilungen wurde 2016/17 auf einem hohen Niveau von 22 Pressemitteilungen sowie weiteren 10 Kurzmitteilungen gehalten. Im aktuellen Berichtszeitraum wurde pro Jahr monatlich eine Pressemitteilung verfasst. Dadurch entstanden im Jahr 2016 137 Medienveröffentlichungen. Im Jahr 2017 waren es 230 Veröffentlichungen. Besonders hervorzuheben ist dabei die Medienkooperation „Eiszeit" mit der „Sächsischen Zeitung", durch die eine Reihe von Print-und Onlineartikeln vor, während und nach der Expedition PS106 des deutschen Forschungseisbrechers „Polarstern" entstanden, die Wolken- und Klimaforschung einem breiten Publikum nahebrachten und verdeutlichten, weshalb die Erwärmung in der Arktis sich auf das Wetter in Sachsen auswirkt. Neben klassischen Reportagen nutzte Wissenschaftsredakteur Stephan Schön die Teilnahme an der Expedition auch für neue journalistische Formen wie ein Multimedia-Essay oder eine 3D-Ausgabe der Zeitung, die zu einem der größten Projekte des Verlages 2017 wuchs. Dass das Experiment für beide Seiten erfolgreich war, zeigt auch seine Einstufung der Polarstern-Expedition PS106 unter Leitung von Prof. Andreas Macke als ein „Highlight der sächsischen Forschung 2017".

Der 2013 erneuerte Internetauftritt wurde weiter ausgebaut. Das Internetangebot richtet sich neben Forschenden zugleich an die breite Öffentlichkeit. Die Rubrik „Entdecken" hat daher zum Ziel, die Forschung für alle Interessierten zu erläutern. Zum „Welttag der Meteorologie 2017" entstand dabei unter dem Titel „Wolken verstehen" ein Überblick zu Leipzig als Zentrum der Wolkenforschung. Um Wissenschaft anschaulicher zu machen, kommen auf www.tropos.de zunehmend Forschende zu Wort, die auch selbst von den Messkampagnen in aller Welt berichten. Dazu wurde unter „Aktuelles" die Rubrik „Messkampagnen" ausgebaut, in der z. B. Berichte und Fotos von Expeditionen wie „Azoren 2017", der Arktis-Expedition PS106, der Antarktisumrundung „ACE 2016/2017" oder dem „Central Asian Dust Experiment" in Tadschikistan zu finden sind.

Mit dem Twitter-Kanal „@TROPOS_de" ist das Institut jetzt auch in den sozialen Medien aktiv. Knapp 300 Personen und Institutionen haben den Kanal abonniert („Follower"). Im Schnitt werden die Meldungen ca. 20.000 Mal pro Monat betrachtet

Transfer in science and society – overview / Transfer in Wissenschaft und Gesellschaft – Überblick

Fig. / Abb. 3: Prof. Dr. Alfred Wiedensohler (TROPOS) and Heiko Rosenthal (Leipzig Major for Environment, Public Policy and Sports) at the press conference presenting the final report of the "Low Emission Zone Leipzig" project. / Prof. Dr. Alfred Wiedensohler (TROPOS) und Heiko Rosenthal (Bürgermeister für Umwelt, Ordnung, Sport der Stadt Leipzig) auf der Pressekonferenz zum Abschlussbericht des Projektes „Umweltzone Leipzig" im Dezember 2017. (Photo: Tilo Arnhold / TROPOS)

the "Augusteum" of the University Leipzig and at the Leibniz monument.

A joint exhibition at the "Wissenschaftsmeile" (science presentation mile) with the other Leibniz institutes in Saxony was organised for the citizen festival in the framework of the Anniversary of German Unity, celebrated in Dresden from October 1-3, 2016, with more than 450.000 visitors.

On February 25, 2017 TROPOS researchers offered dialogue with interested citizens and organised an open day for the "OdCom" project on analysing odour problems in the German-Czech border region.

TROPOS is part of the public relations work of the German Climate Consortium (DKK), the "Klimanavigator" and the Leibniz Association, for example the BMBF Year of Science "Meere und Ozeane" (seas and oceans).

New approaches will be explored through the BMBF project "WTimpact" to develop gain of knowledge as a transfer instrument and to move on from knowledge transfer to knowledge exchange. In this consortium project of four Leibniz institutions TROPOS will contribute through citizen science research on air quality to allow subsequent analyses on this form of knowledge transfer.

Selected topics and activities during the reporting period. In addition to the institute's competence in urban air quality (particulate matter and low emission zones), especially climate relevant expertise about cloud formation processes or the impact of dust in the atmosphere became more important.

On December 14, 2017, TROPOS and LfULG (Saxon State Office for the Environment, Agriculture

("Impressions"). Während der „Polarstern"-Expedition PS106 verdoppelten sich die Zugriffszahlen.

Zusammen mit 60 anderen Institutionen beteiligte sich TROPOS an der alle zwei Jahre stattfindenden „Langen Nacht der Wissenschaften" am 27. Juni 2016, die Einblicke in Labore, Hörsäle, Institute, Kliniken, Magazine und Archive bot und damit auch in die Labore des TROPOS. Anlässlich des Leibniz-Jahres präsentierten sich an diesem Abend die drei Leipziger Leibniz-Institute zentral mit Infoständen und einem Vortrags-und Aktionsprogramm im Zentrum Leipzigs im „Augusteum" der Universität und am Leibniz-Denkmal. Zusammen mit den sächsischen Leibniz-Instituten war TROPOS vom 1. bis 3. Oktober 2016 auf der „Wissenschaftsmeile" in Dresden anlässlich des Bürgerfestes zum Tag der Deutschen Einheit präsent, das insgesamt von mehr als 450.000 Besucherinnen und Besucher zählte. Im direkten Kontakt mit interessierten Bürgerinnen und Bürgern standen auch die Forschenden des „Od-Com"-Projektes zu Geruchsbeschwerden im sächsisch-tschechischen Grenzgebiet beim Tag der offenen Tür am 25. Februar 2017 in Deutschneudorf.

Außerdem ist TROPOS an den Öffentlichkeitsaktionen des Deutschen Klimakonsortiums (DKK), des Klimanavigators und der Leibniz-Gemeinschaft, wie beispielsweise dem BMBF-Wissenschaftsjahr „Meere und Ozeane" aktiv, beteiligt.

Neue Wege wird das im September 2017 gestartete BMBF-Projekt WTimpact gehen, um die kollaborative Wissensentwicklung als ein Transferinstrument zu entwickeln und vom Wissenstransfer zum Wissensaustausch zu gelangen. TROPOS wird in dem Verbundprojekt von vier Leibniz-Instituten u.a. über Citizen Science zu Luftqualität beitragen, dass diese Formen des Wissenstransfers untersucht werden können.

Ausgewählte Themen und Aktivitäten im Berichtszeitraum. Neben der Kompetenz des TROPOS zur urbanen Luftqualität (Feinstaub und Umweltzonen), gewann besonders klimarelevantes Wissen über Prozesse wie Wolkenbildung oder die Auswirkungen von Staub in der Atmosphäre an Bedeutung. Zusammen mit dem LfULG präsentierte TROPOS am 14. Dezember 2017 den Abschlussbericht des Sondermessprogramms zur Umweltzone in Leipzig. Nach sieben Jahren Messungen konnten die Experten dabei belegen, dass die Umweltzone die Gesundheitsbelastung durch Feinstaub und Ruß deutlich gesenkt hat, die Belastung mit Stickoxiden aber trotz moderner Dieselkraftfahrzeuge nahezu konstant geblieben ist. Diese Ergebnisse sind ein wichtiger Beitrag zur aktuellen Diskussion um Diesel-PKWs in den Städten. Die Forschenden

and Geology) jointly presented the final report of the measurement programme accompanying the implementation of the Low Emission Zone Leipzig. After 7 years the experts could verify, that the Low Emission Zone reduced health impacts by particulate matter and soot, but that the load of nitrogen oxides remained constant despite modern diesel vehicles.

These results are an important contribution to the current discussion about Diesel vehicle use in cities.

Subsequently researchers on that subject were on high demand: TROPOS organised an expert forum for the "Week of the Environment" at Schloss Bellevue Park in Berlin, the residence of the Federal President, on June 8, 2016. Here Dr. Dominik van Pinxteren discussed together with experts from UBA (Federal Environmental Agency) and the Berlin senate on the topic "Hotspots of urban air pollution in Europe and worldwide – are measures effective enough?". On March 8, 2017 Prof. Alfred Wiedensohler was invited to speak in front a public meeting of the German Bundestag environment committee entitled "Air pollution by nitrogen oxides in conurbations – causes and possible solutions". Also present in the German Bundestag was Prof. Hartmut Herrmann in the framework of the Leibniz initiative "Leibniz in Bundestag" and talked to members of the Committee for the Environment, Nature Conservation and Reactor Safety and represented TROPOS with the topic "Diesel soot, low emission zones and the wood combustion trend – what is the German status in terms of air quality?".

On the occasion of the 25th anniversary of the Leibniz institutes in Saxony, the Saxon State Minister for Science and the Art Dr. Eva-Maria Stange, acknowledged the significance of the Leibniz institutions as key pillars for the Saxon center of science. The event was mainly organised by TROPOS in collaboration with the other institutes and took place in "Kongresshalle am Zoo Leipzig" with about 300 guests from politics, administrations, business and science.

On November 9, 2017 the Saxon State Minister for Science and the Art Dr. Eva-Maria Stange handed over the new laboratory building for atmospheric chemistry. It was founded by the Federal Government and the Land Saxony with 9,3 million Euro. The minister took the opportunity to obtain information about the laboratory experiments and their relevance for air quality and climate.

A continuously very popular topic among actors of audio-visual media is cloud research. For example ARD, ARTE, MDR, and 3sat reported on the new wind channel at the Cloud Laboratory. "MDR Sachsenspiegel" and "MDR Mittagsmagazin" showed pictures and interviews about the Arctic expedition. The Cape

Fig. / Abb. 4: TROPOS presentation at the citizen festival on the occation of the Anniversary of the German Unity in Dresden 2016. / TROPOS-Stand im Leibniz-Zelt der „Wissenschaftsmeile" auf dem Bürgerfest zum Tag der deutschen Einheit in Dresden 2016. (Photo: Sebastian Zeppenfeld / TROPOS)

des Institutes waren daher bei Politik und Medien gefragte Experten: Zur „Woche der Umwelt" am Sitz des Bundespräsidenten organisierte TROPOS am 08. Juni 2016 in Berlin ein Fachforum. Dr. Dominik van Pinxteren diskutierte dabei u.a. mit Experten des Umweltbundesamtes und dem Berliner Senat über das Thema „Hotspots der urbanen Luftverschmutzung in Europa und weltweit – wie effektiv sind Maßnahmen?". Rede und Antwort stand Prof. Alfred Wiedensohler auf der öffentlichen Sitzung des Umweltausschusses im Bundestag zum Thema „Luftbelastung durch Stickoxide in Ballungsräumen – Ursachen und Lösungsmöglichkeiten" am 08. März 2017. Ebenfalls im Deutschen Bundestag aktiv war Prof. Hartmut Herrmann, der das Institut bei „Leibniz im Bundestag" am 30./31. Mai 2017 im Gespräch mit Abgeordneten des Ausschusses für Umwelt, Naturschutz, Bau und Reaktorsicherheit vertrat zum Thema „Dieselruß, Umweltzonen und der Trend zum Heizen mit Holz - wo steht Deutschland aktuell in Sachen Luftqualität?" vertrat.

Wissenschaftsministerin Dr. Eva-Maria Stange würdigte anlässlich des 25-jährigen Bestehens der sächsischen Leibniz-Institute deren Bedeutung als Säulen des Wissenschaftsstandorts Sachsen. Das Jubiläum wurde am 6. Februar 2017 in der Kongresshalle Leipzig begangen. Die Festveranstaltung wurde federführend von TROPOS zusammen mit den anderen Leibniz-Instituten in Sachsen organisiert und es nahmen rund 300 Gäste aus Politik, Verwaltung, Wirtschaft und Wissenschaft teil.

Am 9. November 2017 übergab die sächsische Staatsministerin für Wissenschaft und Kunst, Dr. Eva Maria Stange, ein neues Laborgebäude an das Institut. Der Neubau für Experimente zur Chemie der Atmosphäre wurde vom Bund und dem Freistaat

Transfer in science and society – overview / Transfer in Wissenschaft und Gesellschaft – Überblick

Verde Island television channel (RTC) reported about the MarParCloud campaign, Czech Television (CT) about lidar measurements in Kosetice. But media also increasingly focus on the topic of air pollution: HR television broadcasted the programme "Tire abrasion as an underestimated environment problem". "Einfach genial" by MDR television and "Planet e" by ZDF joined TROPOS researcher doing mobile soot measurements. The results of the Low Emission Zone Leipzig or the detection of dust from forest fires in Canada were estimated nationwide in print and online media. Outstanding from the array of print articles are for example: the portraits of the institute's "Staubfänger" (dust catcher) in "Welt am Sonntag" or the impressions of the Austrian news magazine "profil" from behind the scenes of the cloud laboratory. Artistic activities by means of drawings and interviews by the illustrator Kerstin Heymach accompanied the works of TROPOS at the Longyearbyen research station and on-board "Polarstern" (Kerstin Heymach: Klimaaufzeichnungen).

Equal opportunities and promotion of young researchers

Equal opportunities are implemented as a leading principle at TROPOS. The institute fulfils the equal opportunity standards of the Leibniz Association, which were worked out by a presidential project group and presented in front of the General Assembly of members 2016.

Already during recruiting processes measures for the absolutely non-discriminatory collaboration are applied at the institute and are improved constantly. TROPOS intends to further increase the proportion of international researchers.

Following the so-called Leibniz cascade model TROPOS also intends to increase the proportion of women, especially in post-doc and leading positions. Therefore, a stage-model was implemented in 2012, which was defined according the current structure of employees at the institute. Particularly worth mentioning here is the SAW funded junior research group "Dust at the interface" leaded by Dr. habil. Kerstin Schepanski and "MARPARCLOUD" leaded by Dr. Manuela van Pinxteren. During the reporting period Dr. Heike Kalesse took part in the Leibniz Mentoring Programme for women and in the end of 2017 she was appointed for a junior professorship at the University Leipzig.

Audit "berufundfamilie": An important prerequisite for equal opportunities and career orientation is the reconciliation of career and family, especially for the promotion of young researchers. On May 25, 2011

Sachsen mit insgesamt 9,3 Millionen Euro finanziert. Die Ministerin nutzte die Gelegenheit, um sich vor Ort ausführlich über die Laborexperimente und deren Relevanz für Luftqualität und Klima zu informieren.

Besonders bei den audiovisuellen Medien ist die Wolkenforschung nach wie vor sehr beliebt. So berichteten beispielsweise ARD, ARTE, MDR und 3sat über den neuen Windkanal im Wolkenlabor. Der MDR-„Sachsenspiegel" und das MDR-„Mittagsmagazin" zeigten Bilder und Interviews zur Arktis-Expedition. Das Fernsehen der Kapverden (RTC) berichtete über die Kampagne „MarParCloud", das tschechische Fernsehen (CT) über die Lidar-Messungen in Kosetice. Aber auch das Thema Luftverschmutzung gerät zunehmend in den Fokus. So berichtete das HR-Fernsehen über „Reifenabtrieb als unterschätztes Umweltproblem". Die Sendung „Einfach genial" des MDR-Fernsehens und „Planet e" vom ZDF begleiteten Forschende des TROPOS bei ihren mobilen Rußmessungen. Die Ergebnisse der Umweltzone oder die Erfassung von Staub aus kanadischen Waldbränden fanden 2017 bundesweit Beachtung in den Printmedien. 2016 hatte bereits ein Bericht der dpa über die Lidar-Messungen von TROPOS für Beachtung gesorgt. Aus der Vielzahl der Printartikel ragen u.a. der Beitrag heraus, der „Die Staubfänger" des Instituts in der „Welt am Sonntag" portraitiert oder der Artikel im österreichischen Nachrichtenmagazin „profil", worin ein Blick hinter die Kulissen des Wolkenlabors geworfen wird. Im Rahmen einer künstlerischen Begleitung der Arktisforschung des Transregio 172 „Arctic Amplifcation" wurden auch die Arbeiten des TROPOS auf der Forschungsstation in Longyearbean und auf der „Polarstern" zeichnerisch und durch Interviews mit den Beteiligten begleitet (Kerstin Heymach: Klimaaufzeichnungen).

Fig. / Abb. 5: NoSoaT-Training School (North South Atlantic Training Transect) on board Polarstern expedition PS102, 2016. / NoSoaT-Training School (North South Atlantic Training Transect) an Bord der Polarsternfahrt PS102, 2016. (Photo: TROPOS)

the TROPOS efforts in this direction were internally and externally manifested in the certificate for the "career and family audit" and the respective measures are applied.

As a result of a re-auditing procedure TROPOS received the certificate for the audit once again on 29 June, 2015. The certificate and thus the framework conditions for an optimal productive achievement of research aims and at the same time realising family responsibilities was confirmed on August 31, 2017 and the re-auditing is now consolidated.

Promotion of young researchers. TROPOS actively promotes young researchers in the bachelor and master education at the Leipzig University as well as during and after doctoral research projects. The institute is involved in the development and implementation of the new bachelor and master programmes and is exclusively responsible for four modules and partially responsible for further two modules.

Highly qualified scientists of the Institute contribute to teaching activities in cooperation with the Leipzig University as joint appointments. In addition to meteorology students also chemistry and physics students are trained at TROPOS (see list, p. 168).

The institute offers young researchers an individualized realization of their dissertation projects supported by the supervision committee in the framework of the structured doctoral training programme. TROPOS scientists give lectures at the Universities of Jena, Beijing, Jinan, and Shanghai, Helsinki and Stockholm, in international summer and winter schools, training courses and networks (see list, p. 166).

The 2012 founded Leipzig Graduate School on "Aerosols, Clouds and Radiation" provided together

Fig. / Abb. 6: Dr. Dietrich Althausen, winner of the science slam "Competition of Cooperation Projects" in the framework of the BMBF Central Asia Day 2017. / Dr. Dietrich Althausen, Gewinner des Science-Slam „Wettbewerb der Kooperationsprojekte" auf dem „Ländertag Zentralasien" des BMBF 2017. (Photo: BMBF)

Chancengleichheit und Nachwuchsförderung

Gleichstellung ist am TROPOS als Leitprinzip implementiert. Das Institut erfüllt damit die Gleichstellungsstandarts der Leibniz-Gemeinschaft, die von einer präsidentiellen Projektgruppe erarbeitet und 2016 der Mitgliederversammlung vorgestellt wurden. Am TROPOS werden Maßnahmen zur absolut diskriminierungsfreien Zusammenarbeit am Institut bereits im Einstellungsverfahren angewendet und fortlaufend verbessert. Das Institut ist weiterhin bestrebt, den Anteil an internationalen Wissenschaftlerinnen und Wissenschaftlern zu erhöhen.

TROPOS will den Anteil von Frauen, vor allem in wissenschaftlichen Führungspositionen, weiter erhöhen und verfolgt dabei das so genannte Kaskadenmodell nach den Empfehlungen der Leibniz-Gemeinschaft, wobei ein an die momentane institutsspezifische Stellensituation angepasstes Stufenmodell im Jahr 2012 definiert wurde. Speziell erwähnt sei hier die Leitung der SAW-geförderten Nachwuchsgruppe „Interdust" durch Frau Dr. habil. Kerstin Schepanski und „MARPARCLOUD" durch Dr. Manuela van Pinxteren. Frau Dr. Heike Kalesse nahm im Berichtszeitraum am Leibniz-Mentoring Programm teil und wurde Ende 2017 auf eine Juniorprofessur der Universität Leipzig berufen.

Nachwuchsförderung. TROPOS fördert aktiv den wissenschaftlichen Nachwuchs in der Bachelor- und Masterausbildung, während der Promotionsvorhaben und darüber hinaus. Das Institut ist eng in die Entwicklung und in die Durchführung der neuen Bachelor- und Masterstudiengänge an der Universität Leipzig eingebunden und ist für vier Module exklusiv und für zwei weitere Module teilweise verantwortlich.

Hochqualifizierte Mitarbeiterinnen und Mitarbeiter beteiligen sich als gemeinsame Berufungen an der Lehre der Universität Leipzig. Neben Studierenden der Meteorologie werden am TROPOS auch Chemie- und Physikstudierende ausgebildet (siehe Liste, S. 168).

Das Institut bietet jungen Wissenschaftlerinnen und Wissenschaftlern individuell abgestimmte und von einem Betreuungsteam begleitete Realisierung ihrer Promotionen im Rahmen der strukturierten Doktorandenausbildung. Mitarbeitende des TROPOS halten Kurse an den Universitäten von Jena, Peking, Jinan und Shanghai, Helsinki und Stockholm und bei internationalen Sommerschulen, Ausbildungskursen und -netzwerken (siehe Liste, S. 166).

Die im Juli 2012 gegründete Leibniz-Graduiertenschule zu „Wolken, Aerosolen und Strahlung" hat die Promovierendenausbildung am TROPOS gemeinsam mit der Universität Leipzig auf eine solide Grundlage

Transfer in science and society – overview / Transfer in Wissenschaft und Gesellschaft – Überblick

Fig. / Abb. 7: Radiosonde ascent at Girl's Future Day at TROPOS 2017. / Radiosondenaufstieg zum Girl's Day 2017 am TROPOS. (Photo: Beate Richter / TROPOS)

with the University Leipzig a solid basis for the doctoral training at TROPOS and combines the expertise of both partners within the coupled research fields "aerosols, clouds, and radiation". By now the Graduate School has 30 members and is located in the Research Academy Leipzig (RAL).

Create future. TROPOS is a partner within the MINT-Individual network to inspire and generate interest in technical and natural science studies, and especially shows career perspectives in tropospheric research. Students get to know research work in a playful manner and have the possibility to directly talk to scientists from the MINT field. In the framework of this initiative the institute regularly participates in the Girls' Day (girls future day). In 2016 and 2017 interested female students could gain insight into laboratories and career opportunities as scientists and other professions at TROPOS. In total 16 practical trainings were supervised by employees of the institute and 11 educational events for pupils, two for students and six for adults were performed during the reporting period.

One BELL project (Besondere Lernleistung, i.e. special learning performance) was supervised.

As in the last years TROPOS will continue to finance an apprentice position.

Cooperations and networking

Numerous grown networks within the Leibniz Association, with Universities, with Max Planck Institutes, with institutes of the Helmholtz Society, and collaborations at the international level demonstrate the actual level of TROPOS networking in the field of interdisciplinary aerosol and cloud research. Similar alike TROPOS is networked on the European and global level and actively develops research programmes (see list, p. 185).

gestellt und bündelt die gemeinsame Expertise in den gekoppelten Bereichen „Aerosole-Wolken-Strahlung". Sie ist mit nunmehr 30 Mitgliedern in der „Research Acadamy Leipzig" (RAL) verortet.

Zukunft schaffen. TROPOS ist Partner im Netzwerk MINT-Individual und unterstützt den Weg zum naturwissenschaftlichen Studium und zeigt berufliche Perspektiven im Bereich der Atmosphärenforschung. Schülerinnen und Schüler lernen die Forschungsarbeit auf spielerische Art kennen und kommen mit Forschenden aus dem MINT-Bereich ins Gespräch. Im Rahmen der MINT-Initiative, die zum Ziel hat, Jugendliche für einen Beruf in den Fächern Mathematik, Informatik, Naturwissenschaften und Technik zu begeistern, beteiligt sich TROPOS auch am Girls' Day, dem Mädchen-Zukunftstag. In den Jahren 2016 und 2017 konnten sich an diesem Tag interessierte Schülerinnen in den Laboren über Ausbildungsmöglichkeiten informieren. Insgesamt wurden in beiden Jahren 16 Schülerpraktika durchgeführt, elf Bildungs- und Informationsveranstaltungen für Schulkinder und zwei für Studierende und sechs für Erwachsene. Eine BELL-Arbeiten (besondere Lernleistungen) wurde betreut.

TROPOS wird auch in den nächsten Jahren mindestens einen Lehrlingsausbildungsplatz aus Haushaltsmitteln finanzieren.

Bedeutende Kooperationen und Vernetzung in der Forschung

Zahlreiche bisher gewachsene Vernetzungen innerhalb der Leibniz-Gemeinschaft, mit Universitäten, mit Max-Planck-Instituten, mit Instituten der Helmholtz-Gemeinschaft sowie auf internationaler Ebene zeigen den derzeitigen Stand der Vernetzung des TROPOS in der interdisziplinären Aerosol- und Wolkenforschung. Ähnlich ist TROPOS auf der europäischen und weltweiten Ebene vernetzt und entwickelt hier aktiv Forschungsprogramme (siehe Liste, S. 185).

Technologische Entwicklungen am TROPOS führen zu internationalen Standards in der experimentellen direkten und indirekten Erfassung von Aerosolen und Hydrometeoren vom Boden bis zur hohen Atmosphäre sowie in der modellmäßigen Beschreibung des komplexen Multiphasensystems.

Im Rahmen des Wettbewerbsfonds der Leibniz-Gemeinschaft werden die Kooperationsmöglichkeiten innerhalb der Leibniz-Gemeinschaft und mit Universitätsinstituten ausgebaut. Durch Kooperationsvereinbarungen ist das Institut mit zahlreichen internationalen Einrichtungen verbunden (siehe Liste,
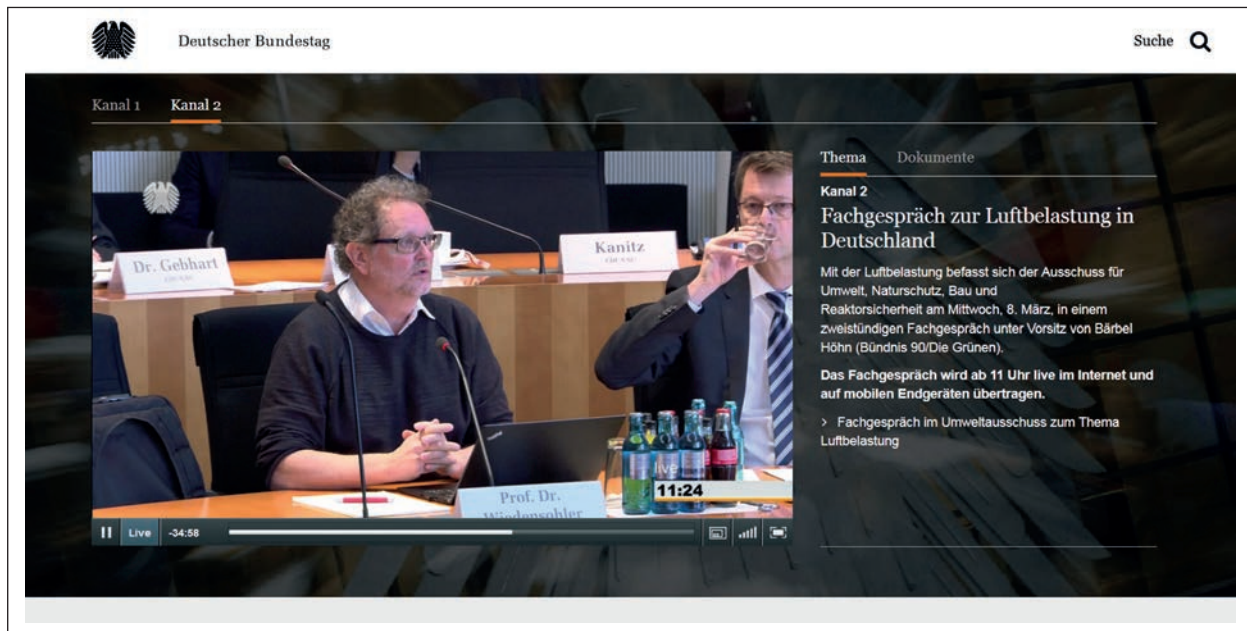
Fig. / Abb. 8: Prof. Dr. Alfred Wiedensohler at the public meeting of the environment committee in German Bundestag on the topic nitrogen oxides in conurbations. / Prof. Dr. Alfred Wiedensohler auf der öffentlichen Sitzung des Umweltausschusses im Deutschen Bundestag zum Thema Stickoxide in Ballungsräumen. (Photo: www.bundestag.de)

Technological developments at TROPOS lead to international standards in the experimental direct and indirect acquisition of aerosols and hydrometeors from ground up to the high atmosphere as well as in model-based descriptions of the complex multiphase system.

In the framework of the Leibniz competition funds cooperation is extended among the Leibniz Association and with university institutes. The ground-based remote sensing and in-situ measurement activities of TROPOS are integrated into the long-term orientated infrastructure ACTRIS and into ESA policy advice. The in-situ measurements of aerosol particles are part of the EMEP and WMO GAW networks. The collaboration with partners from Eastern Europe is being established (see list, p. 185).

S. 185). Die bodengebundenen Fernerkundungs- und in-situ-Messungen sind international eingebunden in die langfristigen ACTRIS-Arbeiten und in Beratungstätigkeiten für die ESA. Die in-situ Aerosolaktivitäten sind international in den EMEP- und WMO-GAW-Netzwerken eingebunden. Die Zusammenarbeit mit Osteuropäischen Partnern zur Umweltbelastung und Aerosolferntransporten im europäischen Raum ist angebahnt und wird weiter ausgebaut (siehe Liste, S. 185).

Articles

Trans-boundary PM10 pollution in Eastern Germany: Results from the "PM-OST" project

Dominik van Pinxteren, Falk Mothes, Gerald Spindler, Khanneh Wadinga Fomba, Hartmut Herrmann

Im Projekt PM-OST wurde eine detaillierte Ursachenanalyse von PM10 Feinstaub-Immissionen für 10 ausgewählte Messstationen der Länder Brandenburg, Berlin, Sachsen, Mecklenburg Vorpommern und des Umweltbundesamtes erstellt. Für den Zeitraum Winter 2016/17 wurden die Konzentration der PM10-Masse sowie ausgewählter Inhaltsstoffe in Abhängigkeit von verschiedenen Belastungssituationen analysiert. Unter Anwendung der positiven Matrixfaktorisierung als Rezeptormodell zur PM10-Quellzuordnung in Kombination mit statistischen Methoden der Rückwärtstrajektorienanalyse konnten lokale, regionale, sowie grenzüberschreitende PM10-Quellbeiträge aus Nachbarländern quantifiziert werden. Im Ergebnis zeigte sich, dass zusätzliches antransportiertes PM10 aus östlicher Richtung je nach meteorologischen Randbedingungen im Mittel über 6 ländliche Hintergrundstationen 0 – 30 µg m^{-3}, an einzelnen Stationen sogar bis zu 50 µg m^{-3} ausmachte. Für meteorologische Bedingungen, die hohe PM10- Massekonzentrationen von > 30 µg m^{-3} zur Folge haben, hatte dieses „Inkrement Ost" im Mittel einen Anteil von 50% an der Gesamtkonzentration. Für Bedingungen mit mittleren Konzentrationen zwischen 20 und 30 µg m^{-3} erklärte es 20% und in Situationen mit geringen PM10- Massekonzentrationen < 20 µg m^{-3} war der grenzüberschreitende Eintrag vernachlässigbar. Die Quellen des importierten PM- Anteils lagen in primären Emissionen der Holz- und Kohleverbrennung, sowie sekundär gebildetem Ammoniumsulfat und organischem Material, das sich während des Transportes der Luftmassen vermutlich überwiegend aus den gasförmigen Verbrennungsemissionen SO$_2$ und VOCs gebildet hatte.

Introduction and Overview

Episodes of air mass inflow from eastern directions frequently lead to elevated PM10 concentrations in Eastern Germany [*Spindler et al.*, 2013; *Spindler et al.*, 2010], which are often attributed to trans-boundary pollution import from eastern neighbouring countries [*van Pinxteren et al.*, 2016]. Within the PM-Ost project, this hypothesis was tested by means of a detailed analysis of pollution situations considering both transport and local meteorological conditions, leading to a quantitative assessment of the contributions of trans-boundary PM import and the identification of its sources.

The project was based on a dataset containing daily PM10 mass and constituents´ concentrations (inorganic ions and carbon sum parameters OC/EC) for 10 selected measurement stations of the federal states of Brandenburg, Berlin, Saxony, Mecklenburg-Western Pomerania and the German Federal Environmental Agency (UBA), which are depicted in Fig. 1 and listed with their abbreviations in Tab. 1. The studied period was from September 2016 to March 2017 and included 80 selected special measurement days (SMD), for which concentrations of polycyclic aromatic hydrocarbons (PAHs), levoglucosan and, for stations in Berlin, trace metals concentrations were determined in addition to the continuously available data.

Days and episodes characterised by high PM10 mass concentrations were particularly considered during the selection of the special measurement days.

Several days showing medium and low concentrations were, however, also included. Figure 2 shows an overview of the PM10 concentration time series at the 10 stations. The special measurement days are displayed in grey while days showing concentrations exceeding the daily limit value ($> 50\ \mu g\ m^{-3}$) are indicated by red dots.

The data show a typical trend of decreasing concentrations, with highest values detected at the traffic stations BEFRA and BBPOT and gradually lower concentrations measured at urban background stations BENAN and BBCOT and stations located in the rural background. A long episode of strongly increased PM10 concentrations even at rural stations is notable from the end of January until mid of February 2017, characterised by a high number of days with exceedance of the daily PM10 limit value at most stations.

Days and episodes showing increased PM concentrations may be due to particularly high emissions caused by, e.g., traffic or domestic heating and/or meteorologically adverse conditions such as, e.g., air mass transport of polluted air masses or weather conditions with limited air exchange and dispersion. Distinguishing these effects is often not easily possible, as they may mutually overlay or reinforce each other. For the investigated time period, it could be shown that air mass trajectories from eastern neighbouring countries correlate with on average i) lower temperatures and thus higher emissions from domestic heating, ii) lower mixing layer heights and thus an increased accumulation of local emissions and iii) less precipitation and thus less wet deposition of PM. Hence, a clear attribution of the increased concentrations during eastern trajectories to transboundary PM import is not unambiguously possible, as typical meteorological conditions during eastern wind episodes very likely result in local and regional accumulation of emissions as well.

Fig. 1: Overview of the measurement station, colour-coded as rural background stations (green), urban background stations (blue) and traffic stations (red) (Source: OpenStreetmap®).

Tab. 1: Measurement stations in "PM-OST" with their abbreviatios and classifications.

State	Station	Abbreviation	Classification
Berlin	Frankfurter Allee	BEFRA	Traffic
	Nansenstraße	BENAN	Urban
Brandenburg	Potsdam	BBPOT	Traffic
	Hasenholz	BBHAS	Rural
	Cottbus	BBCOT	Urban
UBA/Brandenburg	Neuglobsow	UBNEU	Rural
Mecklenburg-Western Pomerania	Löcknitz	MVLOE	Rural
Saxony	Brockau	SNBRO	Rural
	Niesky	SNNIE	Rural
	Melpitz	SNMEL	Rural

Fig. 2: Daily PM10 mass concentrations for all measurement stations during the study period; red dots indicate days with exceedance of the daily PM10 limit value of 50 µg m⁻³; special measurement days are displayed in grey.

Results based on the Lenschow approach

However, an assessment of the local and regional contribution to particularly polluted urban "hotspot" stations is possible by means of the so-called "Lenschow approach" [*Lenschow et al.*, 2001], which compares mean concentrations measured at 3 stations of different type (traffic station, urban and rural background station) that are geographically close. Here, increments for traffic and urban background are derived that are subsequently added to the concentration measured at the rural background station. In this project, this approach was applied to the measuring stations BEFRA, BENAN

and BBHAS. In addition to all measurement days, categories were formed according to special characteristics. These categories contained days with exceedance of the daily PM10 limit value, business days (Monday to Friday) vs. weekend days (Saturday, Sunday, public holidays), as well as categories related to meteorological conditions, i.e., air mass inflow: "East" or "West", based on backward trajectories; "scale" of the air masses: "Regional" or "Long-Range", based on the distance of backward trajectories from the receptor site; temperature: "Warm" or "Cold" with the median of all daily averaged temperatures taken as limit value; mixing layer height: "High" or "Low", with the median of the mixing layer height based on the
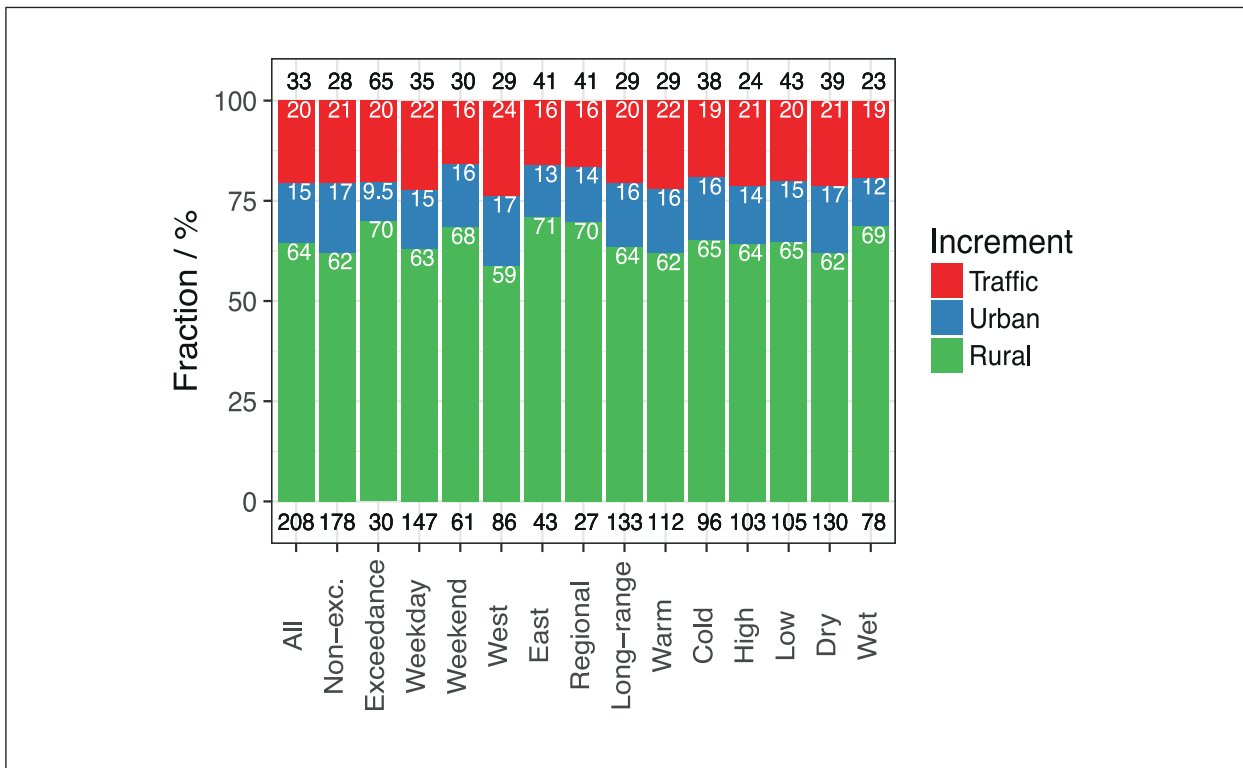
Fig. 3: Spatial contributions according to the Lenschow approach for the BEFRA station in different categories. Black numbers above the bars indicate the mean PM10 mass in µg m⁻³, while the black numbers below the bars indicate the number of measured values in the respective category.

COSMO-CLM model (FU Berlin) taken as limit value; and weather condition: "Dry" or "Wet" with the median of DWD RADOLAN precipitation values of the stations taken as limit value.

Figure 3 shows the relative increments for traffic, urban and rural background for the BEFRA station in dependence on the different categories. Similar to the findings of previous studies, a typical contribution of approximately 20% traffic, 15% urban background and 65% rural background to the mean PM concentration measured at the traffic station was found for all days as well as in most of the categories. In the categories showing the highest mean concentrations at the BEFRA station (41 – 65 µg m⁻³), i.e. "Exceedance", "East" and "Regional" days, the rural background contribution increased to approximately 70%. A major influence of trans-boundary pollution import to these elevated concentrations and rural background contributions can, however, not directly be derived from these observations. This is, on one hand, due to interactions between the meteorological categories, as described above, and on the other hand due to the fact that, for the category showing the highest concentrations ("Exceedance" days), a distinct Eastern inflow could only be detected for about one third of these days.

Quantification of trans-boundary PM import

In order to quantify the influence of trans-boundary long-range transport, a differentiated analysis of combined categories related to meteorological conditions was performed. Therefore, the values of the broad categories scale, temperature, mixing layer height and weather condition were combined into narrow categories containing only the sampling days that fulfilled all given category values, e.g. days with Western air mass inflow on a long-range scale with cold temperature, high boundary layer height and dry weather. These combined categories allowed for a comparison of the mean PM10 mass between air mass inflow West and East within identical or similar meteorological boundaries, thereby significantly reducing the ambiguity of transport vs. local or regional meteorology. For example, the mean mixing layer heights were very similar for "West" and "East" within the combined categories, while the values differed significantly between their respective opposite category:

West_Long-Range_Cold_High_Dry: 700 m
East_Long-Range_Cold_High_Dry: 600 m

In comparison:

West_Long-Range_Cold_Low_Dry: 250 m
East_Long-Range_Cold_Low_Dry: 260 m

A similar effect was observed for the meteorological parameters temperature and precipitation. It has to be noted, though, that building categories based on only two values cannot always level out differences in the meteorological conditions completely, e.g. there is still some variation within the combined "Cold" categories in the mean temperatures. Here, a further differentiation into more than two category values would be necessary. The present dataset of 212 measurement days, however, was not large enough for such further discrimination.

Within the combined meteorological categories, an "increment East" was calculated as the difference between mean concentrations during Western and Eastern air mass inflow episodes. This increment is interpreted as a proxy for the contribution of trans-boundary PM10 import into the study area, since it represents the added contribution from Eastern inflow for otherwise similar meteorological boundary conditions. Figure 4 shows the contribution of the "increment East" to the total PM10 concentration during Eastern inflow within different combined meteorological categories.

The highest increment East was observed for cold, dry days influenced by long-range backward trajectories and low mixing layer heights ("Long-Range_Cold_Low_Dry"). Regardless of measurement station type (traffic, urban, rural), the Eastern increment was approximately 30 µg m^{-3} on average within the study period, which represents about 60% of the observed mean PM10 concentration at the respective station type in that category.

If the mixing layer height changes from "Low" to "High" at otherwise constant boundary conditions ("Long-Range_Cold_High_Dry"), the increment still shows values of approximately 20 µg m^{-3}, representing still about 60% of overall pollution due to equally lower mean concentrations. A change from "Long-Range" to "Regional" ("Regional_Cold_Low_Dry") reduces the Eastern increment to close to 10 µg m^{-3}, while the contribution is decreased to approximately 25% on average for the rural background stations. This may indicate that the major contribution of trans-boundary PM import has its origins in countries further away and not necessarily in directly neighbouring regions of Poland and the Czech Republic. This observation is actually consistent with the outcomes of statistical trajectory analysis methods performed in this project, which equally suggest that the major source regions of the PM10 mass observed in the investigated area is located in more remote Southeast Europe.
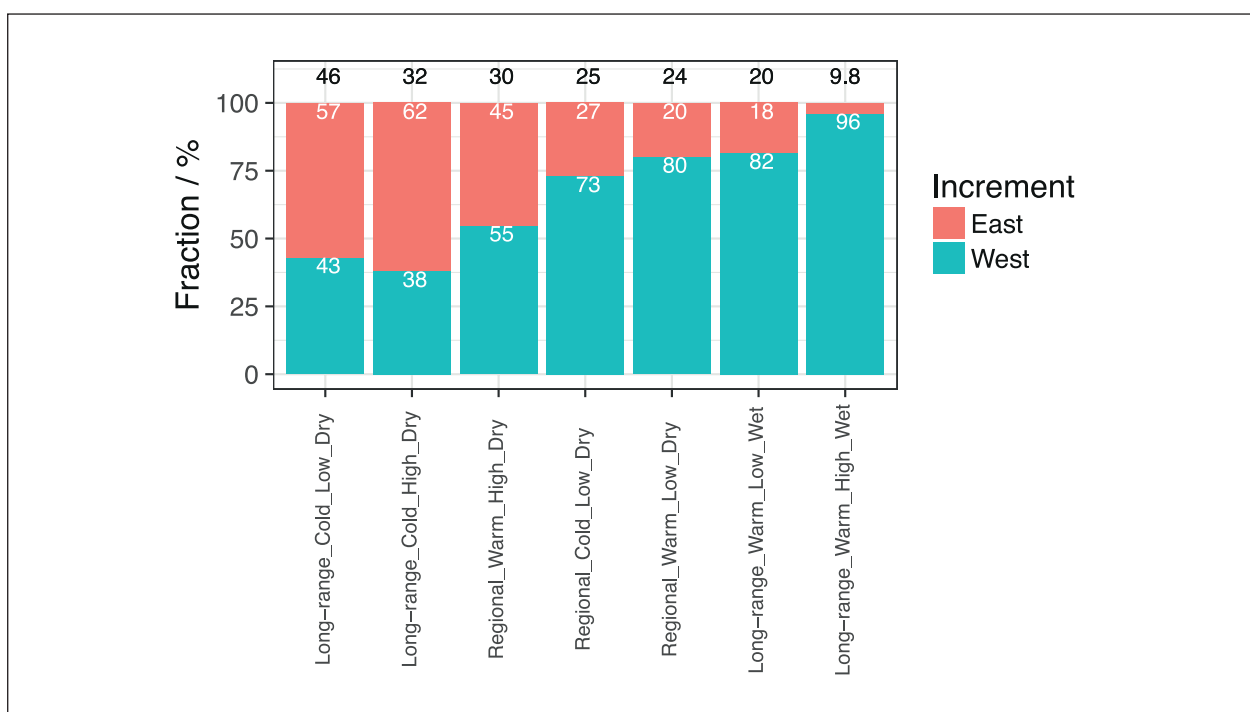
Fig. 4: Mean contributions of trans-boundary PM10 import into the study area ("increment East"), for the respective meteorological conditions using averaged data from all rural background stations. Black numbers above the bars indicate the mean concentration during Eastern air mass inflow in µg m^{-3}, while white numbers indicate the contributions of background levels (West) and the trans-boundary import (East).

Considering the contributions of the increment East in Fig. 4 as a function of the averaged PM10 mass across the combined meteorological categories, the following overall picture emerges: At meteorological boundary conditions leading to a high pollution value of > 30 µg m^{-3} in the rural background, roughly 50% of rural PM can be attributed to transboundary import. At averaged PM10 mass concentrations of approximately 20 – 30 µg m^{-3} this contribution is still about 20%, whereas the contribution is negligible at low pollution levels < 20 µg m^{-3}. It can even be slightly negative, in particularly for warm and wet combined categories, meaning that concentrations are slightly decreased during Eastern as compared to Western wind episodes (not shown here). These values are, on average, valid for the study period, although the combination of categories related to meteorological conditions in some cases lead to a comparably low number of days per combined category. This number ranged from 3 (minimum criterion for forming a category) and 40 across all rural measurement stations. More statistically robust and representative results could be obtained by analysing longer time periods.

Source apportionment using Positive Matrix Factorisation (PMF)

In order to obtain a more detailed source apportionment of the PM10 concentrations observed for the various stations and the increment East, receptor modelling using Positive Matrix Factorisation (PMF) was performed, including PM10 mass concentrations as well as the constituents analysed in the project. PMF runs were carried out on 5 levels with increasing amount of chemical information, but decreasing number of measurement days, as shown below:

Level 1: all 212 measurement days, all stations, PM10 mass, ions, OC/EC
Level 2: 80 SMD, all stations, PM10 mass, ions, OC/EC
Level 3: 80 SMD, all stations, PM10 mass, ions, OC/EC, PAHs
Level 4: 80 SMD, all stations, PM10 mass, ions, OC/EC, PAHs, levoglucosan
Level 5: 80 SMD, 2 stations (Berlin), PM10 mass, ions, OC/EC, PAHs, levoglucosan, metals

Table 2 shows the source categories identified at the various levels, along with their main constituents and characteristic marker compounds, acting as the basis for the physical interpretation of the mathematical PMF factors.

The sources, i.e., fresh salt (sea salt or road salt), chemically aged salt (by replacing chloride with other acids), secondary formation I (mainly ammonium nitrate), secondary formation II (mainly ammonium sulfate and organic matter), combustion, and traffic were resolved by the PMF model on all 5 levels. Based on additional chemical information (levoglucosan and metals), the source category related to combustion could be further split into general combustion, biomass burning, and coal combustion on levels 4/5, while the source category related to traffic was split into traffic wear and resuspension sources by adding metals on level 5.

These source categories explaing varying contributions to the PM10 mass at a given station, as shown in Fig. 5 as average over all 212 project days (PMF level 1).

Tab. 2: Source categories of PM10, resolved by PMF receptor modelling in the PM-Ost study.

Source category	Level	Main constituents	Marker compounds
Salt (fresh)	1-5	sodium, chloride	sodium, chloride
Salt (aged)	1-5	sodium, sulfate, nitrate, OC	sodium, magnesium
Secondary I (AN)	1-5	ammonium, nitrate, OC	nitrate
Secondary II (AS + OC)	1-5	ammonium, sulfate, OC	sulfate
Combustion	1-5	OC, EC	EC, potassium, (PAH)
Combustion (BM)	4-5	OC, EC	potassium, levoglucosan
Combustion (coal)	5	OC, nitrate, ammonium	As
Traffic	1-4	OC, EC, calcium, sulfate, nitrate	EC, calcium
Traffic (wear)	5	EC, Fe	Fe, Cu, Ba
Traffic (resuspension)	5	OC, calcium, sulfate	calcium, Ti, Sr
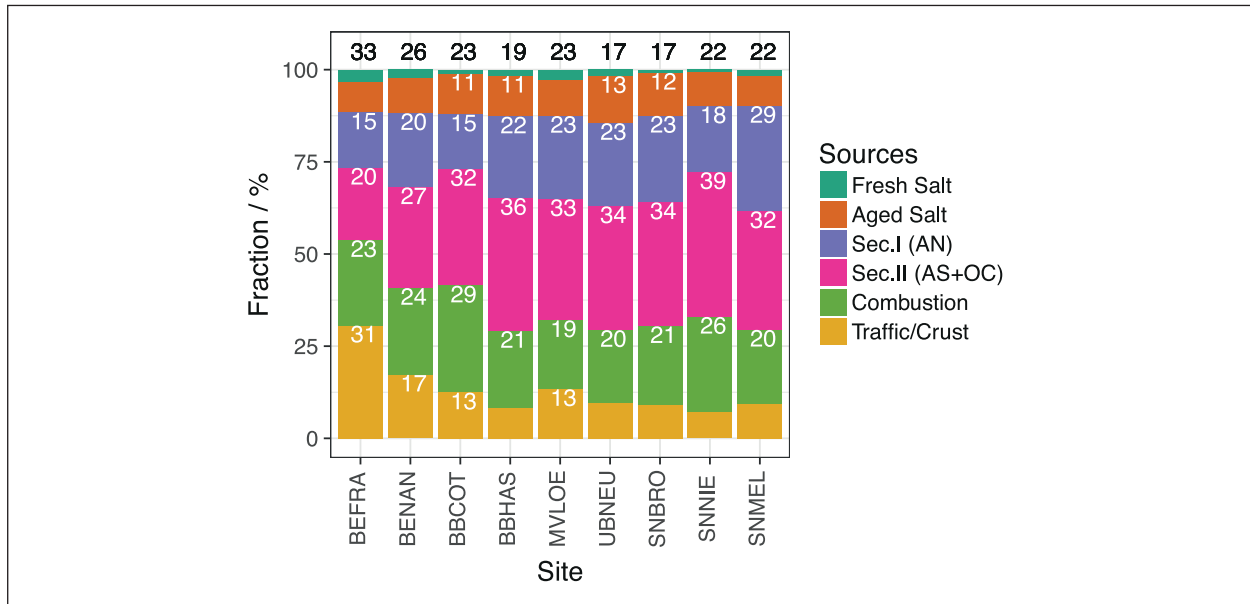
Fig. 5: Mean source contributions to PM10 mass concentrations at the measurement stations of the study area. Black numbers indicate the mean PM10 concentratio, while white numbers indicate the source contribution of the respective source category in percent.

As expected, the traffic contribution was highest at the urban stations, showing values of 30% at the BEFRA station and approximately 15% for the urban background. Emissions resulting from combustion of solid fuels explained about 20 - 30% of PM mass at all stations, secondary formation of ammonium sulfate and organics explained 20 - 40%, while 15 - 30% could be attributed to the formation of ammonium nitrate and approximately 10% to fresh and aged salt.

PMF results were used to identify the sources of trans-boundary PM import by calculating the increment East at equal meteorological boundary conditions for all PMF source categories and integrating them to form an overall picture. In Fig. 6, the combined meteorological categories with a positive increment East are shown, along with the mean PM10 mass concentrations based on PMF and the respective source contributions.

From Fig. 6, it becomes clear that the additionally imported contribution from Eastern directions were, for all meteorological boundary conditions, primarily caused by combustion emissions and secondary ammonium sulfate and organic matter. Given the fact that SO_2 and volatile hydrocarbons, as precursor
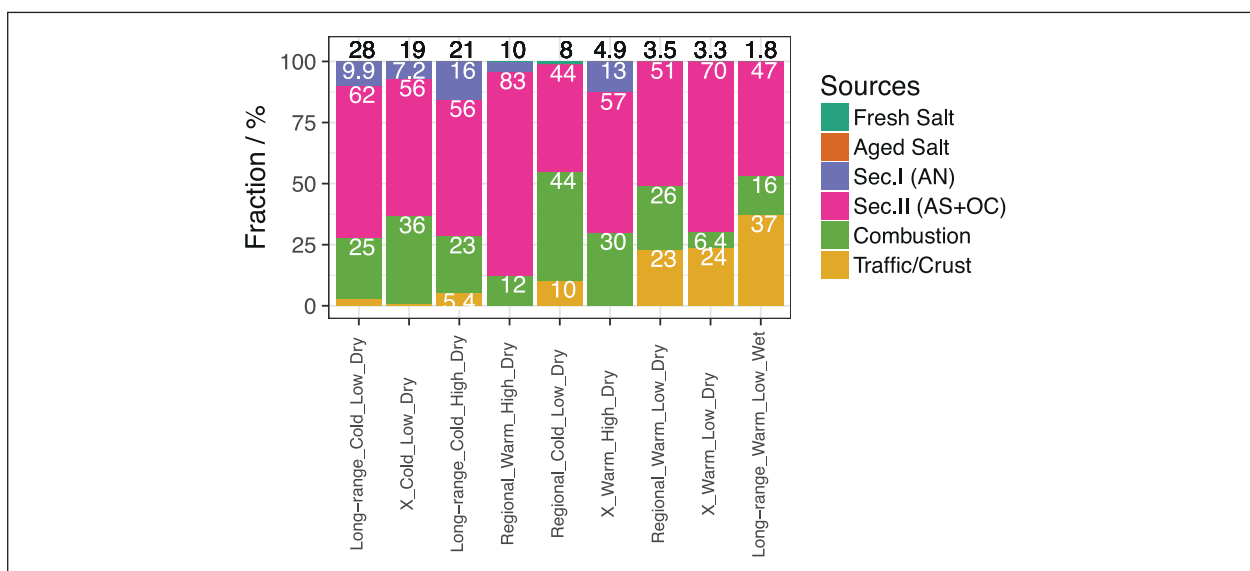
Fig. 6: Source contributions to trans-boundary PM10 import, averaged over all rural background stations. Black numbers indicate the mean PM10 mass concentration based on PMF in µg m⁻³, while white numbers indicate the respective relative contributions of the source categories.

compounds of sulfate and organic matter, are also, to a great extent, emitted during the combustion of coal and biomass, it can be concluded that primary as well as secondary products of solid fuel combustion were the major cause of trans-boundary PM import into the study area. The additional finding that transitioning from warm to cold days results in a strong increase of the absolute increments in the combined categories is an indication that domestic heating emissions in particular were the major source of the imported pollution, as domestic heating emissions, in contrast to industrial emissions or emissions from the energy sector, are highly dependent on temperature.

Conclusion

In the project PM-OST, a quantification as well as a source apportionment of trans-boundary import of PM into the study area in Eastern Germany was performed. The results show that the additionally imported PM10 mass from Eastern directions on average accounted for $0 - 30$ μg m^{-3}, depending on the meteorological conditions. At meteorological conditions leading to high PM10 mass concentrations of > 30 μg m^{-3} in the rural background, this "increment East" contributed on average 50% to the total rural PM10 concentration. For medium concentrations ranging from 20 to 30 μg m^{-3}, the increment East explained 20% of total PM, while the contribution of trans-boundary PM import was negligible for episodes of rural PM10 mass concentrations < 20 μg m^{-3}. For

high PM episodes with easterly winds at the urban traffic station Frankfurter Allee in Berlin (BEFRA), the following approximate contributions from different spatial scales resulted from a combination of increment East and the Lenschow approach:

traffic:	$15 - 20\%$
urban background:	$10 - 15\%$
rural background:	35%
long-range import:	35%

The sources of the imported trans-boundary PM could be attributed to primary emissions from the combustion of wood and coal, as well as ammonium sulfate and organic matter, likely formed during the transport of air masses after emission of gaseous combustion compounds like SO_2 and volatile organic compounds. Given the fact that the Eastern increment increased with lower temperature, emissions from domestic fuel burning are suggested to be a more likely source than industrial emissions or emissions from the energy sector. Furthermore, back trajectories indicated that the primary source regions might lie in more distant Eastern parts of Central and Southeast Europe rather than in the directly neighbouring areas of Poland and the Czech Republic. It has to be noted, however, that these back trajectory analyses carry large uncertainties and further studies would be necessary to identify source regions with more confidence.

References

Lenschow, P., H. J. Abraham, K. Kutzner, M. Lutz, J. D. Preuss, and W. Reichenbacher (2001), Some ideas about the sources of PM10, *Atmos. Environ.*, *35*, S23-S33.

Spindler, G., E. Brüggemann, T. Gnauk, A. Grüner, K. Müller, and H. Herrmann (2010), A four-year size-segregated characterization study of particles PM10, PM2.5 and PM1 depending on air mass origin at Melpitz, *Atmos. Environ.*, *44*(2), 164-173, doi: 10.1016/j.atmosenv.2009.10.015.

Spindler, G., A. Grüner, K. Müller, S. Schlimper, and H. Herrmann (2013), Long-term size-segregated particle (PM10, PM2.5, PM1) characterization study at Melpitz -- influence of air mass inflow, weather conditions and season, *J. Atmos. Chem.*, *70*(2), 165-195, doi: 10.1007/s10874-013-9263-8.

van Pinxteren, D., K. W. Fomba, G. Spindler, K. Müller, L. Poulain, Y. Iinuma, G. Löschau, A. Hausmann, and H. Herrmann (2016), Regional air quality in Leipzig, Germany: detailed source apportionment of size-resolved aerosol particles and comparison with the year 2000, *Faraday Discuss.*, doi: 10.1039/c5fd00228a.

Dust at the interface - modelling and remote sensing

Kerstin Schepanski, James R. Banks, Stefanie Feuerstein, Robert Wagner

Obwohl winzig, wird ihm ein großer Einfluss auf unser Klimasystem zugeschrieben. Obwohl in seinen Quellregionen begrenzt, ist er in jeder Region der Erde anzutreffen. Die Rede ist von Wüsten- staub, kleinen Bodenpartikeln, die in der Atmosphäre schweben und den Energiehaushalt der Erde beeinflussen. Wüstenstaub reflektiert, absorbiert und emittiert Strahlung. Er modifiziert Wolkenbil- dungsprozesse sowie Niederschlagswahrscheinlichkeiten. Seine mineralogische Zusammenset- zung ist vielfältig und regional verschieden. Vom Wind getragen kann er entfernte Kontinente und Ozeane erreichen. Als nährstoffhaltige Fracht des Windes kann er Ökosysteme düngen sowie die Bioproduktivität steigern. Eingeatmet kann er jedoch auch Krankheiten begünstigen.
Wüstenstaub tritt in verschiedenen Formen in das menschliche Bewusstsein: Als imposante und bedrohlich wirkende Staubstürme oder als dünne Schleier am Himmel, als atemraubende Luftfracht oder als kaum wahrnehmbare Beimischung. Entscheidend für die Präsenz und damit auch die Auswirkungen von Staub auf die Umwelt ist das Zusammenspiel von Landoberfläche und Atmo- sphäre. Der Boden stellt die Partikel bereit, die durch den Wind als Staub in die Atmosphäre einge- tragen und anschließend verfrachtet werden können. Der Transport von Staub in der Atmosphäre durch die vorherrschenden Windsysteme lässt sich gut und eindrucksvoll anhand von Satelliten- daten abbilden und verfolgen.
Im folgenden Beitrag werden drei Aspekte der Atmosphärenforschung zum Thema Staub herausge- griffen und diskutiert: (1) Staubquellen – der Ursprung. Obwohl stets unterschiedlich, lassen sich Staubquellen zu einzelnen Typen oder Klassen zusammenfassen. Am Beispiel einer bedeutenden und zugleich komplexen Staubquellregion in der Zentralsahara werden die unterschiedlichen Beiträge von Atmosphäre und Boden zur Variabilität der Staubquellaktivität diskutiert. (2) Staub- emission – was trägt dazu bei? Auch wenn dem Wind eine zentrale Rolle in der Staubemission zugeschrieben werden kann, so kann der Ursprung für Wind vielfältig und manchmal auch überra- schend sein: Kann Staub durch feuerinduzierte Konvektion (sog. Pyrokonvektion) in die Atmo- sphäre eingetragen werden? Und wenn ja, wie sieht der Zusammenhang aus? (3) Staubtransport – wie ist Staub sichtbar? Im abschließenden Teil wird der Frage nachgegangen, welchen Einfluss die optischen Eigenschaften der Staubpartikel auf die Darstellung der atmosphärischen Staubfracht in RGB-Falschfarbendarstellungen von Satellitendaten haben.
Gemeinsam betrachtet tragen die Ergebnisse aus allen drei Teilbereichen der Staubforschung dazu bei, das Verständnis der raum-zeitlichen Variabilität von Staub in der Atmosphäre zu erweitern.

Introduction

Mineral dust, a suspension of tiny soil particles in the atmosphere, is supposed to be a global player in the Earth system. Arguments given to support this role are its omnipresence in the Earth system, its ability to modulate the global thermostat, and its fertilising properties stimulating bio-productivity [*Carslaw et al.*, 2010]. First, dust particles contribute to the atmospheric aerosol burden not only over desert regions. Blowing with the winds, suspended dust particles are transported to remote regions leading to the second prominent argument for dust's significance: dust impacts. Airborne dust modulates the Earth's radiation budget and stimulates cloud and precipitation formation processes ultimately impacting on atmosphere dynamics and balances. Third, mineral dust particles deliver micro-nutrients to remote

ecosystems. The supply of these micro-nutrients can enhance the bio-productivity and ultimately affect the global carbon cycle. However, suspended dust in the atmospheric boundary layer may also impact negatively on human well-being.

Main actor of this article is the dust particle on its journey through the atmosphere. Progressing through the atmospheric dust life-cycle will highlight different aspects of the dust life-cycle as well as the application of different methods. Particular focus is on the dust sources and emission processes – the origin of the dusts' journey through the atmosphere and the 'how'. Here, the interplay of atmospheric and geomorphic controls on dust source activity will be discussed for a frequently active but complex dust source region in the central Sahara. Regarding the winds necessary to ultimately mobilise and entrain dust particles into the atmosphere, the origin of wind may or may not be the most obvious question. Here, we conceptually investigate the ability of pyro-convection for uplifting dust. Once airborne, the formation of dust plumes is observable from space. Due to the benefit of dust observation from space for research and weather forecasting, the demand for quantitative information on the actual dust concentration is high. In a third spotlight, the role of optical properties for the information content of satellite observations is discussed.

The atmospheric dust life-cycle

The journey of dust particles from source to sink is often referred as 'the atmospheric dust life-cycle', which composes of three major and successive elements: 'emission', 'transport', and 'deposition'. The spatial and temporal extent of the dust life-cycle is not predefined; however, the definition is generally used for describing the somewhat general link between predominant source to sink relationships.

Dust emission is controlled by surface characteristics and the supply of momentum required for particle mobilisation. Dense vegetation prevents soil from erosion, but bare soil is susceptible for wind erosion. However, as soils differ regarding their texture, particle size distribution, and composition, which is roughly summarised as 'soil type', the wind erosion potential and thus the emission efficiency varies among soil types, textures, vegetation cover, and soil moisture. In addition to soil conditions favouring wind erosion, momentum is required in order to mobilise and eventually suspend soil particles as dust in the atmosphere. Due to the surface drag, momentum from the wind acts on the soil surface mobilising particles if sufficiently strong. Hence, dust entrainment can be described as threshold problem with soil characteristics and near surface wind speed being the

determining elements [*Kok et al.*, 2012]. Interannual changes in wind speed and vegetation cover are assumed to play a major role to the interannual variability in dust emission and consequent atmospheric dust concentrations and export and deposition fluxes [*Wagner et al.*, 2016].

Once airborne and mixed deep into the atmospheric boundary layer, the dust particles' journey through the atmosphere is to a certain extent remotely controlled. Regional wind regimes and large-scale atmospheric circulation patterns determine the pathway through the atmosphere towards distant regions [*Schepanski et al.*, 2016, 2017].

Originating from the soil, the residence time of dust particles in the atmosphere is limited. Gravitation, scavenging, and turbulent downward mixing remove dust from the atmosphere and deposited on the surface. Depending on the nature of the surface, dust removed from the atmosphere and thus reaching the terminal point of the atmospheric dust life-cycle may enter a new stage, e.g. sinking through the ocean column [*Korte et al.*, 2017], fertilizing ecosystems, or altering the structure of snowpack.

Dust source activity controlled by wind regimes and sediment supply

The characteristics of dust sources vary regarding their sediment supply and availability. But also the transport capacity of the atmosphere is a crucial determinant in the system soil-atmosphere for Aeolian erosion. Dust sources can be distinguished regarding their geomorphic unit, which also moderates the soil's emissivity and thus the potential to emit lots of dust – or just little. The variability in dust emission and dust emission flux can be described as a function of the soil characteristic, wind and prevailing weather regimes. In the following, we will examine in depth a known dust source region located in the central Sahara (Fig. 1a) regarding the controlling contribution by soil characteristic (i.e. geomorphic unit and vegetation) and wind occurrence.

First, dust sources inevitably need to become known and somewhat classified regarding their dominant characteristic. Most obvious criterion is the surface characteristic. As local visits were not an option due to the geopolitical situation in Niger, a land cover classification algorithm was applied to Sentinel-2 imagery and adapted to the specifics of the central Saharan dust source regions. The resulting classification scheme clusters similar land covers and thus reveals a spatial inhomogeneity regarding surface types across the dust source region. In particular, the spatial distribution of surface classes such as alluvial sediments, rocks, or sand becomes visible.

By applying the land cover classification algorithm to multiple dates, temporal changes in extent of alluvial sediments can be determined.

The formation of alluvial sediments, that were found to dominate a significant portion of the study area, is strongly dependent on precipitation and consequent surface water runoff. By combining information on precipitation fluxes (estimated from TRMM (Tropical Rainfall Measuring Mission) rainfall products) and vegetation cover (estimated from NDVI (Normalized Difference Vegetation Index)), changes in surface type can be linked to antecedent rainfall events.

Wind erosion and consequent dust emission is controlled by both sediment availability and transport capacity, ergo wind. Whereas the sediment availability from alluvial sediments is enhanced a certain time after strong rain events [*Reheis and Kihl*, 1996], the wind speed distribution is controlled by the atmospheric circulation regime superimposed by local effects such as caused by orography. The availability of sediments and transport capacity

(wind) lead to a local seasonality of the dust emission flux. This is evident for the central Saharan dust source region, where the combination of different characteristics contribute to the local variability: First, different surface cover classes are evident and the study area's surface is characterised by an inhomogeneous layout. Second, the predominant wind regime changes across the source region in meridional direction as the monsoon front enters the study area during wet season.

To examine the diverse characteristics of the central Saharan dust source region in more detail and to eventually contrast the first-order controls on the seasonal variability of observed dust source activity and consequent dust emission flux, four subdomains were defined (Fig. 1b). Thereby, each domain can be assigned to one water catchment and clusters similar dust source activation behaviours. The first is of particular of relevance as alluvial sediments formed by surface water runoff from the mountains are the dominant surface cover class acting as dust source.
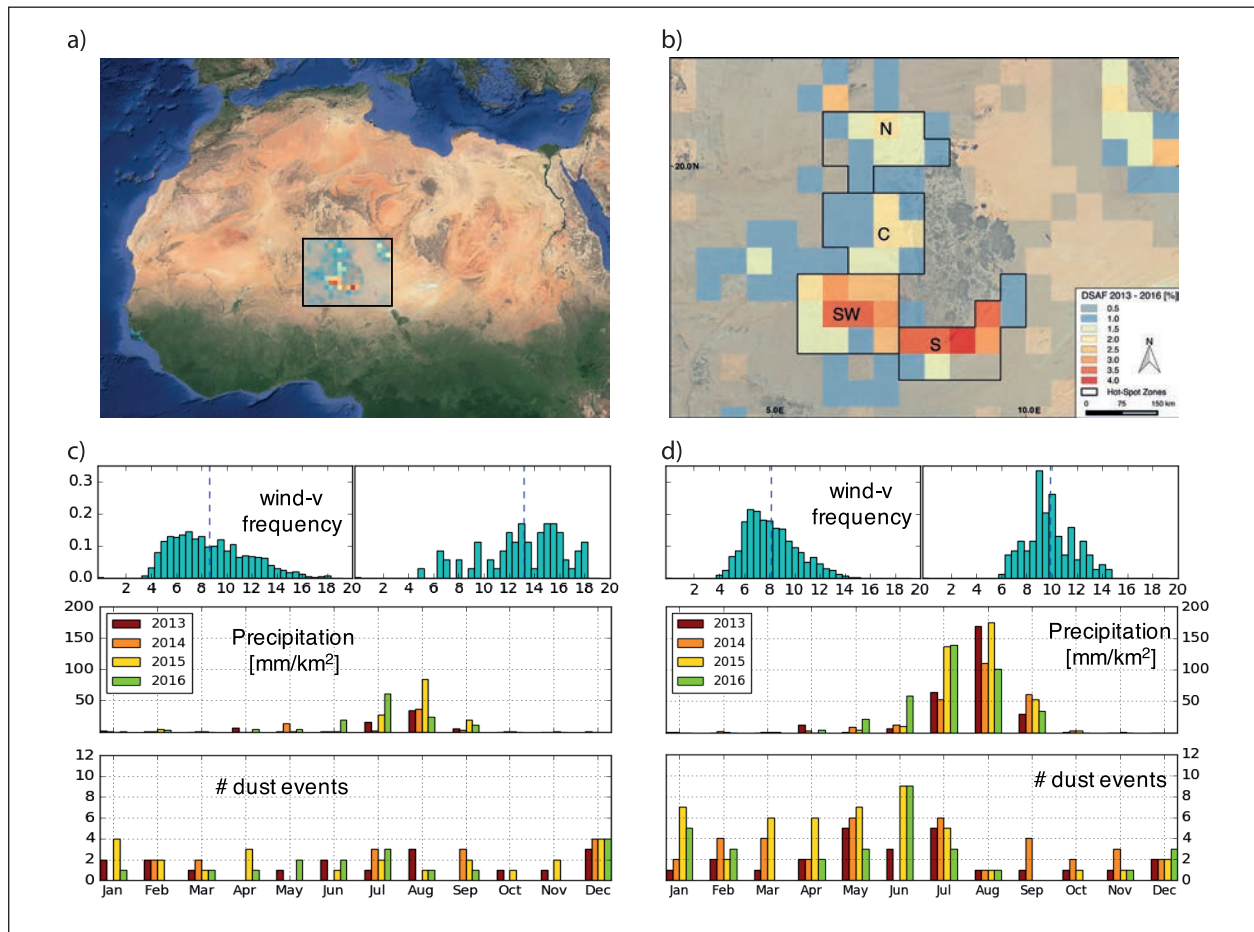
Fig. 1: (a) Overview on the study area. (b) Dust source activation frequency map (DSAF) for the study area covering the Aïr Massif for the four-year period 2013-2016. DSAFs are identified from MSG desert dust RGB images. (c) Panel summarizing the key meteorological controls wind and precipitation together with dust source activity shown as number of dust events for the northern 'N' domain as outlined in panel (b). (d) Same as for (c) but for the southwestern 'SW' domain.

Figures 1c and 1d summarizes the first-order controlling characteristics on the central Saharan dust source region. The northern subdomain (Fig. 1c) is less affected by precipitation and temporary vegetation cover, the seasonal variability in dust source activation is predominantly defined by the variability in the trade wind regime (Harmattan). The southwestern subdomain (Fig. 1d), in contrast to the northern subdomain, shows significant seasonality regarding precipitation and vegetation cover with enhanced vegetation cover during and after the monsoon season. The seasonal variability in dust source activation is predominantly related to the onset and duration of the monsoon season as rainfall and growing vegetation suppresses dust mobilisation. Comparing both subdomains, the following can be concluded: In the northern zone, dust emission is mainly wind driven, whereby sufficiently strong winds are associated with the Harmattan. Rock and bare sediments cover the surface in most parts of the subdomain suggesting that suitable sediments have been eroded by strong winds in the past. Due to low precipitation fluxes, the sources are only little recharged. In the southwestern zone, precipitation and consequent surface water runoff during the monsoon season affect the sediment formation and thus sediment availability for wind erosion. Regularly, strong rain events occurring over the mountain regions and consequent torrential water runoff form fresh layers of alluvial sediments – waiting to be eroded by sufficiently high wind events once vegetation died off.

In a nutshell, main outcomes from this study illustrate the necessity of a holistic approach when investigating the variability of the atmospheric dust life-cycle, in particular dust emission fluxes which ultimately also directly impact on atmospheric dust concentrations and deposition fluxes.

Dust emission associated with wind fields modulated by pyro-convection

The classical concept of wind erosion describing the process of dust emission and finally the suspension of dust in the boundary layer can be sketched as following: Lose and dry soil particles of optimum size are lofted either directly via turbulent eddies pushing and pulling the dust grain into the air, or via saltation. Thereby, wind drag forces entrain dust particles into the air, but, however, as these particles are too heavy to remain aloft although experiencing buoyancy due to turbulence, these particles return to the ground quickly. Their trajectory of motion follows that of a ballistic projectile. Crashing down onto the ground, the saltating particle may splash into small fragments or break other particles due to an inelastic collision [Kok et al., 2012]. Due to the impact, these small brittle fragments spread out eventually being entrained into the air. Being smaller and thus lighter than the
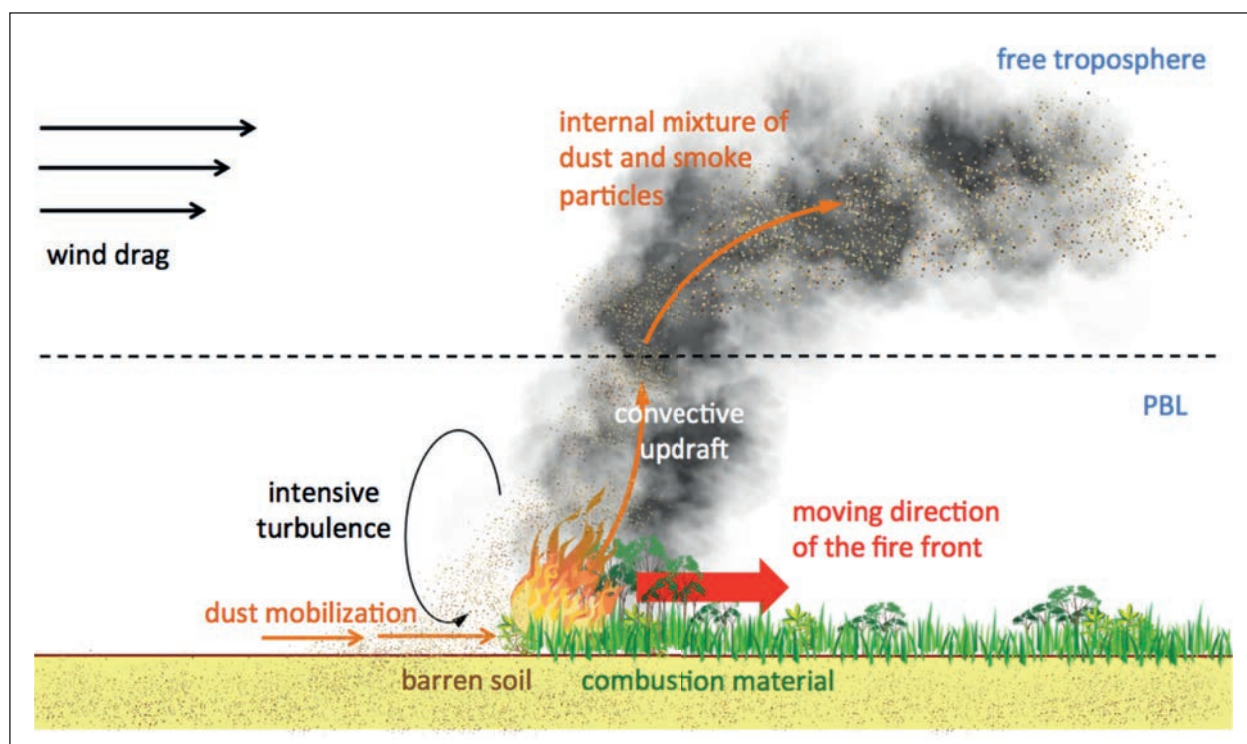
Fig. 2: Conceptual model of dust emission driven by pryo-convection. The figure is taken from Wagner et al. [2018].
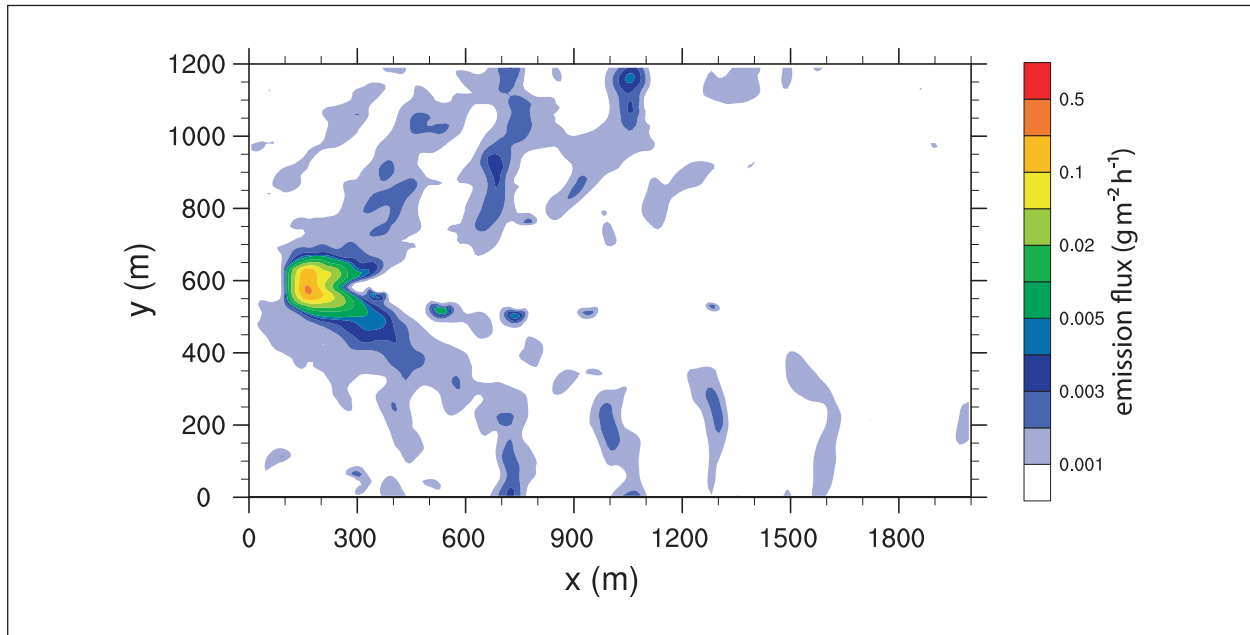
Fig. 3: Dust emission flux calculated using wind fields from LES simulations as described by Wagner et al. [2018].

saltating grains, the fragments may experience buoyancy due to turbulence and become mixed deep into the boundary layers.

However, there is more than one way to uplift and suspend dust particles into the atmosphere. Wildfires generate strong winds in both horizontal and vertical direction. Sufficiently strong to entrain dust particles although the ambient wind itself would be too low. Figure 2 illustrates the conceptual model on dust emission via pyro-convection as it is suggested by the literature so far [e.g., *Clements et al.*, 2008]. The main driver for dust entrainment, again, is the wind. However, in this case the wind is at least enhanced if not completely generated by the thermal updraft caused by the heat source of the fire. It may not be the most obvious natural wind generator, however, its contribution to dust emission and ultimately the global atmospheric dust burden is still un-quantified. Nevertheless, dust mixed into the atmosphere by pyro-convection shows a strong potential to easily being mixed into the free troposphere.

Although several measurement studies find dust particles in smoke plumes originating from wildfires [*Nisantzi et al.*, 2014; *Schlosser et al.*, 2017], the concurring occurrence of smoke and dust entrainment is not considered in state-of-the-art aerosol models. Towards developing a parameterisation considering dust emission in the vicinity of wildfires, we performed a first study based on Large Eddy Simulations (LES) using the model ASAM (All Scale Atmosphere Model, [*Jähn et al.*, 2015]). In such a simplified model framework, the impacts of a fire on the ambient wind field and the local dust emission potential can be explicitly analysed. We tested different fire intensities, sizes and shapes for various ambient wind conditions. By designing these test cases, we were inspired by natural and prescribed grassland and shrubland fires as they occur frequently in the Sahel zone.

In essence, results from this study illustrate that (1) wildfires impact on the ambient winds in such a way, that the near-surface wind speed probability density function (PDF) is shifted towards higher wind speeds regarding its maximum, but also the tail towards higher wind speeds is longer. This means that higher wind speeds occur more often and thus the dust emission potential is significantly increased. Also for cases for which the ambient wind speed per se would be too low to foster dust mobilisation. (2) The spatial impact on the ambient wind field is not limited to the burning area itself. A modulating effect, in particular the superposition of turbulence enhanced by the fire and the ambient wind flow, is evident also some kilometres downstream. There, the modulated winds may still be sufficiently strong to mobilise dust as illustrated in Fig. 3.

Although an idealized set up, this numerical experiment clearly supports the hypothesis on dust emission via pyro-convection as suggested from several measurement studies. It furthermore is a first step towards implementing a novel dust emission mechanism into state-of-the-art aerosol models in order to quantify the amount of dust emitted and to enable the research community to assess the relevance of internally mixed dust and soot for e.g. cloud and precipitation formation processes.

Shades of pinkness – dust optical properties strongly impact its representation in the MSG dust product

Satellite enthusiasts know the MSG (Meteosat Second Generation) SEVIRI (Spinning Enhanced Visible and Infra-Red Imager) instrument and its famous dust product highlighting the presence of dust in the atmosphere by pinkish colour shades. Available during day and night, one image every 15 minutes of the entire hemisphere centred at 0°E over the Equator, MSG SEVIRI's dust product is used by both forecasters and scientists longing for information on the presence of dust over bright desert surfaces such as the northern and southern African deserts, Arabia and the Middle East.

Although heavily used for identifying dust sources [*Schepanski et al.*, 2017, 2012; *Ashpole and Washington*, 2012; *Vickery et al.*, 2013] and dust plumes, the information gained remained at a qualitative level due to the complexity of the different shades of pinkness [*Brindley et al.*, 2012]. Nevertheless, quantitative retrievals of dust aerosol optical thickness are possible during daytime involving radiation transfer modelling and making use of additional meteorological input data [*Brindley and Russell*, 2009; *Banks et al.*, 2013].

By combining atmosphere - dust modelling using the model system COSMO-MUSCAT (COSMO: COnsortium for Small-scale MOdelling; MUSCAT: MUltiScale Chemistry Aerosol Transport Model) and radiation transfer modelling using the Radiative Transfer for TOVS (RTTOV) program, synergetic satellite scenes as would be seen by the IR channels of MSG-SEVIRI if the COSMO-MUSCAT simulated dust distribution represents the reality, are calculated. These artificial satellite images retrieved by presuming the real world is a model simulation and the satellite flying above the Earth is RTTOV, provide a unique environment for systematically examining the uncertainties in the information gained from these satellite observations. For our study, we calculated synergetic images for the 6-month period June – July 2011, 2012, and 2013 and examined them regarding the impacts on the colour shading in the original RGB (red-green-blue) rendering leaving airborne dust in a pinkish colour shading.

As outlined by *Brindley et al.* [2012], different shades of pinkness result predominantly from variability in atmospheric humidity, optical properties of
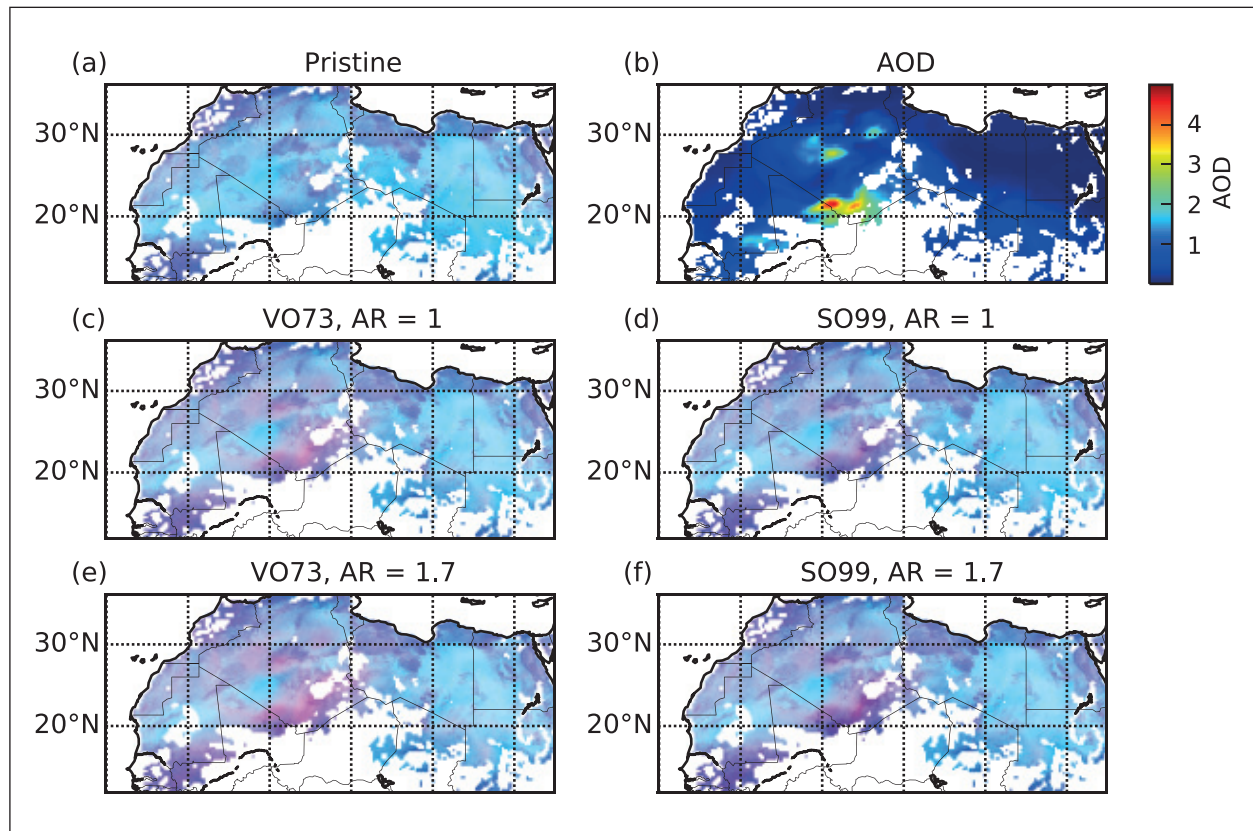

Fig. 4: Desert dust RGB images simulated from COSMO-MUSCAT dust concentrations for 25 June 2013, 12 UTC. (a) Pristine sky. (b) Dust AOD at 550 nm. (c, e) Using VO73 dust for AR of 1 (spheroid) and AR 1.7 (spheroidal). (d, f) Using SO99 dust for AR of 1 and 1.7. Figure taken from Banks et al. [2018].

dust particles, and surface emissivity. All are of relevance and demand to be investigated closely, which we aim for. In the following, the influence of dust optical properties, in particular refractive index and particle shape, on the shades of pinkness in simulated MSG-SEVIRI dust images will be discussed in a proof-of-concept design.

Dust concentrations simulated by COSMO-MUSCAT were used as input for RTTOV in order to simulate MSG SEVIRI dust images, and thus the dust size distribution follows the five size bins resolved by COSMO-MUSCAT. Regarding the optical properties, in particular the refractive index, two sets of data published by *Volz* [1973] (hereafter: VO73) and *Sokolik & Toon* [1999] (hereafter: SO99) were considered. As dust particles are not spheres, spheroidal particles with different aspect ratios (AR) were studied, however, here we present for an AR of 1.7 as found be previous field studies [e.g., *Kandler et al.*, 2009] in comparison to an AR value of 1, which represents a spherical particle. In the further course of the study, the shades of pinkness obtained from RTTOV simulations using the VO73 or SO99 in order to describe the optical properties (i.e. refractive indices and AR) of mineral dust were compared against the observed shades of pinkness with respect to atmospheric dust loading, surface emissivity, and dust layer height and depth. A throughout assessment on different influences on the pink colour was performed examining the individual contribution of the red, green and blue colour beam to the final colour shade.

The pinkness in all its shades representing airborne dust is due to a composite of three colour beams: red (R), green (G), and blue (B). Each colour beam spans a range of values from 0 to 255, the combination of all RGB values results in a colour out of the rainbow colour palette. Focussing on pink as this colour represents dust in the chosen set of wavelength bands (given by the design of the MSG SEVIRI IR dust index), various shades of pinkness result from varying configurations of R, G, and B values. Brightness temperature differences (BTD) are assigned to the individual RGB beam and as the BTD depends on the refractive index of the dust particle, size distribution, and concentration, different shades of pinkness result for changes in at least one of the parameters. Figure 4 summarises the sensitivity of the pink colour indicating airborne dust against the two set of refractive indices applied, VO73 and SO99, and further sketches the expected impact of an aspect ratio AR of 1.7 accounting for the shape of the spheroidal particles as introduced above. Compared to the colour shades given by the satellite product, COSMO-MUSCAT-RTTOV simulations represent these colours the best for the VO73 data set and spheroidal particles.

In summary, the above sketched impact of dust optical properties on the appearance of airborne mineral dust in the colour related index product is highly dependent on the dust properties. Given that dust sources are never identical but at best similar, meteorological conditions and surface emissivity together with the diversity of dust characteristics have a strong influence on the final product – the colour appearing in the satellite product telling the observer whether there is dust or not and implicitly making a suggestion on the quantity. The bottom line is that similar size distributions and concentrations but different sources can make a big difference to the colour of the imagery.

Summary

Dust matters. And knowing about its origin, about how it is getting into the atmosphere, where it appears, and what its properties matters, too. This article aimed for highlighting selected and exciting aspects contributing to the research on mineral dust. The spotlights addressed can be summarised as: (1) Different dust source types show varying emission activities and require sophisticated representation in dust production models. (2) Dust emission processes are diverse and sometimes unexpected. Pyro-convection enhances the ambient winds fostering dust entrainment opening up a new field of feedbacks and impacts. (3) Detailed knowledge of dust optical properties, in particular the refractive index, particle size and shape, are essential for quantifying retrievals of atmospheric dust loading from satellites.

In a nutshell, dust comprises tiny particles suspended in the atmosphere but with far-reaching impact on the Earth system. Research on dust including all related processes, controls and feedbacks is vital in order to assess the Earth system today, in the past and in future.

Acknowledgement

References

Ashpole, I., and R. Washington (2012), An automated dust detection using SEVIRI: A multi-year climatology of summertime dustiness in the central and western Sahara, *J. Geophys. Res.*, 117, doi:10.1029/2011JD016845.

Banks, J. R., and H. E. Brindley (2013), Evaluation of MSG-SEVIRI mineral dust retrieval products over North Africa and the Middle East, *Remote Sens. Environ.*, 128, 58-73, doi:10.1016/j.rse.2012.07.017.

Banks, J. R., K. Schepanski, B. Heinold, A. Hünerbein, and H. E. Brindley (2018), The influence of dust optical properties on the colour of simulated MSG-SEVIRI Desert Dust imagery, *Atmos. Chem. Phys.*, submitted.

Brindley, H.E., P. Knippertz, C. Ryder, and I. Ashpole (2012), A critical evaluation of the ability of the Spinning Enhanced Visible and InfraRed Imager (SEVIRI) thermal infrared red-green-blue rendering to identify dust events: Theoretical analysis, *J. Geophys. Res.*, 117, doi:10.1029/2011JD017326.

Brindley, H. E., and J. E. Russell (2009), An assessment of Saharan dust loading and the corresponding cloud-free longwave direct radiative effect from geostationary satellite observations, *J. Geophys. Res.*, 114, doi:10.1029/2008JD011635.

Carslaw, K. S., O. Boucher, D. V. Spracklen, G. W. Mann, J. G. L. Rae, S. Woodward, and M. Kulmala (2010), A review of natural aerosol interactions and feedbacks with the Earth system, *Atmos. Chem. Phys.*, 10, 1701-1737, doi:10.5194/acp-10-1701-2010.

Clements, C. B., S. Zhong, Y. Bian, W. E. Heilman, D. W. Byun (2008), First observations of turbulence generated by grass fires, *J. Geophys. Res.*, 113,D22102, doi:10.1029/2008JD010014

Jähn, M., O. Knoth, M. König, and U. Vogelsberg (2015), ASAM v2.7: A compressible atmospheric model with a Cartesian cut cell approach, *Geosci. Model Dev.*, 8, 317-340, doi:10.5194/gmd-8-317-2015.

Kandler, K., L. Schütz, C. Deutscher, M. Ebert, H. Hofmann, S. Jäckel, R. Jaenicke, P. Knippertz, K. Lieke, A. Massling, A. Petzold, A. Schladitz, B. Weinzierl, A. Wiedensohler, S. Zorn, and S. Weinbruch (2009), Size distribution, mass concentration, chemical and mineralogical composition and derived optical parameters of the boundary layer aerosol at Tinfou, Morocco, during SAMUM 2006, *Tellus B*, 61, 32-50, doi:10.1111/j.1600-0889.2008.00385.x.

Kok, J. F., E. J. R. Parteli, T. I. Michaels, and D. Bou Karam (2012), The physics of wind-blown sand and dust, Rep. on Prog. in Phys., 75, 106901.

Korte, L. F., G.-J. A. Brummer, M. van der Does, C. V. Guerreiro, R. Hennekam, J. A. van Hateren, D. Jong, C. I. Munday, S. Schouten, and J.-B. W. Stuut (2017), Downward particle fluxes of biogenic matter and Saharan dust across the equatorial North Atlantic, Atmos. Chem. Phys., 17, 6023-6040, doi:10.5194/acp-17-6023-2017.

Nisantzi, A., R. E. Mamouri, A. Ansmann, and D. Hadjimitsis (2014), Injection of mineral dust into the free troposphere during fire events observed with polarization lidar at Limassol, Cyprus, *Atmos. Chem. Phys.*, 14, 12155-12165, doi:10.5194/acp-14-12155-2014.

Reheis, M. C., and R. Kihl (1995), Dust deposition in southern Nevada and California, 184-1989: Relations to climate, source area, and source lithology, J. Geophys. Res., 100(D5), 8893-8918, 1995.

Schepanski, K., I. Tegen, B. Laurent, B. Heinold, and A. Macke (2007), A new Saharan dust source activation frequency map derived from MSG-SEVIRI IR-channels, *Geophys. Res. Letts.*, 34, L18803, doi:10.1029/2007GL030168.

Schepanski, K., I. Tegen, and A. Macke (2012), Comparison of satellite based observations of Saharan dust source areas, *Remote Sens. Environ.*, 123, 90-97, doi:10.1016/j.rse.2012.03.019.

Schepanski, K., M. Mallet, B. Heinold, and M. Ulrich (2016), North African dust transport toward the western Mediterranean basin: atmospheric controls on dust source activation and transport pathways during June-July 2013, *Atmos. Chem. Phys.*, 16, 14147-14168, doi:10.5194/acp-16-14147-2016.

Schepanski, K., B. Heinold, and I. Tegen (2017), Harmattan, Saharan heat low, and West African monsoon circulation: modulations on the Saharan dust outflow towards the North Atlantic, *Atmos. Chem. Phys.*, 17, 10223-10243, doi:10.5194/acp-17-10223-2017.

Schlosser, J. S., R. A. Braun, T. Bradley, H. Dadashazar, A. B. MacDonald, A. A. Aldhaif, M. A. Aghdam, A. H. Mardi, X. Peng, and A. Sorooshian (2017), Analysis of aerosol composition data for western United States wildfires between 2005 and 2015: Dust emission, chloride depletion, and most enhanced aerosol constituents, *J. Geophys. Res.*, 122, 8951-8966, 2017.

Sokolik, I. N., and O. B. Toon (1999), Incorporation of mineral composition into models of the radiative properties of mineral aerosol from UV to IR wavelengths, *J. Geophys. Res.*, 104, 9423-9444, doi:10.1029/1998JD200048.

Vickery, K. J., F. D. Eckardt, and R. G. Bryant (2013), A sub-basin scale dust plume source frequency inventory for southern Africa, 2005-2008, Geophys. Res. Lett., 40, 1-6, doi:10.1002/grl50968.

Volz, F. E. (1973), Infrared Optical Constants of Ammonium Sulfate, Sahara Dust, Volcanic Pumice, and Flyash, *Appl. Optics*, 12, 564-568, doi:10.1364/AO.12.000564

Wagner, R., K. Schepanski, B. Heinold, and I. Tegen (2016), Interannual variability in the Saharan dust source activation – Toward understanding the differences between 2007 and 2008, *J. Geophys. Res.*, 121, 4538-4562, doi:10.1002/2015JD024302.

Wagner, R., M. Jähn, and K. Schepanski (2018), Wildfires as a source of airborne mineral dust – Revisiting a conceptual model using Large-Eddy simulations (LES), *Atmos. Chem. Phys.*, submitted.

Study of cloud condensation nuclei and ice nucleating particles in the Southern Ocean during the Antarctic Circumnavigation Expedition (ACE)

Silvia Henning[1], André Welti[1], Markus Hartmann[1], Mareike Löffler[1], Andrea Baccarini[2], Martin Gysel[2],
Danny Rosenfeld[3], Heini Wernli[4], Ken Carslaw[5], Julia Schmale[2], Frank Stratmann[1]

[1] Leibniz Institute for Tropospheric Research (TROPOS), Leipzig, Germany
[2] Paul Scherrer Institute (PSI), Villigen, Switzerland
[3] Hebrew University of Jerusalem, Jerusalem, Israel
[4] ETH Zurich, Zurich, Switzerland
[5] University of Leeds, Leeds, United Kingdom

Der Südliche Ozean (SO) ist die anthropogen am geringsten beeinflusste Region der Erde [*Hamilton et al.*, 2014], jedoch in Bezug auf Aerosolpartikel, als wichtiger und klimarelevanter Bestandteil der Atmosphäre, nur sehr wenig bis gar nicht untersucht. Als Partner des Projekts „Study of Preindustrial-like-Aerosol Climate Effects" (SPACE) nahmen wir von Dezember 2016 bis März 2017 am bisher beispiellosen Antarctic Circumnavigation Expedition (ACE) teil. ACE-SPACE, als Teilprojekt von ACE, bot uns die einmalige Gelegenheit, Aerosolmessungen von hoher Qualität im SO durchzuführen. ACE-SPACE allgemein zielt auf eine detaillierte Charakterisierung des von anthropogener Verschmutzung unbeeinflussten Aerosols ab, welches mit dem in der vorindustriellen Atmosphäre vergleichbar ist. Der Fokus des TROPOS im Rahmen von ACE-SPACE liegt auf jenen Aerosolpartikeln, die an Aerosol-Wolken-Wechselwirkungen beteiligt sind, insbesondere solchen, die als Wolkenkondensationskerne (CCN) oder eisnukleierende Partikel (INP) fungieren können. Wir untersuchen die örtlichen Veränderungen der CCN- und INP-Konzentration in der Umgebung des antarktischen Kontinents, die CCN-Hygroskopizität und die Gefriereigenschaften von INPs. Mit Hilfe von Rückwärtstrajektorien werden mögliche CCN- und INP-Quellen identifiziert. Die bereitgestellten INP- und CCN-Daten repräsentieren einen extrem wertvollen Datensatz, der maßgeblich zur Verbesserung der Qualität zukünftiger Klimamodelle und von Produkten der Satellitenfernerkundung beitragen wird.

Introduction

It is a great challenge to assign exact numbers to the human influence on climate change. While we know the effect of carbon dioxide emissions quite well, there are anthropogenic emissions of other substances that effect climate through complex chains of interactions with atmospheric processes, that are not yet well characterized [*IPCC*, 2013]. This lack of knowledge causes uncertainties in the quantification of how human activities influence weather and climate [*Carslaw et al.*, 2013].

To isolate the anthropogenic contribution, we need to characterize the atmosphere as it was before industrialization - before large emissions of gases and particles to the air began. The effects of gases and particles in the pre-industrial atmosphere need to be "subtracted" from what we observe today. The region that qualifies best to observe pristine, pre-industrial like conditions is the Southern Ocean (SO) as discussed in the paper by *Hamilton et al.* [2014].

Natural sources of atmospheric aerosol particles are e.g. volcanic eruptions, desert dust, wild fires and sea spay, or of biological origin like pollen or dimethyl sulfide (DMS) e.g. *Andreae and Raemdonck* [1983] and *Pruppacher and Klett* [1997]. Volcanic eruptions or dust storms can dramatically change the particle concentration in the atmosphere, but also far away

from such sources, in so called pristine areas, number concentrations can vary over a wide range depending on location and season [*Asmi et al.*, 2013].

The influence of atmospheric aerosol particles on the microphysical properties of clouds is complex and depends on the particle number size distribution and on their optical and chemical properties [*Heintzenberg and Charlson*, 2009]. Particles serving as cloud condensation nuclei (CCN, [*Köhler*, 1936]), affect properties such as cloud albedo [*Twomey*, 1974] and cloud life-time [*Rosenfeld et al.*, 2014]. At which supersaturation an aerosol particles may act as CCN is dictated by its size and chemical composition [*Dusek et al.*, 2006].

Aerosol particles also affect the glaciation of clouds by initiating droplet freezing at temperatures warmer than the homogenous freezing temperature of minus 38°C [*Pruppacher and Klett*, 1997]. These particles are called ice nucleating particles (INPs). INPs influence both, the microphysical and radiative properties of clouds, and thereby play a significant role in the formation of precipitation and cloud influences on climate [*Hoose and Mohler*, 2012; *Murray et al.*, 2012]. Properties and nature of INPs is a hot topic in current lab and field studies [*Augustin-Bauditz et al.*, 2014; *DeMott et al.*, 2016].

CCN over the SO: Our knowledge of aerosol and aerosol-cloud interaction in the SO is based on only few observations. In the 1990 two intensive field campaigns took place in the area: the Southern Ocean Cloud Experiment (SOCEX, 40° to 43° S, 143° to 145°E), an aircraft campaign divided into a summer and a winter flight phase [*Boers et al.*, 1998] and the first Aerosol Characterization Experiment (ACE-1, 40° to 55° S, 135° to 160° E, [*Bates et al.*, 1998a]).

The focus of SOCEX was cloud microphysical properties and their seasonality. They found a strong effect of season on the cloud droplet concentration, with summer concentration being three times higher than winter concentration [*Boers et al.*, 1996; *Boers and Krummel*, 1998]. The air masses were presumably not influenced by anthropogenic emissions and a natural aerosol source was suspected to cause the observed difference. But as no comprehensive aerosol equipment was available at that time, this hypothesis could not be strengthened by, e.g., the observation of new particle formation in the marine boundary layer during summer.

ACE-1 took place in the austral summer (mid November to mid December 1995) and was aiming for quantification of the chemical and physical processes controlling the evolution and properties of the atmospheric aerosol relevant to radiative forcing and climate. During this intensive field campaign aerosol, cloud and radiation measurements were conducted

at two ground stations, but also ship-based measurements on two research vessels and on a research aircraft were conducted [*Bates et al.*, 1998a; *Bates et al.*, 1998b]. During ACE-1 several sources of aerosol were identified and investigated in this remote marine region. It was found that biogenically produced dimethyl sulfide (DMS) is a major source of marine sulfate aerosol [*Bates et al.*, 1998a] and that sea-spray aerosol formed in dependence of wind strength [*Bates et al.*, 1998b], but also subsidence of free-tropospheric aerosol into the marine boundary layer was found, and the possibility of homogenous particle formation in the vicinity of clouds was discussed [*Clarke et al.*, 1998; *Weber et al.*, 1998]. Still to date the role of DMS in new particle formation is highly controversial [*Quinn and Bates*, 2011].

A more recent campaign (2009 - 2011), the HIAPER Pole-to-Pole Observations (HIPPO) program [*Wofsy et al.*, 2011] also delivered aerosol and cloud data over the SO as far south as 67°S. However, their focus was on the whole Pacific Ocean and not specifically on the SO.

Ground-based aerosol and CCN measurements close to the SO region are available. On the mainland of Antarctica e.g. from Neumayer and South Pole station [*Asmi et al.*, 2013], during austral summer at Princess Elisabeth Antarctica Research Station and at Palmer station [*Defelice et al.*, 1997], and also from Tasmania. However, measurements on the Antarctic continent do not necessarily reflect the conditions over the SO, and aerosol sources and their evolution in the atmosphere can differ significantly. While Antarctic aerosol has been observed to have strong stratospheric and upper tropospheric source components [*Fiebig et al.*, 2014] a source apportionment study in the SO shows that local biogenic and aged marine particles without upper atmospheric influence are the main sources [*Schmale et al.*, 2013]. However, despite the few aircraft and ship campaigns, the SO region itself remains largely unsampled. No mission has yet attempted to capture comprehensive aerosol properties around the Antarctic continent. Most missions have so far focused on particular sectors of the SO. The importance of further investigations of the SO region, with respect to natural particle sources, and aerosol-cloud-interactions, for our deeper process understanding, has also been pointed out in the SOCRATES White paper by [*Marchand et al.*, 2014]. The strong seasonality in the aerosol and CCN number [*Asmi et al.*, 2013; *Ayers and Gras*, 1991; *Boers and Krummel*, 1998; *Gras*, 1995] leads the authors to the hypothesis, that there are different sources active during different seasons. Biogenically-derived aerosol is supposedly the major CCN source in summer time, whereas in winter time sea-spray

aerosol is the main source. These questions, however, have not been systematically addressed yet. Somewhat similar sources are suggested for INPs, however the respective information is extremely scarce.

INP over the SO: Satellite observations with MODIS [*Huang et al.*, 2012; *Morrison et al.*, 2011] and measurements during HIPPO [*Chubb et al.*, 2016] document a frequent occurrence of super-cooled water droplets over the SO. Also, ground-based Lidar observations [*Kanitz et al.*, 2011] reflect lower cloud glaciation temperatures in the southern hemisphere, which might be due to the lack of INP in the remote marine environment. Knowledge of the cloud phase is essential for the correct representation of the cloud-radiative properties in climate models. Satellite retrieval show that currently models consist-ently underestimate the outgoing short-wave radiation in the oceanic regions of the southern hemisphere [*Trenberth and Fasullo*, 2010].

In absence of the dominant INP sources of the northern latitudes, such as dust and aerosol of anthropogenic origin, aerosol particles of a different nature have to be the important INP over the Southern Ocean. Available INP concentration meas-urements in the SO region date back to the 1970's [e.g. *Bigg*, 1973]. They found that the number concen-tration is very low compared to continental regions

[*Pruppacher and Klett*, 1997], but nearly nothing is known on the nature of the ice nucleating particles (and thereby sources), their number concentration and spatial variation over the SO.

DeMott et al. [2016] stresses the importance of marine INP being emitted from the ocean together with sea spray aerosol (SSA) ejection, based on la-boratory measurements. They observed an increase in INP concentration associated with phytoplankton blooms. Even low concentrations of biological INP from biological productive oceans could influence cloud properties as other INP (mineral dust or secondary aerosol) are not able to initiate freezing at as high temperatures as some bio-aerosol do. However, weather SO waters provide ice active bio-aerosol has not yet been investigated.

In summary, information concerning both CCN and INP abundance, their chemical and physical properties, and their sources in the SO region is rare, but urgently needed to better understand and quantify climate change and the importance of aero-sol-cloud-interactions therein.

Antarctic Circumnavigation Expedition

Scientific focus. The interdisciplinary approach of ACE-SPACE connecting on board in-situ and remote sensing measurements, satellite observations
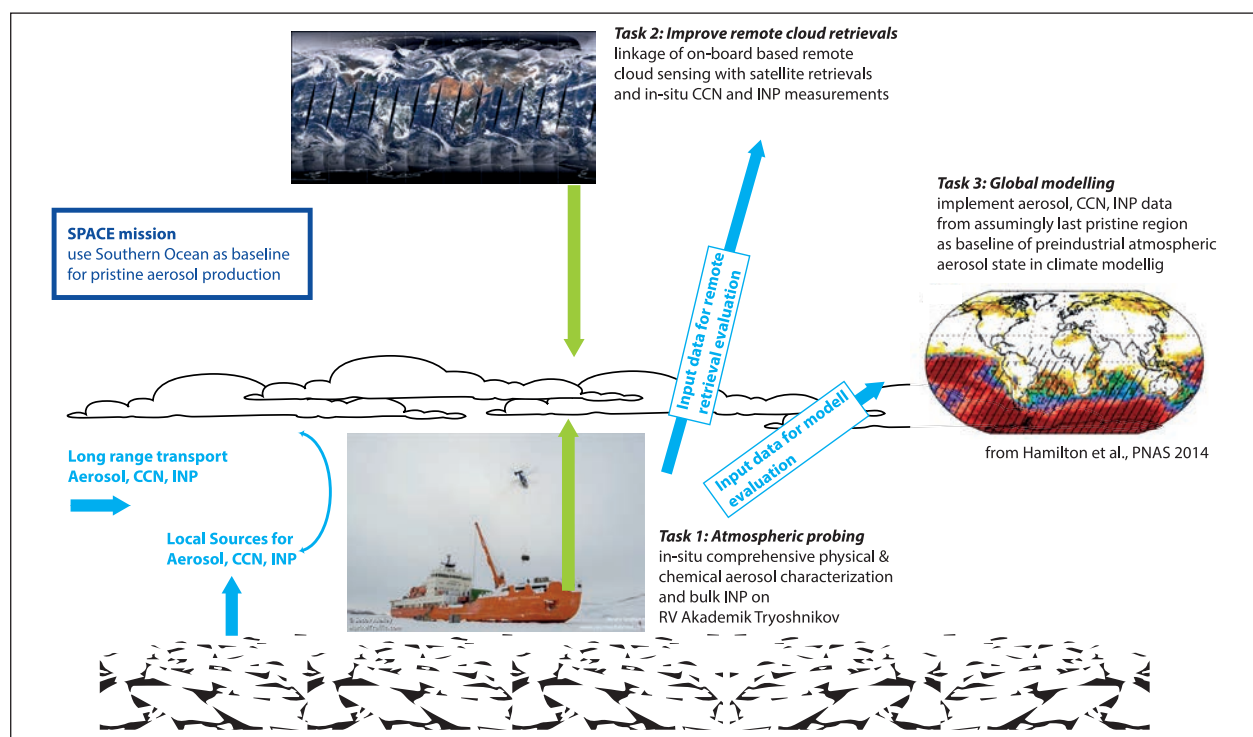
Fig. 1: Overview on the ACE-SPACE project. Cooperation partners in this project are the Paul Scherrer Institute (CH) with Julia Schmale as PI, the University of Leeds, Leeds (UK), The Hebrew University of Jerusalem, Jerusalem (Israel), University of Cranfield, (UK), Federal Institute of Technology Zurich, (CH).
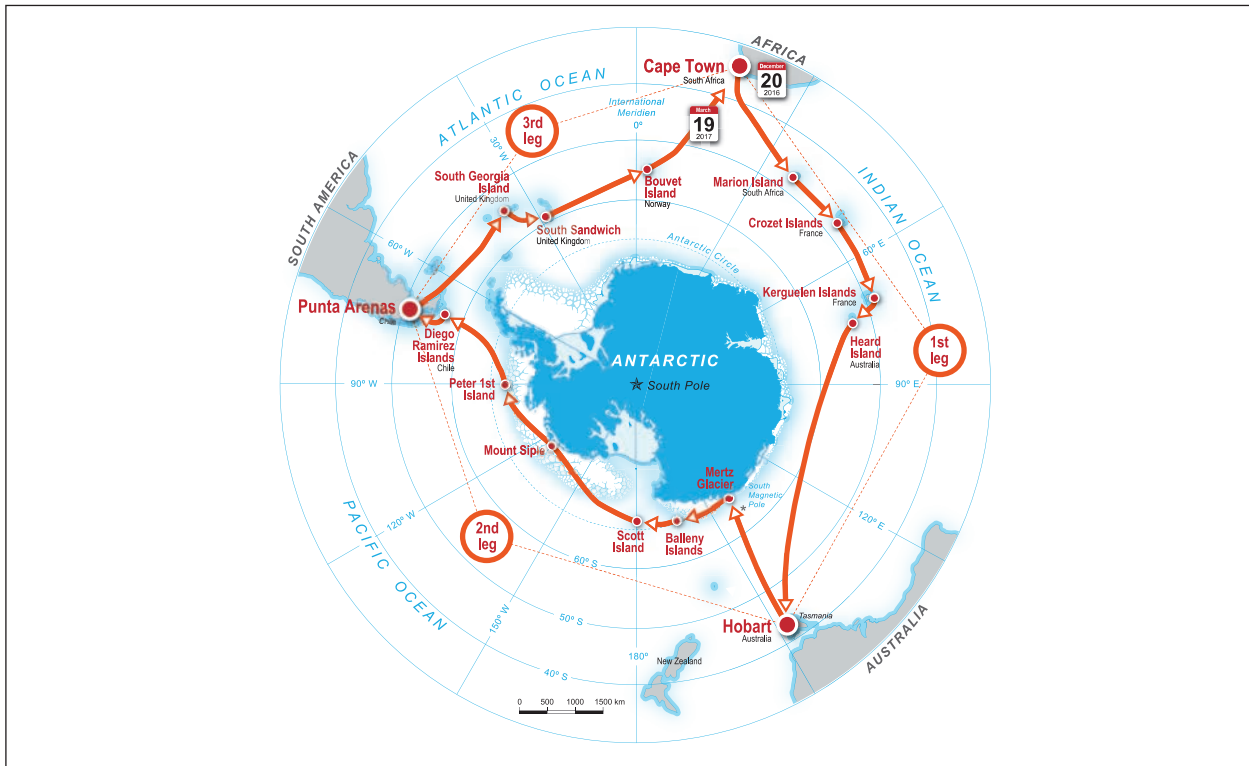
Fig. 2: Overview of the 3 month lasting ACE cruise leading from Cape Town via Hobart and Punta Arenas back to Cape Town (map by courtesy of Swiss Polar Institute).

and global climate modeling, promises to exceed the knowledge gain of in-situ observations alone (cf. Fig. 1). The performed measurements provide the first comprehensive data sets concerning circum-Antarctic aerosol properties. Together with on board remote sensing, satellite retrievals and modeling studies, the collected data will significantly improve the definition of preindustrial aerosol baseline conditions. Better defined preindustrial aerosol baseline conditions make possible a more accurate quantification of anthropogenic climate effects, and thereby improve the quality of future climate predictions.

ACE cruise. The ACE expedition took place in the Austral summer months from December 2016 to March 2017. On the first leg the RV "Akademik Tryoshnikov" outbound from Cape Town December 20th, 2016, passed the Subantarctic Island groups of Marion, Crozet, Kerguelen and Heard and hereby the polar front. The expedition reached Hobart on January 19th, 2017. With 67°S, the cruise reached the highest latitudes during the second leg and several times the vessel passed through the drift ice zone close to the Antarctic continent. Punta Arenas was reached in the end February 22th, 2017. The final leg back to Cape Town, which was reached March 19th, 2017, passed the Islands of South Georgia, South Sandwich and Bouvet.

Measurement setup. As partner of ACE-SPACE, TROPOS focused on the measurement of cloud condensation nuclei (CCN), as well as particles able to nucleate ice (INP). A CCN counter was situated in the aerosol measurement container of the PSI (Fig. 3, red container in picture on the left), which was positioned in the front of the upper deck. The CCN-100 instrument (DMT, Boulder, USA) was continuously operated during all 3 legs at 5 supersaturations (0.15%, 0.2%, 0.3%, 0.5%, 1%). It was connected to a common aerosol inlet and operated side by side with other aerosol characterization equipment measuring e.g. total particle concentration and aerosol particles size distribution.

Filter sampling for the off-line INP analysis was done by means of two DIGITEL instruments (Riemer Messtechnik, Germany) with automatic filter exchange. Both instruments were placed on the observation deck and fixed to the railing (Fig. 3 right picture). The high-volume instrument DHA-80 was operated with a 24h sampling interval and 150mm quartz fiber filters as filter material with a PM10 inlet. The low volume instrument DPA-14 was run on an 8h sampling interval and the filter material was polycarbonate (Nuclepore) with 200nm pore size. The sampled filters were collected regularly from the instruments storage and stored at minus 20°C onboard of the vessel. The high-volume filters will be

Fig. 3: All online aerosol measurements were operated side by side in a container placed on the upper deck (red container in the left picture). The aerosol inlet can be seen on the right hand side on top of the red container. The DIGITEL filter units DHA-80 and DPA-14 were fixed to the railing on the observation deck (right picture).

shared between, chemical analysis and INP analysis, the low volume filters are used for INP analysis only.

Cloud Condensation Nuclei

Continuous CCN measurements were conducted during the whole ACE cruise. Periods of contamination from ship exhaust are erased from the data-set by applying a filtermask. The filtermask is compiled based on extreme values of total particle number concentration, black carbon and carbon dioxide indicating exhaust periods.

Figure 4 shows an overview of CCN numbers at all supersaturation increasing from 0.15% to 1% (colour code indicating supersaturation is included in the figure). Often the CCN concentration reflects the total particle number with only some exceptions. Typical concentrations are between 5 cm^{-3} to
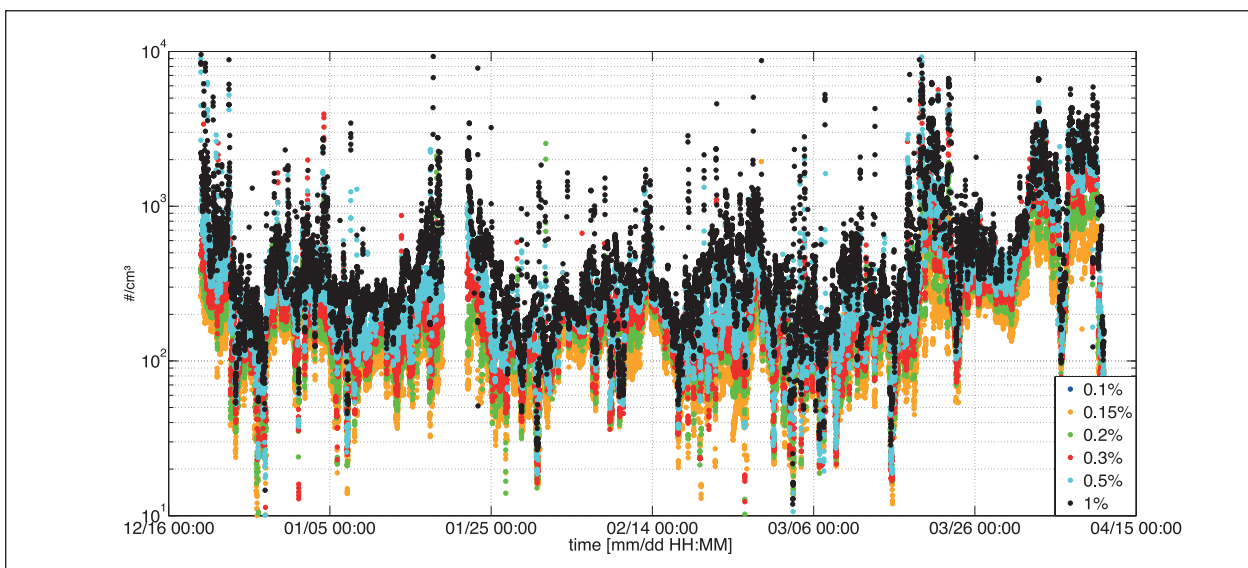
Fig. 4: Overview of the CCN number concentration over the whole cruise. Different colored dots give the CCN number concentration for increasing supersaturation between 0.15% and 1%.
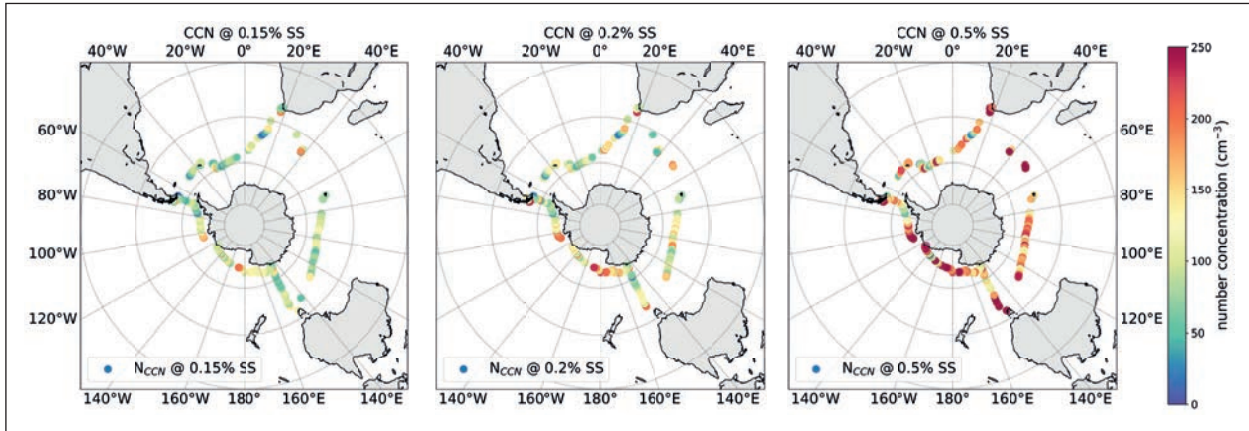
Fig. 5: CCN number concentration along the track of the RV "Akademic Tryoshnikov" at 0.15%, 0.2% and 0.5% supersaturation, from left to right. The gaps in the data are due to filtering the data for stack influences. 30% of the data points remained for the currently applied preliminary data filter.

Tab. 1: Preliminary median values for the entire cruise of CCN number concentration, total particle number concentration (CN), critical particle daiamter as derived from the for all 5 supersaturations.

SS (%)	CCN (cm⁻³)	CN (cm⁻³)	Dcrit (nm)	κ
0.15	106	323	104.25	0.57
0.20	136	326	79.15	0.73
0.30	156	324	61.39	0.69
0.50	193	331	45.69	0.60
1.00	252	349	30.79	0.48

1300 cm⁻³. For 0.2% in supersaturation 15 to 260 cm⁻³ CCN were observed. This is generally higher than suggested by the GLOMAP model [*Pringle et al.*, 2009], where concentrations between 0 and 25 cm⁻³ are predicted for the entire SO.

Along the 3-month lasting cruise track, we observed several periods of special interest, such as several days with high number concentrations of small particles, a cold air outbreak, and air masses originating from the outflow of a volcano plume. Figure 5 shows the CCN concentrations for 0.15, 0.2 and 0.5% supersaturation along the ship track. The CCN number is surprisingly constant over the whole cruise, with an overall mean value at 0.2% of 110 cm⁻³. However, extreme values were found close to the Antarctic continent. At Mertz Glacier, very low CCN concentrations (around 15 cm⁻³, January 30, 2017) were observed, but also the highest pristine concentrations (up to 260 cm⁻³, February 6, 2017) were measured close to this region. Possible factors (e.g., air mass origin) influencing CCN concentration

and hygroscopicity will be investigated during the course of the project with help of back-trajectories and compared to predictions of current models, e.g. GLOMAP.

Hygroscopicity. By integrating the particle size distributions, from the largest particle diameter down to the size where the sum reaches the number of measured CCN, the minimal activated or critical particle diameter can be determined. Using the formalism given in *Petters and Kreidenweis* [2007] the hygroscopicity parameter κ (Tab. 1) can be calculated from the critical particle diameter. The hygroscopicity parameter indicates the average chemical composition of activated CCN as a function of supersaturation. Averaged over all SS we get a value for κ of 0.61, this is lower than the model based value for the SO of about 0.8 to 1 given by *Pringle et al.* [2010], but similar to other measurements in the region of coastal Antarctica and the Weddel sea, reporting a similar median κ over all SS of 0.66 [*O'Shea et al.*, 2017].

Ice Nucleating Particles

The meteorological most important INP are those that form ice crystals at relatively low supercooling. It is they who initiate the glaciation of supercooled, liquid- to mixed-phase clouds. Besides the temperature where INP convert cloud droplets into ice crystals, their abundance determines the overall effect on a cloud, i.e., changes in cloud optical properties or the formation of precipitation and cloud dissipation. Modelling studies suggest that INP concentrations as low as 0.01 L⁻¹ are sufficient to have an effect, if at the same time CCN concentrations are optimal to favour secondary ice formation [*Sullivan et al.*, 2017].

On the continent, main sources of INP are soil and desert dusts, industrial emissions, biomass
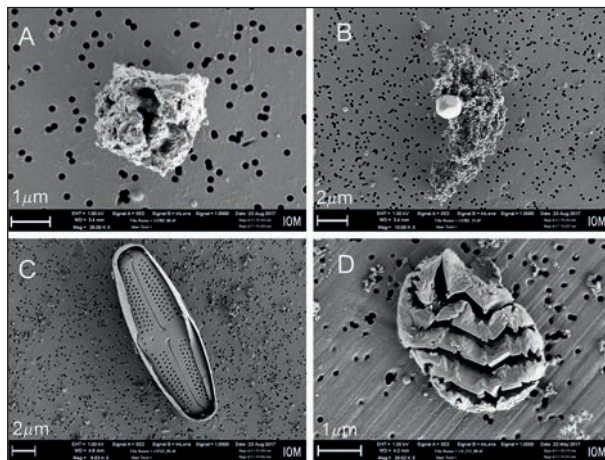
Fig. 6: SEM images of particles found in the marine ambient air along the ACE track. (A) Sea salt with organic material, (B) aggregate of micro colloids, (C) and (D) fragments of organisms.

Some can be be identified as fragments of diatoms (Fig. 6 C), mineral dust, salt (Fig. 6 A), soot (probably from the ship exhaust) or organic conglomerates of probably biological origin.

Method for polycarbonate (low-volume) filters. Measurements were conducted using a technique capable to determine ambient INP concentrations in the temperature range -20°C<T<0°C, most important for the onset of cloud glaciation. During the 8 hour sampling intervals, aerosol particles were extracted from defined volume of air and deposited on filters utilizing the DIGITEL DPA-14 low-volume sampler. The filter samples were sealed and preserved for analysis in the lab. There the aerosol was washed off the filter, and the washing water divided into 96 subsamples and exposed to decreasing temperatures. The freezing temperature of each individual subsample is registered. This data allows to derive the concentration of active INP as function of temperature in the air volume sampled initially. So far only every third of the polycarbonate filters has been analysed for INP. The analysis of the remaining polycarbonate filters and the quartz fibre filters will complete the picture.

burning and biological aerosol. On the other 70% of the planet, the oceans, INP from these sources are often highly diluted after long range transport. Marine sources of INP have been identified and it is found that they can be active in the relevant temperature range (-20°C<T<0°C). The unanswered question is their abundance. It was suggested by *Burrows et al.* [2013], that distant from the continental sources, the marine INP contribution can play a role in cloud glaciation. Figure 6 shows a selection of particles collected in the marine environment during ACE.

Figure 7 depicts temperature spectra, i.e., INP number concentrations as function of temperature, as determined for all up to now analysed low-volume filter samples (blue). Compared to three widely used parametrizations [*Cooper*, 1986; *Fletcher*, 1962; *Meyers et al.*, 1992] measured concentrations are
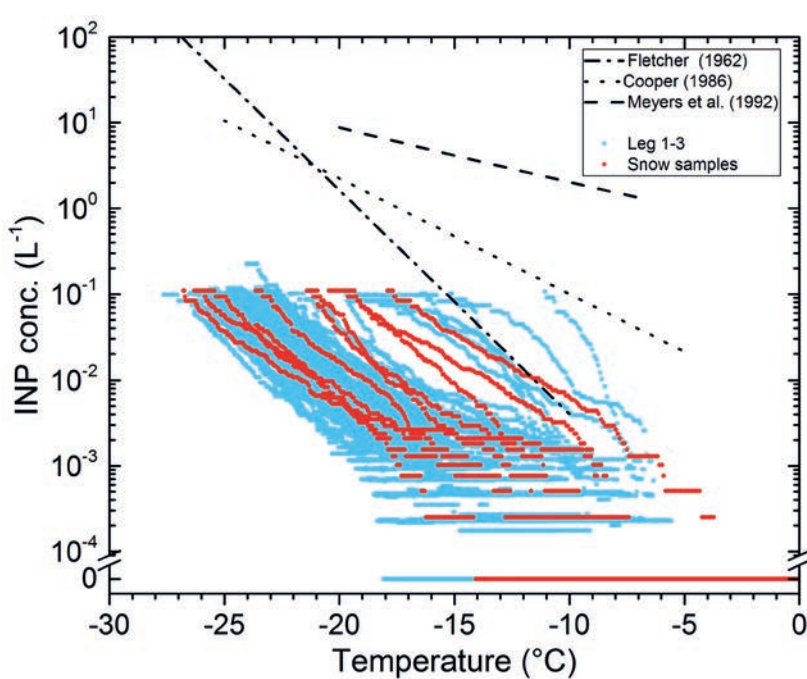
Fig. 7: Temperature spectra of INP concentrations measured during ACE. Filter measurements are given in blue, snow samples in red. Parametrizations from Fletcher [1962], Cooper [1986] and Meyers et al. [1992] are added for comparison.
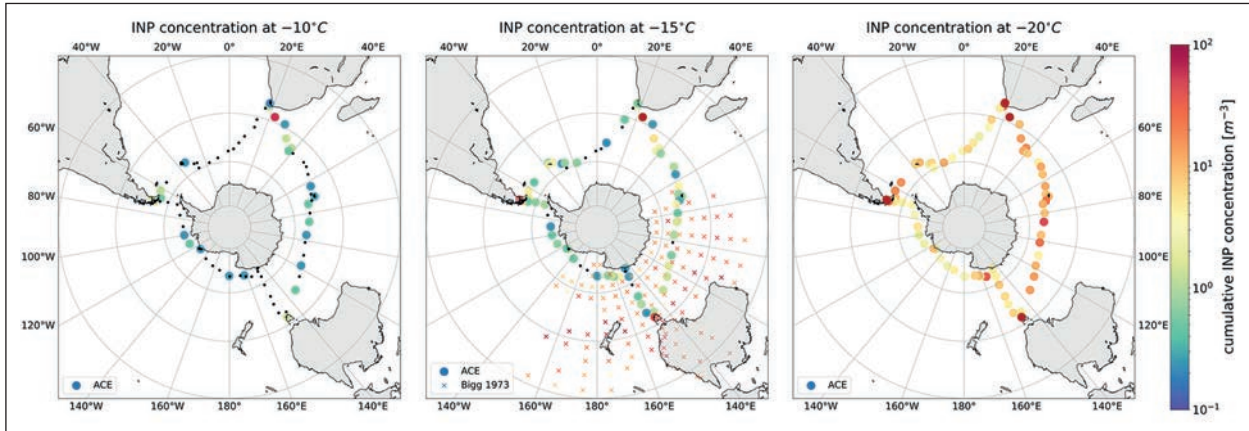
Fig. 8: INP concentrations measured at -10°C, -15°C and-20°C along the ACE track. Black points indicate concentrations below the detection limit. INP concentrations at -15°C from Bigg (1973) are given for comparison.
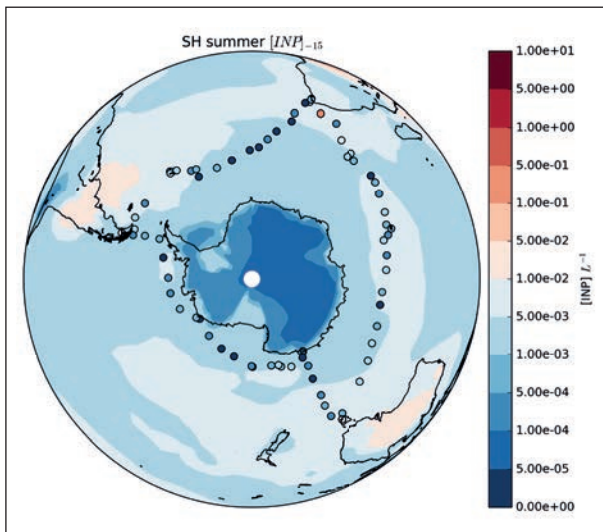
Fig. 9: Comparison of measured INP concentrations at -15°C to the GLOWMAP model prediction of INP concentrations in the SO (courtesy of Jesus Vergara-Temprado).

much lower, confirming that the absence of INP could be one reason for the presence of liquid, supercooled clouds in this part of the globe.

To test if the filter sample technique underestimates INP concentration, the INP concentration in snow samples collected on islands, icebergs and on the ship during snow fall events are given for comparison (red data in Fig. 7). Both datasets are in agreement on the mostly low INP concentration.

Maps showing the spacial variation in INP concentration at -10°C, -15°C and -20°C arround Antarctica are given in Fig. 8. We find that concentrations are constantly low on the open Ocean, but increase in the vicinity to the ports of Cape Town, Hobart and Punta Arenas. Temperature spectra of measurements close to ports can be seen as steep increase in INP concentration between -5°C to -15°C

in Fig. 7. On the open Ocean, concentrations of INP active at -10°C are often below 0.1m^{-3}, the limit of detection. On the map showing INP concentrations at -15°C, literature data reported by *Bigg* [1973] is given for comparison. Mesurements during ACE show a one order of magnitude lower abundance of potential INP at this temperature.

Bigg [1973] suggested that the INP observed in the SO could be of continental origin, transported over a long distance and brought to sea level by convective mixing. This point of view is supported by reports that even at the South Pole, some particles found in snowflakes are composed of mineral dusts [*Kumai*, 1976]. The backtrajectories along the ACE track, indicate a primary marine origin of INP in the SO. This is in agreement with the interpretation of *Schnell and Vali* [1976], who provided an alternative interpretation for Bigg's measurements. They showed evidence that revealed a strong dependence of INP concentration on marine biological productivity.

A comparison of INP concentrations along the ACE track to model predictions of INP concentrations in the same season as the measurements is shown in Fig. 9. The GLOWMAP model prediction uses concentrations of K-feldspar and marine organics as sources of INP. Measured concentrations are often lower than the model prediction.

Summary

Information concerning both CCN and INP abundance, their chemical and physical properties, and their sources in the SO region is rare, but urgently needed to better understand and quantify climate change and the importance of aerosol-cloud-interactions therein. To meet these needs, we took part in the Antarctic Circumnavigation Expedition (ACE), and as collaboration partner of the PSI within the

ACE-SPACE project, carried out comprehensive CCN and INP measurements. The sample and data analysis is still ongoing and results gained up to now can be summarized as follows:

- CCN concentrations range between about 5 and 1300 cm^{-3}
- Hygroscopicity parameter κ ranges between roughly 0.5 and 0.7
- No clear dependence of CCN number concentration on geographical location or trajectory source region
- INP concentrations vary in the range from 0.1 to 100 m^{-3} at -20°C<T<-5°C

- Highest concentrations (10-100 INP m^{-3}) are measured closest to continents
- Observed INP concentrations at -15°C are lower than Bigg's measurements in 1969-1972, and closer to concentrations predicted by the global GLOMAP model

Together with remote sensing, satellite retrievals and modelling studies carried out within ACE-SPACE, the collected data will significantly improve the definition of preindustrial aerosol baseline conditions, make possible a more accurate quantification of anthropogenic climate effects, and thereby improve the quality of future climate predictions.

References

Andreae, M. O., and H. Raemdonck (1983), Dimethyl Sulfide in the Surface Ocean and the Marine Atmosphere: A Global View, *Science*, *221*(4612), 744.

Asmi, A., et al. (2013), Aerosol decadal trends - Part 2: In-situ aerosol particle number concentrations at GAW and ACTRIS stations, *Atmos. Chem. Phys.*, *13*(2), 895-916, doi:10.5194/acp-13-895-2013.

Augustin-Bauditz, S., H. Wex, S. Kanter, M. Ebert, D. Niedermeier, F. Stolz, A. Prager, and F. Stratmann (2014), The immersion mode ice nucleation behavior of mineral dusts: A comparison of different pure and surface modified dusts, *Geophys. Res. Lett.*, *41*, doi:10.1002/2014gl061317.

Ayers, G. P., and J. L. Gras (1991), Seasonal Relationship Between Cloud Condensation Nuclei And Aerosol Methanesulfonate In Marine Air, *Nature*, *353*(6347), 834-835, doi:10.1038/353834a0.

Bates, T. S., B. J. Huebert, J. L. Gras, F. B. Griffiths, and P. A. Durkee (1998a), International Global Atmospheric Chemistry (IGAC) project's first aerosol characterization experiment (ACE 1): Overview, *J. Geophys. Res. - Atmos.*, *103*(D13), 16297-16318, doi:10.1029/97jd03741.

Bates, T. S., V. N. Kapustin, P. K. Quinn, D. S. Covert, D. J. Coffman, C. Mari, P. A. Durkee, W. J. De Bruyn, and E. S. Saltzman (1998b), Processes controlling the distribution of aerosol particles in the lower marine boundary layer during the First Aerosol Characterization Experiment (ACE 1), *J. Geophys. Res. - Atmos.*, *103*(D13), 16369-16383, doi:10.1029/97jd03720.

Bigg, E. K. (1973), Ice Nucleus Concentration in Remote Areas, *J. Atmos. Sci.*, *30*, 1153-1157.

Boers, R., J. B. Jensen, and P. B. Krummel (1998), Microphysical and short-wave radiative structure of stratocumulus clouds over the Southern Ocean: Summer results and seasonal differences, *Q. J. R. Meteorol. Soc.*, *124*(545), 151-168, doi:10.1002/qj.49712454507.

Boers, R., J. B. Jensen, P. B. Krummel, and H. Gerber (1996), Microphysical and short-wave radiative structure of wintertime stratocumulus clouds over the Southern Ocean, *Q. J. R. Meteorol. Soc.*, *122*(534), 1307-1339, doi:10.1002/qj.49712253405.

Boers, R., and P. B. Krummel (1998), Microphysical properties of boundary layer clouds over the southern ocean during ACE 1, *J. Geophys. Res. - Atmos.*, *103*(D13), 16651-16663, doi:10.1029/97jd03280.

Burrows, S. M., C. Hoose, U. Pöschl, and M. G. Lawrence (2013), Ice nuclei in marine air: biogenic particles or dust?, *Atmos. Chem. Phys.*, *13*(1), 245-267.

Carslaw, K. S., et al. (2013), Large contribution of natural aerosols to uncertainty in indirect forcing, *Nature*, *503*(7474), 67-+, doi:10.1038/nature12674.

Chubb, T., Y. Huang, J. Jensen, T. Campos, S. Siems, and M. Manton (2016), Observations of high droplet number concentrations in Southern Ocean boundary layer clouds, *Atmos. Chem. Phys.*, *16*(2), 971-987, doi:10.5194/acp-16-971-2016.

Clarke, A. D., J. L. Varner, F. Eisele, R. L. Mauldin, D. Tanner, and M. Litchy (1998), Particle production in the remote marine atmosphere: Cloud outflow and subsidence during ACE 1, *J. Geophys. Res. - Atmos.*, *103*(D13), 16397-16409, doi:10.1029/97jd02987.

Cooper, W. A. (1986), Precipitation Enhancement - A Scientific Challenge, edited by R. R. Braham, pp. 29-32, Am. Meteorol. Soc.

Defelice, T. P., V. K. Saxena, and S. C. Yu (1997), On the measurements of cloud condensation nuclei at Palmer Station, Antarctica, *Atmos. Environ.*, *31*(23), 4039-4044.

DeMott, P. J., et al. (2016), Sea spray aerosol as a unique source of ice nucleating particles, *Proceedings of the National Academy of Sciences of the United States of America*, *113*(21), 5797-5803, doi:10.1073/pnas.1514034112.

Dusek, U., et al. (2006), Size matters more than chemistry for cloud-nucleating ability of aerosol particles, *Science*, *312*(5778), 1375-1378.

Fiebig, M., D. Hirdman, C. R. Lunder, J. A. Ogren, S. Solberg, A. Stohl, and R. L. Thompson (2014), Annual cycle of Antarctic baseline aerosol: controlled by photooxidation-limited aerosol formation, *Atmos. Chem. Phys.*, *14*(6), 3083-3093, doi:10.5194/acp-14-3083-2014.

Fletcher, N. H. (1962), *The physics of rainclouds*, Cambridge University Press.

Gras, J. L. (1995), CN, CCN And Particle-Size In Southern-Ocean Air At Cape-Grim, *Atmos. Res.*, *35*(2-4), 233-251, doi:10.1016/0169-8095(94)00021-5.

Hamilton, D. S., L. A. Lee, K. J. Pringle, C. L. Reddington, D. V. Spracklen, and K. S. Carslaw (2014), Occurrence of pristine aerosol environments on a polluted planet, *Proceedings of the National Academy of Sciences of the United States of America*, *111*(52), 18466-18471, doi:10.1073/pnas.1415440111.

Heintzenberg, J., and R. Charlson (Eds.) (2009), *Clouds in the Perturbed Climate System: their relationship to engery balance, atmospheric dynamics, and precipitation*, 597 pp., The MIT press, Cambridge.

Hoose, C., and O. Mohler (2012), Heterogeneous ice nucleation on atmospheric aerosols: a review of results from laboratory experiments, *Atmos. Chem. Phys.*, *12*(20), 9817-9854, doi:10.5194/acp-12-9817-2012.

Huang, Y., S. T. Siems, M. J. Manton, A. Protat, and J. Delanoe (2012), A study on the low-altitude clouds over the Southern Ocean using the DARDAR-MASK, *J. Geophys. Res. - Atmos.*, *117*, 15, doi:10.1029/2012jd017800.

IPCC (2013), IPCC report 2013: Working Group I contribution to the AR5 on Climate Change 2013: The Physical Science Basis*Rep.*, Cambridge, United Kingdom and New York, NY, USA.

Kanitz, T., P. Seifert, A. Ansmann, R. Engelmann, D. Althausen, C. Casiccia, and E. G. Rohwer (2011), Contrasting the impact of aerosols at northern and southern midlatitudes on heterogeneous ice formation, *Geophys. Res. Lett.*, *38*, 5, doi:10.1029/2011gl048532.

Köhler, H. (1936), The nucleus and the growth of hygroscopic droplets, *Trans. Faraday Soc.*, *32*, 1152-1161.

Kumai, M. (1976), Identification of nuclei and concentrations of chemical species in snow crystals sampled at the South Pole, *J. Atmos. Sci.*, *33*, 833-841.

Marchand, R., R. Wood, C. Bretherton, G. McFarquhar, A. Protat, P. Quinn, S. Siems, C. Jakob, S. Alexander, and B. Weller (2014), The Southern Ocean Clouds, Radiation, Aerosol Transport Experimental Study.

Meyers, M. P., P. J. DeMott, and W. R. Cotton (1992), New Primary Ice-Nucleation Parametrisation in an Explicit Cloud Model, *J. Appl. Meteor.*, *31*, 708-721.

Morrison, A. E., S. T. Siems, and M. J. Manton (2011), A Three-Year Climatology of Cloud-Top Phase over the Southern Ocean and North Pacific, *J. Clim.*, *24*(9), 2405-2418, doi:10.1175/2010jcli3842.1.

Murray, B. J., D. O'Sullivan, J. D. Atkinson, and M. E. Webb (2012), Ice nucleation by particles immersed in supercooled cloud droplets, *Chem. Soc. Rev.*, *41*(19), 6519-6554, doi:10.1039/c2cs35200a.

O'Shea, S. J., et al. (2017), In situ measurements of cloud microphysics and aerosol over coastal Antarctica during the MAC campaign, *Atmos. Chem. Phys.*, *17*(21), 13049-13070, doi:10.5194/acp-17-13049-2017.

Petters, M. D., and S. M. Kreidenweis (2007), A single parameter representation of hygroscopic growth and cloud condensation nucleus activity, *Atmos. Chem. Phys.*, *7*(8), 1961-1971.

Pringle, K. J., K. S. Carslaw, D. V. Spracklen, G. M. Mann, and M. P. Chipperfield (2009), The relationship between aerosol and cloud drop number concentrations in a global aerosol microphysics model, *Atmos. Chem. Phys.*, *9*(12), 4131-4144, doi:10.5194/acp-9-4131-2009.

Pringle, K. J., H. Tost, A. Pozzer, U. Poschl, and J. Lelieveld (2010), Global distribution of the effective aerosol hygroscopicity parameter for CCN activation, *Atmos. Chem. Phys.*, *10*(12), 5241-5255, doi:10.5194/acp-10-5241-2010.

Pruppacher, H. R., and J. D. Klett (1997), *Microphysics of clouds and precipitation*, 2 ed., 954 pp., Kluwer Academic Publishers, Dordrecht [etc.].

Quinn, P. K., and T. S. Bates (2011), The case against climate regulation via oceanic phytoplankton sulphur emissions, *Nature*, *480*(7375), 51-56, doi:10.1038/nature10580.

Rosenfeld, D., et al. (2014), Global observations of aerosol-cloud-precipitation-climate interactions, *52*(4), 750 - 808.

Schmale, J., J. Schneider, E. Nemitz, Y. S. Tang, U. Dragosits, T. D. Blackall, P. N. Trathan, G. J. Phillips, M. Sutton, and C. F. Braban (2013), Sub-Antarctic marine aerosol: dominant contributions from biogenic sources, *Atmos. Chem. Phys.*, *13*(17), 8669-8694, doi:10.5194/acp-13-8669-2013.

Schnell, R., and G. Vali (1976), Biogenic Ice Nuclei: Part I. Terrestrial and Marine Sources, *J. Atmos. Sci.*, *33*, 1554-15564.

Sullivan, S. C., C. Hoose, A. Kiselev, T. Leisner, and A. Nenes (2017), Initiation of secondary ice production in clouds, *Atmos. Chem. Phys. Discuss.*, *2017*, 1-22, doi:doi:10.5194/acp-2017-387.

Trenberth, K. E., and J. T. Fasullo (2010), Simulation of Present-Day and Twenty-First-Century Energy Budgets of the Southern Oceans, *J. Clim.*, *23*(2), 440-454, doi:10.1175/2009jcli3152.1.

Twomey, S. (1974), Pollution and the planetary albedo, *Atmos. Environ.*, *8*, 1251-1256.

Weber, R. J., A. D. Clarke, M. Litchy, J. Li, G. Kok, R. D. Schillawski, and P. H. McMurry (1998), Spurious aerosol measurements when sampling from aircraft in the vicinity of clouds, *J. Geophys. Res. - Atmos.*, *103*(D21), 28337-28346, doi:10.1029/98jd02086.

Wofsy, S. C., H. S. Team, T. Cooperating Modellers, and T. Satellite (2011), HIAPER Pole-to-Pole Observations (HIPPO): fine-grained, global-scale measurements of climatically important atmospheric gases and aerosols, *Philosophical Transactions of the Royal Society a-Mathematical Physical and Engineering Sciences*, *369*(1943), 2073-2086, doi:10.1098/rsta.2010.0313.

Cooperation

Paul Scherrer Institute, Villigen, Switzerland;
University of Leeds, Leeds, United Kingdom;
The Hebrew University of Jerusalem, Jerusalem, Israel;
ETH Zurich, Zurich, Switzerland:
University of Cambridge, Cambridge, United Kingdom

Cloud, aerosol and radiation measurements during the Polarstern expedition PS106 (PASCAL) in June - July 2017

Andreas Macke, Carola Barrientos, Thomas Conrath, Ulrike Egerer, Ronny Engelmann, Susanne Fuchs, Xianda Gong, Hannes Griesche, Markus Hartmann, Simonas Kecorius, Manuela van Pinxteren, Martin Radenz, Kay Szodry, Teresa Vogl, Andre Welti, Jonas Witthuhn, Sebastian Zeppenfeld, Hartmut Herrmann, Frank Stratmann, Alfred Wiedensohler

TROPOS war federführend an der Vorbereitung und Durchführung der POLARSTERN-Expedition PS106.1 in die zentrale Arktis beteiligt. Die Expedition hatte das Ziel, möglichst umfassend das Aerosol-Wolkensystem der arktischen Troposphäre und die Energieflüsse über dem Ozean und dem Meereis sowie vertikale Profile der Energieflüsse in der arktischen Grenzschicht zu untersuchen. Die Messungen tragen dazu bei, Ursachen für die schnelle Klimaerwärmung in der Arktis, die so genannte „Arktische Verstärkung", besser zu verstehen. Der folgende Beitrag fasst die Arbeiten des TROPOS während der Expedition PS106.1 und der Folge-Expedition PS106.2 zusammen. Diese sind ein wesentlicher Beitrag zum Sonderforschungsbereich TR172 „Arktische Verstärkung".

Introduction

The Polar Regions are important components in the global climate system. The widespread surface snow and ice cover in Polar Regions strongly impacts the surface energy budget, which is tightly coupled to global atmospheric and oceanic circulations. Here, the interaction of different Arctic feedback mechanisms is not yet completely understood. For example, the coupling of sea ice, clouds and aerosol in the transition zone between Open Ocean and sea ice is not fully understood so far. Therefore, this issue has been addressed in the **PASCAL** (Physical feedbacks of Arctic PBL, Sea ice, Cloud And Aerosol) project to improve our understanding of the recent dramatic reduction in Arctic sea-ice in the boreal summer. For this purpose the TROPOS-OCEANET and aerosol instrumentation on board of POLARSTERN during the cruise PS106 in June and July 2017 have provided broadband radiation measurements to determine the surface energy budget and a detailed characterization of surface, cloud and aerosol properties. The observations on the ship and most importantly on a two week ice floe camp have been closely coordinated with collocated airborne activities of the POLAR 5 and

POLAR 6 AWI aircraft operating between Longyearbyen along the gradient of sea ice concentration and POLARSTERN. These airborne observations were supplemented by observations of the boundary layer structure (mean and turbulent quantities) from tethered balloon and several small Unmanned Airborne Vehicles UAV's, which were operated during the ice station nearby POLARSTERN. The atmospheric measurements were to a large degree performed in the framework of the Collaborative Research Cluster TR 172 "Arctic Amplification".

The article provides an overview of the TROPOS contributions with a focus on the time period of the ice floe camp. Several other groups from other institutions have participated in PS106 as well. For a complete description of all measurements during PS106, we refer to the cruise report to be published by the Alfred Wegener Institute (AWI) in 2018. Here, we show some preliminary results covering radiation budget and remote sensing, in-situ aerosol measurements, tethered-balloon based boundary layer profiling, and surface micro layer (SML) probing. A concluding outlook also addresses the coming one-year ice drift of POLARSTERN in 2019/2020, where TROPOS will contribute with similar equipment.
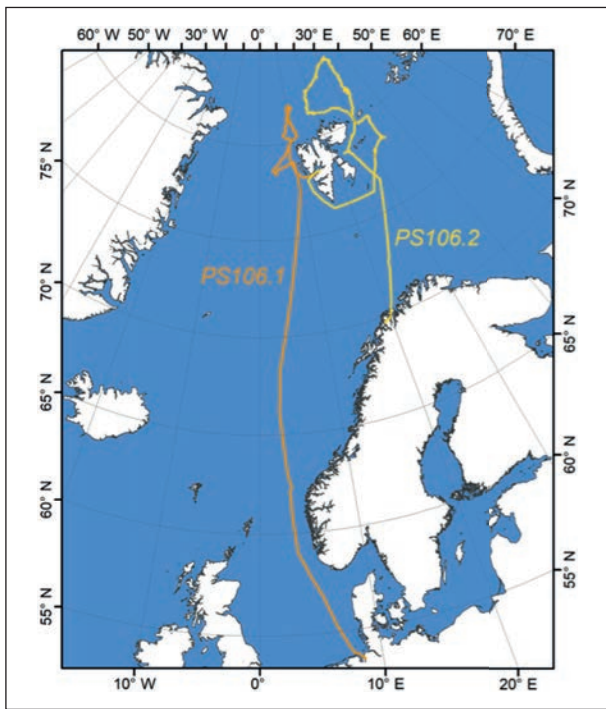
Fig. 1a: Cruise track of POLARSTERN Expedition PS106. Figure by Anna Nikolopoulos, AquaBiota.
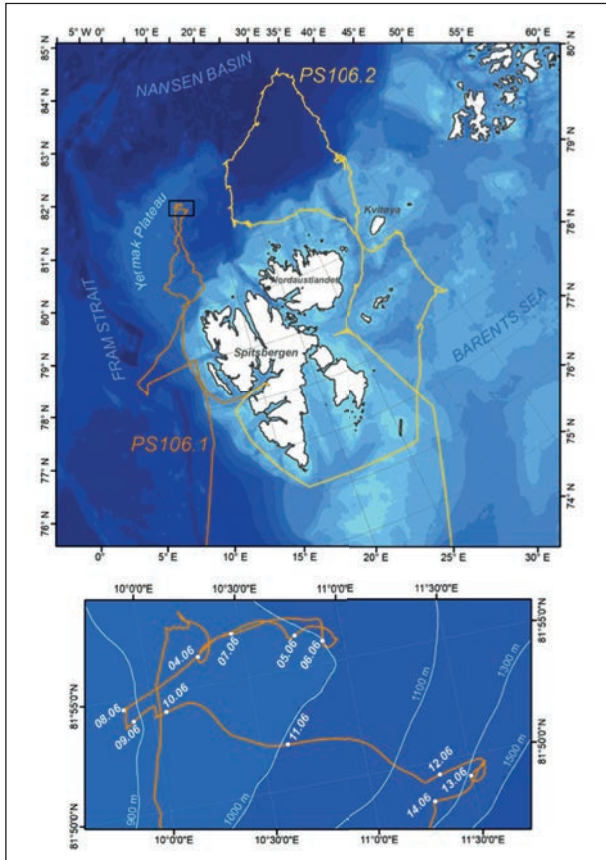
Fig. 1b: Cruise track of POLARSTERN in operational area near Svalbard and during the ice floe camp. Figure by Anna Nikolopoulos, AquaBiota.

Itinerary

On May 24 2017 POLARSTERN set sails in Bremerhaven and reached a suitable nearly circular ice floe with a diameter of roughly 4 km at (82° 57.7' N, 10° 14.6' E) in the morning of June 3. On the ice floe camp continuous measurements of the energy budget at the surface and the state of the cloudy atmosphere were performed from June 4 to June 15. In parallel, sea ice physical, biological and biogeo-chemical measurements were carried out. Due to bad visibility conditions the measurements on the ice floe were cancelled for parts of June 6 and June 9 as well as completely for June 12. On June 16 POLARSTERN continued to Longyearbyen with arrival on June 21. The continuous ship-based atmospheric meas-urements were operating until the end of PS106 in Tromsø on July 20 2017. Figure 1a shows the entire cruise track of PS106. Figure 1b provides a zoom into the operational area north of Svalbard and the drift of the ice floe camp, respectively.

As the focus of this overview article is on the measurements during the ice floe camp, Fig. 2 provides an overview on the weather and sky condi-tions during that two-weeks period. Fortunately, a variety of different weather and cloud conditions occurred during that time, and most importantly, a melting period with warm air intrusion from the south was observed in the second week.

Objectives and first results

a) Radiation budget & atmosphere remote sensing

The objectives of the radiation and remote aerosol, cloud and water-vapor measurements are to obtain both the radiation budget and the state of the cloudy atmosphere as accurate as possible to provide realistic atmosphere-radiation relationships for use in climate models and in remote sensing. While similar experiments have been performed from land [*Macke et al.*, 2017] and open ocean stations [*Kalisch and Macke*, 2012], only few data from measurements exist over the Central Arctic.

For the second time during the OCEANET activ-ities, a stabilized cloud radar (MIRA 35 GHz) was utilized on POLARSTERN to obtain continuous time series of vertical profiles of cloud and ice water as well as vertical velocity throughout the entire tropo-sphere. To obtain accurate vertical velocities from the cloud-radar observations, the cloud radar was installed on a stabilization platform. PS106 was thus the first POLARSTERN cruise ever with a stabilized 35-GHz clour radar on board. The radar observations
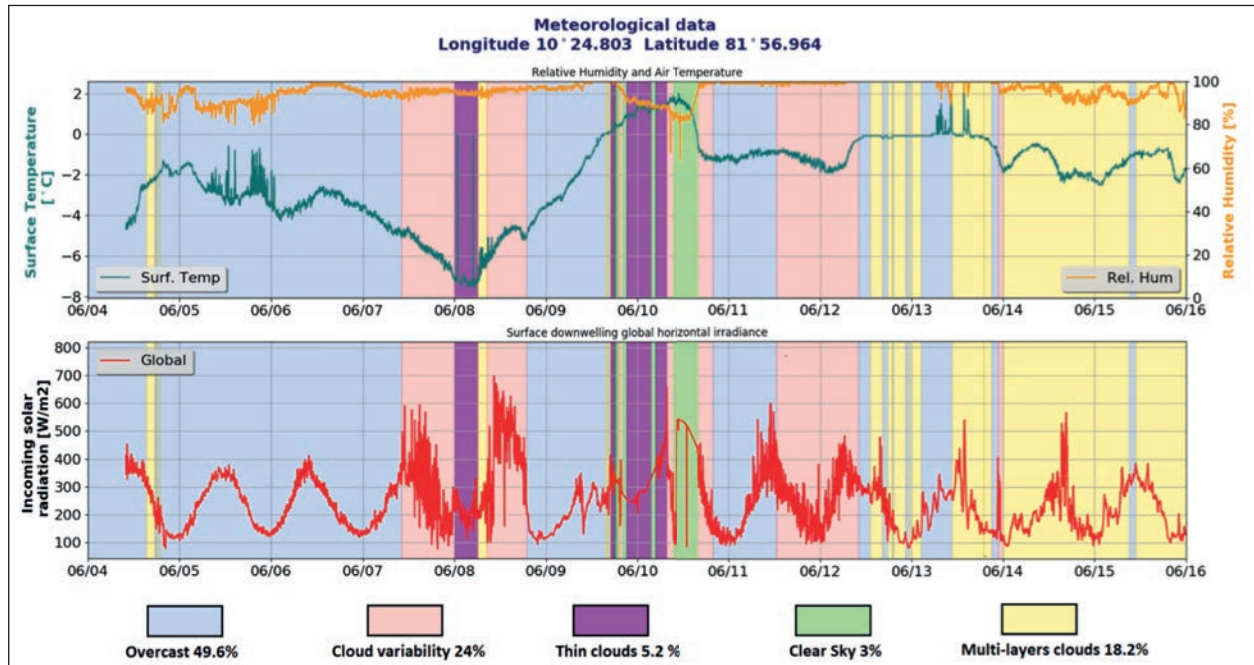
Fig. 2: Overview of weather and sky conditions during the ice floe camp. Figure by Carola Barrientos. Polarstern meteorological data by Holger Schmitthüsen, AWI.

provide the key data to resolve two dimensional cloud processes for comparison with high-resolution dynamical models and with remote sensing from space for radiation closure studies. The algorithms to convert radar reflectivity measurements into cloud physical properties have been developed over the years within the framework of the European ACTRIS project [*Bühl et al.*, 2016].

The TROPOS lidar system Polly-XT, a semi-autonomous multiwavelength polarization Raman lidar, was operated inside the OCEANET container together with the radiation and microwave sensing equipment. The lidar is able to measure independently profiles of particle backscatter at three wavelengths and extinction at two wavelengths, which allows identifying particle type, size, and concentration [*Kanitz et al.*, 2013; *Engelmann et al.*, 2016]. Additionally, the particle depolarisation ratio is measured in order to discriminate between spherical and non-spherical particles, e.g. water clouds vs. ice clouds. The data are used to characterize long-range transport of aerosol and to identify pollution. Both, radar and lidar were able to measure profiles from as low as 150 m above the ground to identify the shallow Arctic boundary layer and connect the remote measurements with the ground-based in-situ measurements.

A multichannel microwave radiometer (HATPRO) was applied to continuously retrieve integrated water vapor (IWV) and cloud liquid water path (LWP). Time series of these data resolve small-scale atmospheric structures as well as the effects of the mean state of

the atmosphere and its variability on the co-located measurements of the downwelling shortwave and longwave radiation to allow intercomparison with model and satellite data [*Hanschmann et al.*, 2012]. Most instruments were integrated in the container-based atmosphere observatory OCEANET. A network of autonomous pyranometer stations allowed to retrieve the spatiotemporal variability of the downwelling solar irradiance (see [*Madhavan et al.*, 2017]), that may have an influence on the melting processes of the Arctic sea ice and melt pond mix.

The time series of IWV and LWP from measurements with the microwave radiometer HATPRO within the OCEANET container are shown in Fig. 3. IWV values were found to be around 20-30 kg/m² during departure from Bremerhaven. Upon arrival in the Arctic, the IWV decreased occasionally even below 5 kg/m². Most observed values were about 10 kg/m². LWP values were mostly found between 0 and 200 g/m² with frequent values around 40-60 g/m².

Measurements with the Raman lidar PollyXT were generally very difficult, as the sky over POLARSTERN was mostly cloudy. In low clouds, the laser beam was attenuated after a few tens of meters. Therefore, only the rare clear-sky situations allowed an aerosol profiling. Nevertheless, on 9 and 10 June 2017 a lofted aerosol layer between 1 and 3 km was observed. First analysis of backward trajectories provided by German Meteorological Service (DWD) showed that the air masses were transported to the Arctic from Central Europe.
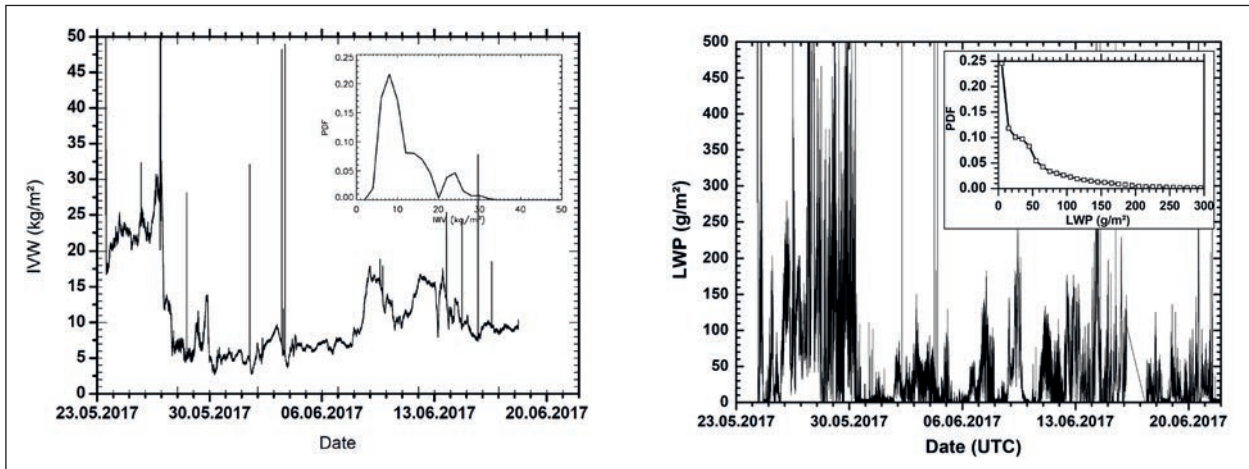
Fig. 3: Integrated water vapor and liquid-water path measured with the microwave radiometer during PS106.1. The inset shows the histogram of the time series. Distinctive spikes in the IWV time series were caused by obstructions to the sky during maintenance operations. Figure by Ronny Engelmann.

The combination of cloud radar, lidar, and microwave-radiometer measurements allow a detailed identification and characterisation of vertically resolved aerosol and cloud properties, taking advantage of the long-year algorithm development in the framework of the European EARLINET and CLOUDNET activities [*Baars et al.*, 2017, *Illingworth et al.*, 2007]. Figure 4 shows an exemplary time series of a combined aerosol/cloud target classification (upper diagram) and data quality characterization (lower diagram). Especially the identification of ice formation or ice melting provides valuable information on thermodynamical processes and aerosol-cloud interaction for process studies and for comparison with model results. For example, on June 5, the MIRA-35 radar and PollyXT lidar detected the occurrence of ice particle formation in low boundary layer clouds at

temperatures of about -7 °C. This case is currently under intense investigation to identify the physical mechanisms for the occurrence of these rather warm ice layers. The ground-based remote sensing of the vertical aerosol and cloud structure was performed nearly continuously during the full two months of the POLARSTERN cruise PS106 thus providing an unprecedented data set in the Central Arctic.

The pyranometer network, for the first time to our knowledge, provided the spatiotemporal variability of the downwelling solar irradiance at the surface in the Arctic. Figure 5 shows an example snapshot of the spatial variability of the broadband solar transmittance (downwelling irradiance at the surface divided by downwelling irradiance at the top of the atmosphere). Currently, these data are statistically analysed in terms of cloud types. Further analysis will show to
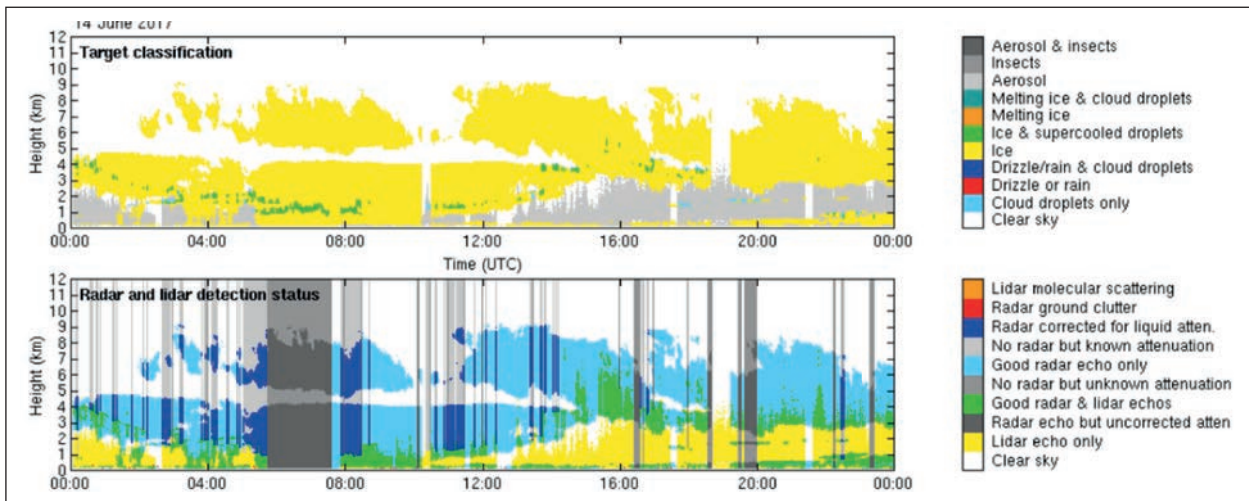
Fig. 4: Target classification (upper plot) and quality characterization (lower plot) of combined lidar/radar tropospheric profiling. Figure by Holger Baars.
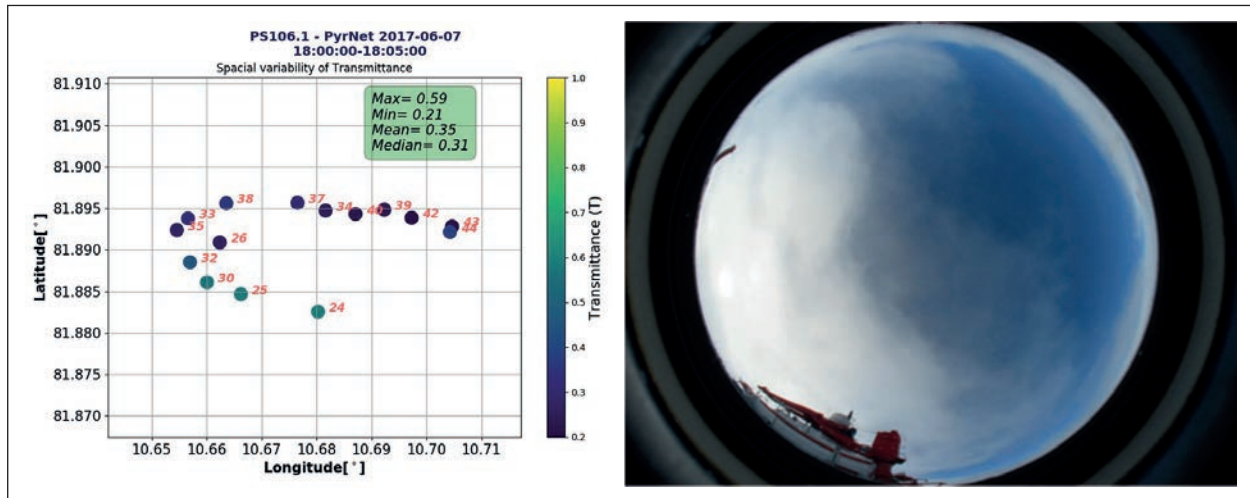
Fig. 5: Example for spatial variability of solar radiation transmissivity together with corresponding sky image. Figure by Carola Barrientos.

what extent a spatially variable irradiance imposed on a heterogeneous ice surface provides different melting conditions compared to a homogeneous irradiance.

b) Aerosol in-situ measurements

The portfolio of the Aerosol Group at TROPOS includes the in-situ characterization of atmospheric aerosols in urban as well as remote background atmospheres, the characterization of regional and urban air quality, the examination of hygroscopic particle properties, the measurement and simulation of in-situ aerosol optical properties, the investigation of atmospheric transport processes, and the development of new and improved instruments for physical aerosol characterization.

Ice Nucleating Particles (INP) and Cloud Condensation Nuclei (CCN) may significantly influence the microphysical and radiative properties of Arctic clouds. Information concerning the concentrations of Arctic INP, their chemical nature (mineral and/or organic), and their origin (local sources or long range transport) is sparse, therefore the Cloud Group at TROPOS investigated and quantified the Arctic aerosol in respect to its ability to form ice and liquid cloud droplets. In collaboration with the chemical analysis performed by *d) Sea surface microlayer (SML) measurements* we may able to identify potential sources of INP and CCN.

Onboard POLARSTERN all measurements were conducted inside a temperature-controlled container laboratory with focus on the particle characterization using high-end scientific instruments in order to study:

- physical aerosol properties using an Aerodynamic Sizer (APS) and Scanning Mobility Particle Sizer (SMPS) for particle number size distributions from 10 nm to 10 µm, and a Volatility and Humidifying Tandem Differential Mobility Particle Sizer (VH-TDMPS) for the hygroscopic growth of the particles;
- Optical properties using a nephelometer and an absorption photometer to measure the particle light scattering and absorption coefficients, respectively; and
- Particle chemical composition using a High Resolution Time of Flight Aerosol Mass Spectrometer (HR-ToF-AMS) for the non-refractory PM1.
- Cloud Condensation Nuclei (CCN) number size distribution and particle number size distribution to determine the particle hygroscopicity using a DMT CCN counter-100 and a Scanning Mobility Particle Sizer (SMPS)
- Ice Nucleating Particle (INP) number concentration using a DMT Spectrometer for Ice Nuclei (SPIN)

In addition to the on-line instrumentations, a PM10 Digitel high volume filter sampler (3 day sampling) and a PM1 Digitel low volume filter sampler (8 hour sampling) are installed on the roof of the aerosol container. A cloud water sampler in front of the container collected fog droplets. All these offline samples will be analyzed at TROPOS for their ice nucleating behavior and in close collaboration with the Atmospheric Chemistry Department these will be also characterized chemically. SML, bulk seawater, snow and ice core samples collected around the ship and on the ice floe are also shared between the cloud group (measurement of ice nucleating behavior) and the ACD (chemical characterization).

Figure 6 shows the number concentration of small aerosol particles within the size range of 10
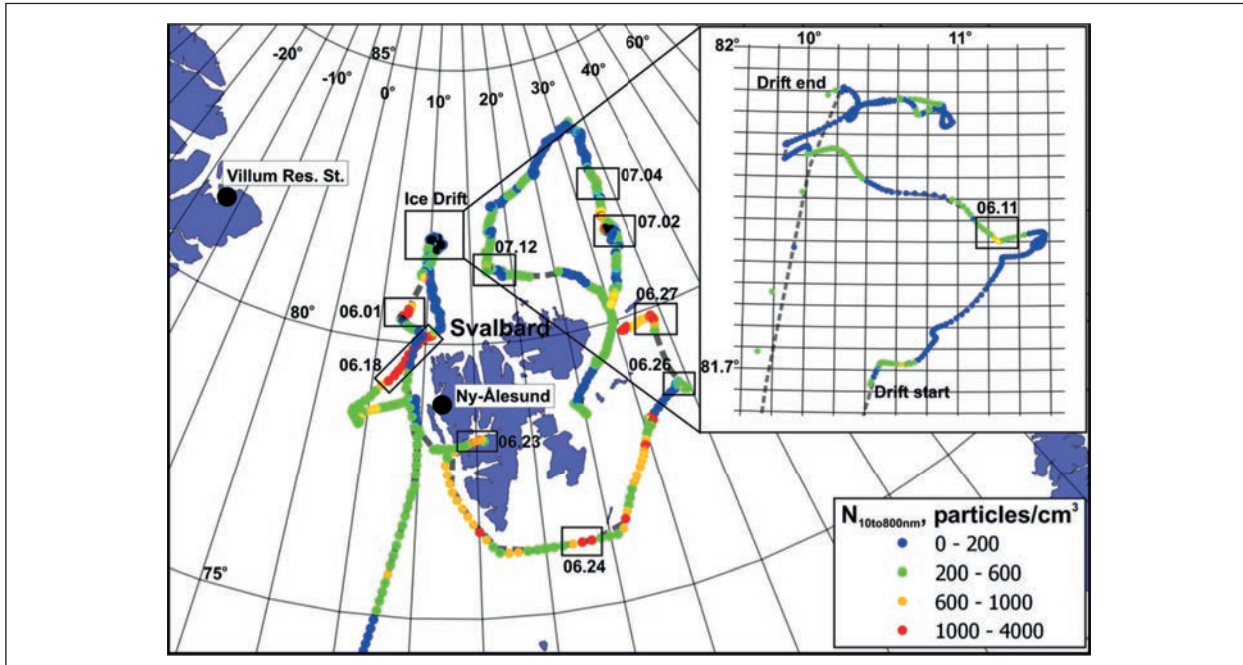
Fig. 6: Number concentration of small aerosol particles within the size range of 10 to 800 nm in diameter for the entire POLARSTERN cruise PS106. Figure by Simonas Kecorius.

to 800 nm in diameter for the entire POLARSTERN cruise PS106. Large concentrations indicate local new particle formation (NPF) processes. NPF was found in the open ocean near Svalbad and only to a small extend in the sea ice indicating the sea surface origin of freshly formed aerosol particles. However, there is some NPF variability in the sea ice, possibly due to changing occurrences of polynyas. The low NPF indicates that the sources of cloud condensation nuclei (CCN) are most likely not local but from remote locations.

During PS106.1 and PS106.2 the cloud condensation nuclei (CCN) number concentration at 6 distinct supersaturations (0.1, 0.15, 0.2, 0.3, 0.5 and 1%) were measured with a CCN-100, see Fig. 7. Here the CCN number concentration at a supersaturation typical for clouds (0.2%) and the total particle number concentration are presented. The presented data are
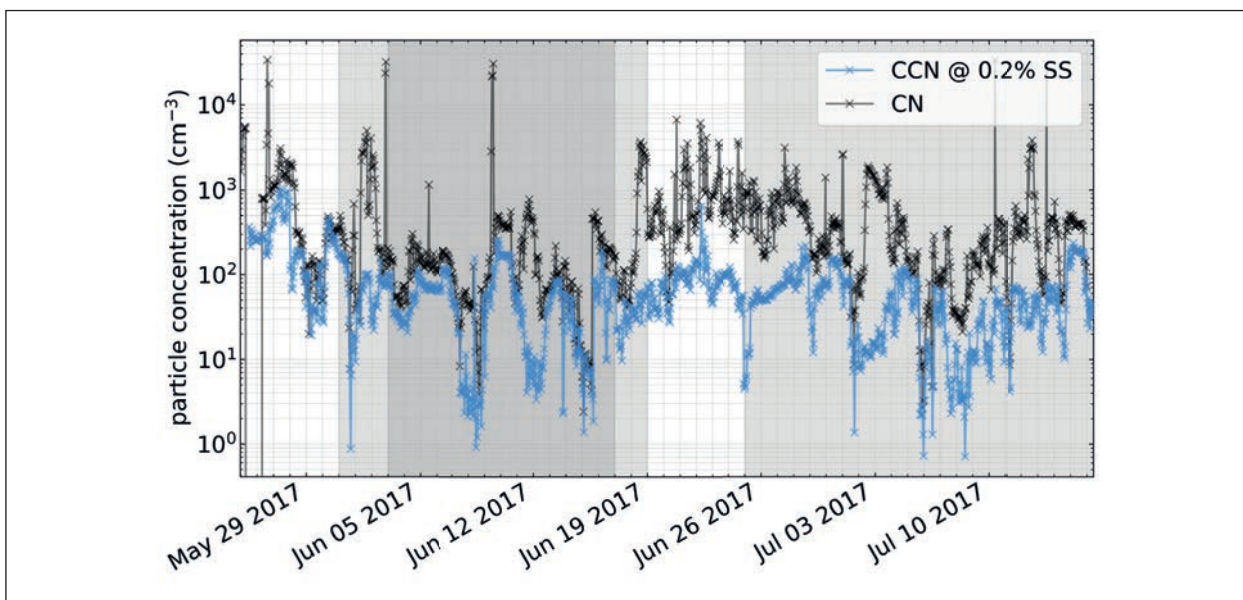
Fig. 7: Cloud condensation nuclei (CNN) concentration at a reference supersaturation of 0.2% during the entire cruise of PS106. Figure by Markus Hartmann.

low pass-filtered and averaged for 10 min intervals. Over the whole measurement period CCN concentrations are generally low with a median of 54.89 cm^{-3}, but vary over three orders of magnitude (min.: 0.71 cm^{-3}; max.: 1039.62 cm^{-3}), where higher values are often, but not solely, associated with open water conditions, as indicated above from the NPF measurements. Periods where increasing total number concentrations, but constant or even decreasing CCN concentrations are observed (e.g. 11.6. – 12.6.17) are due to a pronounced Aitken mode, which originates from a New Particle Formation (NPF) event.

The concentrations of Ice Nucleating Particles (INP) were measured in-situ and offline with different instruments/measurement setups. The combination of both methods allows to cover the full mixed-phase cloud temperature regime (-38°C – 0°C). The corresponding INP concentration is shown in Fig. 8. The in-situ measurements were carried out with the Spectrometer for Ice Nuclei (SPIN by DMT, Boulder, USA), which allows measurements at varying temperatures and supersaturations. The data presented here are measured in the immersion mode (SS$_{water}$ > 1) and represent 30min-averages at specific temperatures. The offline measurements included sampling on both polycarbonate and quartz fiber filters with subsequent laboratory analysis by freezing array techniques based on the ones by *Budke & Koop* [2015] and *Conen et al.* [2012]. The laboratory analysis is time-intensive and not all filter samples have been analysed yet. The data shown here is based on polycarbonate filter samples only, with each day being represented by at least one filter sample. Sampling time per filter

sample was 8 hours at an air flow rate of ca. 30 L/min. Filters were washed of and the washing water was analyzed concerning its ice nucleation behavior utilizing the Leipzig Ice Nucleation Array (LINA, based on the setup of *Budke & Koop* [2015]. Overall the INP concentrations are low. In comparison with a global, only on temperature dependent parametrization like *Fletcher* [1962], the concentrations are about one order of magnitude lower. Also, no clear association between INP concentration and the periods within the pack ice has been observed, whereas in the proximity to the Longyearbyen harbor a clear increase in INP concentrations was found.

c) Tethered balloon-borne measurements of energy budget of the cloudy atmospheric boundary layer in the central Arctic

The quantification of the energy fluxes (turbulent fluxes of sensible and latent heat, momentum and radiative fluxes) within the Atmospheric Boundary Layer (ABL) in the central Arctic represents a key issue for an improved understanding of the Arctic response to Global Warming ("Arctic Amplification"), see *Jeffries et al.*, [2012, 2013], *Overland et al.*, [2012], *Wendisch et al.*, [2017]. The melting of Arctic sea ice is decisively linked with the surface energy fluxes. Surface sensible and latent turbulent heat fluxes are comparably low over sea ice and in this case the energy budget is dominated by the solar and terrestrial radiative fluxes, which are mostly influenced by the local cloud situation (e.g., [*Curry*, 1986]). If sea-ice is noticeably reduced, as observed within the past 20 years, the mean surface temperature increases and the typical low-level temperature inversion is weakened (lower stability). This would increase the turbulent energy fluxes in the Arctic ABL including the moisture flux, which would promote cloud formation.

Arctic low-level clouds exhibit several typical features compared to mid-latitude clouds, which cause important and specific effects (e.g., in terms of radiative transfer) and challenge the numerical modeling of Arctic low-level clouds. In particular, the often mixed-phase character of Arctic low-level clouds and the more complicated vertical structure of the ABL cause major issues compared to mid-latitudes. Arctic low-level clouds mostly warm the ABL. They are frequently organized in several distinct layers and the turbulent energy fluxes can be de-coupled from the surface fluxes (e.g., [*Shupe et al.*, 2013]). Occasionally, moisture inversions coincide with the temperature inversion and the cloud layers penetrate the inversions, that is, the temperature inversion is not necessarily capping the cloud layer.
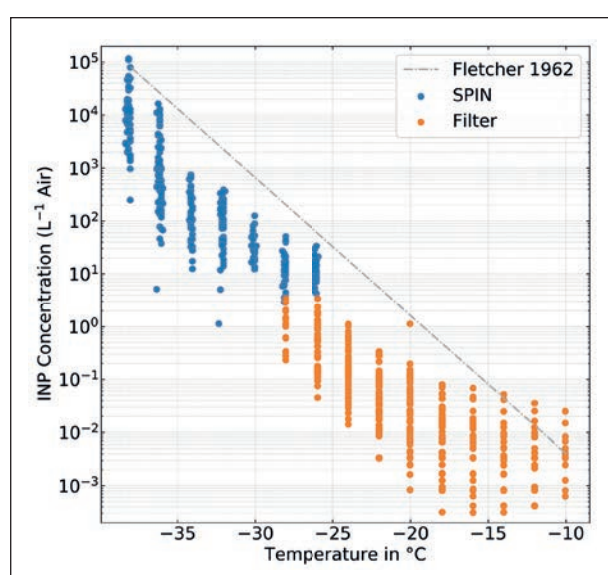
Fig. 8: Ice nucleating particle (INP) concentration as a function of temperature. Figure by Markus Hartmann.
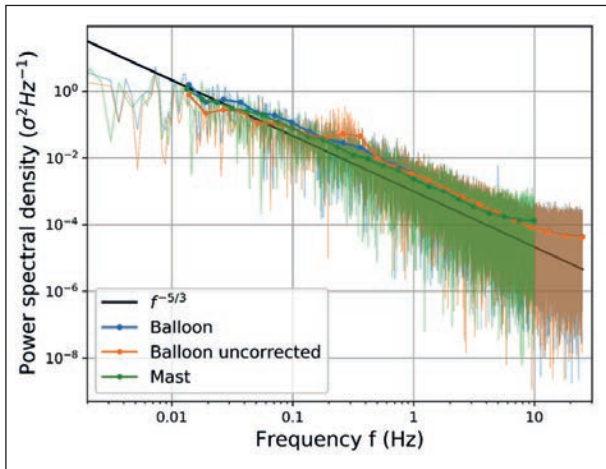
Fig. 9: Power-spectra of high frequency Sonic anemometer vertical wind measurements on June 5, performed at the balloon and at a 10 m meteorology mast, both at the same height. Figure by Ulrike Egerer.

For an improved understanding of the cloudy ABL in the Arctic tethered balloon–borne measurements of turbulent and radiative energy fluxes were performed under different cloudy conditions and thermal stratification during the ice camp. A 90 m^3-helium-filled balloon with a maximum payload of 10 kg was deployed to profile the ABL from the ground up to 1500 m altitude. Several measurement units were fixed at the tether below the balloon to study vertical profiles of turbulent and radiative energy fluxes. The balloon site was situated about 200 m away from the ship. Balloon flights were performed on nine days in different weather conditions, which included clear sky, a low level jet (up to 14 m/s), low clouds of different thickness and multiple cloud layers.

Turbulence parameters were measured alternatively with a lightweight hot-wire anemometer package and a three-dimensional ultrasonic anemometer. The balloon-borne turbulent energy flux measurements were complemented by measurements of humidity, temperature and virtual temperature at high frequencies. Radiative fluxes were measured with two broadband packages to complete the energy budget profiles. Radiance was measured within the solar spectral range by two spectrometers to retrieve cloud optical thickness and the effective radius of the clouds. In addition, a filter aerosol sampler of the TROPOS chemistry department was attached to the tether on June 10, which measured over a period of 3 hours above the inversion layer.

Figure 9 shows power-spectra of high frequency Sonic anemometer vertical wind measurements on June 5, performed at the balloon and at a 10 m meteorology mast, both at the same height. It can be seen that the boundary layer wind follows the

expected -5/3 slope for both the stationary mast and the mobile balloon measurements as expected for isotropic 3d turbulence. The ballon-based spectrum shows an artifact due to the tumbling of the instrument, which however could be corrected for based on inertial measurements at the balloon anemometer. This comparison proofs that the balloon-based system accurately provides turbulence and turbulence fluxes as well as their profiles.

d) Sea surface microlayer (SML) measurements

The oceans are suggested to be a significant source for aerosol particles in the marine boundary layer. In this context not only the bulk water but especially the uppermost layer of the ocean, the sea surface microlayer (SML), might play an important role in the transport of matter to the atmosphere as it is the interface for all gaseous, liquid and particulate mass transfer between sea and air (e.g. [*Cunliffe et al.*, 2013]). The role of the SML is poorly understood to date. However, especially in the Arctic region the SML is supposed to be the origin of organic biopolymers, among them acidic polysaccharides, which are suggested to be transported into the atmosphere via bubble bursting processes ([*Orellana et al.*, 2011], [*Wilson et al.*, 2015]). These compounds might be important in aerosol and cloud processes, e.g. acting as ice nuclei (IN). We aim for a detailed chemical investigation of the SML and the bulk water with emphasis on studying the broad spectrum of carbohydrate composition and transparent exopolymer particles (TEP). Simultaneously, we will study the ice nucleating abilities of the SML and the bulk water to combine the chemical information with their potential physical effects. We will also collect data of possible biogeochemical drivers for the marine biopolymers.

The sampling of the SML was performed with an established glass plate technique (e.g. [*van*

Fig. 10: Surface microlayer (SML) sampling at the ice edge. Picture by Marcel Nicolaus, AWI.

Pinxteren et al., 2012]), while bulk seawater was sampled in glass bottles from a depth of ca. 1 m., see Fig. 10. All collected SML, and bulk water samples (for contrasting SML and bulk water) are stored and frozen. The chemical analysis will be performed after the cruise in the laboratories of TROPOS. A first analysis of TEP could be performed on board and showed positive signals in the SML and in the bulk aerosol particles. This is a strong indicator for possible air sea transfer of the TEP. A comprehensive qualitative and quantitative analysis will deliver information about the abundance of organic matter and especially the marine biopolymers in the diverse marine compartments. Enrichment factors will be calculated and their concentration in dependence of different environmental factors (wind speed, chlorophyll-a concentration) will be studied. Such data, together with a simultaneous analysis of the local aerosol particles are very limited to date. Finally, through a combination of the chemical information together with the detection of INPs in marine aerosol particles and seawater we will explore the hypothesis if local marine sources influence the Arctic ice nucleating (and cloud condensation) population.

Outlook

The summarized TROPOS activities during the Arctic expedition PS106 have successfully provided the complex atmospheric composition and the corresponding energy fluxes in a polar environment. A large variety of different aerosol, cloud and weather conditions were encountered which enables a number of interesting case studies, especially on cloud and ice formation. In the near future, radiation closure studies will be performed to see to what extend the observed tropospheric conditions explain the observed surface radiation budgets given our present capabilities of capturing the state of the troposphere and realistically desribe the radiative transfer. The in-situ aerosol and SML-sampling will show to what extend local sources of organic matter contribute to the polar aerosol distribution and its ability to form water droplets and ice particles. The occurrence of relatively warm ice clouds in the marine boundary layer and the role of local and long-range transported CCN and INP requires further analysis, also in combination with modelling activities in the framework of the TR 172. Also the role of humidity transports in cloud life cycles (not discussed here) will be further analysed. In general, the wealth of observations provides a valuable test-bed for model validation both for thermodynamic and microphysical parameter.

The POLARSTERN expedition PS106, especially the ice floe camp, also served successfully as a proof of concept for the "Multidisciplinary drifting Observatory for the Study of Arctic Climate" MOSAiC campaign, where POLARSTERN will be drifting for one year through the Central Arctic, accompanied by several aircraft activities from the AWI polar research aircrafts and the German HALO research aircraft. TROPOS will contribute to the POLARSTERN- and aircraft activities with a focus on aerosols, mixed-phase clouds, and the role of CCN and INP along a full year.

Acknowledgements

References

Baars, H., Seifert, P., Engelmann, R., Wandinger, U.: Target categorization of aerosol and clouds by continuous multiwavelength-polarization lidar measurements, *Atmos. Meas. Tech.*, 10, 3175-3201 p., doi:10.5194/amt-10-3175-2017

Budke & Koop 2015, *Atmos. Meas. Tech.*, doi: 10.5194/amt-8-689-2015.

Bühl, J., Seifert, P., Myagkov, A., and Ansmann, A.: Measuring ice- and liquid-water properties in mixed-phase cloud layers at the Leipzig Cloudnet station, *Atmos. Chem. Phys.*, 16, 10609-10620, doi:10.5194/acp-16-10609-2016, 2016.

Conen et al., 2012, Atmos. Meas. Tech., doi: 10: .5194/amt-5-321-2012.

Cunliffe M, et al. (2013) Sea surface microlayers: A unified physicochemical and biological perspective of the air–ocean interface. *Prog. Oceanogr.*, 109, 104-116.

Curry, J. A.: Interactions among turbulence, radiation and microphysics in Arctic stratus clouds. *J. Atmos. Sci.*, 43, 90–106, 1986.

Fletcher 1962, The Physics of Rainclouds, Cambridge University Press.

Engelmann, R., Kanitz, T., Baars, H., Heese, B., Althausen, D., Skupin, A., Wandinger, U., Komppula, M., Stachlewska, I. S., Amiridis, V., Marinou, E., Mattis, I., Linné, H., and Ansmann, A.: The automated multiwavelength Raman polarization and water-vapor lidar PollyXT: the neXT generation, *Atmos. Meas. Tech.*, 9, 1767-1784, https://doi.org/10.5194/amt-9-1767-2016, 2016.

Hanschmann, T., Deneke, H., Roebeling, R., and Macke, A.: Evaluation of the shortwave cloud radiative effect over the ocean by use of ship and satellite observations, *Atmos. Chem. Phys.*, 12, 12243–12253, 2012, doi:10.5194/acp-12-12243-2012

Illingworth, A.J., R.J. Hogan, E.J. O'Connor, D. Bouniol, J. Delanoë, J. Pelon, A. Protat, M.E. Brooks, N. Gaussiat, D.R. Wilson, D.P. Donovan, H.K. Baltink, G. van Zadelhoff, J.D. Eastment, J.W. Goddard, C.L. Wrench, M. Haeffelin, O.A. Krasnov, H.W. Russchenberg, J. Piriou, F. Vinit, A. Seifert, A.M. Tompkins, and U. Willén, 2007: Cloudnet. *Bull. Amer. Meteor. Soc.,* 88, 883–898, https://doi.org/10.1175/BAMS-88-6-883

Jeffries, M. O., Richter-Menge, J. A., and Overland, J. E. E.: Arctic Report Card 2012, http://www.arctic.noaa.gov/reportcard, 2012.

Kalisch, J. and Macke, A.: Radiative budget and cloud radiative effect over the Atlantic from ship-based observations, *Atmos. Meas. Tech.*, 5, 2391-2401, doi:10.5194/amt-5-2391-2012, 2012.

Kanitz, T., A. Ansmann, R. Engelmann, and D. Althausen (2013), North-south cross sections of aerosol layering over the Atlantic Ocean from multiwavelength Raman/polarization lidar during Polarstern cruises, *J. Geophys. Res.*, 118, 2642–2655, doi: 100 10.1002/jgrd.50273.

Macke, A., Seifert, P., Baars, H., Barthlott, C., Beekmans, C., Behrendt, A., Bohn, B., Brueck, M., Bühl, J., Crewell, S., Damian, T., Deneke, H., Düsing, S., Foth, A., Di Girolamo, P., Hammann, E., Heinze, R., Hirsikko, A., Kalisch, J., Kalthoff, N., Kinne, S., Kohler, M., Löhnert, U., Madhavan, B. L., Maurer, V., Muppa, S. K., Schween, J., Serikov, I., Siebert, H., Simmer, C., Späth, F., Steinke, S., Träumner, K., Trömel, S., Wehner, B., Wieser, A., Wulfmeyer, V., and Xie, X.: The HD(CP)[2] Observational Prototype Experiment (HOPE) – an overview, *Atmos. Chem. Phys.*, 17, 4887-4914, doi:10.5194/acp-17-4887-2017, 2017.

Madhavan, B. L., Deneke, H., Witthuhn, J., and Macke, A.: Multiresolution analysis of the spatiotemporal variability in global radiation observed by a dense network of 99 pyranometers, *Atmos. Chem. Phys.*, 17, 3317-3338, doi:10.5194/acp-17-3317-2017, 2017.

Orellana, M.V., et al. (2011), Marine microgels as a source of cloud condensation nuclei in the high Arctic, *Proc. Natl. Acad. Sci. USA*, 108, 13612–13617.

Overland, J. E., Wood, K. R., and Wang, M.: Warm Arctic–cold continents: Impacts of the newly open Arctic Sea, *Polar Res.*, 30, 15 787, doi:10.3402/polar.v30i0.15 787, 2011.

Shupe, M. D., Persson, P. O. G., Brooks, I. M., Tjernström, M., Sedlar, J., Mauritsen, T., Sjogren, S., and Leck, C.: Cloud and boundary layer interactions over the Arctic sea ice in late summer, *Atmos. Chem. Phys.*, 13, 9379-9399, 2013.

van Pinxteren M, et al. (2012) Chemical characterization of dissolved organic compounds from coastal sea surface microlayers. *Environ. Sci. Technol.*,46, 10455–10462, DOI: 10.1021/es204492b

Wendisch, M., M. Brückner, J. P. Burrows, S. Crewell, K. Dethloff, K. Ebell, Ch. Lüpkes, A. Macke, J. Notholt, J. Quaas, A. Rinke, and I. Tegen, 2017: Understanding causes and effects of rapid warming in the Arctic. *Eos*, 98, doi:10.1029/2017EO064803.

Wilson, T.W. et al. (2015)*, Nature,* 525, 234-238.

Towards an enhanced characterization of aerosol-cloud-dynamics-precipitation interaction with ground-based remote-sensing techniques

Patric Seifert, Holger Baars, Johannes Bühl, Hannes Griesche, Heike Kalesse, Martin Radenz, Ronny Engelmann, Albert Ansmann, Dietrich Althausen, Ulla Wandinger

**Eine Vielzahl komplexer Prozesse beeinflusst die Wechselwirkung zwischen Aerosol, Wolken, Dynamik und Niederschlag. Aerosole bestimmen die grundlegenden Eigenschaften von Wolken, da sie die nötigen Wolkenkondensations- und Eiskeime liefern. Dynamische Prozesse bestimmen die spätere zeitliche Entwicklung der Wolkenprozesse. Die Interaktion zwischen Aerosol, Wolken und Dynamik wiederum bestimmt die Art und Menge des gebildeten Niederschlages. Um die Rolle von Aerosolpartikeln und deren raumzeitlicher Variabilität in Wolkenprozessen besser verstehen zu können, wird am TROPOS daran gearbeitet, die für den Lebenszyklus einer Wolke verantwortlichen Prozesse möglichst vollständig mit bodengebundenen Fernerkundungsmethoden zu erfassen. Ziel ist die kontinuierliche Beobachtung der Atmosphäre in klimatologischen Schlüsselregionen, in denen konkrete Fragen zur Aerosol-Wolken-Niederschlags-Interaktion beantwortet werden können. Die für die Messungen nötigen Geräte sind in der mobilen LACROS Messstation zusammengefasst und umfassen unter anderem das am Institut entwickelte Lidarsystem Polly^{XT}, ein 35-GHz Wolkenradar, ein Dopplerlidar sowie passive Fernerkundung mittels Mikrowellenradiometer, Sonnenphotometer und einer Strahlungsmessstation. Im Rahmen dieses Artikels wird eine Reihe an Studien vorgestellt, die in den vergangenen Jahren zu einem verbesserten Verständnis der Aerosol-Wolken-Niederschlags-Wechselwirkung geführt haben. Diese umfassen neue Methoden zur Aerosol-Typisierung, zur Bestimmung von wolkenmikrophysikalischen Eigenschaften, zur Ableitung der Temperaturabhängigkeit von Eisbildung und Niederschlag, sowie zur Trennung von Partikelfallgeschwindigkeit und Vertikalwinden innerhalb von Wolken und Niederschlag.
Ziel der Arbeiten ist es, die neuentwickelten Techniken im Rahmen von Feldexperimenten in klimatologischen Schlüsselregionen einzusetzen, um so die Sensitivität von Wolken und Niederschlagsprozessen auf eine Variation der Aerosoleigenschaften untersuchen zu können. Neben Aktivitäten im stark mit Wüstenstaub und anthropogener Verschmutzung belasteten östlichen Mittelmeerraum, ist für 2018 der Start des Projektes Dynamics, Aerosol, Cloud and Precipitation Observations in the Pristine Environment of the Southern Ocean (DACAPO-PESO) geplant, das in Punta Arenas, Chile, dem südlichsten Festlandspunkt Südamerikas durchgeführt werden soll, um eine Kontrastierung der Wolkeneigenschaften der nördlichen und südlichen mittleren Breiten zu ermöglichen.**

Introduction

Clouds and aerosols are inseparably linked via complex pathways of interaction whose outcome defines the macroscopic properties of precipitation and radiation fields. On the one hand, aerosol particles are required as cloud condensation nuclei from which cloud droplets form. On the other hand, primary ice formation in the temperature range of heterogeneous freezing between 0 and approximately -40°C requires ice nucleating particles (INP) which need to be present in the aerosol reservoir. The ways in which aerosol and cloud particles interact are however also controlled by the air dynamics and thermodynamics of the atmospheric environment. Thermodynamics are considered to dominate the cloud microphysical properties because they control the amount of water vapour that is available for forming
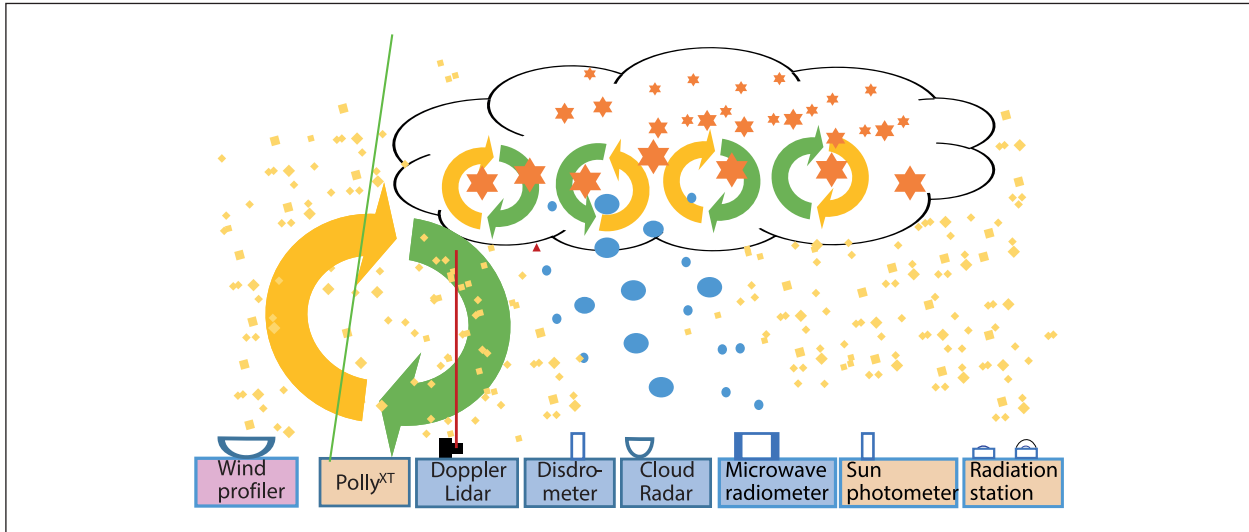
Fig. 1: Illustration of the different ground-based remote sensing instruments utilized in studies of TROPOS to characterize aerosol-cloud-dynamics-precipitation interaction.

liquid water or ice. This dominance makes it difficult to isolate aerosol-related effects in observations of cloud properties. Also the direct numerical simulation of aerosol-cloud-precipitation interaction processes is challenging because the spatiotemporal scales that are needed to be covered reach from the turbulent microscale up to the scale of precipitation systems. It is thus subject to observations to disentangle the signal of aerosol-cloud interaction processes from the dynamically and thermodynamically dominated observable meteorological features. The suite of remote-sensing instruments required for capturing aerosol and cloud microphysics and dynamics simultaneously is schematically shown in Fig. 1.

This article aims on presenting the progress that was achieved in the last years at TROPOS to investigate aerosols, clouds, precipitation, atmospheric dynamics, and their interaction simultaneously with ground-based remote sensing techniques. First, the utilized instrumentation and data analysis tools involved in the scheme illustrated in Fig. 1 are introduced. In subsequent sections, studies of TROPOS that address the retrieval of cloud and aerosol properties, atmospheric dynamics, and their interaction are presented. The article is concluded with an outlook.

Instrumentation

To enable the simultaneous, vertically resolved observation of aerosols, clouds, precipitation and atmospheric dynamics, a wide range of active remote sensing instruments is required. Motivated by this need, the mobile multi-instrument platform Leipzig Aerosol and Cloud Remote Observations System – LACROS – was established at TROPOS.

LACROS comprises a unique set of active and passive remote sensing instruments, which are available for deployment in field campaigns. The active remote sensing branch spans the wavelength range from the UV to microwave radiation which is covered with multiwavelength Raman-polarization lidar Polly^{XT} [*Baars et al.*, 2016], a Ceilometer Jenoptik CHM15kx, a Doppler lidar Halo Photonics Streamline, and a 35-GHz cloud radar Mira-35. Passive instrumentation that helps to interpret the active remote measurements consists of a Cimel Sun photometer, a microwave radiometer HATPRO, an all-sky imager, as well as visible and infrared radiometers and spectrometers. Meteorological surface data and radiosondes are available in addition.

Besides the mobile instrumentation, methodological developments in terms of retrievals for cloud microphysical properties are employed in the stationary lidar system MARTHA, which is installed in the upper floor of the main building of TROPOS. MARTHA provides 30 W of total laser power at 355, 532, and 1064 nm wavelength, and sufficient workspace for experimental lidar setups. It currently contains multiple detection channels for the acquisition of co- and cross-polarized components of the returned elastic and Raman-backscatter signals at two different fields of view.

An auxiliary instrument used by TROPOS for studies of atmospheric vertical motions, even within precipitation, is a 482-MHz radar wind profiler (RWP). The RWP is operated by the German Meteorological Service (DWD) at the Meteorological Observatory Lindenberg - Richard-Aßmann Observatory (MOL-RAO) in Lindenberg, Germany, where cloud radar, lidar and microwave radiometers are available, as

well, to allow for studies similar to those possible with LACROS.

Comparable instrumentation to the one of LACROS is also provided by the Atmospheric Radiation Measurement (ARM) facilities of the Unites States (U.S.) Department of Energy (DOE). Techniques that were developed for LACROS are thus to a large extent also applicable to ARM site observations, which was utilized in one of the studies presented below.

Data processing

The datasets recorded by the LACROS instrument suite are processed entirely on a single server. Data of the Polly[XT] lidar are processed within PollyNet that provides quality-assured automatically derived profiles of particle backscatter and extinction coefficients [*Baars et al.*, 2016]. Synergistic retrievals that are based on data of cloud radar, lidar, microwave radiometer, Doppler lidar radiation measurements and ancillary systems are implemented into the Cloudnet processing chain [*Illingworth et al.*, 2007]. The Cloudnet framework is in addition the basis for novel retrievals that have been developed by TROPOS or in collaboration with partners within the Aerosol, Clouds and Trace Gases Research InfraStructure (ACTRIS) project in which TROPOS has a leading role.

For fast access to the measurement data and retrieved products, the real-time data analysis and display software package LARDA (Lidar and Radar Data Analyzer, http://larda.tropos.de) was recently developed at TROPOS. LARDA provides on the one hand an online interface to plot arbitrary subsets of recorded observables, on the other hand it provides

a Python-based Application Programming Interface (API) for statistical analyses of the LACROS observations.

In the following, applications of the above-mentioned instrumentation and algorithms for the characterization of aerosol-cloud-dynamics-precipitation interaction are introduced.

Target categorization of aerosol and clouds by continuous multiwavelength-polarization lidar measurements

As explained above, it is essential to observe aerosol and clouds preferably in 4-D, but realistically round the clock and vertically resolved in order to better quantify the spatiotemporal distribution of aerosol and clouds as well as to improve the determination of their interaction. A step towards approaching this goal was achieved in a study of *Baars et al.* [2017] in the frame of HD(CP)[2]. Here, calibrated signals at 532 and 1064 nm wavelength and the depolarization ratio from the multiwavelength lidar Polly[XT] are used to categorize primary aerosol but also clouds in high temporal and spatial resolution. Automatically derived particle backscatter coefficient profiles in low temporal resolution (30 min) are applied to calibrate the lidar signals. From these calibrated lidar signals, new atmospheric parameters in temporally high resolution (quasi-particle-backscatter coefficients) are derived. By using thresholds obtained from multiyear, multisite EARLINET (European Aerosol Research Lidar Network) measurements, four aerosol classes (small; large, spherical; large, non-spherical; mixed, partly nonspherical) and several cloud classes (liquid, ice) are defined. Thus, particles are classified
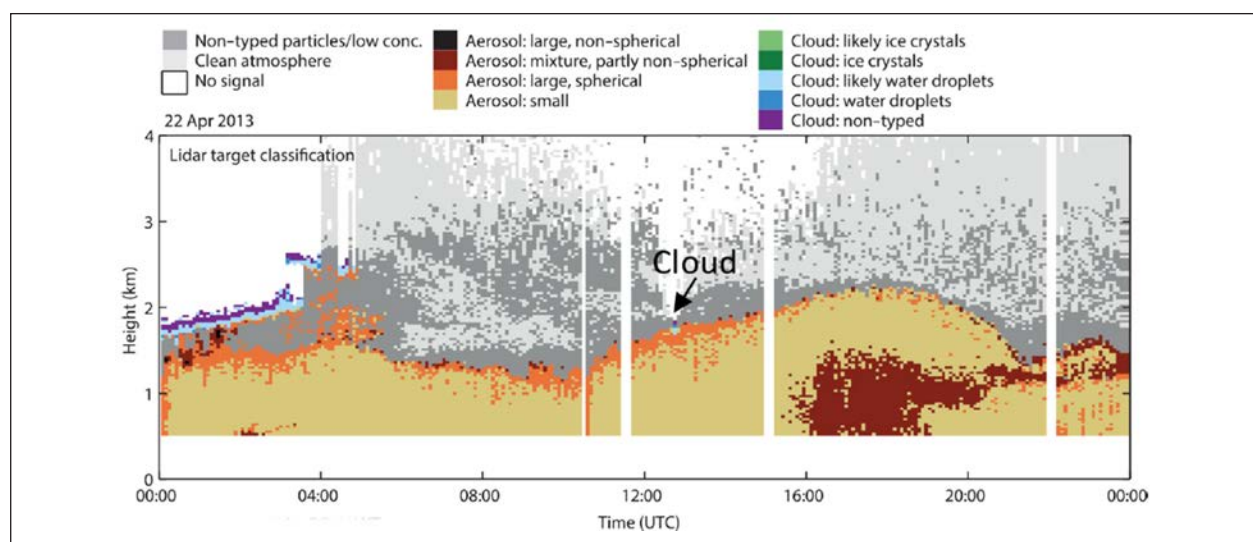
Fig. 2: Lidar-based aerosol and cloud target categorization for 24 hours of continuous observations performed on 21 April 2013 in Krauthausen, Germany.

by their physical features (shape and size) instead of by their source. Figure 2 provides an example of the lidar-based aerosol and cloud classification scheme, based on 24 hours of continuous observations of Polly[XT] on 22 April 2013 in Krauthausen, Germany. These observations were part of the HD(CP)[2] Observational Prototype Experiment HOPE [*Macke et al.*, 2017]. It can be seen that large, non-spherical particles where mixed from the ground into the boundary layer in the afternoon of the day.

The retrieval of the particle type and the underlying automatic, continuous retrieval of the aerosol optical properties builds the basis for enhanced retrievals of aerosol microphysical properties. One example is a method for the estimation of profiles of INP and CCN from measurements of the particle backscatter coefficient and depolarization ratio that was developed by *Mamouri and Ansmann* [2016].

Relationship between temperature and apparent shape of pristine ice crystals derived from polarimetric cloud radar observations

Similar to aerosols as discussed above, also cloud hydrometeors can be distinguished by means of their shapes. This was recently demonstrated in studies of *Myagkov et al.* [2016a, 2016b] who presented first quantitative estimations of apparent ice particle shape at the top of mixed-phase-topped clouds. The analysed ice particles were formed under mixed-phase conditions in the presence of

Fig. 3: Temperature dependence of polarizability ratios, i.e., apparent particle shapes, for ice crystals grown in the free-fall chamber (blue filled circles) and for ones located close to tops of mixed-phase clouds, retrieved from MIRA-35 cloud radar observations (red filled circles). Note that $\rho_e > 1$ corresponds to prolate particles and $\rho_\varepsilon < 1$ corresponds to oblate particles. Vertical red bars represent 1 standard deviation of observed polarizability ratios. Data from the free-fall chamber (Takahashi et al., 1991) were provided by Prof. Takahashi, Hokkaido University of Education, Sapporo, Japan.

supercooled liquid water in the temperature range from −20 to −3 °C. The retrieval is based on polarizability ratios of ice particles measured by a Ka-band 35-GHz cloud radar MIRA-35 with hybrid polarimetric configuration. The polarizability ratio is a function of the geometrical axis ratio and the dielectric properties of the observed hydrometeors and thus is a measure of particle shape. For the study, 22 cases observed during the ACCEPT (Analysis of the Composition of Clouds with Extended Polarization Techniques) field campaign [*Myagkov et al.*, 2016b] performed in fall 2014 at Cabauw Experimental Site for Atmospheric Research (CESAR) observatory in Cabauw, the Netherlands, were used. Polarizability ratios retrieved for cloud layers with cloud-top temperatures of ~−5, ~−8, ~−15, and ~−20 °C were 1.6, 0.9, 0.6, and 0.9, respectively. Such values correspond to prolate, quasi-isotropic, oblate, and quasi-isotropic particles, respectively. Data from a free-fall chamber were used for the comparison. A good agreement of detected apparent shapes with well-known shape-temperature dependencies observed in laboratories was found, as is shown in Fig. 3. Polarizability ratios used for the analysis were estimated for areas located close to the cloud top, where aggregation and riming processes do not strongly affect the ice particles. From the study, it was concluded that, in microwave scattering models, ice particles detected in these areas, can be assumed to have pristine shapes. It was also found that even slight variations of ambient conditions at the cloud top with temperatures warmer than ~−5 °C can lead to rapid changes of ice crystal shape.

Retrievals of microphysical properties of liquid water clouds. New approach: dual field of view depolarization lidar

Knowledge about the shape of cloud hydrometeors, as it can be retrieved with the technique presented in the previous section, is of value for the understanding of mixed-phase cloud processes. Nevertheless, for the quantification of mixed-phase cloud particles, knowledge about the mass and number of involved hydrometeors is required. This includes both, the liquid as well as the ice phase. Especially at temperatures of above -25°C the liquid and the ice phase are strongly linked to each other, because it is meanwhile widely accepted that heterogeneous ice formation in this temperature range does occur entirely from liquid-phase particles. Liquid water cloud microphysical properties can be retrieved with the Dual Field of View (DFOV) Raman lidar from TROPOS [*Schmidt et al.*, 2014]. However, this technique can only be applied during night-time and with long averaging periods, and it requires sophisticated

Fig. 4: (b) Application of three different lidar methods for the retrieval of liquid cloud microphysical properties for a case study (Fig. a) observed with the TROPOS lidar system MARTHA on 2 April 2017 in Leipzig.

optical setups, which are so far only implemented into the stationary lidar MARTHA. In 2016 a Single-FOV (SFOV) depolarization lidar procedure to obtain these microphysical properties was additionally implemented. Based on experiences made with both techniques, a new DFOV depolarization lidar approach was developed, implemented and tested in the MARTHA setup during summer 2017. This new approach is also available for daytime observations and can in principle also be implemented into the mobile PollyXT lidar systems. As is shown in Fig. 4, a comparison between the three lidar methods in terms of the microphysical properties of liquid water clouds reveals good agreement in the DFOV Raman lidar and the DFOV depolarization lidar approaches. A rather weak performance was found for the SFOV depolarization lidar approach that requires too many a-priori information for the retrieval of liquid cloud microphysical properties. In conclusion, the new DFOV depolarization lidar approach was found to be a promising tool for the observation of liquid-cloud microphysical properties during day- as well as during night-time.

Improving the detection of supercooled liquid water in optically thick mixed-phase clouds

The maximum lidar observation range is determined by complete signal attenuation at a penetrated optical depth of about three. Thus, when penetrated optical depths reach higher values, the above-mentioned retrieval for liquid-cloud properties cannot be applied anymore. The characterization of the entire vertical profile of phase-partitioning in mixed-phase clouds is thus a challenge which can be addressed by synergistic profiling measurements with ground-based polarization lidars and cloud radars. While lidars are sensitive to small particles and can thus detect supercooled liquid layers (SCL), cloud radar returns are dominated by larger particles (like ice crystals). In contrast, cloud radars are able to penetrate multiple liquid layers and can thus be used to expand the identification of cloud phase to the entire vertical column beyond the lidar extinction height, if morphological features in the radar Doppler spectrum can be related to the existence of SCL. Relevant spectral signatures such as bimodalities and spectral skewness can be
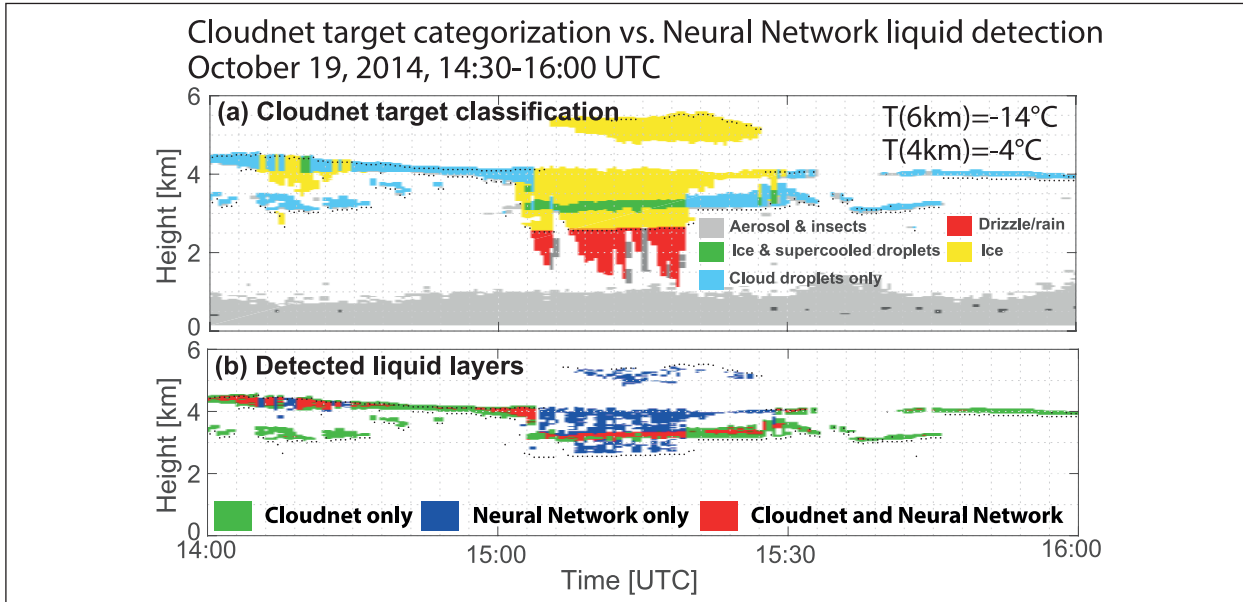
Fig. 5: Evaluation of the performance of (a) Cloudnet and (b) a Neural Network Approach to identify liquid clouds. Cloudnet performs well in thin cloud layers, e.g., between 14:30 and 15:00 UTC. The neural network approach shows good performance in thick, multi-layer clouds, e.g., between 15:00 and 15:30 UTC.

related to cloud phase by training a neural network appropriately in a supervised learning scheme, with lidar measurements functioning as supervisor. The neural network output (prediction of SCL location) derived using cloud radar Doppler spectra can be evaluated with several parameters such as liquid water path (LWP) detected by microwave radiometer and (liquid) cloud base detected by lidar. The technique has been previously tested on data from DOE-ARM instruments in Barrow, Alaska and is here utilized for observations from LACROS during the ACCEPT field experiment. Figure 5(b) shows that the neural network approach enhances the liquid-phase retrieval in optically thick mixed-phase cloud systems, as it was the case between 15:00 and 15:30 UTC. In case of single-layer liquid clouds (e.g., Fig. 5: 14:30 to 15:00 UTC), the original Cloudnet approach (Fig. 5a) was however found to perform better because the cloud radar alone is not very sensitive to these thin liquid clouds. Thus, the combination of Cloudnet and the neural network approach can well provide information about the existence of liquid water layers even under conditions of full attenuation of the lidar signal, which is a step toward an extended classification of deep mixed-phase cloud processes.

Understanding rapid changes in phase partitioning between cloud liquid and ice in stratiform mixed-phase clouds

The formation of pristine ice crystals within layers of supercooled liquid water is the only prerequisite for a large number of complex, inter-related mixed-phase cloud processes that finally determine the properties of precipitation reaching the surface. Understanding phase transitions in mixed-phase clouds is of great importance because the hydrometeor phase controls the lifetime and radiative effects of clouds. In high latitudes, these cloud radiative effects have a crucial impact on the surface energy budget and thus on the evolution of the ice cover. For a springtime low-level mixed-phase stratiform cloud case from Barrow, Alaska, a unique combination of instruments and retrieval methods was combined with multiple modelling perspectives to determine key processes that control cloud phase partitioning [Kalesse et al., 2016]. The interplay of local cloud-scale versus large-scale processes was considered. Rapid changes in phase partitioning were found to be caused by several main factors. Major influences were the large-scale advection of different air masses with different aerosol concentrations and humidity content, cloud-scale processes such as a change in the thermodynamical coupling state, and local-scale dynamics influencing the residence time of ice particles. Other factors such as radiative shielding by cirrus and the influence of the solar cycle were found to only play a minor role for the specific case study (11-12 March 2013). From this study it can be concluded that for an even better understanding of cloud phase transitions, observations of key aerosol parameters such as profiles of cloud condensation nuclei and ice nuclei concentration are desirable. As mentioned above, a step towards fulfilling this requirement was recently done

by means of a study of *Mamouri and Ansmann* [2016] who showed that profiles of concentrations of INP and CCN can be estimated from lidar measurements of aerosol optical properties.

Measuring ice- and liquid-water properties in mixed-phase cloud layers at the Leipzig Cloudnet station

Long-term observations with LACROS provide the possibility to derive statistics of certain key aspects of clouds. In a study of *Bühl et al.* [2016], a Cloudnet data set collected at Leipzig was analysed with special focus on mixed-phase layered clouds. Goal was to investigate the amount of ice formed as a function of temperature in the temperature regime of heterogeneous freezing. An overview of the results presented by *Bühl et al.* [2016] is shown in Fig. 6. Basic input parameters for the analysis were the liquid- and ice-water content which were derived together with vertical motions of ice particles falling through the liquid cloud base. The ice water content produced in the supercooled liquid clouds was found to depend strongly on cloud top temperature (Fig. 6a). Also the ice mass flux (Fig. 6b) was calculated by combining measurements of ice-water content and particle Doppler velocity. The efficiency of heterogeneous ice formation and its impact on cloud lifetime could thus be estimated for different cloud-top temperatures by relating the ice mass flux to the liquid water content at cloud top (Fig. 6c). Cloud radar measurements of linear depolarization ratio (LDR), shown as fill colour in Fig. 6., and Doppler velocity (not shown) indicate that ice crystals which formed in the analysed mixed-phase cloud layers with a geometrical thickness of less than 350 m are mostly pristine when they fall out of the cloud.

Constraining the microphysical processes involved in precipitation formation

The formation of precipitation at mid latitudes is well known to occur via ice-phase processes. Only via the Wegener-Bergeron-Findeisen process, which describes the efficient growth of ice crystals at relative humidities below liquid water saturation, hydrometeors can grow to sizes that lead to significant amounts of precipitation, i.e., so-called cold rain. Warm-rain formation at mid-latitudes is limited to drizzle because the cloud thermodynamical processes are too weak to produce large raindrops solely by coagulation of cloud droplets.

One study at TROPOS thus aimed at the investigation of the relevance of different heterogeneous liquid-dependent freezing processes for the total amount of precipitation observed with LACROS. Measurements of the vertically-pointing 35-GHz cloud radar Mira-35 and and the optical disdrometer were used to identify the cloud vertical extent and the amount of precipitation reaching the ground, respectively. A quasi-continuous dataset for the period from August 2011 to March 2014 obtained in Leipzig was analysed.

Figure 7 shows the statistics derived for Leipzig, Germany, and Limassol, Cyprus. It was found that precipitation formation without deposition freezing and homogeneous freezing can still lead to high precipitation rates of about 20 mm / hour. Up to about 40% of the time the total amount the precipitation formed at cloud-top temperatures between -25 and 0 °C. On average, the precipitation intensity caused by clouds with top temperatures between -25 and 0 °C was 3 mm per hour which is also similar to the average total precipitation intensity of all cold-rain processes. Peak precipitation rates of 100 mm per hour and more were restricted to events of deep-convection
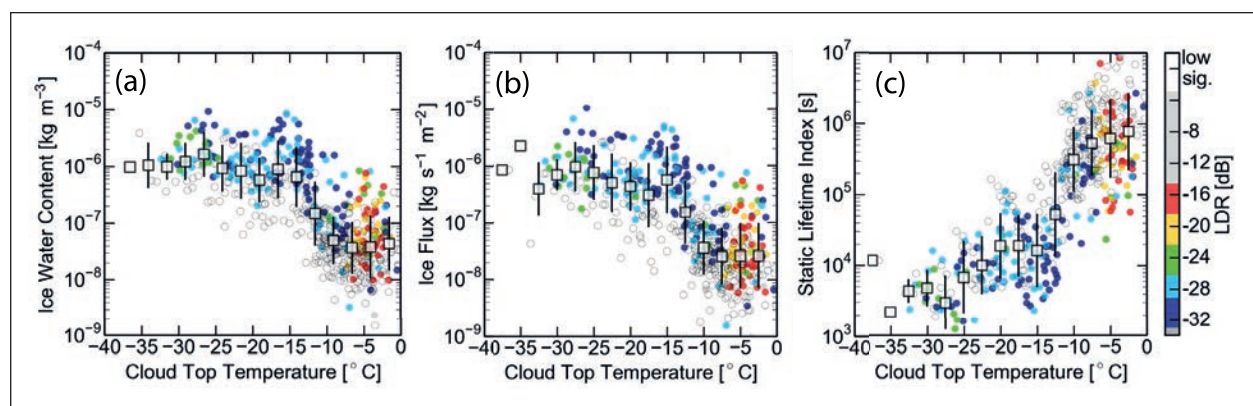
Fig. 6: Long-term statistics of heterogeneous ice formation in thin supercooled liquid cloud layers for a 3-year dataset observed with LACROS in Leipzig. Shown are (a) ice water content, (b) ice mass flux, and (c) static lifetime index as a function of cloud top temperature. Color shades show the LDR of the observed ice particles, which is a proxy for particle shape.
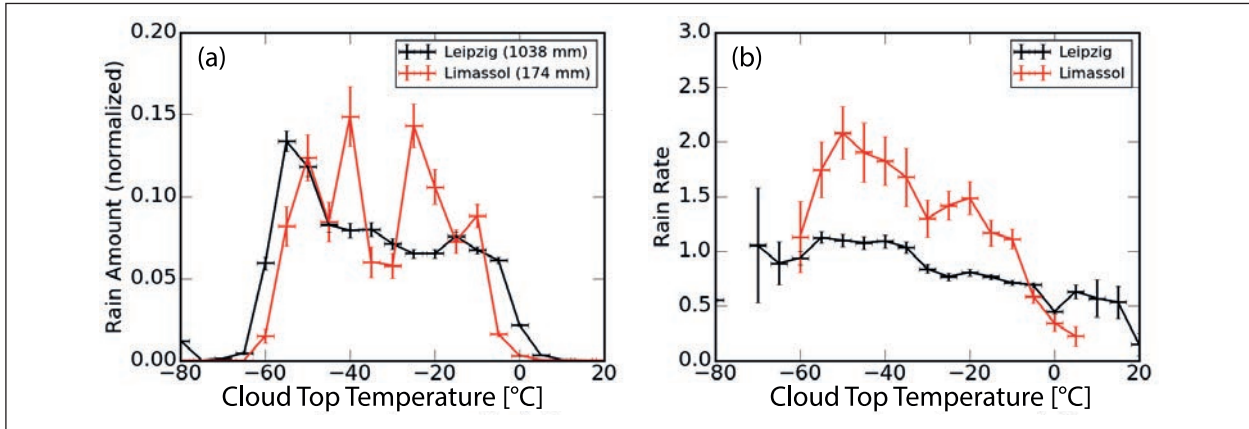
Fig. 7: Relationship of (a) the total rain amount and (b) rain rate as a function of cloud top temperature derived from 3 years of observations in Leipzig and 1-year of observations in Limassol.
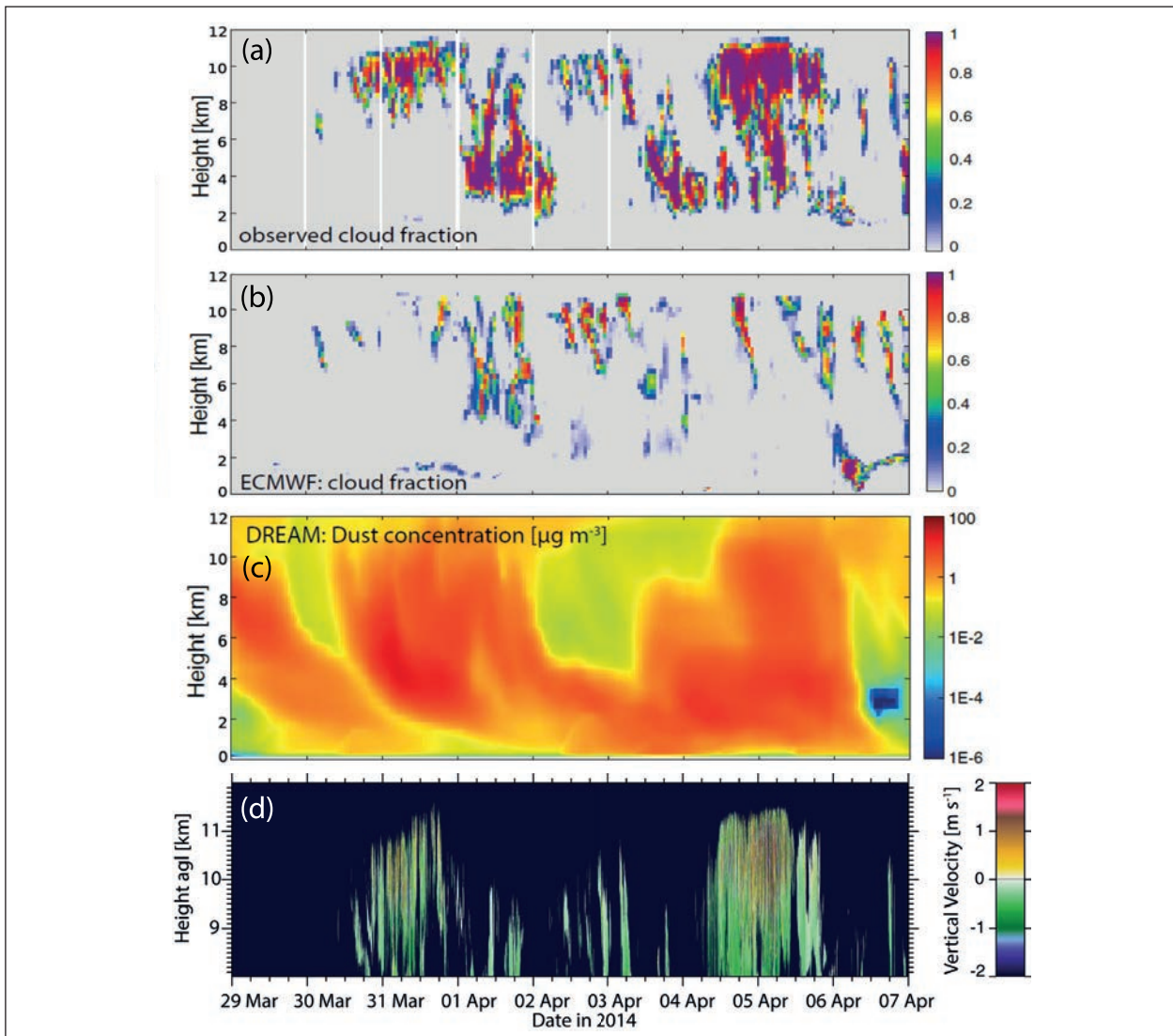
Fig. 8: Cloud observations at Leipzig during a strong dust outbreak that occurred from 29 March to 07 April 2014. Shown are (a) the cloud fraction observed with LACROS, (b) the cloud fraction predicted with the IFS model of ECMWF, (c) the modelled dust concentration, and (d) the vertical velocity field for the height range between 8 and 12 km. Especially on 29 March and on 4 April the forecast of cirrus clouds showed strong deficiencies in comparison to the observations, which correlates with high dust loads and a strong variability in vertical velocities at cloud level.

that usually reaches the tropopause level and thus cloud-top temperatures of -50°C and below. The derived high fraction of precipitation caused solely by liquid-dependent heterogeneous freezing processes implies an important role of the concentration and type of ice nuclei in the formation of precipitation.

Relationship between aerosol load and the forecast skill of weather prediction models

Mineral dust contributes strongest to the total atmospheric aerosol burden, but it also has a high spatio-temporal variability. Operational numerical weather prediction (NWP) models, in turn, currently do consider neither the spatiotemporal variability of the aerosol burden nor its semi-direct and indirect aerosol effects. Even the direct aerosol effects on the radiation field are only based on, if at all, a seasonally averaged aerosol climatology. Hence, short-term variations in the atmospheric aerosol burden can lead to large deviations between NWP model forecasts and the actual atmospheric state.

One study of TROPOS that considers LACROS observations and the model evaluation capabilities of Cloudnet demonstrates to which extent the presence of Saharan dust can cause observable deficiencies in atmospheric model predictions. The investigated time period covers 8 days in March/April 2014 during which both, dust-free and dust-laden conditions were present over Central Europe. From the LACROS observations model-relevant parameters such as cloud fraction and ice and liquid water content were derived with Cloudnet. These parameters were scaled to the respective grids of the NWP models ECMWF-IFS, COSMO-DE, and COSMO-EU in order to enable an evaluation of the NWP forecasts against the observations.

Figure 8 presents an overview of the meteorological conditions that were present at Leipzig between 29 March and 7 April 2014. As can be seen from Fig. 8c, Saharan dust was predicted by the Dust Regional Aerosol Model (DREAM) to reach up to 12 km height. Especially on 29 March and 04 April, when high concentrations of mineral dust occurred at high altitudes, the observed cloud fraction (Fig. 8a) and the cloud fraction modeled with ECMWF-IFS (Fig. 8b) deviate strongly from each other. This suggests a lack of the models to forecast cirrus clouds under strongly dust-laden conditions. Nevertheless, the explanation for that was found to be two-fold. First, the presence of large amounts of Saharan dust up to the tropopause provided ice nuclei concentrations that were much higher than it is

assumed in the cloud parameterizations of the NWP models. Second, strong turbulence was observed in the cirrus layer, which was apparently not resolved by the NWP models. Updrafts of up to 4 m s^{-1} were detected which can lead to strong supersaturation and thus to more efficient ice nucleation (Fig. 8d).

Separation of vertical air motion and fall velocities of hydrometeors

Vertical air motions strongly determine the microphysical evolution of clouds and precipitation. Nevertheless, a continuous, ground-based observation of vertical air motion within clouds is hardly achievable because usually the velocity field is masked by the velocity of falling cloud hydrometeors. The collaborative study of TROPOS and DWD Combined Observations with Lidar, RAdar and WInd profiler (COLRAWI), aimed on utilizing measurements of a 482-MHz RWP, collocated with a Cloudnet station (Ceilometer, 35 GHz cloud radar and microwave radiometer) to measure vertical motions inside of clouds over Lindenberg, Germany. To remove the influence of falling particles in the wind profiler signal, a correction scheme using the Doppler spectra of the cloud radar and radar wind profiler was developed. To demonstrate the capabilities of the novel algorithm, Fig. 9 presents a case study of a warm front passage that was observed at Lindenberg on 19 June 2015. Shown are in (a) and (b) the vertical velocities observed with the RWP and the cloud radar respectively. By combining both observations, the vertical air motion (c) and particle terminal velocity (d) can be separated from each other. This technique thus allows direct measurements of in-cloud vertical air velocity by means of ground-based remote sensing. The method can be incorporated into the Cloudnet software and can be operationally applied for further studies of aerosol-cloud-dynamics interaction and model evaluation.

A Monte Carlo simulation with artificial spectra was used to quantify the accuracy of the correction procedure. The mean bias in the velocity estimate was found to be around 0.1 m s^{-1}. The benefit of this dataset is twofold: Firstly, long term statistics can be assembled. It was found, that the mean vertical velocity of clear air and within clouds concurs within the measurement uncertainty. But the standard deviation within clouds is slightly higher than in the clear atmosphere. Secondly, the dynamic field associated with single clouds can be investigated in detail providing more insight into aerosol-cloud-dynamics interaction.
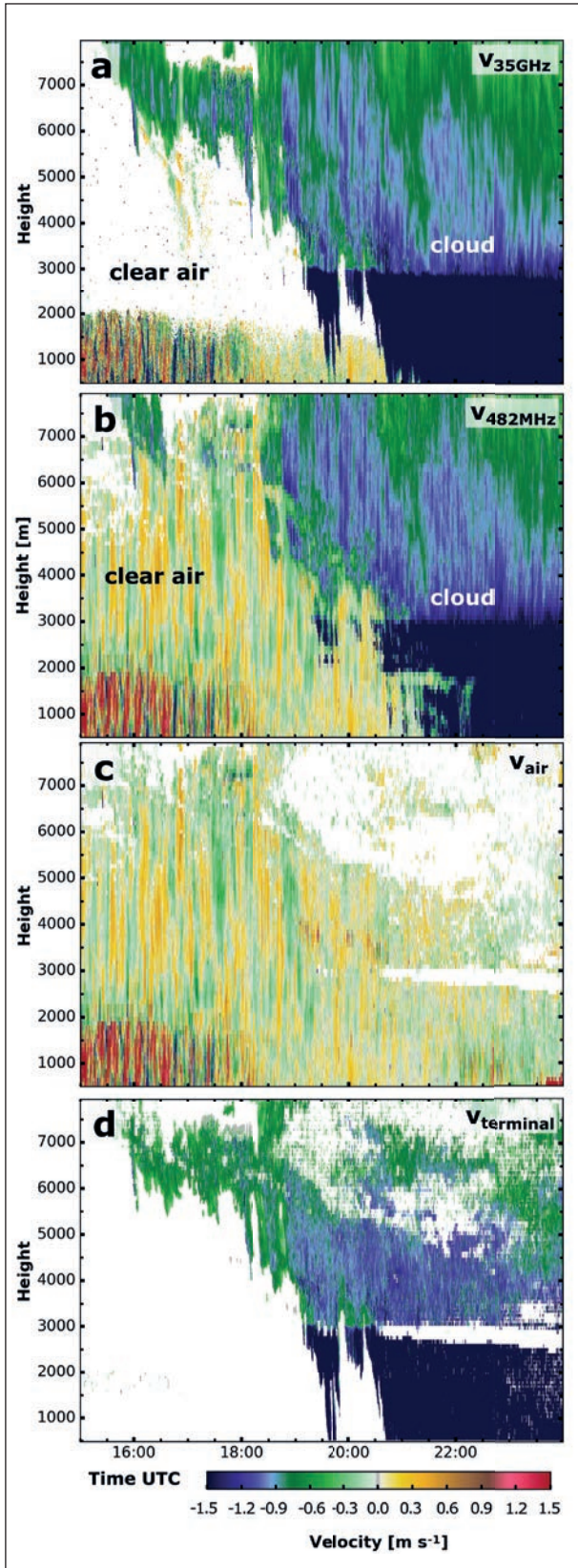
Fig. 9: Observation of vertical-velocity fields during the passage of a warm front over Lindenberg, Germany, on from 15:00-24:00 UTC. Shown are (a) raw observations of a 35-GHz cloud radar, (b) raw observations of a 482-MHz wind profiler and the retrieved fields of (c) vertical air velocity and (d) terminal fall velocity of hydrometeors.

Summary & Outlook

During the last years, considerable progress was achieved at TROPOS in profiling aerosol-cloud-dynamics-precipitation interaction. All presented studies together demonstrate the focused efforts to be once able to perform a closure between the microphysics of aerosols, clouds, and precipitation, taking into account the atmospheric dynamical and thermodynamical properties as additional constraints.

The presented techniques and approaches rely to a large extent on the availability of long-term datasets. Achieving such qualitatively high data record is another focus of the research at TROPOS, realized by means of the continuous observations with the Polly[XT] lidar systems and the LACROS instrument suite, which incorporate steady instrument improvements.

Finally, by performing long-term field experiments in climatological key regions, valuable datasets are derived for the investigation of defined aspects of aerosol-cloud-dynamics-precipitation interaction. E.g., motivated by our lidar-only observations of strong contrasts in heterogeneous ice formation efficiency between northern-hemispheric Leipzig (Germany) and southern hemispheric Punta Arenas, Chile, the project Dynamics, Aerosol, Cloud and Precipitation Observations in the Pristine Environment of the Southern Ocean (DACAPO-PESO) will be conducted from fall 2018 to fall 2019 in a collaboration with the University of Magallanes, Punta Arenas, Chile. A major goal of this field experiment is to derive an aerosol and cloud dataset for one of the most pristine regions on Earth. This will enable to study the contrasts between the rather polluted northern-hemispheric datasets of TROPOS, e.g., the ones from Limassol, Cyprus, or Leipzig, and pristine conditions in order to enhance knowledge on the role of aerosols on cloud and precipitation processes.

References

Baars, H., P. Seifert, R. Engelmann, and U. Wandinger (2017), Target categorization of aerosol and clouds by continuous multiwavelength-polarization lidar measurements, *Atmos. Meas. Tech.*, *10*(9), 3175-3201, doi: doi:10.5194/amt-10-3175-2017.

Baars, H., T. Kanitz, R. Engelmann, D. Althausen, B. Heese, A. Ansmann, and U. Wandinger (2016), Polly[NET]: An emerging network of automated Raman-polarization lidars for continuous aerosol profiling paper presented at OSA Light, Energy and the Environment Congress 2016, Optical Society of America (OSA), Leipzig, Germany, 14-17 November 2016.

Bühl, J., P. Seifert, A. Myagkov, and A. Ansmann (2016), Measuring ice- and liquid-water properties in mixed-phase cloud layers at the Leipzig Cloudnet station, *Atmos. Chem. Phys.*, *16*(16), 10609-10620, doi: doi:10.5194/acp-16-10609-2016.

Kalesse, H., G. d. Boer, A. Solomon, M. Oue, M. Ahlgrimm, D. Zhang, M. D. Shupe, E. Luke, and A. Protat (2016), Understanding Rapid Changes in Phase Partitioning between Cloud Liquid and Ice in Stratiform Mixed-Phase Clouds: An Arctic Case Study, *Mon. Wea. Rev.*, *144*(12), 4805-4826, doi: 10.1175/mwr-d-16-0155.1.

Macke, A., P. Seifert, H. Baars, C. Barthlott, C. Beekmans, A. Behrendt, B. Bohn, M. Brueck, J. Bühl, S. Crewell, T. Damian, H. Deneke, S. Düsing, A. Foth, P. Di Girolamo, E. Hammann, R. Heinze, A. Hirsikko, J. Kalisch, N. Kalthoff, S. Kinne, M. Kohler, U. Löhnert, B. L. Madhavan, V. Maurer, S. K. Muppa, J. Schween, I. Serikov, H. Siebert, C. Simmer, F. Späth, S. Steinke, K. Träumner, S. Trömel, B. Wehner, A. Wieser, V. Wulfmeyer, and X. Xie (2017), The HD(CP)2 Observational Prototype Experiment (HOPE) – an overview, *Atmos. Chem. Phys.*, *17*(7), 4887-4914, doi: 10.5194/acp-17-4887-2017.

Mamouri, R., and A. Ansmann (2016), Potential of polarization lidar to provide profiles of CCN- and INP-relevant aerosol parameters, *Atmos. Chem. Phys.*, *16*(9), 5905-5931, doi: doi:10.5194/acp-16-5905-2016.

Myagkov, A., P. Seifert, M. Bauer-Pfundstein, and U. Wandinger (2016a), Cloud radar with hybrid mode towards estimation of shape and orientation of ice crystals, *Atmos. Meas. Tech.*, *9*(2), 469-489, doi: doi:10.5194/amt-9-469-2016.

Myagkov, A., P. Seifert, U. Wandinger, J. Bühl, and R. Engelmann (2016b), Relationship between temperature and apparent shape of pristine ice crystals derived from polarimetric cloud radar observations during the ACCEPT campaign, *Atmos. Meas. Tech.*, *9*(8), 3739-3754, doi: doi:10.5194/amt-9-3739-2016.

The Cyprus Aerosol, Clouds and Rain Experiment (CyCARE)

Johannes Bühl[1], Patric Seifert[1], Ronny Engelmann[1], Albert Ansmann[1], Rodanthi Mamouri[2], Argyro Nisantzi[2], Bernadett Weinzierl[3], Volker Freudenthaler[4]

[1] Leibniz Institute for Tropospheric Research (TROPOS), Leipzig, Germany
[2] Cyprus University of Technology, Limassol, Cyprus
[3] LMU Munic, Munic, Germany
[4] University of Vienna, Vienna, Austria

Das östliche Mittelmeer ist ein idealer Ort für Studien der komplexen Wechselwirkung zwischen Aerosolen und Wolken. Aus diesem Grund hat TROPOS eine einjährige Messkampagne mit der kombinierten Lidar/Radar Plattform LACROS in Limassol (Zypern) von Oktober 2016 bis April 2018 durchgeführt. Andere Forschungsgruppen schlossen sich der Kampagne für eine intensive Messphase im April 2017 an. Die Messkampagne repräsentiert den Beginn einer intensiven Langzeitkooperation von TROPOS mit der Technischen Universität Limassol (CUT-TEPAK).

Introduction

Cyprus is a hot spot for observations of transport of anthropogenic and natural emissions like dust and biomass burning aerosol. It is hence an ideal place for investigation of the complex interaction between aerosols and clouds. In the course of the BACCHUS project, a historic dust storm was observed on Cyprus with never before observed values of aerosol optical thickness [*Mamouri et al.*, 2016]. A further motivation to closely investigate the atmospheric patterns of cloud and rain patterns in that region is that future climate projections indicate a strong decrease of precipitation properties in the whole eastern Mediterranean area [*Boucher et al.*, 2014] In the framework of the BACCHUS project, TROPOS performed a field campaign at Limassol, Cyprus together with other partners, partly from the BACCHUS consortium.

Methods

The Leipzig Aerosol and Cloud Remote Observation System (LACROS) was shipped to Limassol in October 2016 and has been performing continuous observations of aerosols, clouds and atmospheric dynamics together with ground-based radiation measurements. The LACROS station consists of a MIRA-35 cloud radar, a Polly[XT] Raman lidar and a HATPRO microwave radiometer. Up to now, a one-year synergistic Cloudnet dataset has been derived. During the campaign, special emphasis was laid on the determination of the microphysical composition of clouds. For this purpose, regular cloud radar scans were performed in order to measure particle shapes [*Myagkov et al.*, 2016].

Example case studies

An example measurement of cloud mixing with desert dust is shown in Fig. 1. The measurements originate from LACROS and were combined using the synergistic target categorization mask of Cloudnet [*Illingworth et al.*, 2007] and the new multi-wavelength-lidar based EARLINET aerosol classification [*Baars et al.*, 2017].

In April 2017, an intensive operation period (IOP) was performed. During this month, a variety of aerosol observations were performed with ground-based in-situ instruments (TROPOS), unmanned aerial vehicles (Cyprus Institute, Nicosia) and
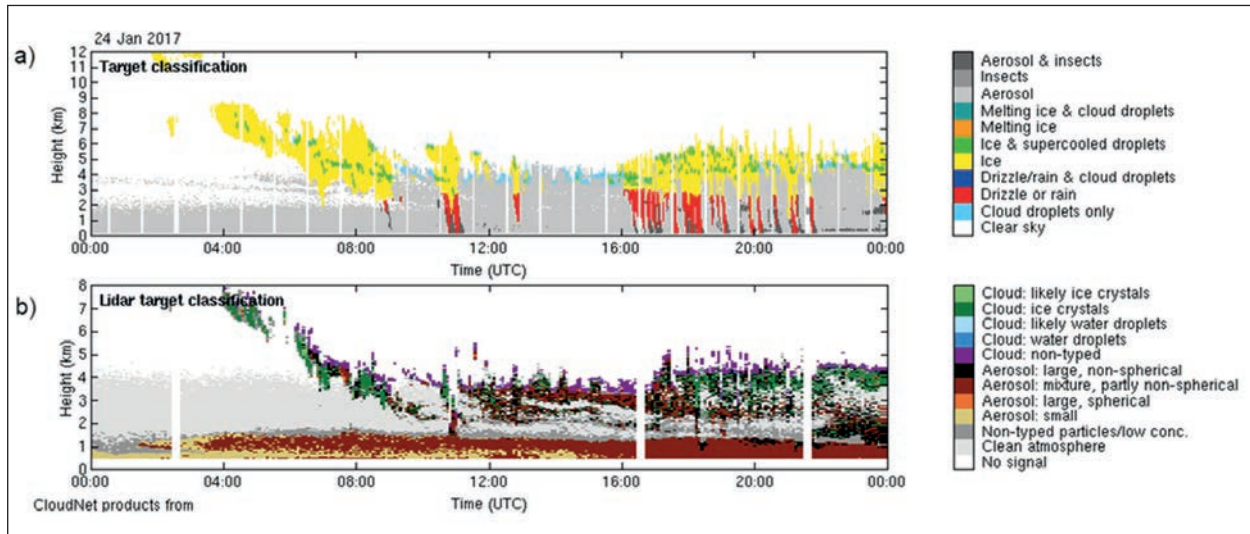
Fig 1: Upper panel: Cloudnet target classification with discrimination of cloud-particle phase and a basic aerosol detection. Lower panel: Advanced aerosol classification on the basis of measurements of PollyXT multi-wavelength Raman/Depolarization lidar.

additional Raman-/Depolarization lidar measurements (LMU Munich). The DLR Falcon research aircraft was stationed at Pafos, Cyprus and performed combined airborne in-situ/lidar observations of aerosol properties, clouds and wind in the eastern Mediterranean with special focus on absorbing aerosols. The flights were performed in the context of the Absorbing aerosol layers in a changing climate: aging, lifetime

and dynamics (A-LIFE) ERC Starting Grant of Bernadett Weinzierl.

Figure 2 shows an illustration of a dust plume observed during the CyCARE IOP phase. The figure shows a preliminary evaluation of the measurements of several Polly^{XT} Raman lidar measurements taken in the region during several flights with in-situ probing of DLR Falcon. Lidar-derived concentrations of cloud
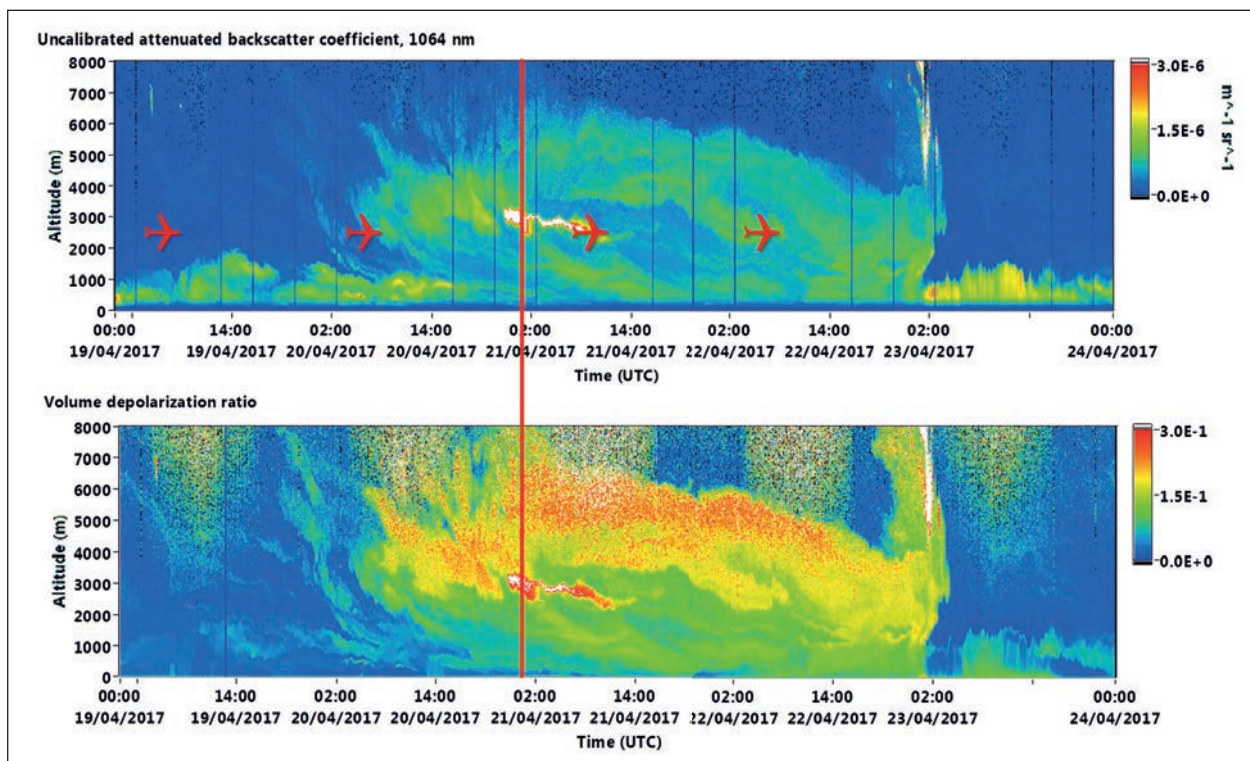
Fig. 2: Raman lidar observations of a dust plume at Limassol, Cyprus. Aircraft symbols indicate time when DLR Falcon overflew the LACROS station at Limassol and probed the same air mass.
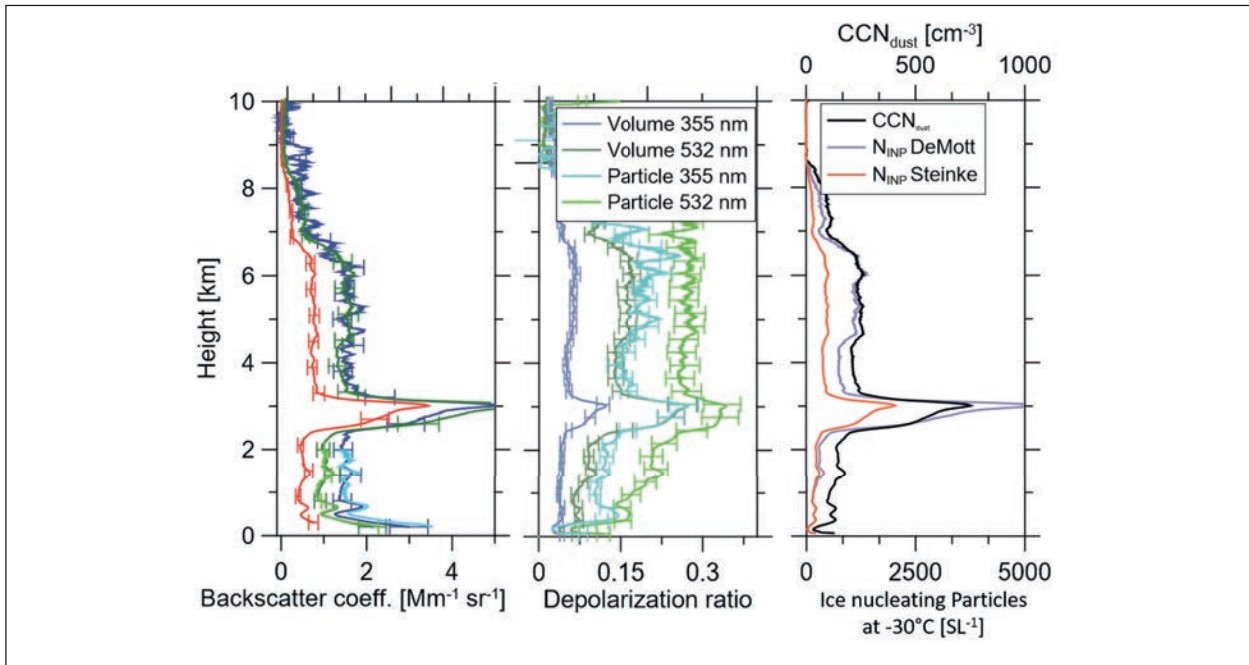
Fig. 3: Lidar profile of aerosol microphysical properties derived at the position of the red bar in Fig. 2. CCN and INP have been derived by the method of Mamouri and Ansmann (2015).

condensation particles (CCN) and ice nucleating particles (INP) are shown in Fig. 3. These results were obtained with the method of *Mamouri and Ansmann* [2015].

Air quality on Cyprus is mainly affected by the far transport of aerosols from the European mainland and surrounding deserts. The bay of Limassol additionally creates complex wind fields affecting the daily cycles of mixing layer development. The LACROS Doppler lidar was used to measure profiles of the wind vector and local turbulence over Limassol. The Doppler lidar was pointed vertically during most of the

time. Each half hour a conical scan was performed for measurement of a horizontal wind profile in the boundary layer. These measurements of wind speed and turbulence are vital for aerosol mixing studies, including the identification and disentangling of local and remote sources of aerosols (e.g. desert dust) on local air quality. Figure 4 shows a vector average of all wind vectors that have been observed from April to September 2016. The data show the daily cycle of land-sea-breeze effects over Limassol and underline the complexity of the wind situation in this location.
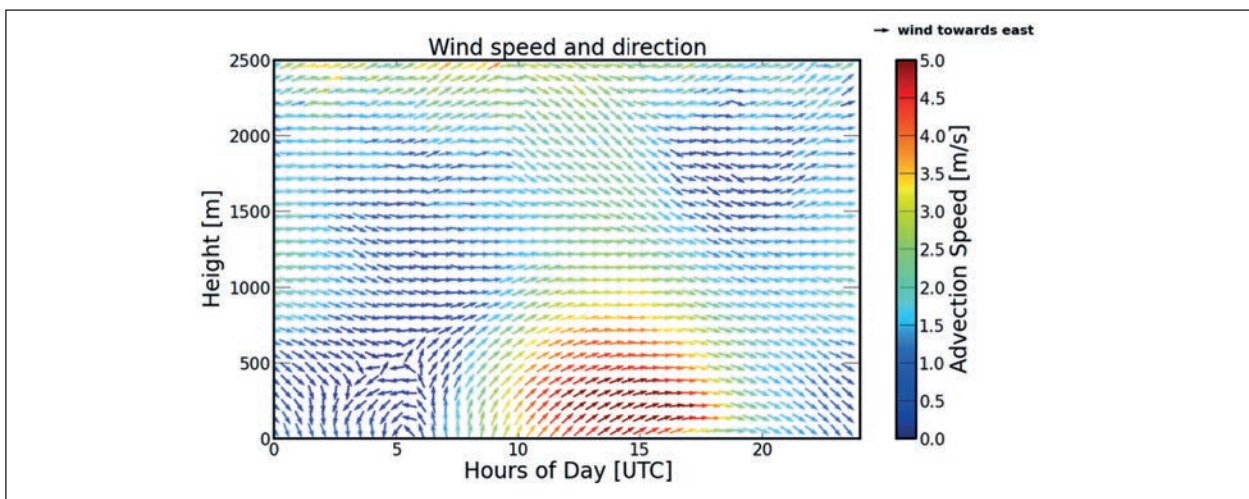
Fig. 4: Vector averaged horizontal wind at Limassol, averaged across the summer period (April to September). Color indicates wind speed. Arrows show the averaged wind vectors at a given height and time.

Summary and Outlook

CyCARE is an esult of the BACCHUS project and spiked a variety of other activities in the eastern Mediterranean, which eventually brought together a critical mass of observers in order to study transport of air masses influenced by desert dust and biomass burning aerosol in the eastern Mediterranean. Collocated lidar/radar observations of clouds together with aircraft in-situ probing will allow contrasting aerosol and cloud properties under various conditions like the influence of Saharan dust, Middle East desert dust and continental aerosol. The campaign will be continued until April 2018.

References

Baars, H., Seifert, P., Engelmann, R., and Wandinger, U., 2017. Target categorization of aerosol and clouds by continuous multiwavelength-polarization lidar measurements, *Atmos. Meas. Tech.*, 10, 3175-3201.

Illingworth, A.J., R.J. Hogan, E.J. O'Connor, D. Bouniol, J. Delanoë, J. Pelon, A. Protat, M.E. Brooks, N. Gaussiat, D.R. Wilson, D.P. Donovan, H.K. Baltink, G. van Zadelhoff, J.D. Eastment, J.W. Goddard, C.L. Wrench, M. Haeffelin, O.A. Krasnov, H.W. Russchenberg, J. Piriou, F. Vinit, A. Seifert, A.M. Tompkins, and U. Willén, 2007. Cloudnet. *Bull. Amer. Meteor. Soc.*, 88, 883–898.

Boucher, O., Randall, D., Artaxo, P., Bretherton, C., Feingold, G., Forster, P., Kerminen, V. M., Kondo, Y., Liao, H., Lohmann, U., Rasch, P., Satheesh, S. K., Sherwood, S., Stevens, B. & Zhang, X. Y. 2014. Climate Change 2013: The Physical Science Basis. Contribution of Working Group I to the Fifth Assessment Report of the Intergovernmental Panel on Climate Change. *In:* STOCKER, T. F., QIN, D., PLATTNER, G. K., M, T., ALLEN, S. K., BOSCHUNG, J., NAUELS, A., XIA, Y., BEX, V. & MIDGLEY, P. M. (eds.) *Climate Change 2013: The Physical Science Basis. Contribution of Working Group I to the Fifth Assessment Report of the Intergovernmental Panel on Climate Change.* Cambridge University Press, Cambridge, United Kingdom and New York, NY, USA.

Mamouri, R. E. and Ansmann, A. 2016. Potential of polarization lidar to provide profiles of CCN- and INP-relevant aerosol parameters. *Atmos. Chem. Phys.,* 16**,** 5905-5931.

Mamouri, R. E., Ansmann, A., Nisantzi, A., Solomos, S., Kallos, G. & Hadjimitsis, D. G. 2016. Extreme dust storm over the eastern Mediterranean in September 2015: satellite, lidar, and surface observations in the Cyprus region. *Atmos. Chem. Phys.,* 16**,** 13711-13724.

Myagkov, A., Seifert, P., Bauer-Pfundstein, M. & Wandinger, U. 2016. Cloud radar with hybrid mode towards estimation of shape and orientation of ice crystals. *Atmos. Meas. Tech.,* 9**,** 469-489.

Cooperation
Cyprus University of Technology, Cyprus;
University of Vienna, Austria;
LMU Munich, Germany;
Deutsches Zentrum für Luft und Raumfahrt (DLR), Germany

SALTRACE Highlights: Vertical resolved optical properties of aged Saharan dust and wet and dried marine aerosol particles with a triple-wavelength polarization lidar at Barbados

Moritz Haarig[1], Dietrich Althausen[1], Albert Ansmann[1], André Klepel[1], Holger Baars[1], Ronny Engelmann[1], Martin Radenz[1], Josef Gasteiger[2], Volker Freudenthaler[3], Silke Groß[4], Eleni Marinou[5], Konrad Kandler[6], Sharon P. Burton[7], Rodanthi Mamouri[8], Carlos Toledano[9], David Farrell[10], Damien Prescod[10]

[1] Leibniz Institute for Tropospheric Research (TROPOS), Leipzig, Germany
[2] Faculty of Physics, University of Vienna, Austria
[3] Meteorological Institute, Ludwig Maximilian University, Munich, Germany
[4] German Aerospace Center, Oberpfaffenhofen, Germany
[5] National Observatory Athens, Greece
[6] Technical University Darmstadt, Germany
[7] NASA Langley Research Center, Hampton, VA, USA
[8] Cyprus University of Technology, Limassol, Cyprus
[9] Group of Atmospheric Optics, University of Valladolid, Spain
[10] Caribbean Institute for Meteorology and Hydrology, Barbados

Der Ferntransport von Saharastaub aus Nordafrika in die Karibik wurde in der SALTRACE Kampagne untersucht. Der Frage, wie sich das Saharastaub-Aerosol durch trockene und feuchte Deposition, chemische Alterung und Wolkenprozesse ändert, wurde 2013 und 2014 in umfangreichen Experimenten auf der Karibikinsel Barbados nachgegangen. Flugzeug- und Bodenmessungen wurden zu einem ganzheitlichen Bild kombiniert. Hier werden drei Highlights der am Boden mit einem dreiwellenlängen Polarisations-/Raman-Lidar durchgeführten Vertikalmessungen vorgestellt. 1.) Auf dem Weg nach Barbados (5000-6000 km westlich der Hauptstaubquellen) und von dort nach Missouri (nach weiteren 6000 km Transport) verändern sich die optischen Eigenschaften des Staubes fast nicht. 2.) Auf dem Weg von Afrika in die Karibik reduziert sich der Anteil großer Partikel (mit Durchmessern > 5 µm) merklich. 3.) Die optischen Eigenschaften abgetrockneter, würfelartiger mariner Salzpartikel konnten erstmals mit einem Lidar vermessen werden.

Introduction

The Saharan Aerosol Long-range TRansport and Aerosol–Cloud-interaction Experiment (SALTRACE) aims to characterize the modifications of Saharan dust after long-range transport [*Weinzierl et al.,* 2017]. Comprehensive field campaigns took place at Barbados (13°N, 59°W) in the summer months of 2013 and 2014 and in February–March 2014. Three highlights from the active remote sensing are presented. The research to compare the airborne in situ data with the ground-based remote sensing observations is ongoing.

Highlight 1: Saharan dust transport over > 12000 km observed at Barbados and Missouri

A unique case was observed during SALTRACE-3 on 6 July 2014 [*Haarig et al.*, 2017a]. A 3 km deep Saharan dust layer crossed Barbados and traveled westward towards the United States (see backward trajectories in Fig. 1). Coincidentally, this aged dust layer was observed with an airborne triple-wavelength polarization lidar (high-spectral-resolution lidar HSRL-2) one week later [*Burton et al.*, 2015]. We use this unexpected opportunity to
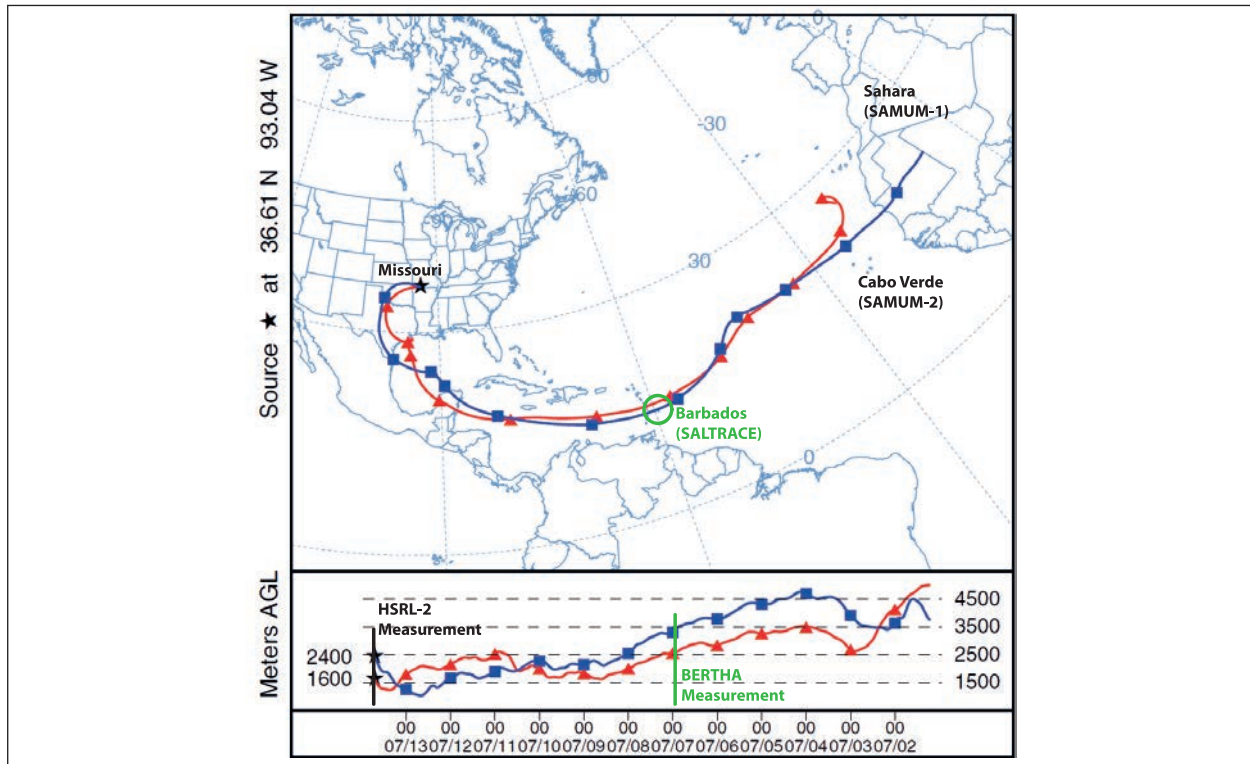
Fig. 1: The 12.5-day HYSPLIT backward trajectories for 13 July 2014 arrive at the measurement location of the HSRL-2 measurement over southern Missouri. The location (Barbados) and time of the corresponding BERTHA lidar measurement is indicated by a green vertical line. The locations of SAMUM-1 (Morocco) and SAMUM-2 (Cabo Verde) are marked.
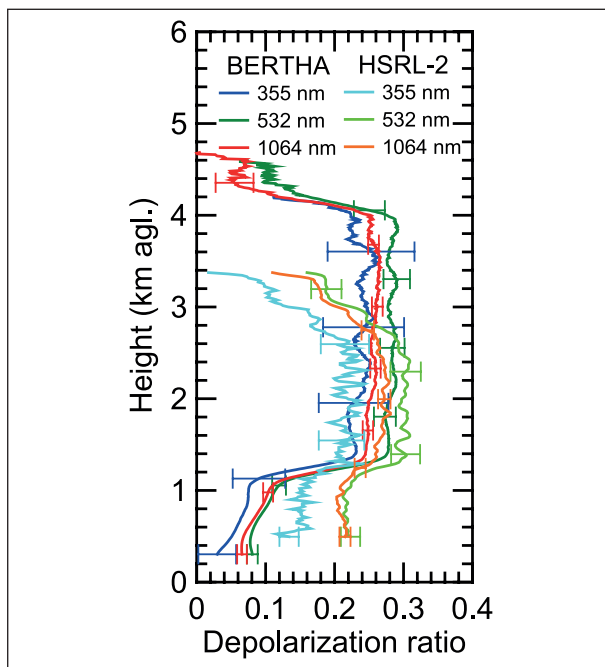
Fig. 2: The vertical profiles of the particle linear depolarization ratio (PLDR) at three wavelengths measured with BERTHA on Barbados, 6–7 July 2014, 23:18–01:33 UTC. For comparison, height profiles of PLDR measured with the airborne triple-wavelength polarization lidar (HSRL-2) on 13 July 2014, 17:00 UTC are shown. The airborne lidar observations were performed in Missouri about 6000 km and 7 days downwind of Barbados.

compare the triple-wavelength depolarization observations (Fig. 2) of aged dust after long-range transport over 6000 km (Barbados) and 12 000 km (Missouri, midwestern USA). The 12.5-day backward trajectories indicate that the dust observed over Barbados at 2.5 and 3.5 km height descended towards 1.6 and 2.4 km height over Missouri. After leaving the African continent, the dust layers arrived after 5 and 12 days over Barbados and Missouri, respectively.

An excellent agreement between the two lidar data sets of depolarization-ratio profiles was found (Fig. 2). Similar dust optical properties and depolarization features were observed over both sites indicating almost unchanged dust properties within this one week of travel from the Caribbean to the United States.

Highlight 2: Depolarization ratio of Saharan dust: From SAMUM-1 and SAMUM-2 to SALTRACE

To investigate the changes in the dust optical properties from Africa towards the Caribbean, the SALTRACE results [*Haarig et al.,* 2017a] are set into the context of the SAMUM-1 (Morocco, 2006) [*Freudenthaler et al.*, 2009] and SAMUM-2 (Cabo Verde, 2008) [*Groß et al.*, 2011] depolarization ratio studies (Fig. 3).
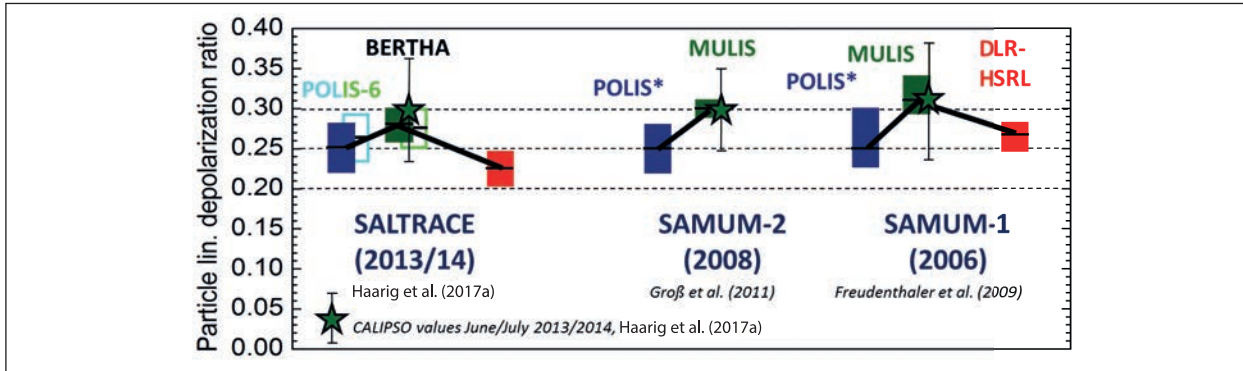
Fig. 3: Comparison of dust-layer mean particle linear depolarization ratios measured along the transport way from Morocco (SAMUM-1) [Freudenthaler et al., 2009] to Cabo Verde (SAMUM-2) [Groß et al., 2011] and to Barbados (SALTRACE) [Haarig et al., 2017a]. Colored bars show the range of the observed depolarization ratios at 355 nm (blue), 532 nm (green), and 1064 nm (red). The lidar systems BERTHA, POLIS, MULIS and the airborne high-spectral-resolution lidar (HSRL) of DLR (Deutsches Zentrum für Luft- und Raumfahrt) were used to collect this data set. In addition, CALIOP dust-layer mean values of depolarization ratios considering all observations during the 4 SALTRACE summer months (June and July in 2013 and 2014) are shown. The mean values consider all CALIOP overpasses of selected areas in southeastern Morocco, in the Cabo Verde region, and around Barbados.

There is almost no change of the mean 355 and 532 nm particle depolarization ratio with distance from the dust source. The slow decrease of the mean 532 nm depolarization value from 0.31 (Morocco) to 0.30 (Cabo Verde) to 0.28 (Barbados) is not significant. The comparison with the CALIOP (Cloud-Aerosol Lidar with Orthogonal Polarization) satellite observations also shows no significant change in the 532 nm depolarization ratio across the Atlantic.

More information conveys the spectral slope of the depolarization ratio of Saharan dust over Barbados as shown in Fig. 3, with the maximum at 532 nm (0.28±0.02) and lower values at 355

(0.25±0.03) and 1064 nm (0.23±0.02). The spectral slope contains particle size information reflecting the different influence of the fine-mode (<1 μm) and coarse-mode (>1 μm) dust fractions on the overall (fine + coarse) particle depolarization ratio at the three wavelengths [*Mamouri and Ansmann*, 2014, 2017].

The available 1064 nm depolarization ratios indicate a significant decrease from a Morocco mean value of 0.27 to a Barbados mean value of 0.23. We speculate that a substantial fraction of large dust particles causing depolarization ratios of 0.40 is present over areas close to the Sahara but that these large particles are strongly removed before reaching Barbados. The other two wavelengths (355 and 532 nm) are more sensitive to fine-mode dust, for which the removal by gravitational settling is less efficient.

Highlight 3: Dry and wet marine particles: RH dependence of the depolarization ratio

During the SALTRACE-2 (winter) campaign, pure marine conditions prevailed for some days over Barbados. This offered the unique opportunity to study the relation between marine particle shape and relative humidity (RH) under atmospheric conditions [*Haarig et al.,* 2017b]. The shape of sea salt particles strongly depends on RH. At typical values of RH >80 % in the marine boundary layer, sea salt particles are liquid solution drops and thus spherical in shape. When RH decreases below 45 %, they crystallize and become mostly cubic-like in shape. The change in shape leads to different optical properties, especially to an enhancement in the linear depolarization ratio.
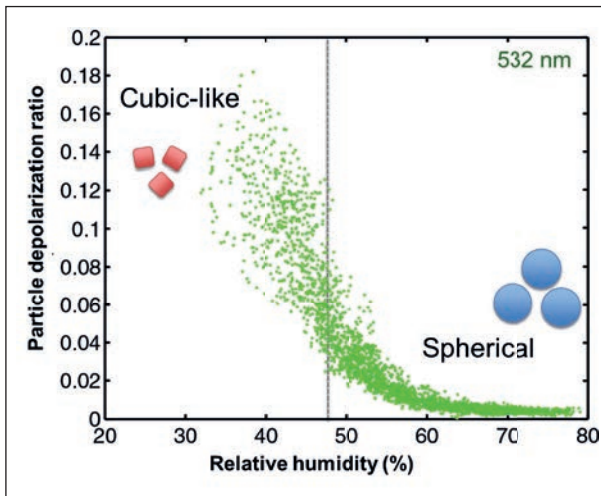
Fig. 4: Correlation of the particle linear depolarization ratio at 532 nm with RH. The BERTHA measurements of 23 February 2014, 23:38–01:08 UTC, at 375–1100 m height are used (3 min temporal and 35 m vertical resolution). The dashed line marks the sea salt efflorescence point (48% RH), around which the phase transition from spherical solution droplets (low depolarization ratio) to non-spherical sea salt crystals (high depolarization ratio) occurs.

The radiosonde and water-vapor Raman lidar observations show a drop in RH below 50 % in the marine aerosol layer simultaneously with a strong increase in particle linear depolarization ratio, which reaches values up to 0.12 ± 0.08 at 355 nm, 0.15 ± 0.03 at 532 nm, and 0.10 ± 0.01 at 1064 nm. The correlation between the shape-dependent PLDR and RH for 23 February 2014 is shown in Fig. 4. The phase transition from spherical sea salt particles (PLDR < 0.03) to cubic-like sea salt crystals is clearly visible. The lidar ratio (extinction-to-backscatter ratio) remained almost unchanged between 19 and 27 sr.

Outlook

In the next steps, the lidar measurements on Barbados will be used to estimate vertical profiles of concentrations of cloud condensation nuclei and ice nucleating particles [according to *Mamouri and Ansmann*, 2016], which can be compared to airborne in situ measurements. After the discussion and publication of the above presented highlights in the study the Saharan aerosol long-range transport, the aerosol-cloud interaction will be in the focus to complete the Saharan Aerosol Long-range Transport and Aerosol–Cloud-interaction Experiment (SALTRACE).

References

Burton, S. P., Hair, J. W., Kahnert, M., Ferrare, R. A., Hostetler, C. A., Cook, A. L., Harper, D. B., Berkoff, T. A., Seaman, S. T., Collins, J. E., Fenn, M. A., and Rogers, R. R. (2015), Observations of the spectral dependence of linear particle depolarization ratio of aerosols using NASA Langley airborne High Spectral Resolution Lidar, *Atmos. Chem. Phys., 15,* 13453–13473, https://doi.org/10.5194/acp-15-13453-2015.

Freudenthaler, V., Esselborn, M., Wiegner, M., Heese, B., Tesche, M., Ansmann, A., Müller, D., Althausen, D., Wirth, M., Fix, A., Ehret, G., Knippertz, P., Toledano, C., Gasteiger, J., Garhammer, M., and Seefeldner, M. (2009), Depolarization ratio profiling at several wavelengths in pure Saharan dust during SAMUM 2006, *Tellus B*, *61*, 165–179, https://doi.org/10.1111/j.1600-0889.2008.00396.x.

Groß, S., Tesche, M., Freudenthaler, V., Toledano, C., Wiegner, M., Ansmann, A., Althausen, D., and Seefeldner, M. (2011), Characterization of Saharan dust, marine aerosols and mixtures of biomass-burning aerosols and dust by means of multi-wavelength depolarization and Raman lidar measurements during SAMUM 2, *Tellus B, 63*, 706–724, https://doi.org/10.1111/j.1600-0889.2011.00556.x.

Haarig, M., Ansmann, A., Althausen, D., Klepel, A., Groß, S., Freudenthaler, V., Toledano, C., Mamouri, R.-E., Farrell, D. A., Prescod, D. A., Marinou, E., Burton, S. P., Gasteiger, J., Engelmann, R., and Baars, H. (2017a), Triple-wavelength depolarization-ratio profiling of Saharan dust over Barbados during SALTRACE in 2013 and 2014, *Atmos. Chem. Phys*., *17*, 10767–10794, https://doi.org/10.5194/acp-17-10767-2017.

Haarig, M., Ansmann, A., Althausen, D., Gasteiger, J., and Kandler, K. (2017b), Linear depolarization ratio of dried marine particles: SALTRACE lidar observations and modeling, *Atmos. Chem. Phys., 17,* 14199–14217, https://doi.org/10.5194/acp-17-14199-2017.

Mamouri, R. E. and Ansmann, A. (2014), Fine and coarse dust separation with polarization lidar, *Atmos. Meas. Tech., 7,* 3717–3735, https://doi.org/10.5194/amt-7-3717-2014.

Mamouri, R. E. and Ansmann, A. (2016), Potential of polarization lidar to provide profiles of CCN- and INP-relevant aerosol parameters, *Atmos. Chem. Phys., 16,* 5905-5931, doi:10.5194/acp-16-5905-2016.

Mamouri, R. E. and Ansmann, A. (2017), Potential of polarization/Raman lidar to separate fine dust, coarse dust, maritime, and anthropogenic aerosol profiles, *Atmos. Meas. Tech., 10*, 3403–3427, https://doi.org/10.5194/amt-10-3403-2017.

Weinzierl, B., Ansmann, A., Prospero, J. M., Althausen, D., Benker, N., Chouza, F., Dollner, M., Farrell, D., Fomba, W. K., Freudenthaler, V., Gasteiger, J., Groß, S., Haarig, M., Heinold, B., Kandler, K., Kristensen, T. B., Mayol-Bracero, O. L., Müller, T., Reitebuch, O., Sauer, D., Schäfler, A., Schepanski, K., Spanu, A., Tegen, I., Toledano, C., and Walser, A. (2017), The Saharan Aerosol Long-range Transport and Aerosol-Cloud-Interaction Experiment (SALTRACE): overview and selected highlights, *B. Am. Meteorol. Soc., 98,* 1427–1451, https://doi.org/10.1175/BAMSD-15-00142.1.

Cooperation

Deutsches Luft- und Raumfahrtzentrum (DLR), Oberpfaffenhofen, Germany;
Caribbean Institute for Meteorology and Hydrology (CIMH), Husbands, Barbados;
Ludwig-Maximilians-Universität (LMU), München, Germany;
Faculty of Physics, University of Vienna, Wien, Austria;
Technische Universität Darmstadt, Darmstadt, Germany

Dust forecasts versus lidar observations: New options of comparison

Albert Ansmann[1], Franziska Rittmeister[1], Ronny Engelmann[1], Sara Basart[2], Oriol Jorba[2], Christos Spyrou[3], Samuel Remy[4], Annett Skupin[1], Holger Baars[1], Patric Seifert[1], Fabian Senf[1], Thomas Kanitz[5]

[1] Leibniz Institute for Tropospheric Research (TROPOS), Leipzig, Germany
[2] Barcelona Supercomputing Center, Dep. of Earth Sciences, Barcelona, Spain
[3] National and Kapodistrian University of Athens, Dep. of Physics, Athens, Greece
[4] Laboratoire de Météorologie Dynamique, IPSL, UPMC/CNRS, Paris, France
[5] ESTEC, Noordwijk, The Netherlands

Während einer vierwöchigen Forschungsreise von Guadeloupe nach Mindelo, Kap Verde, im Frühjahr 2013 wurden mit einem Lidar auf dem Forschungsschiff Meteor Saharastaubfahnen vermessen. Die beobachteten Staubprofile wurden mit entsprechenden Staubvorhersagen eines regionalen (SKIRON) und zweier globaler Vorhersage-Modelle (NMMB/BSC-Dust, MACC/CAMS) verglichen. Neue Wege des Vergleichs wurden genutzt. Mit einer verfeinerten Lidar-Methode lassen sich nun zum einen Staub, Rauch, und marine Aerosolkomponenten besser trennen und zum anderen Fein- und Grobstaubanteile (mit Partikeldurchmessern von >1µm) unterscheiden. Die drei wichtigsten Ergebnisse der Studie sind: a) Staubvorhersagen sind akzeptabel bis zu einer Entfernung von etwa 2000 km von den Quellgebieten, b) die Verminderung der Staubkonzentration durch trockene Deposition ist in den globalen Modellen generell zu effizient, und c) das Verhältnis von feinen zu groben Staubpartikeln ist in den globalen Modellen zu hoch und deutet auf einen zu hohen Anteil an feinen Staubpartikeln bei der modellierten Emission in den Quellgebieten hin.

Introduction

We performed continuous Saharan dust observations with a multiwavelength polarization/Raman lidar aboard the German research vessel Meteor across the tropical Atlantic Ocean between the Caribbean and Africa (over 4500 km) from 29 April to 23 May 2013 [*Rittmeister et al.*, 2017]. These dust profiles were compared with dust forecasts obtained with the regional model SKIRON (the name SKIRON, one of the eight gods of winds, is taken from the Greek mythology), and the global models MACC (MACC/CAMS: Monitoring Atmospheric Composition and Climate /Copernicus Atmosphere Monitoring Service) and NMMB (NMMB/BSC -Dust: Nonhydrostatic Multiscale Model on the B Grid, BSC: Barcelona Super- computing Center). Polarization lidars allow us to separate dust from smoke and marine particles. Recently, it was shown that even fine dust and coarse dust can be distinguished [*Mamouri and Ansmann*, 2017] so that one of the most important modeling aspects which deals with the emitted and transported dust particle size spectrum [*Kok*, 2011a, b; *Kok et al.*,

2017] can now be illuminated in model-observation comparisons.

Results

Figure 1 shows key findings of the comparison in the case of the NMMB/BSC-Dust model. The results are similar for the comparison with the MACC/CAMS dust profiles. In the SKIRON model the fine-to-coarse dust ratio is set constant to avoid an overestimation of the fine dust fraction. A detailed discussion is presented by *Ansmann et al.* [2017]. As a main result, a moderate to strong underestimation of the coarse dust mass concentration and of the respective 532 nm extinction coefficient was found (NMMB, MACC), disregarding the distance from Africa (cases 1,2,3, and 4: 1000, 1700, 3300, and 4300 km west of Africa, respectively). The ratio of fine dust to coarse dust especially in terms of the particle extinction coefficient is too high in the two global models. The relative overestimation of the fine dust optical effects was already suggested by *Kok et al.* [2017], but is now clearly demonstrated by observations. A too high fine dust
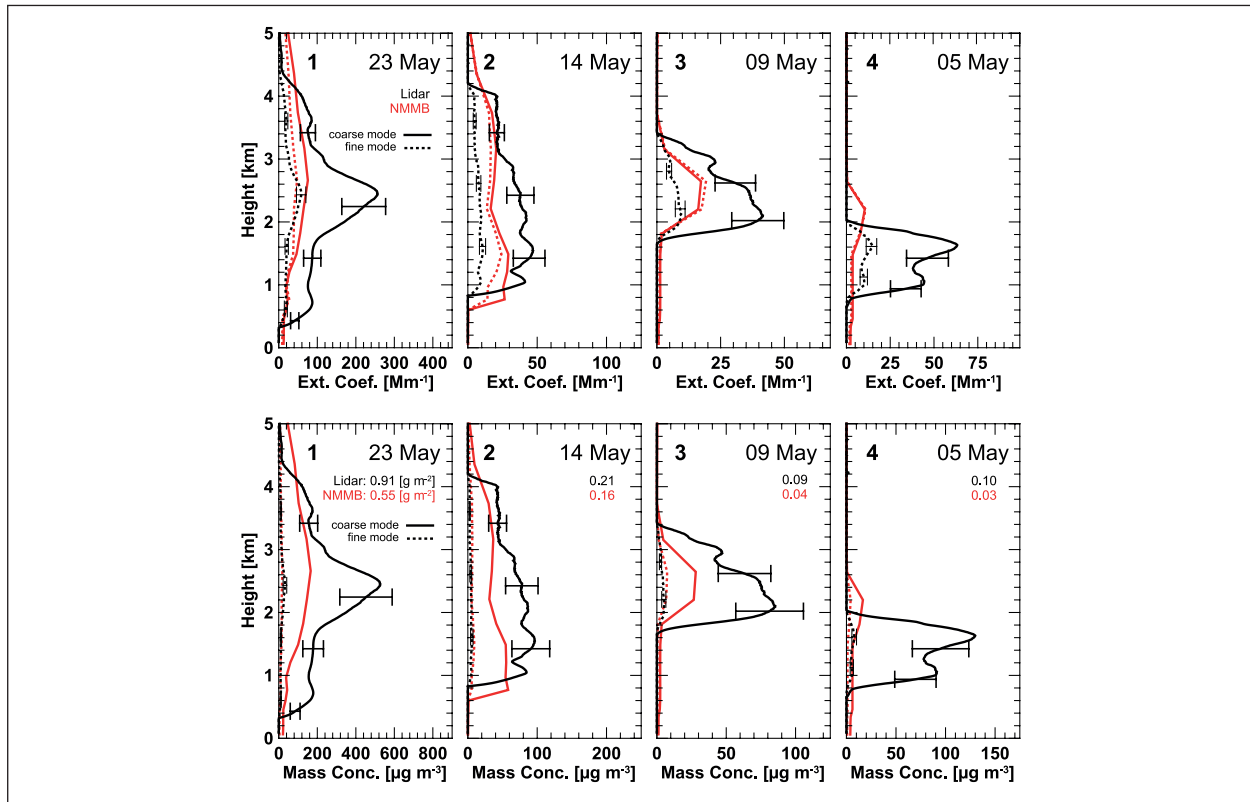
Fig 1: (Top) Comparison of fine (dotted) and coarse (solid) dust extinction coefficients derived from lidar observations (black) and simulated with NMMB/BSC-Dust (red) for cases 1 (1000 km), 2 (1700 km), 3 (3300 km), and 4 (4300 km) west of the African coast. (Bottom) Respective fine (dotted) and coarse (solid) dust mass concentrations derived from the lidar measurements (black) and the simulations (red). Column-integrated total dust mass concentrations are given as numbers. The underestimation of the total mass concentration by the model increases with distance from Africa.

fraction leads to an overestimation of the dust radiative effect and to wrong estimates of cloud condensation nuclei and ice-nucleating particle concentrations.

Since the overestimation of the relative contribution of fine dust to total dust is already visible in the observations close to Africa (cases 1 and 2), we conclude that too much fine dust or, correspondingly, too less coarse dust was emitted in the simulations.

References

Ansmann, A., Rittmeister, F., Engelmann, R., Basart, S., Jorba, O., Spyrou, C., Remy, S., Skupin, A., Baars, H., Seifert, P., Senf, F., and Kanitz, T.: Profiling of Saharan dust from the Caribbean to western Africa – Part 2: Shipborne lidar measurements versus forecasts, *Atmos. Chem. Phys.*, 17, 14987-15006, https://doi.org/10.5194/acp-17-14987-2017, 2017.

Kok, J. F.: A scaling theory for the size distribution of emitted dust aerosols suggests climate models underestimate the size of the global dust cycle, *Proc. Natl. Acad. Sci. USA*, 108, 1016–1021, doi:10.1073/pnas.1014798108, 2011a.

Kok, J. F.: Does the size distribution of mineral dust aerosols depend on the wind speed at emission?, *Atmos. Chem. Phys.*, 11, 10149-10156, doi:10.5194/acp-11-10149-2011, 2011b.

Kok, J. F., Ridley, D. A., Zhou, Q., Miller, R. L., Zhao, C., Heald, C. L., Ward, D. S., Albani, S., and Haustein, K.: Smaller desert dust cooling effect estimated from analysis of dust size and abundance, *Nat. Geosci.*, 10, 274–278, doi:10.1038/ngeo2912, 2017.

Mamouri, R.-E. and Ansmann, A.: Potential of polarization/Raman lidar to separate fine dust, coarse dust, maritime, and anthropogenic aerosol profiles, *Atmos. Meas. Tech.*, 10, 3403-3427, https://doi.org/10.5194/amt-10-3403-2017, 2017.

Rittmeister, F., Ansmann, A., Engelmann, R., Skupin, A., Baars, H., Kanitz, T., and Kinne, S.: Profiling of Saharan dust from the Caribbean to western Africa – Part 1: Layering structures and optical properties from shipborne polarization/Raman lidar observations, *Atmos. Chem. Phys.*, 17, 12963-12983, https://doi.org/10.5194/acp-17-12963-2017, 2017.

Smoke over Clouds – Radiative Effects Assessed with MSG (SCREAM)

Daniel Merk[1], Hartwig Deneke[1], Martin de Graaf[2], Jan Fokke Meirink[2]

[1] Leibniz Institute for Tropospheric Research (TROPOS), Leipzig, Germany
[2] Royal Netherlands Meteorological Institute (KNMI), de Bilt, the Netherlands

Absorbierende Aerosole können die solaren Strahlungsflüsse signifikant verändern. Der hieraus resultierende direkte Strahlungseffekt ist bisher nur unzureichend bekannt und ist besonders stark für Situationen, in denen solche Aerosole über hellen Oberflächen wie z.B. Stratokumulus-Wolken-feldern auftreten. Gleichzeitig wird in solchen Situationen die Genauigkeit von passiven Verfahren zur Bestimmung von Wolkeneigenschaften beeinträchtigt. Diese Effekte wurden hier unter Verwendung von Beobachtungen des geostationären Satelliten Meteosat genauer untersucht. Durch Nutzung der SEVIRI-Kanalkombination mit 1.6 and 3.9 um Wellenlänge konnte abgeschätzt werden, dass herkömmliche Methoden die Wolken-optische Dicke in stark Aerosol-belasteten Situationen um bis zu 15% unterschätzen. Beobachtungen des Geostationary Earth Radiation Budget (GERB) Instruments zeigen für diese Fälle einen direkten Strahlungseffekt der absorbierende Aerosole bis zu 35W/m², konsistent mit vorherigen Untersuchungen.

Introduction

The radiative effect of aerosols remains a highly uncertain factor in our understanding of the Earth's climate system. The direct radiative effect (DRE) is defined as the change in net radiative flux at the top of atmosphere (TOA) caused by aerosols, and is still poorly known. The combined DRE of all aerosols is negative, i.e., results in a cooling of the atmosphere. A special situation occurs for absorbing aerosols above clouds, where the DRE can change sign and thus causes a warming of the atmosphere, which strongly depends on the brightness of the underlying surface.

Absorbing aerosols above clouds frequently occur over the South-East (SE) Pacific and SE Atlantic, where also persistent stratocumulus cloud decks are found. Fires in Southern Africa during the local dry period and driven by the monsoon result in one third of the world's biomass burning emissions, and are transported westwards over the Atlantic. This results in haze overlying the marine stratocumulus clouds. The maximum direct radiative effect is found over the SE Atlantic between 0° and 20° S during August and September [*Chand et al.*, 2008]. Several studies have assessed the DRE for the SE Atlantic region using different instruments and methods, and

generally agree on a mean DRE of about 30 Wm² for these months [e.g., *de Graaf et al.*, 2012; 2014], which is not correctly reproduced by current climate models [*Boucher et al.*, 2013; *Myhre et al.*, 2013].

The aim of the present study was (a) to retrieve cloud properties from the SEVIRI instrument using the 1.6 and 3.9 um channel combination instead of the standard 0.6 and 1.6 um channel combination as it is unaffected by the presence absorbing aerosols, (b) to determine typical uncertainties of retrieved standard cloud products for aerosol above cloud conditions, and (c) to estimate the DRE using observations from Meteosat's GERB instrument.

Data and Method

For this study, observations from the SEVIRI and GERB instruments on-board the geostationary Meteosat Second Generation (MSG) satellites from August 2006 are used together with the absorbing aerosol index (AAI) derived from the Ozone Monitoring Instrument (OMI) on-board the polar-orbiting AURA satellite, which is used to detect the presence of absorbing aerosol above clouds [*Alfaro-Contreras et al.*, 2014]. SEVIRI is a multispectral passive imager with 12 narrowband channels covering solar and thermal
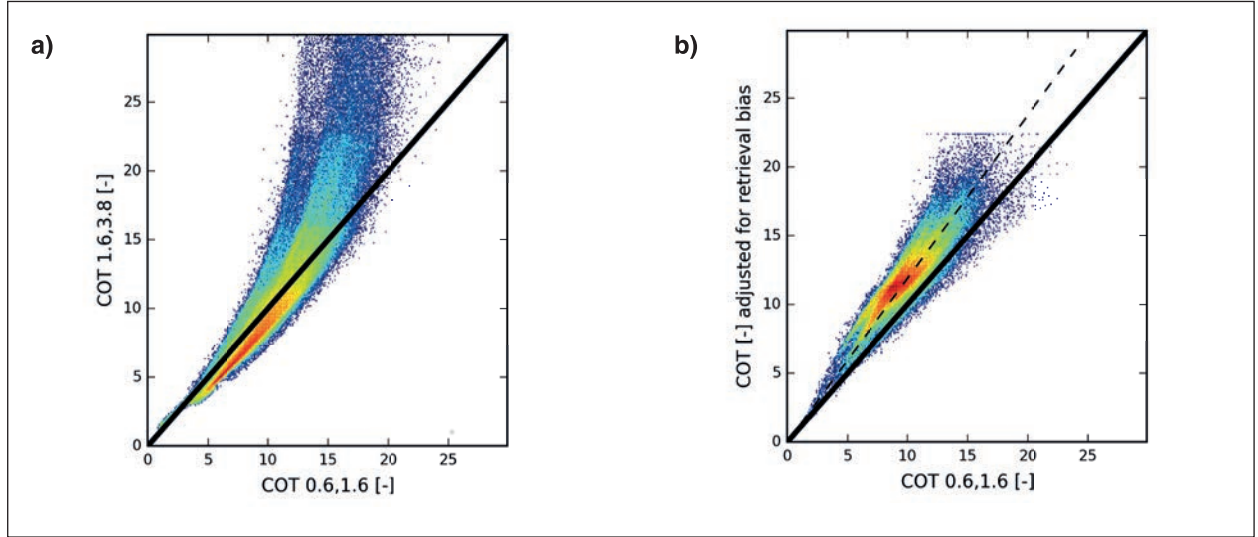
Fig. 1: Joint histograms of the MSG SEVIRI-based estimates of cloud optical thickness derived from the standard 0.6 um /1.6 um and the experimental 1.6/3.9 um channel combination; (a) for unpolluted conditions and (b) for polluted conditions and after applying a bias-correction, obtained for observations during August 2006 and a region of 0-10°S and 10-20°E.

wavelengths, with spatial and temporal resolutions of 3x3 km² and 15 minutes, respectively. Its 0.6 and 1.6 um channels are commonly used for the retrieval of cloud properties, specifically optical depth and droplet effective radius. Compared to other satellites, its 3.9 um channel is relatively wide, and overlaps with water vapour and CO2 absorption, which limits its information content for retrievals of cloud properties. Despite these limitations, KNMI's Cloud Physical Properties retrieval [CPP, *Roebeling et al.*, 2006] has been modified to utilize the weakly and strongly absorbing wavelengths of 1.6 and 3.9 um, as they are unaffected by the presence of smoke above clouds. In addition, the reflected solar broadband flux observed by the GERB instrument is used to assess changes in the radiation budget.

Results and Discussion

A comparison of the experimental and standard SEVIRI-based retrieval of cloud optical thickness is shown in Fig. 1a) for unpolluted conditions (AAI<0), and in Fig. 1b) for heavily polluted conditions (AAI>3). For unpolluted conditions, the experimental retrieval exhibits relatively large scatter, and saturates already for moderate optical thicknesses larger than 12-15 due to the absorption of cloud particles. A negative retrieval bias is also evident for small optical thicknesses, which turns positive as cloud optical thickness increases, and might be due to calibration uncertainties. To quantify the effects of pollution on standard cloud retrievals, a histogram matching technique has been applied to the results shown in
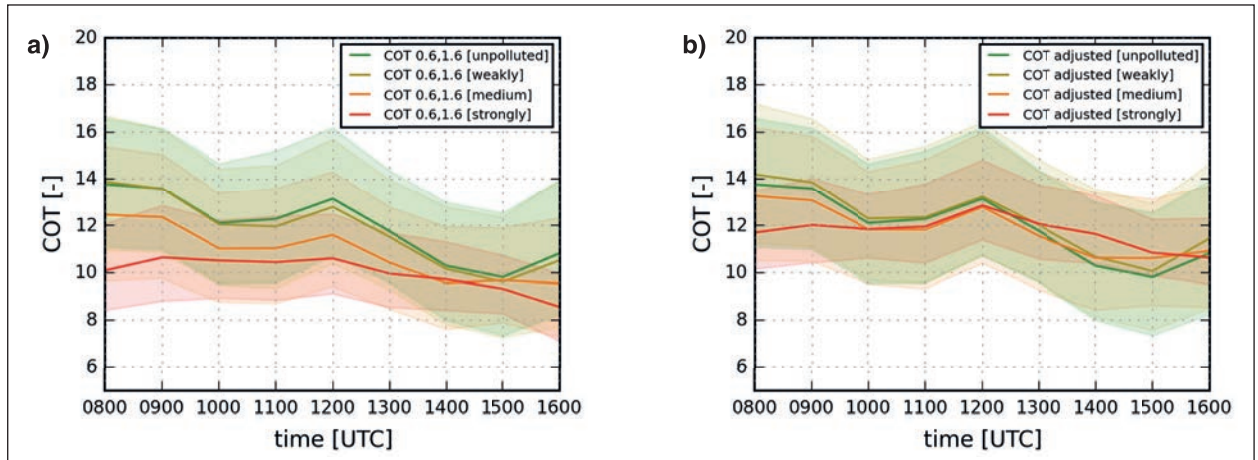
Fig. 2: Mean diurnal cycle of cloud optical thickness derived from MSG SEVIRI, separated for unpolluted, weakly, medium and strongly polluted conditions derived with (a) the 0.6 um /1.6 um and (b) the 1.6/3.9 um channel combination, and the same region and period as in Fig.1.

Fig. 1b) to correct for this bias. After this correction, a positive bias of 15% remains, which is likely attributable to an underestimate of cloud optical thickness for the standard retrieval resulting from the presence of absorbing aerosols

Figure 2 shows the diurnal cycle of cloud optical thickness obtained by a) the standard retrieval, and by b) the experimental retrieval. While for the standard retrieval a reduction of optical thickness with pollution strength is observed, this behaviour is not found for the experimental retrieval, indicating that this is probably an artefact caused by the presence of absorbing aerosols. Only for strongly polluted conditions, a significant change of the diurnal cycle can be identified, which might be due to the reduced solar insolation resulting from the aerosol layer above the clouds.

Mean diurnal cycles of the reflected solar radiation observed by GERB have been determined for different pollution classes. The difference of these mean diurnal cycles is interpreted as DRE here, and is shown in Fig. 3. Changes range from 10 W/m^2 for weakly polluted to about 35 W/m^2 for strongly polluted conditions, consistent with the results of previous studies. Note that changes in the reflected solar radiation could also be caused by differences in cloud properties.

While the observed scatter and saturation effects make retrievals based on the 1.6 and 3.9 um channel combination less accurate than standard retrievals, they nevertheless offer valuable information
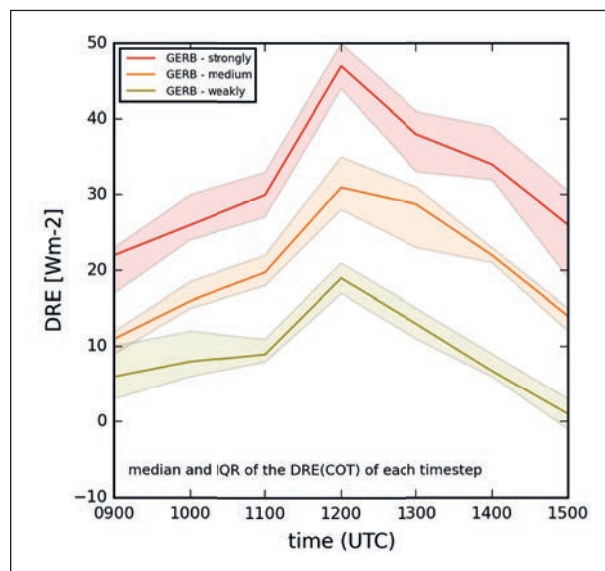
Fig. 3: Difference in the mean diurnal cycle of reflected solar radiation for weakly, moderately and strongly polluted conditions obtained from the MSG GERB instrument and compared to unpolluted conditions, interpreted here as the direct radiative effect of absorbing aerosols above clouds, and the same region and period as in Fig.1.

for aerosol-above-cloud conditions as demonstrated by our results. While our results show a reduction in reflected solar radiation by up to 40 W/m^2, it remains a future challenge to accurately separate the direct effect of aerosol absorption and indirect effects caused by changes in cloud properties.

References

Alfaro-Contreras, R., J. Zhang, J. Campbell, R. Holz, and J. Reid (2014), Evaluating the impact of aerosol particles above cloud on cloud optical depth retrievals from MODIS, *J. Geophys. Res. Atmos.*, 119, 5410–5423, D021270.

de Graaf, M., L. Tilstra, P. Wang, and P. Stammes (2012), Retrieval of the aerosol direct radiative effect over clouds from spaceborne spectrometry, , *J. Geophys. Res. Atmos.*, 117, D07 207.

de Graaf, M., N. Bellouin, L. Tilstra, J. Haywood, and P. Stammes (2014), Aerosol directradiative effect of smoke over clouds over the southeast Atlantic Ocean from 2006 to 2009, *Geophys. Res. Lett.*, 41, GL061103.

Chand, D., T. Anderson, R. Wood, R. Charlson, Y. Hu, Z, Liu, and M. Vaughan (2008), Quantifying above-cloud aerosol using spaceborne lidar for improved understanding of cloudy-sky direct climate forcing, *J. Geophys. Res. Atmos.*, 113, D13 206.

Roebeling, R. A., A. Feijt, and P. Stammes (2006), Cloud property retrievals for climate monitoring: Implications of differences between Spinning Enhanced Visible and Infrared Imager (SEVIRI) on METEOSAT-8 and Advanced Very High Resolution Radiometer (AVHRR) on NOAA-17, *J. Geophys. Res.*, 111, D20 210.

Funding

Cooperation
Royal Netherlands Meteorological Institute, De Bilt, the Netherlands.

Metrics for the evaluation of warm convective cloud fields in a large-eddy simulation with Meteosat images

Sebastian Bley[1], Hartwig Deneke[1], Fabian Senf[1], Leonhard Scheck[2]

[1] Leibniz Institute for Tropospheric Research (TROPOS), Leipzig, Germany
[2] Meteorological Institute Munich, Ludwig Maximilian University Munich (LMU), Munich, Germany

Die hohe raumzeitliche Variabilität von konvektiven Wolken hat erhebliche Auswirkungen auf die Quantifizierung des Wolkenstrahlungseffektes. Da konvektive Wolken in atmosphärischen Modellen üblicherweise parametrisiert werden müssen, sind Beobachtungsdaten notwendig, um deren Variabilität sowie Modellunsicherheiten zu quantifizieren. Die raumzeitliche Variabilität von warmen konvektiven Wolkenfeldern wurde mithilfe von Meteosat Beobachtungen sowie hochaufgelösten Modellergebnissen von ICON-LEM charakterisiert. Verschiedene Metriken wurden untersucht, um Unsicherheiten in Modell- und Satellitendaten zu quantifizieren.
Die raumzeitlichen Skalen der Wolkenfelder hängen signifikant von der räumlichen Auflösung der Wolkenfelder ab. Für die Quantifizierung dieser Sensibilität wurden ICON-LEM (ICON Large Eddy Model) Simulationen mit einer räumlichen Auflösung von 156 m verwendet. Die simulierten Wolkenfelder können keine räumliche Skalen unterhalb der effektiven Modellauflösung von 1.2 km auflösen. Dadurch wird die Größe von kleinen konvektiven Wolken von ICON-LEM überschätzt. Dies impliziert, dass eine noch höhere Auflösung notwendig ist, um Wolkeneffekte unterhalb der 1 km Skala auflösen zu können.

Introduction

The realistic representation of clouds in general circulation models (GCMs) remains a fundamental challenge of climate research [*Bony et al.*, 2015]. This difficulty arises in part from the coarse horizontal resolution (~100 km) of GCMs, which does not allow to resolve individual clouds nor the underlying turbulent, microphysical and convective processes. Instead, subgrid-scale processes below the model resolution have to be parametrized. To evaluate and improve these parametrizations, and to advance our understanding of the effects of such small-scale processes, the characterization of the spatio-temporal characteristics of convective clouds across all relevant scales based on observations and high-resolution models is essential. Towards this goal, suitable metrics for comparing observations and model results are required, and their sensitivity to the spatial resolution of the underlying data needs to be quantified.

One challenge for the evaluation of high-resolution and large-domain simulations is the lack of suitable reference observations. Polar-orbiting satellite instruments like MODIS provide global datasets with high spatial resolution (~250–1000 m), but do not allow evaluating the temporal evolution of convective cloud fields. In contrast, the geostationary Meteosat satellites observe Central Europe with a 5 min repeat cycle, but only at a nadir resolution of ~3 km, which is relatively coarse in comparison to the typical size of warm convective clouds. Nevertheless, Meteosat offers the unique opportunity to characterize both the spatial and the temporal variability of small-scale convective cloud fields, and to use these characteristics for model evaluation. Towards this goal, *Bley et al.* [2016] introduced metrics to characterize the spatio-temporal evolution of convective cloud fields by calculating a decorrelation time scale as a measure of the average cloud lifetime as well as a decorrelation length.

Method

We use simulations from the ICON-LEM model which is based on the ICON model, developed at the DWD, and extended to a LES within the HD(CP)²
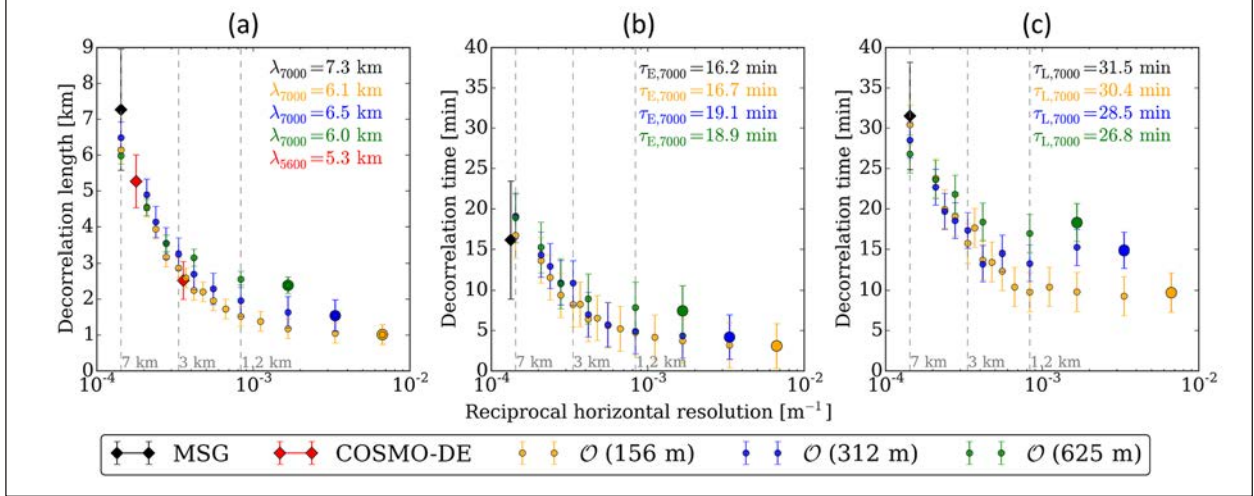
Fig. 1: (a) Spatial decorrelation length and (b) Eulerian and (c) Lagrangian decorrelation times in relation to the reciprocal horizontal resolution of simulations from ICON-LEM O(156 m) (yellow), O(312 m) (blue) and O(625 m) (green), COSMO-DE (red) and observations by MSG (black) of warm convective cloud fields on a local scale averaged over ten 62×62 km² LWP fields. The large circles represent the ICON-LEM scales for their native resolution, and smaller circles indicate the coarse-grained ICON-LEM scales. The vertical error bars indicate the standard deviation between the different cases for ICON-LEM, COSMO-DE and MSG.

project. ICON-LEM simulations were carried out with three different horizontal resolutions, 156 m, 312 m and 625 m. This allows us to analyze differences in the cloud fields arising from different model resolutions, and to separate model-inherent resolution effects from those resulting from a coarse-graining of the model outputs. Satellite data are taken from SEVIRI, which is the main payload on board the geostationary Meteosat Second Generation (MSG) satellites operated by EUMETSAT. The LWP is calculated using the Cloud Physical Properties retrieval [CPP; *Roebeling et al.,* 2006] developed in the framework of the Satellite Application Facility on Climate Monitoring [CM SAF; Schulz et al., 2009]. The lower part of the LWP distribution might be under-represented by MSG due to its detection limit, which mainly affects thin cirrus clouds and low small cumulus clouds.

We emphasize that there can be an inherent difference between the resolution at which the data are provided, called the native resolution here, and the optical or effective resolution for satellite observations and model simulations, respectively. For Meteosat observations, the optical resolution is lower than the native resolution by a factor of 1.6 [*Deneke and Roebeling,* 2010]. For numerical simulations, the effective resolution is always coarser than the native grid resolution and represents a range at which the variability of physical processes can be resolved. The ICON-LEM cloud fields are sequentially coarse-grained to an average pixel resolution of 7 km to allow comparisons with observations from Meteosat. We follow the methodology of *Bley et al.* [2016] and investigate the decorrelation scales and their resolution sensitivity in ICON-LEM warm convective cloud fields
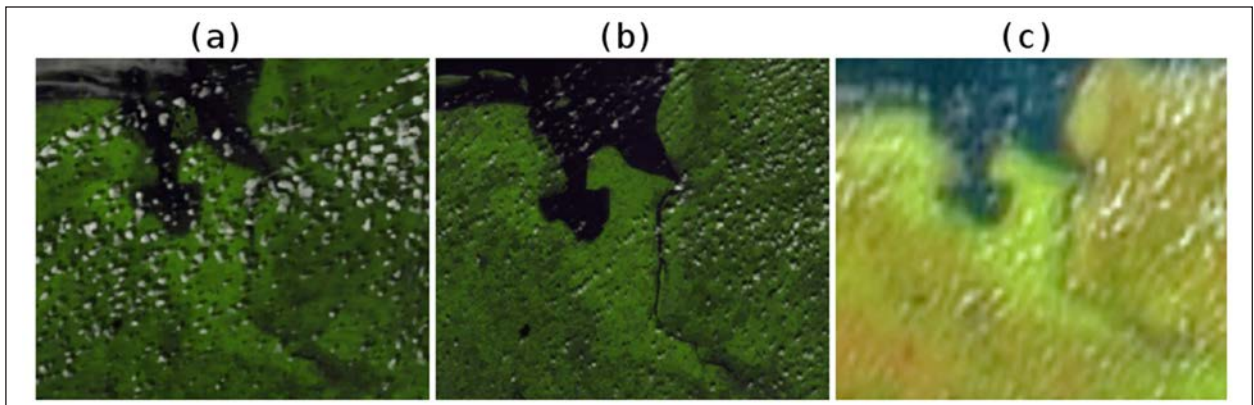
Fig. 2: (a) Forward simulation using fast radiative transfer calculations [Scheck et al., 2016] on ICON-LEM O(156 m), (b) shows the MODIS satellite image at 250x250 km² resolution and (c) the HRV RGB composite from Meteosat with 1.2x2.2 km² resolution.

by approaching a Lagrangian perspective to estimated the average cloud lifetime.

Results and Discussion

Figure 1 shows the decorrelation length (a), Eulerian (b) and Lagrangian decorrelation time (c) as averages of ten ICON-LEM and COSMO-DE fields of warm convective clouds in relation to the reciprocal horizontal resolution [*Bley et al.*, 2017]. While the Lagrangian decorrelation time is expected to be generally larger than the Eulerian decorrelation time, the latter is also beneficial to estimate the impact of advective processes onto the local decorrelation behaviour. An excellent agreement is found between the observed and the ICON-LEM scales at 7 km resolution. In contrast, ICON-LEM cloud fields at 156 m resolution exhibit substantially lower decorrelation lengths of 1 km and Lagrangian decorrelation times of 10 min. This result also demonstrates a high amount of unresolved cloud variability in the coarse-grained ICON-LEM and MSG cloud fields, which causes the high-resolution sensitivity of the decorrelation scales.

With the MSG SEVIRI rapid scan, we are able to characterize the changes in convective cloud fields with an update frequency of 5 min, which is sufficient for its spatial resolution. The biggest limit of MSG is the spatial resolution, which leads to a substantial overestimation of the decorrelation scales. The future generation of European geostationary satellites, the Meteosat Third Generation, will give great opportunity to bring down these limits to a spatial resolution of 1 km or even 500 m for selected channels [*Stuhlmann et al.,* 2005].

Recent atmospheric models with comparable spatial resolution as ICON-LEM are still unable to fully resolve cloud processes in the so-called gray zone [*Dorrestijn et al.,* 2012]. Although the model runs on a 156 m grid, it indicates remarkable deficits below the effective resolution, which was found to be about 1.2 km. This is also supported by Fig. 2, which shows an example cloud field over Northern Germany as synthetic radiances from ICON-LEM results (a) and satellite images from MODIS (b) and Meteosat (c). The ICON-LEM simulation overestimates the cloud sizes in comparison to the MODIS observation, which has 250 m resolution. Errors in the vertical and horizontal cloud dimensions have substantial effects on the distribution of cloud water and the quantification of cloud radiative effects and should be considered carefully. Therefore, a further increase in the ICON-LEM model resolution would be desirable in order to improve the representation of convective clouds below 1 km length scale.

References

Bley, S., H. Deneke, and F. Senf (2016), Meteosat-based characterization of the spatiotemporal evolution of warm convective cloud fields over Central Europe, *J. Appl. Meteorol. Climat.*, 55, 2181–2195.

Bley, S., H. Deneke, F. Senf, and L. Scheck (2017), Metrics for the evaluation of warm convective cloud fields in a large-eddy simulation with Meteosat images, *Q.J.R. Meteorol. Soc.*, 143, 2050–2060.

Bony, S., B. Stevens, D. M. W. Frierson, C. Jakob, M. Kageyama, R. Pincus, T. G. Shepherd, S. C. Sherwood, A. P. Siebesma, A. H. Sobel, M. Watanabe, and M. J. Webb (2015), Clouds, circulation and climate sensitivity, *Nat. Geosci.*, 8, 261–268.

Deneke, H. M. and R. A. Roebeling (2010), Downscaling of Meteosat SEVIRI 0.6 and 0.8 μm channel radiances utilizing the high-resolution visible channel, *Atmos. Chem. Phys.*, 10, 9761–9772.

Roebeling, R. A., Feijt, A. J., and Stammes, P. (2006), Cloud property retrievals for climate monitoring: Implications of differences between Spinning Enhanced Visible and Infrared Imager (SEVIRI) on METEOSAT-8 and Advanced Very High Resolution Radiometer (AVHRR) on NOAA-17, *J. Geophys. Res.*, 111, D20 210.

Scheck L., P. Frérebeau, R. Buras-Schnell, B. Mayer (2016), A fast radiative transfer method for the simulation of visible satellite imagery. *J. Quant. Spectrosc. Radiat. Trans.* 175: 54–67.

Stuhlmann R, Rodriguez A, Tjemkes S, Grandell J, Arriaga A, Bézy JL, Aminou D, Bensi P. (2005), Plans for EUMETSATs Third Generation Meteosat geostationary satellite programme. *Adv. Space Res.* 36: 975–981.

Schulz, J., Albert, P., Behr, H.-D., Caprion, D., Deneke, H., Dewitte, S., Dürr, B., Fuchs, P., Gratzki, A., Hechler, P., Hollmann, R., Johnston, S., Karlsson, K.-G., Manninen, T., Müller, R., Reuter, M., Riihelä, A., Roebeling, R., Selbach, N., Tetzlaff, A., Thomas, W., Werscheck, M., Wolters, E., and Zelenka, A. (2009), Operational climate monitoring from space: the EUMETSAT satellite application facility on climate monitoring (CM-SAF), *Atmos. Chem. Phys.*, 9, 1687–1709.

Articles

The Azores: A unique location to study stratocumulus and aerosol layering of the atmosphere in the North-East Atlantic

Holger Siebert[1], Silvia Henning[1], Birgit Wehner[1], Ulrike Egerer[1], Felix Lauermann[2], Frank Stratmann[1], Kai Szodry[1], Manfred Wendisch[2]

[1] Leibniz Institute for Tropospheric Research (TROPOS), Leipzig, Germany
[2] Institute for Meteorology, University of Leipzig, Leipzig, Germany

Im July 2017 wurde durch das TROPOS in Kooperation mit dem LIM eine Feldmesskampagne mit internationaler Beteiligung zur Untersuchung von Aerosol-, Wolken-, Strahlung- und Turbulenzwechselwirkungen über den Azoren im Nord-Ost-Atlantik durchgeführt. Grundlage dieser Messungen waren 17 Hubschrauberflüge mit den Schleppsonden ACTOS und SMART-Helios; der Einsatz erfolgte von dem Flugplatz der Insel Graciosa in direkter Nachbarschaft zur ENA-ARM Messstation. Die kontinuierlichen Messungen der ENA-ARM Station wurden um zusätzliche Aerosolmessungen erweitert und ergänzen zusammen mit Daten von einer weiteren Messstation auf dem Gipfel des Mt. Pico (2300 m, Ihla do Pico) die Hubschraubermessungen. In diesem Bericht werden an Hand zweier Messbeispiele Ergebnisse dargestellt, welche den Fokus der weiteren Auswertung skizzieren und einen kurzen Einblick in den komplexen Aufbau und die Schichtung der maritimen Atmosphäre unter bewölkten und unbewölkten Bedingungen im Nord-Ost-Atlantik geben.

Introduction

Persistent low-level stratocumulus (Sc) clouds are widespread over the globe and cover on average about 20% of the Earth's surface [*Wood*, 2012]. In particular, Sc clouds play a key role in maintaining the turbulent and radiative energy balance of the Sc-topped boundary layer (STBL), mainly due to their role in adjusting the turbulent and radiative fluxes.

Closely connected to the stratification of the STBL is the spatial distribution of aerosol particles. Aerosol particles strongly interact with clouds, serving on the one hand side as cloud condensation nuclei (CCN). On the other hand, clouds are also known as aerosol sources, due to new particle formation in their outflow regions. These processes may have significant influences on both particle and droplet number concentrations in the STBL. Furthermore, long-range transport of aerosol plays a significant role for the local balance. Due to the different sources and sinks of aerosol particles the spatial aerosol distribution is often characterized by complex layering closely linked to the boundary layer structure.

Although the marine boundary layer structure over the oceans is considered simpler compared to continental boundary layers, decoupled layers with multi-levels often characterize the layering. This holds true for cloudy and cloud-less situations. Besides the investigation of more fundamental questions of the physics of stratocumulus and aerosol, one major topic of the "Azores stratoCumulus measurements Of Radiation, turbulEnce and aeroSols" (ACORES) project is the detailed study of the thermal stratification and layering of the marine boundary layer in terms of clouds and aerosol.

The archipelago of the Azores (39° N, 28° W) is located about 1200 km west of Portugal and, therefore, considered as being representative for the undisturbed North-East Atlantic. The unique location has been already considered as a suitable place for atmospheric studies on stratocumulus and aerosol properties with ASTEX (Atlantic Sc Transition EXperiment, [*Albrecht et al.*, 1995]) probably being the most comprehensive field campaign in that region. A more recent project - the CAP-MBL (Clouds, Aerosol, and Precipitation in the Marine Boundary Layer, [*Remillard et al.*, 2012] - had
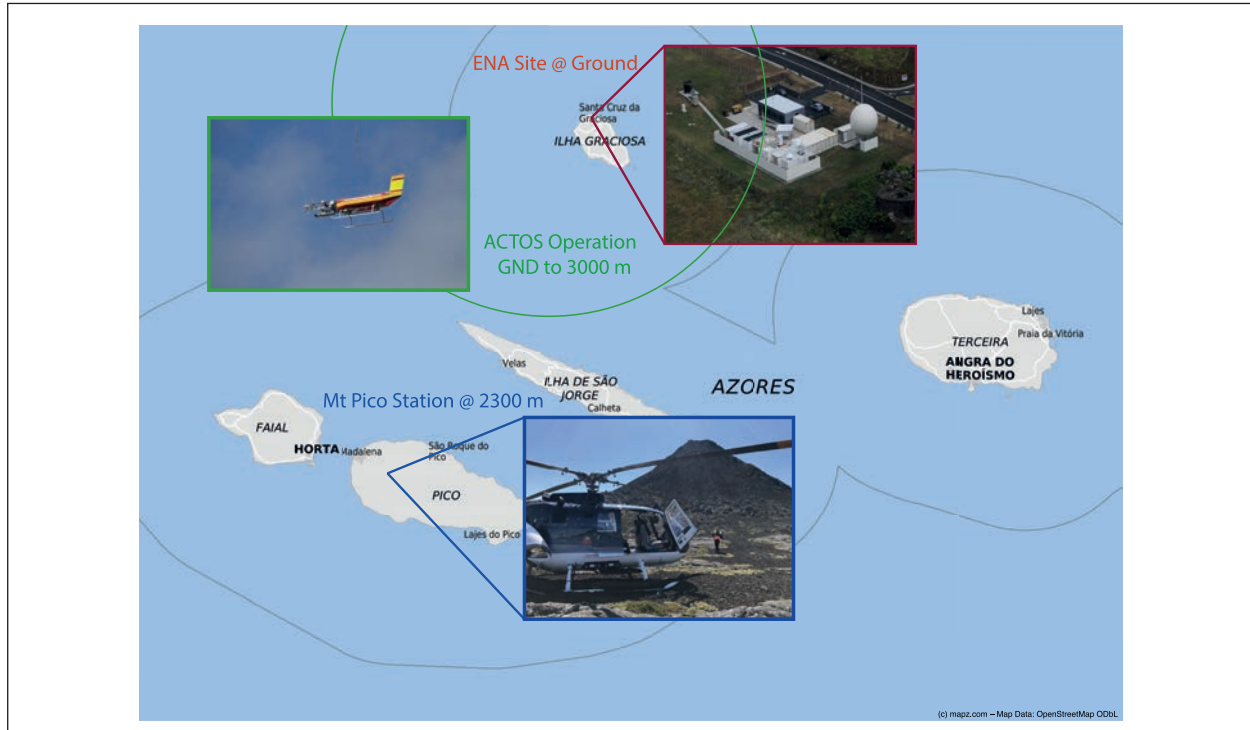
Fig. 1: A map of the central islands of the Azores with Graciosa Island in the north. At Graciosa airport the helicopter was based with ACTOS and Smart-Helios. The green circle roughly marks the operational area of the helicopter. Next to Graciosa airport the ENA site is located. In the southwest Mt Pico (Ilha do Pico) with a small aerosol sampling station is located. The picture shows the helicopter after landing at the mountain top for a cargo lift.

a somewhat different sampling strategy compared to previous studies because it was based on a long-term deployment of the ARM Mobile Facility (AMF) ENA (East North Atlantic) which has been set up on Graciosa Island/Azores in 2009 and turned recently into a permanent site.

The ACORES experiment

The ACORES experiment comprises three different sampling approaches: i) the permanent ARM site located at the airport of Graciosa island, ii) a smaller station on top of the Mt Pico in a height of 2300 m, and iii) the helicopter-borne ACTOS and SMART-Helios payloads, which sample in the vicinity of Graciosa almost from sea level up to 3000 m and, therefore, bridge the continuous ground and mountain-based observations. This approach is illustrated in Fig. 1.

For the period between July 3rd and July 22nd 2017, data sets from 17 research flights with ACTOS and SMART-Helios are available supported by the continuous aerosol observations at Mt Pico and ENA site. The presented ACTOS data includes high-resolution data of horizontal wind vector components (u_E, v_E), potential temperature Θ, and absolute humidity a, but also aerosol particle number size distribution and total number concentration of aerosol particles N_p and CCN

at 0.2% supersaturation (N_{CCN}). A new pyrano- and pyrgeometer combination provides up- and down welling irradiance observations in the terrestrial and solar band. Furthermore, a Cloud Droplet Spectrometer (CDP), a hot-wire probe (LWC-300) and a Particle Volume Monitor (PVM-100A) provide cloud droplet number concentration N_d, liquid water content LWC and droplet size distribution.

Two case studies and discussion

The main focus of this report is to show a typical stratification for cloudy and cloud-free situation. Figure 2 shows the vertical profile observed shortly after take-off on July 9th 2017 with a 150 m thick Sc layer present between 1100 and 1250 m. The first 200 m of the profile are still influenced by the island, which is most obvious in temperature and wind. The scale for the aerosol particle concentration was cut at 500 cm^{-3} because close to the airport the concentration was much higher due to local sources. However, for higher altitudes the observations are considered to be unaffected by the island and representative for the undisturbed North-East Atlantic. The Sc layer as observed during the first profile is characterized by comparable low LWC with maximum values around 0.3 g m^{-3} and small mean droplet diameters of up to 12 μm. The signal of the cloud layer in the terrestrial down-welling irradiance F_{down} is obvious as a local
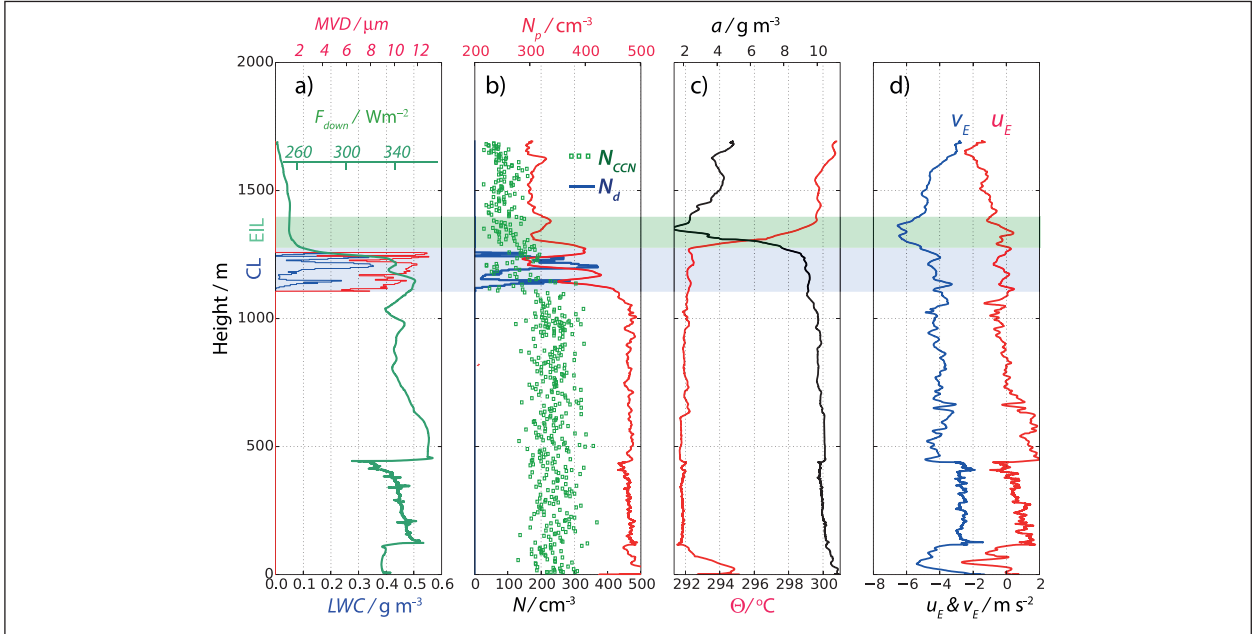
Fig. 2: Vertical profiles of a) LWC, mean volume diameter MVD, and terrestrial down-welling irradiance F_{down}, b) particle (N_p), droplet (N_d), and CCN (N_{CCN}) number concentration, c) absolute humidity a and potential temperature Θ, and d) horizontal wind velocity components v_E and u_E. The blue-shaded area marks the cloud layer (CL) whereas the green-shaded area represents the entrainment interfacial layer (EIL).

maximum around cloud base and a sharp jump at cloud top. From down- and upwelling irradiance the cooling rate at cloud top will be estimated in future analysis.

The droplet number concentration is of order 300 cm^{-3} whereas typical N_p is of order 450 cm^{-3} below the cloud layer and 200 cm^{-3} above cloud. The cloud is topped by a strong temperature inversion: Θ increases by almost 8 K over a height range of 100 m whereas a drops by 8 g m^{-3}. This inversion above the cloud is called entrainment interfacial layer (EIL). It is worth mentioning that above the EIL the humidity increases with height indicating advection of humid air masses in the free troposphere, which is quite unusual. In literature (e.g., [*Nichols and Leighton*, 1986]) humidity typically decrease and the free troposphere is characterized by low humidity. One feature, which was observed quite often during the ACORES campaign, is the wind shear in the EIL and above. Both types of wind shear, an increase of wind velocity but also a change of wind direction with height has been observed. For our case study in Fig. 2 the wind speed increased only from 4 to 6 m s^{-1} but stronger shear has been observed during other days.

The balance between wind shear as a major source for turbulence and the typical stable stratification in the cloud top region is one of the most important open questions in terms of cloud-top entrainment. Based on the experience of previous work of the ACORES team [*Katzwinkel et al.*, 2012; *Malinowski et al.*, 2013] this topic will be – together with the role of radiative cooling at cloud top - one major focus of further cloud data

analysis. The sampling strategy with Dolphin-like flight patterns around the cloud tops (see next paragraph) provides a perfect data set and preliminary data analysis is very promising.

Figure 3 shows a section of Dolphin flights for July 9th, 2017. The sharp jump of virtual temperature T'_v at the inversion is one obvious feature of this record. The lower panel of Fig. 3 shows the LWC as a cloud indicator and the aerosol particle number concentration N_p. One obvious feature of N_p is the strong variability inside the clouds with values ranging from almost zero to values of 450 cm^{-3} typical for the sub-cloud layer (cf. Fig. 2). Although sharp minima corresponding with maxima in LWC are visible – the typical picture of cloud droplet activation that results in a reduction of interstitial aerosol – several sharp spikes of N_p in the green-shaded areas have been observed with maxima twice of the sub-cloud layer concentration. This phenomenon is considered as a clear indication for new particle formation in the cloud region [*Wehner et al.*, 2015] – a feature frequently observed during the ACORES campaign.

A probability density function (PDF) of droplet sizes around cloud top (red line) and in the lower part of the cloud (dark blue line) is shown in arbitrary units. This PDF is estimated from the final cloud profile during the Dolphin flights marked with a black box. A clear shift from smaller droplets in the lower cloud part to larger cloud droplets close to cloud top is obvious. To which extend the bigger droplets are due to pure condensational

growth or how turbulent mixing at cloud top plays a role will be another focus of further investigation.

The second case study from 5th of July shows an example under cloud-free conditions with a focus on physical aerosol properties and stratification. In the left panel of Fig. 4 the vertical profile as sampled shortly after take-off is shown. The potential temperature Θ and absolute humidity a clearly indicate a 700 m thick well-mixed layer (ML) with height-independent total aerosol concentration of $N_p = 350$ cm^{-3} and $N_{CCN} = 100$ cm^{-3}, respectively. Above 700 m the atmosphere is stably stratified up to the maximum height of the profile (2000 m) with a generally decreasing humidity but several distinguished humidity layers and a pronounced minimum just above the ML.

Aerosol concentration exhibit in general higher values above ML but organized in several well-separated layers including one thin layer in 1550 m with concentrations even lower compared to the ML. Interestingly, these aerosol layers are not necessarily qualitatively correlated with humidity layers. The physical properties of the aerosol population indicate a clear cut between aerosol in the ML and above. Several flight legs in a constant height are used for estimating aerosol number size distributions that are shown in the right panel of Fig. 4. The yellow-shaded area shows the distribution for the ML aerosol and

is characterized by two clearly separated modes, an Aitken mode with a peak at 50 nm and an Accumulation mode with a peak at 200 nm. The distributions observed in 120 and 430 m by ACTOS compares qualitatively well with the distribution observed at the ENA site. This is worth mentioning because the ACTOS distributions are based on the average over 3-5 scans of about 2 minutes each whereas the ENA and Mt Pico distributions are averaged over the entire ACTOS flight of about two hours which results in much more robust statistics.

The upper right panel of Fig. 4 shows the distributions observed in 1000, 1600, and 2000 m respectively – all well above the ML. These distributions show a significant accumulation mode with a peak slightly shifted to diameters below 200 nm compared to the ML observations but without a pronounced Aitken mode. Only a small shoulder around 60 nm is visible for all distributions. Interestingly this shoulder is most obvious for the leg in 1600 m with the minimum in total aerosol number concentration. In addition to the three distributions based on ACTOS observations the data from Mt Pico in 2300 m are shown. Qualitatively, this distribution also compares well with the ACTOS observations in comparable heights and shows the same accumulation mode and small shoulder around 60 nm for an Aitken mode.
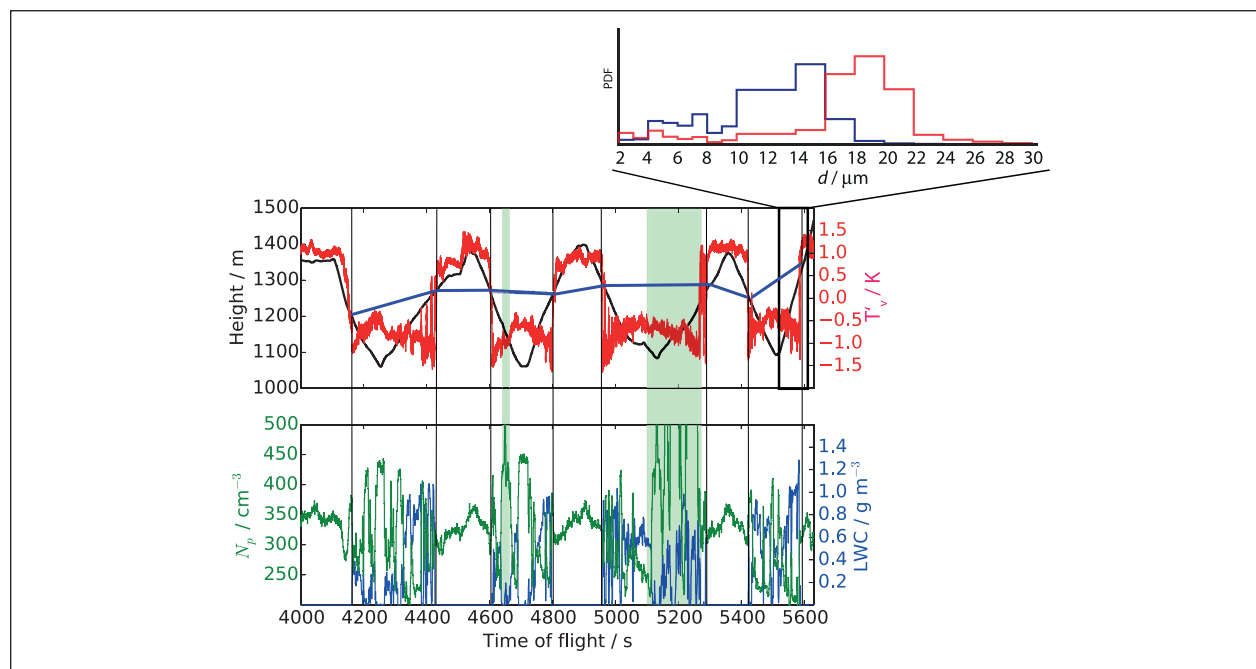
Fig. 3: Time series of (upper panel) barometric height (black line) including estimated cloud top (blue line), fluctuations of the virtual temperature T' as derived from the ultrasonic anemometer (red line) and in the lower panel of N_p and LWC during a sequence of Dolphin flights. Green-shaded periods exhibit several spikes in N_p that are cut in this plot for more detailed presentation. As an inlay, the PDF of the droplet sizes close to cloud top (red curve) and in the lower cloud part (dark blue curve) is shown with arbitrary units. This PDF is based on observations during the final ascent marked with the black box.
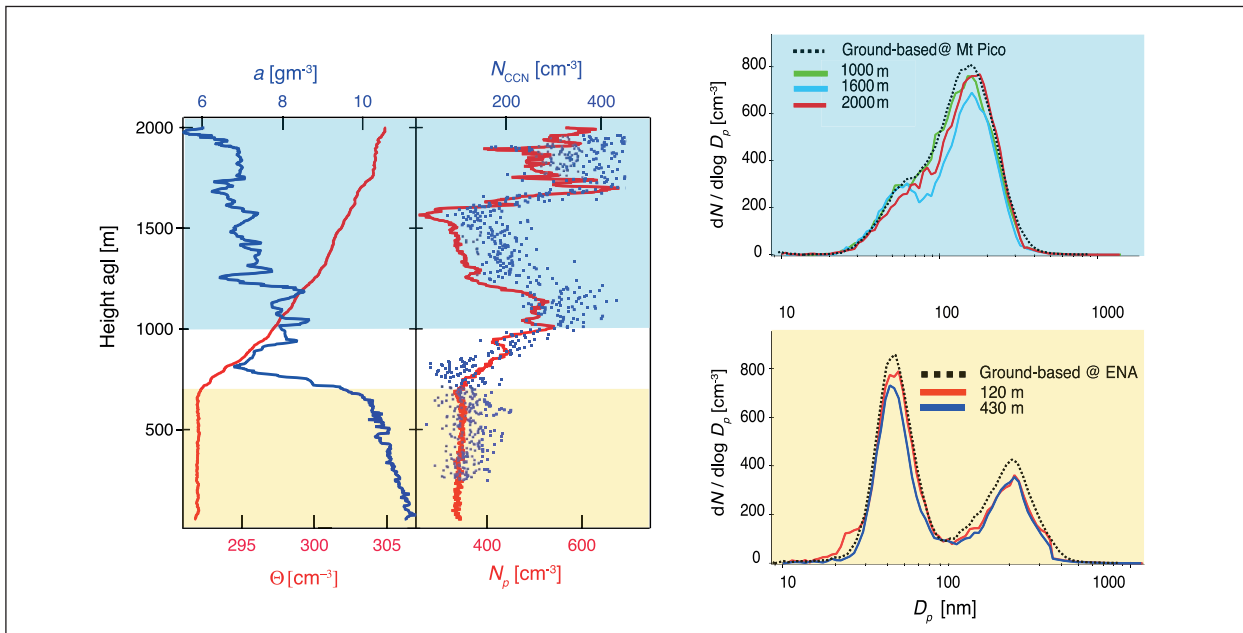
Fig. 4: The left panel shows a vertical profile of Θ (red line), a (blue line), N_{CCN} at 0.2% supersaturation (blue dots) and N_P (red line) as observed during a cloud-free day on July 5th, 2017. The right panels shows aerosol particle size distributions as observed by ACTOS in different heights. The background color indicates the height region in the corresponding profile of the left panel. Additionally, ground-based size distributions at the ENA site (at sea level) and on Mt Pico in 2300 m height are added.

The complex aerosol layering is in contrast to previous observations (e.g., [*Collins et al.*, 2000]) in the North-East Atlantic. Based on the profiles shown in Fig. 4 it seems even impossible to define a clear transition from the ML to the free troposphere. This layering is even more complex in combination with cloud layers and it turns out that general layering and stratification – under cloudy and cloud-free conditions – will become one of the major topics of the ACORES project.

References

R. Wood. Stratocumulus clouds. *Q. J. R. Meteorol. Soc.*, 140:2373 – 2423, DOI:10.1175/MWR–D–11– 00121.1, 2012.

B. A. Albrecht, C. S. Bretherton, D. Johnson, W. H. Scubert, and A. S. Frisch. The Atlantic Stratocu- mulus Transition Experiment – ASTEX. *Bull. Am. Meteor. Soc.*, 76:889–904., 1995.

J. Katzwinkel, H. Siebert, and R. A. Shaw. Observation of a self-limiting, shear-induced turbulent inversion layer above marine stratocumulus. *Boundary-Layer Meteorol.*, 145:131 – 143, 2012.

D. R. Collins, H. H. Jonsson, J. H. Seinfeld, R. C. Flagan, S. Gasso, D. A. Hegg, P. B. RusselL, B. Schmid, J. M. Livongston, E. O. Ström, L. M. R. K. J. Noone, and J. P. Putaud. In situ aerosol-size distributions and clear-column radiative closure during ace-2. *Tellus*, 52(B):498 – 525, 2000.

S. P. Malinowski, H. Gerber, I. J.-L. Plante, M. K. Kopec, W. Kumala, K. Nurowska, P. Y. Chuang, D. Khelif, and K. E. Haman. Physics of Stratocumulus Top (POST): turbulent mixing across capping inversion. *Atmos. Chem. Phys.*, 13:12171–12186, 2013.

S. Nicholls and J. Leighton. An observational study of the structure of stratiform cloud sheets: Part I. Structure. *Q. J. R. Meteorol. Soc.*, 112:431–460, 1986.

J. Remillard, P. Kollias, E. Luke, and R. Wood. Marine boundary layer cloud observations in the Azores. *J. Climate*, 25(DOI: 10.1175/JCLI-D-11-00610.1):7381 – 7398, 2012.

B. Wehner, F. Werner, F. Ditas, R. A. Shaw, M. Kulmala, and H. Siebert. Observations of new particle formation in enhanced UV irradiance zones near cumulus clouds. *Atmos. Chem. Phys. Discuss.*, 15:12423 – 12452, 2015.

Spatial distribution of black carbon and PM in Rome: Case study for highly quality-assured mobile measurements

Honey Dawn Alas[1], Kay Weinhold[1], Thomas Mueller[1], Sascha Pfeiffer[1], Francesca Costabile[2], Antonio Di Ianni[2], Luca Di Liberto[2], Alfred Wiedensohler[1]

[1] Leibniz Institute for Tropospheric Research (TROPOS), Leipzig, Germany
[2] Institute of Atmospheric Science and Climate, National Research Council (CNR-ISAC), Italy

Der Ansatz, Luftschadstoffe mit mobilen Geräten zu messen, hat aufgrund seiner großen Anwendbarkeit in den letzten zehn Jahren an Popularität gewonnen. Die Erfassung der realen räumlichen Verteilung von Schadstoffen mit hoher Messqualität bleibt jedoch eine Herausforderung. Daher wird in dieser Studie eine Standardmethodologie vorgeschlagen, um Daten mit hoher Qualität aus mobilen Messungen zu erhalten. Zum einen ermöglicht eine feste Messstation entlang der Strecke regelmäßige Qualitätskontrollen der mobilen Geräte gegenüber den qualitätsgesicherten Referenzinstrumenten. Zweitens ermöglichte die Durchführung paralleler mobiler Messungen eine konstante Überwachung ihrer Qualität entlang der gesamten Route, welche zur Repräsentativität des räumlichen Durchschnitts führte. Drittens werden Partikelgrößenverteilungen optischer Partikelgrößenspektrometer mit begrenztem Messbereich mit qualitätsgesicherten Messungen an der festen Station korrigiert, um a) das gesamte Partikelgrößenspektrum des gesamten feinen Partikelgrößenbereichs zu erhalten und b) um PM-Massenkonzentrationen abzuleiten. Die vorgeschlagene Methodik befasst sich mit einigen der wichtigsten Fragen in Bezug auf die Qualität mobiler Messungen, insbesondere unter Berücksichtigung von Studien zur gesundheitlichen Auswirkungen, zur Validierung der modellierten räumlichen Verteilung und zur Entwicklung von Strategien zur Verringerung der Luftverschmutzung.

The approach of measuring air pollutants with mobile measurements have gained popularity over the last decade due to its wide range of applicability. However, capturing the real world scenario of spatial distribution of pollutants in a high quality level remains a challenge [*Van den Bossche et al.*, 2015]. Hence, this study proposed a standard methodology to achieve highly quality-assured data from mobile measurements. First, including a fixed station in an urban background area along the route allowed for regular quality check of the mobile instruments against the reference instruments. Second, performing parallel mobile measurements provided a constant monitoring of their performance along the entire route leading to representativeness of the spatial average. Third, optical instruments with limited size range of the particle number size distributions have been corrected to include the whole particle size spectrum (particularly the entire fine mode) to derive mass concentrations of PM. The proposed methodology addressed some of the main issues regarding quality of mobile measurements especially when considered for health impact studies, validation of modelled spatial distribution, and development of air pollution mitigation strategies.

Methods

An intensive campaign called Carbonaceous Aerosols in Rome Environs (CARE) was conducted in the downtown area of Rome, Italy for 4 weeks in February of 2017. The aim of this campaign was to characterize the carbonaceous aerosols in the Mediterranean urban background area of Rome [*Costabile*
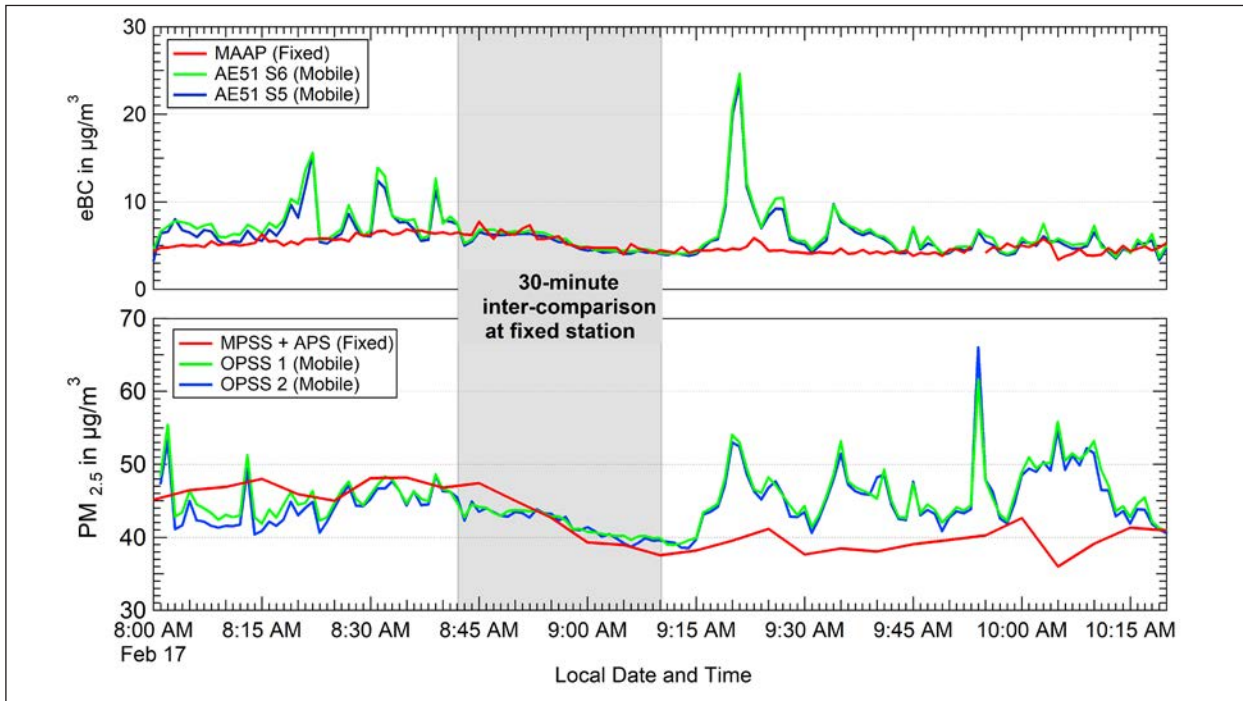
Fig. 1: Time series of parameters measured on the 17th of February (single run) using the parallel approach. The grey area shades the period of inter-comparison at the fixed station. The top panel shows the eBC mass concentrations measured using two AE51s (green and blue) compared against the reference eBC measurements MAAP. The bottom panel shows PM$_{2.5}$ concentrations derived from measurements obtained from two OPSSs compared against the PM$_{2.5}$ mass concentrations reconstructed from MPSS and APS data.

et al., 2017]. Simultaneously, mobile measurements for equivalent black carbon (eBC, microAeth Model AE51) and particle number size distribution (PNSD; TSI Optical particle size spectrometer-OPSS Model 3330) were acquired using two identical platforms (backpacks). Daily (weekday and weekends) parallel measurements were conducted along a fixed route during three periods: morning rush hour, midday, and evening rush hour with a 30-minute inter-comparison against the reference station for each mobile measurement (Multi-angle Absorption Photometer or MAAP for eBC and combined data of TROPOS Mobility Particle Size Spectrometer and Aerodynamic Particle Size Spectrometer or APSS for particulate matter or PM). PM mass concentrations were derived from the OPSS PNSD after correcting for refractive index effects according to the Mie scattering theory. The volume fraction of the fine mode (300 nm – 1000 nm) of the OPSS was corrected according to the volume fraction measured by the MPSS (10 nm – 10000 nm) in the fixed station.

Results

Exemplary data from the mobile measurement campaign allowed for the evaluation of the proposed methodology. First, the parallel measurements resulted in constant quality check of data, increasing the representativeness of the spatial average. Figure 1 shows the time series of the eBC mass concentration, resulting from a single measurement period. From this approach, we found that the unit-to-unit variability of the mobile instruments were +/- 5% and the small differences were noted to be dependent on the distance from the source. Second, results of regular 30-minute inter-comparison at fixed station showed that the mobile instruments for eBC mass concentration are well within 5% of the reference instruments MAAP. Third, the analysis of volume particle size distributions obtained from OPSS and the MPSS showed that the OPSS underestimates the fine mode by a factor ranging from 2 -11 throughout the measurement period as the peak of the volume size distribution varied as well. Furthermore, the refractive index to correct the data (OPSS calibration was done with polystyrene latex (PSL) particles) was 1.50 + 0.001i, similar to literature values for Rome [*Costabile et al.*, 2013]. The derived PM$_{2.5}$ mass concentrations from the mobile instruments were within +/- 20% of the reference instruments (reconstructed PM using MPSS and APSS). Finally, the resulting spatial distribution of eBC and PM$_{2.5}$ mass concentrations (Fig. 2) shows the dependence of eBC and PM$_{2.5}$ mass concentrations on traffic emissions, human activities, and meteorology. This also shows that the spatial distribution of eBC and PM mass concentrations are
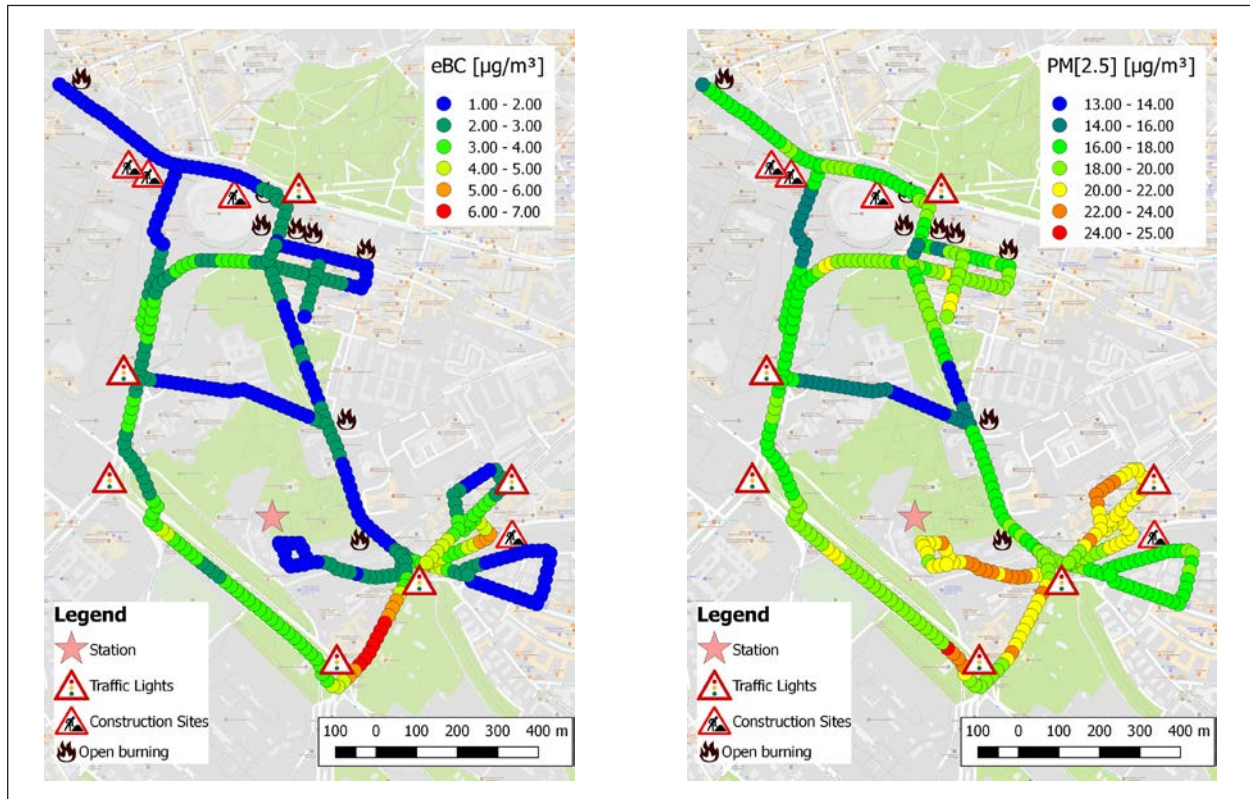
Fig. 2: Overall averaged spatial distribution of eBC mass concentration (left) and PM$_{2.5}$ (right). Locations of the fixed reference station, construction areas, traffic lights, and combustion activities are indicated. Image source: Google Maps.

not well correlated. Hence, when considering personal exposure to near-surface air pollution, the smaller and more toxic eBC mass concentration should also be given more importance.

Data of this quality can be beneficial to health studies related to air pollution and validation of microscale models. Moreover, the high spatial resolution data can prove valuable for policy-makers and urban planners in developing strategies to mitigate air pollution.

References

Costabile, F., et al. (2013) Identification of Key Aerosol Populations through Their Size and Composition Resolved Spectral Scattering and Absorption, *Atmos. Chem. Phys., vol. 13, no. 5, May 2013,* 2455–2470.

Costabile, F., et al. (2017) First Results of the "Carbonaceous Aerosol in Rome and Environs (CARE)" Experiment: Beyond Current Standards for PM$_{10}$. *Atmosphere.* 8(12):249.

Van den Bossche, J., Peters, J., Verwaeren, J., Botteldooren, D., Theunis, J., & Baets, B. D. (2015). Mobile monitoring for mapping spatial variation in urban air quality: Development and validation of a methodology based on an extensive dataset. *Atmos. Environ., 105,* 148-161.

Cooperation

Institute of Atmospheric Science and Climate, National Research Council (CNR-ISAC), Italy

Indoor particles exposure and its relationship to the outdoor concentrations in private homes

Jiangyue Zhao[1], Birgit Wehner [1], Thomas Tuch[1], Kay Weinhold[1], Maik Merkel[1], Ulrich Franck[2], Wolfram Birmili[3], Anja Lüdecke[3], Tareq Hussein[4], and Alfred Wiedensohler[1]

[1] Leibniz Institute for Tropospheric Research (TROPOS), Leipzig, Germany
[2] Helmholtz Centre for Environmental Research, Leipzig, Germany
[3] German Environment Agency (UBA), Berlin, Germany
[4] University of Jordan, Amman, Jordan

Heutzutage verbringen Menschen einen großen Teil ihrer Zeit in geschlossenen Räumen. Gegenwärtig sind nur begrenzte Informationen über die Exposition mit ultrafeinen Innenraum-Partikeln verfügbar, die entweder aus Innen- oder Außenquellen stammen können. Es ist daher wichtig, den Beitrag von Wohnaktivitäten zur Innenraumluft und die Veränderung der Partikelgrößenverteilung (PNSD) in der Außenluft zu untersuchen, die durch die Penetrationsprozesse verursacht wird. Im Auftrag des Umweltbundesamtes (UBA) wurde deshalb dem Leibniz-Institut für Troposphärenforschung (TROPOS) ein Projekt zur Untersuchung der Aerosolpartikel-Exposition und deren Zusammenhang mit der städtischen und ländlichen Atmosphäre erteilt. In dieser Studie werden die Ergebnisse der ersten Messperiode in Leipzig vorgestellt, einschließlich der Variation der Partikelzahlkonzentrationen (PNC) sowie Innen/Außen (I/O)-Verhältnisse für verschiedene feine - und ultrafeine Partikelgrößenbereiche. Ergebnisse für verschiedene Wohnaktivitäten sowie die Entwicklung von Partikelgrößenverteilungen einer spezifischen Innenraumquelle sind beispielhaft dargestellt. Äquivalente Ruß-Massenkonzentrationen werden mit der PNC verschiedener Größenbereiche verglichen, um ein besseres Verständnis für den Größenbereich von Rußpartikeln zu erhalten, die aus den verschiedenen Innenraum-Quellen stammen können.

Introduction

Nowadays, people spend a large fraction of their time indoors [*Brasche and Bischof*, 2005; *Kousa et al.*, 2002]. Currently, only limited information is available about the exposure of residents to indoor ultrafine particles, which can originate from either indoor or outdoor sources [*Chen and Zhao*, 2011; *Morawska et al.*, 2013]. It is thus important to study the contribution of residential activities to the indoor air and the modification of outdoor particle number size distribution (PNSD) caused by the penetration processes. Therefore, on behalf of the German Environment Agency (UBA), a project to study the indoor aerosol particle exposure and its relationship to the urban and rural atmosphere has been granted to the Leibniz Institute for Tropospheric Research (TROPOS). This article presents results from the first measurement period in Leipzig, including the

variation in the particle number concentration (PNC) and Indoor/Outdoor (I/O) ratios in different fine and ultrafine particle size ranges. Results from different residential activities as well as the evolution the particle number size distributions of a certain indoor source are shown exemplary. Equivalent black carbon mass concentrations are compared to PNC of different size ranges to obtain a better understanding of the size range of black carbon particles, originating from different indoor sources.

Indoor sources such as cooking, candles, open fires, cleaning and smoking are understood to be primary drivers of increased indoor particle number and mass concentrations [*Koistinen et al.*, 2004; *Lai et al.*, 2010; *Lazaridis et al.*, 2006; *Semple et al.*, 2012]. This work shows the characteristic of PNSD of different indoor sources in several private homes. Indoor and outdoor particle concentration have been

proven to be strongly correlated in the absence of major indoor sources [*Franck et al.*, 2006; *Hussein et al.*, 2006; *Talbot et al.*, 2016]. However, there is a gap in the knowledge of the relationship between indoor and outdoor ultrafine particles in real homes. This work measures PNC and PNSD between 10 and 800 nm and illustrates that in the situation of closed windows indoor and outdoor particle concentrations are still highly correlated. This is caused by penetration processes. The quantification of the modification of PNSD caused by these processes will be the next goal of this work.

Methods

Measurements are or will be performed in 40 households in two German cities: Leipzig and Berlin. The first measurement period took place in Leipzig in 2017. Households are located in the urban, suburban, and rural area, for obtaining an understanding of the regional influences to PNC. Each household was or will be probed twice for one week, covering both, the cold and warm season to observe the seasonal differences in the PNC.

In each household, indoor measurements took place in the living room, in which people mainly spend their time. Outdoor measurements took place on the balcony, terrace, or in a connected yard. Indoor and outdoor measurements were performed simultaneously. The measured parameters for indoor and outdoor air have been the PNC and PNSD (0.01 – 0.8 µm), using mobility particle size spectrometers (build by TROPOS), and PM_1, $PM_{2.5}$, PM_{10} mass concentrations, using optical particle size spectrometers (Grimm Model 1.108). Additional indoor measurements were the equivalent black carbon mass concentration (microAeth Model AE51) to obtain a better understanding of the composition of indoor sources. As well as the indoor CO_2 concentration (CO_2 sensor, GMP252 Vaisala) to document the room ventilation. The measurements are accompanied by a questionnaire, which documents the room characteristics and a digital notebook, capturing the residential activities.

Results

The indoor and outdoor particles relationship can be quantified by the ratio between indoor and outdoor concentrations (I/O ratio). Figure 1 shows the time series of the median PNC and I/O ratio measured indoors and outdoors at 20 households in Leipzig. The
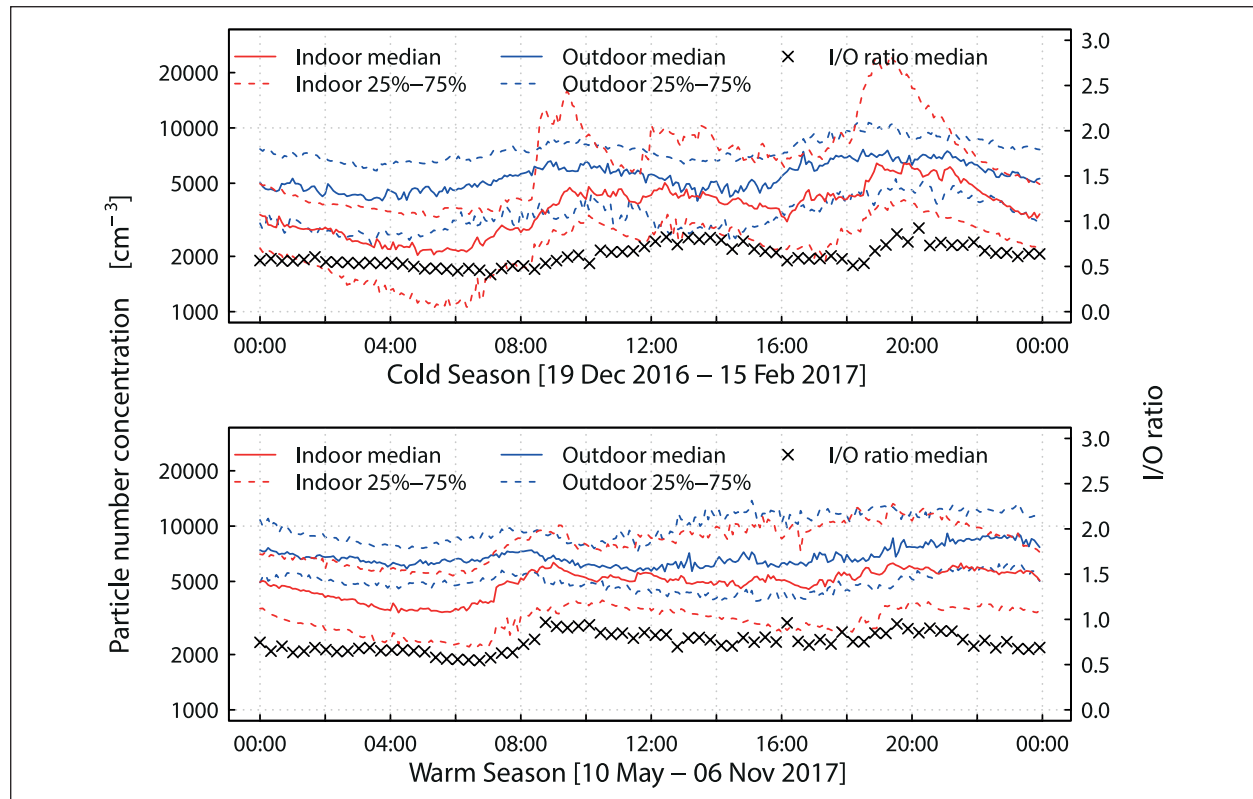
Fig. 1 Time series of indoor and outdoor median PNC measured during the cold season (19 Dec 2016 – 15 Feb 2017) and warm season (10 May 2017 – 11 Sep 2017). The shaded areas are in between the 25% - 75% percentiles of all corresponding data points. The time resolution of the data set is five minutes. In this figure 00:00 - 07:00 is defined as sleeping time and 07:00 – 24:00 is defined as active time.
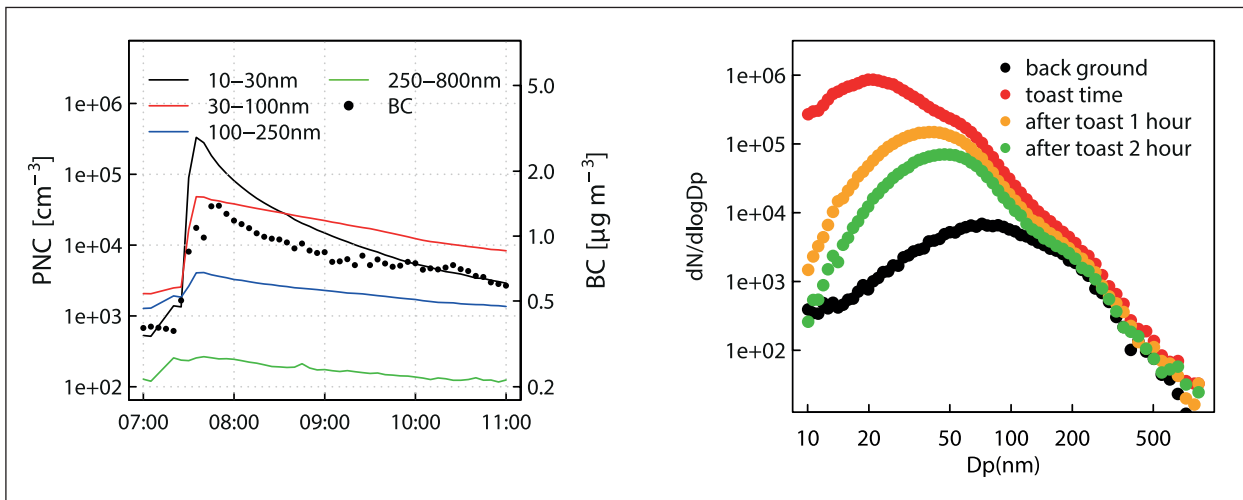
Fig. 2 Example of toasting. a). Time series of indoor PNC in the size ranges of 10-50 nm, 50-100 nm, 100-250nm, 250-800nm and the black carbon (BC) mass concentration. The shaded area is marking the toasting time. b). PNSD of before toasting, during toasting, after toasting 1 hour and 2 hours of the same toasting activity as a).

outdoor concentration generally exceeds the indoor concentration. The I/O ratio was calculated by dividing the indoor PNC by the outdoor PNC for each pair of data points separately. The 24 hours median I/O ratio ranges from 0.4 to 1.

During sleeping time, indoor and outdoor PNCs decreased constantly in both seasons, since neither was influenced by traffic and nor were there indoor sources. The I/O ratio is relatively constant, indicating that indoor and outdoor PNCs are highly related, even in the cold season, when no household had open windows during the night.

During active time, the indoor concentration and I/O ratio show stronger peaks during breakfast, lunch and dinner time in cold season, because more people are at home at these times and have activities such as roasting, baking, etc., causing particles production. On the other hand, outdoor concentrations show an increase in the morning and evening because of rush hour time.

While in warm season, indoor and outdoor PNCs both increase during active time, the peaks patterns

are not as clear as in the cold season. The reason is probably that the average outdoor temperature is around 20°C and people open windows more often. This also lets indoor-produced particles quickly exchange with the outside air.

Figure 2 shows an example for toasting. In Figure 2a) PNCs and BC mass concentration rapidly increased. The PNC increase by approximately two orders of magnitude for particles in the size range 10-30 nm. With increasing particle size, the increase in PNC gets smaller and smaller. The increase in PNC for the size range 250-800 nm is barely visible. This indicates that toasting activities mainly and significantly contributes to ultrafine particles. Figure 2b) shows the particle number size distribution with a peak around 20 nm in particle diameter. After that, the freshly emitted ultrafine particles undergo rapid coagulation or are lost by diffusion to the existing surface area in the room. This is shown by a shift of the particle number size distribution towards the accumulation mode. At the same time, the total number concentration decreases.

References

Brasche, S., and W. Bischof (2005), Daily time spent indoors in German homes – Baseline data for the assessment of indoor exposure of German occupants, *Int. J. Hyg. Environ. Health*, 208(4), 247-253, doi: https://doi.org/10.1016/j.ijheh.2005.03.003.

Chen, C., and B. Zhao (2011), Review of relationship between indoor and outdoor particles: I/O ratio, infiltration factor and penetration factor, *Atmos. Environ.*, 45(2), 275-288, doi: 10.1016/j.atmosenv.2010.09.048.

Franck, U., T. Tuch, M. Manjarrez, A. Wiedensohler, and O. Herbarth (2006), Indoor and outdoor submicrometer particles: exposure and epidemiologic relevance ("the 3 indoor Ls"), Environ. Toxicol., 21(6), 606-613.

Hussein, T., T. Glytsos, J. Ondráček, P. Dohányosová, V. Ždímal, K. Hämeri, M. Lazaridis, J. Smolík, and M. Kulmala (2006), Particle size characterization and emission rates during indoor activities in a house, *Atmos. Environ.*, 40(23), 4285-4307.

Koistinen, K. J., R. D. Edwards, P. Mathys, J. Ruuskanen, xfc, N. nzli, and M. J. Jantunen (2004), Sources of fine particulate matter in personal exposures and residential indoor, residential outdoor and workplace microenvironments in the Helsinki phase of the EXPOLIS study, *Scand. J. Work Environ. Health*, 30, 36-46.

Kousa, A., J. Kukkonen, A. Karppinen, P. Aarnio, and T. Koskentalo (2002), A model for evaluating the population exposure to ambient air pollution in an urban area, *Atmos. Environ.*, 36(13), 2109-2119, doi: https://doi.org/10.1016/S1352-2310(02)00228-5.

Lai, S., K. Ho, Y. Zhang, S. Lee, Y. Huang, and S. Zou (2010), Characteristics of residential indoor carbonaceous aerosols: a case study in guangzhou, pearl river delta region, *Aerosol Air Qual. Res.*, 10(5), 472-478.

Lazaridis, M., V. Aleksandropoulou, J. Smolík, J. E. Hansen, T. Glytsos, N. Kalogerakis, and E. Dahlin (2006), Physico-chemical characterization of indoor/outdoor particulate matter in two residential houses in Oslo, Norway: measurements overview and physical properties – URBAN-AEROSOL Project, *Indoor Air*, 16(4), 282-295, doi: 10.1111/j.1600-0668.2006.00425.x.

Morawska, L., A. Afshari, G. N. Bae, G. Buonanno, C. Y. Chao, O. Hanninen, W. Hofmann, C. Isaxon, E. R. Jayaratne, P. Pasanen, T. Salthammer, M. Waring, and A. Wierzbicka (2013), Indoor aerosols: from personal exposure to risk assessment, *Indoor Air*, 23(6), 462-487, doi: 10.1111/ina.12044.

Semple, S., C. Garden, M. Coggins, K. Galea, P. Whelan, H. Cowie, A. Sánchez-Jiménez, P. Thorne, J. Hurley, and J. Ayres (2012), Contribution of solid fuel, gas combustion, or tobacco smoke to indoor air pollutant concentrations in Irish and Scottish homes, *Indoor Air*, 22(3), 212-223.

Talbot, N., L. Kubelova, O. Makes, M. Cusack, J. Ondracek, P. Vodička, J. Schwarz, and V. Zdimal (2016), Outdoor and indoor aerosol size, number, mass and compositional dynamics at an urban background site during warm season, *Atmos. Environ.*, 131, 171-184.

Power plant ash as atmospheric ice nucleating particles

Sarah Grawe[1], Stefanie Augustin-Bauditz[1+], Hans-Christian Clemen[2], Johannes Schneider[2], Jasmin Lubitz[1], Naama Reicher[3], Yinon Rudich[3], Frank Stratmann[1], and Heike Wex[1]

[1] Leibniz Institute for Tropospheric Research (TROPOS), Leipzig, Germany
[2] Max Planck Institute for Chemistry, Mainz, Germany
[3] Weizmann Institute of Science, Rehovot, Israel
[+] Now at: Deutscher Wetterdienst, Hamburg, Germany

Im Rahmen einer Messkampagne im November 2016 wurden verschiedene Flugaschen aus deutschen Kohlekraftwerken bezüglich ihrer Eiskeimfähigkeit analysiert. Simultan zu Messungen mit dem Leipzig Aerosol and Cloud Interaction Simulator (LACIS) wurden die Flugaschepartikel mithilfe eines Einzelpartikel-Massenspektrometers untersucht. Aufgrund der Ergebnisse zum Immersionsgefrierverhalten in Kombination mit Informationen zur chemischen Zusammensetzung der Partikel wird vermutet, dass kalzium- und schwefelhaltige Substanzen in den Flugaschen Eisnukleation induzieren. Zusätzlich wurde beobachtet, dass Flugaschepartikel, die zuvor in Wasser suspendiert waren, wesentlich weniger effektive Eiskeime sind als trocken zerstäubte Partikel. Dies könnte im Zusammenhang mit einer Hydrierung der oben genannten Substanzen stehen.

Introduction

Fly ash is emitted during solid fuel combustion processes and contains fine particles which are largely composed of mineral inclusions in the fuel [*Flagan and Seinfeld*, 1988]. Coal fly ash (CFA) has been in the focus of aerosol research since the 1970s, mainly because of its negative effects on air quality and human health due to an enhancement of toxic elements in the, for the most part, submicron particles [*Block and Dams*, 1976; *Davison et al.*, 1974; *Gladney et al.*, 1976; *Kaakinen et al.*, 1975]. Since then, knowledge has been gained in terms of CFA particle characterization but to date there are only few studies investigating the effect of CFA particles on atmospheric ice nucleation [*Grawe et al.*, 2016; *Havlíček et al.*, 1993; *Umo et al.*, 2015]. These publications show that CFA is ice nucleation active, however, it is still unclear what makes CFA efficient ice nuclei.

Methods

Four anonymous CFA samples from different German power plants were investigated with respect to their immersion freezing behavior and chemical composition.

Immersion freezing instrumentation. Two different approaches were chosen for the ice nucleation experiments. Firstly, CFA particles where dispersed, size-selected (300 nm) and led into the Leipzig Aerosol Cloud Interaction Simulator (LACIS; *Hartmann et al.* [2011]), where they were activated to cloud droplets, which subsequently froze due to further cooling. At the outlet of LACIS, an optical particle spectrometer registered the ice fraction f_{ice}, i.e., the number of frozen droplets divided by the total number of droplets. With LACIS, it is possible to examine the effect of different particle generation
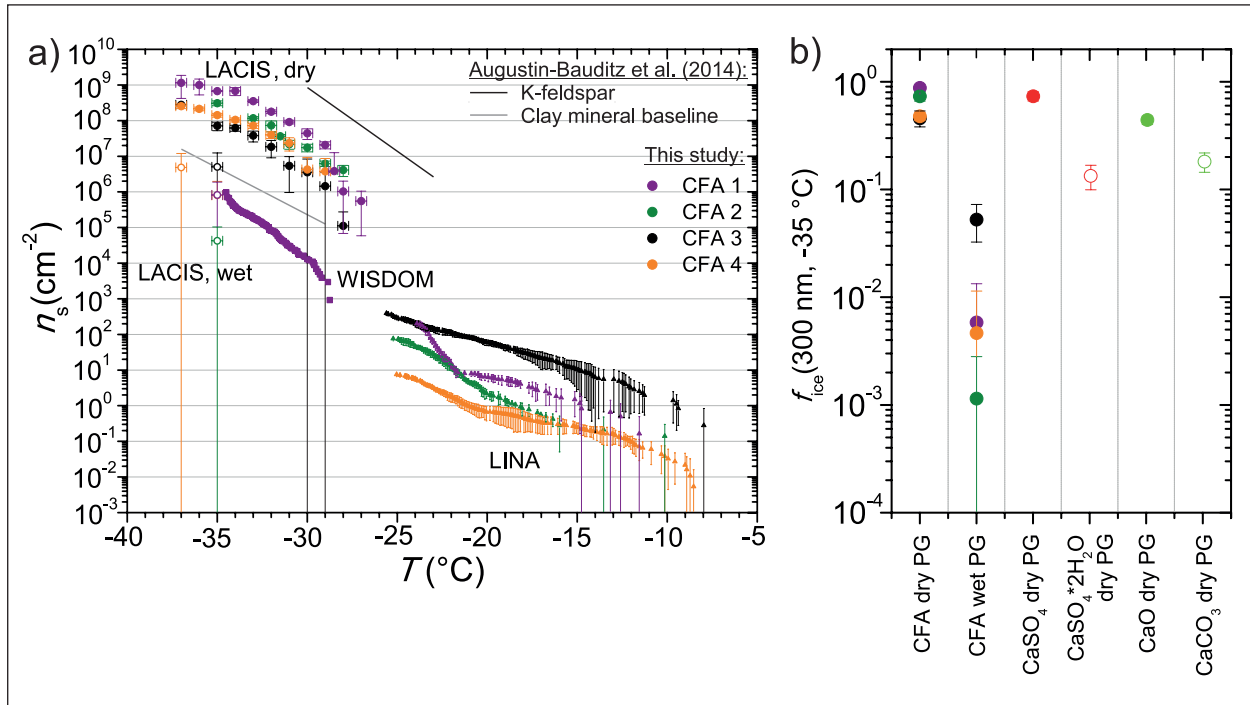
Fig. 1: Results of the immersion freezing experiments. a) Ice nucleation active surface site densities $n_s(T)$ derived from LACIS, WISDOM, and LINA measurements with the four CFA samples. b) Ice fraction f_{ice} from LACIS measurements at -35 °C with 300 nm particles where compounds contained in CFA are compared to CFA in their dehydrated and hydrated forms (PG: particle generation).

techniques. Firstly, the CFA was dry-generated, i.e., via dispersion of the dry powder. Secondly, CFA was suspended in water and particles were wet-generated via spraying of the suspension.

Apart from LACIS, another measurement technique was used, where suspension droplets were put on a substrate and cooled down. Freezing was then observed with the help of a camera. Two different instruments using different droplet sizes were employed in this context to span a broad temperature range. Firstly, the Leipzig Ice Nucleation Array (LINA; *Chen et al.* [2017]) was used, where 1 μl sized droplets were placed on a hydrophobic glass slide supported by a cooled stage. Secondly, the Weizman Supercooled Droplets Observation on Microarray (WISDOM; *Reicher et al.* [2017]) setup was used, where droplets of roughly 0.5 nl were produced with the help of a microfluidic device and placed in an array situated in a cryostage.

Chemical composition analysis.
Simultaneously to the LACIS measurements, the size selected CFA particles were led into the Aircraft-based Laser Ablation Aerosol Mass spectrometer (ALABAMA; *Brands et al.* [2011]), which is a single particle time-of-flight mass spectrometer. For each CFA sample, averaged anion and cation spectra were obtained.

Results

Figure 1 a) shows the results of the immersion freezing measurements with LACIS, WISDOM, and LINA. A normalization with respect to the total particle surface area contained in the droplets (ice nucleation surface site density $n_s(T)$; *DeMott* [1995]) was applied so that the three instruments could be compared.

Dry-generated CFA particles are comparable to mineral dust (gray line: clay minerals, black line: K-feldspar; *Augustin-Bauditz et al.* [2014]) in their immersion freezing behavior. However, when LACIS measurements are done using particles generated from a suspension, the ice nucleation efficiency decreases by at least one order of magnitude. This is supported by WISDOM measurements with CFA1, which agree with LACIS. A temperature overlap could not be achieved between WISDOM and LINA but extrapolation suggests that both instruments could yield similar results.

From the ALABAMA mass spectra (Fig. 2), it follows that Ca- and S- containing compounds contribute to differences in the immersion freezing efficiency between the four CFA samples. $CaSO_4$ and CaO were chosen as test substances for further LACIS measurements (Fig. 1 b). Both substances are comparable to CFA particles in their ice nucleation efficiency. f_{ice} of the hydration products $CaSO_4 \cdot 2H_2O$ and $CaCO_3$ (hydration of CaO yields $Ca(OH)_2$,
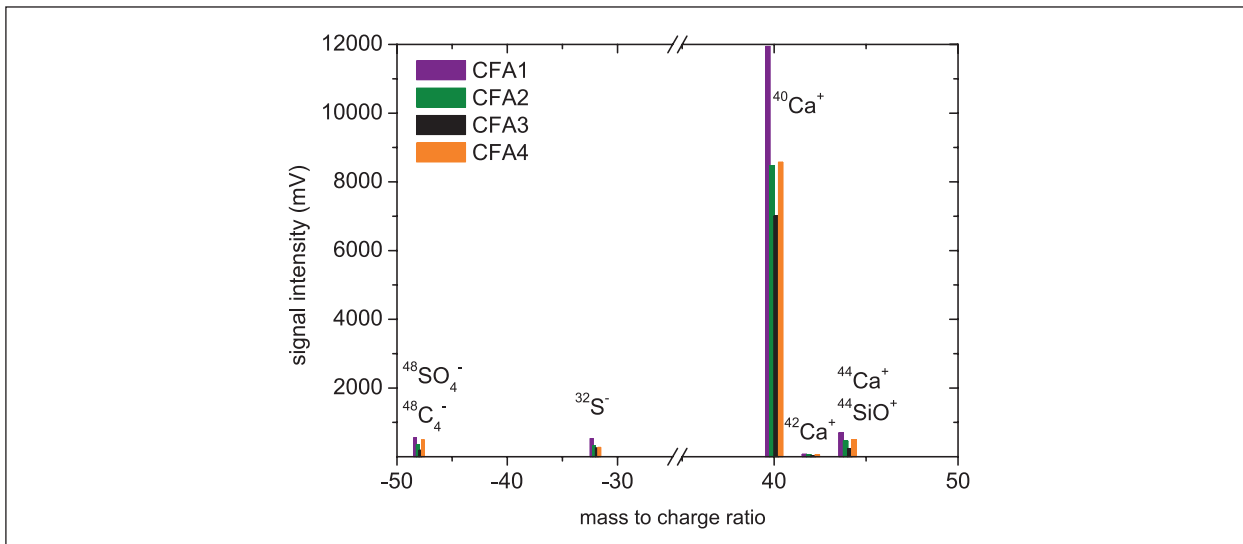
Fig. 2: Chemical composition of 300 nm CFA particles from ALABAMA measurements. Only those peaks are shown for which the signal intensity correlates with the immersion freezing efficiency of the dry-generated CFA samples (i.e., CFA1>CFA2>CFA4>CFA3 or CFA1>CFA4>CFA2>CFA3).

carbonation of $Ca(OH)_2$ yields $CaCO_3$; *Steenari et al.* [1999]) is lower than for the dehydrated compounds by factor 6 and 2, respectively, i.e., $CaSO_4$ and CaO and their hydration products feature the same qualitative behavior as dry- and wet-dispersed CFA. However, the observed decrease is not as substantial as for CFA, which is an indication for other, at this stage unknown, processes/compounds being involved in the reduction of the immersion freezing efficiency of CFA in suspension.

In summary, the immersion freezing ability of CFA particles is partly caused by the presence of Ca-containing compounds such as $CaSO_4$ and CaO, and is reduced through interactions with water (hydration).

References

Augustin-Bauditz, S., H. Wex, S. Kanter, M. Ebert, D. Niedermeier, F. Stolz, A. Prager, and F. Stratmann (2014), The immersion mode ice nucleation behavior of mineral dusts: A comparison of different pure and surface modified dusts, *Geophys. Res. Lett.*, *41*(20), 7375-7382, doi: 10.1002/2014gl061317.

Block, C., and R. Dams (1976), Study of Fly-Ash Emission during Combustion of Coal, *Environ. Sci. Technol.*, *10*(10), 1011-1017, doi: 10.1021/es60121a013.

Brands, M., M. Kamphus, T. Böttger, J. Schneider, F. Drewnick, A. Roth, J. Curtius, C. Voigt, A. Borbon, M. Beekmann, A. Bourdon, T. Perrin, and S. Borrmann (2011), Characterization of a Newly Developed Aircraft-Based Laser Ablation Aerosol Mass Spectrometer (ALABAMA) and First Field Deployment in Urban Pollution Plumes over Paris During MEGAPOLI 2009, *Aerosol. Sci. Tech.*, *45*(1), 46-64, doi: 10.1080/02786826.2010.517813.

Chen, J., Z. Wu, S. Augustin-Bauditz, S. Grawe, M. Hartmann, X. Pei, Z. Liu, D. Ji, and H. Wex (2017), Ice nucleating particle concentrations unaffected by urban air pollution in Beijing, China, *Atmos. Chem. Phys. Discuss.*, *2017*, 1-33, doi: 10.5194/acp-2017-884.

Davison, R. L., D. F. S. Natusch, J. R. Wallace, and C. A. Evans (1974), Trace-Elements in Fly Ash - Dependence of Concentration on Particle-Size, *Environ. Sci. Technol.*, *8*(13), 1107-1113, doi: 10.1021/es60098a003.

DeMott, P. J. (1995), Quantitative Descriptions of Ice Formation Mechanisms of Silver Iodide-Type Aerosols, *Atmos. Res.*, *38*(1-4), 63-99, doi: 10.1016/0169-8095(94)00088-U.

Flagan, R. C., and J. H. Seinfeld (1988), *Fundamentals of air pollution engineering*, Prentice Hall.

Gladney, E. S., J. A. Small, G. E. Gordon, and W. H. Zoller (1976), Composition and Size Distribution of in-Stack Particulate Material at a Coal-Fired Power-Plant, *Atmos. Environ.*, *10*(12), 1071-1077, doi: 10.1016/0004-6981(76)90116-5.

Grawe, S., S. Augustin-Bauditz, S. Hartmann, L. Hellner, J. B. C. Pettersson, A. Prager, F. Stratmann, and H. Wex (2016), The immersion freezing behavior of ash particles from wood and brown coal burning, *Atmos. Chem. Phys.*, *16*(21), 13911-13928, doi: 10.5194/acp-16-13911-2016.

Hartmann, S., D. Niedermeier, J. Voigtländer, T. Clauss, R. A. Shaw, H. Wex, A. Kiselev, and F. Stratmann (2011), Homogeneous and heterogeneous ice nucleation at LACIS: operating principle and theoretical studies, *Atmos. Chem. Phys.*, *11*(4), 1753-1767, doi: 10.5194/acp-11-1753-2011.

Havlíček, D., R. Přibil, and O. Školoud (1993), The Chemical and Mineralogical Composition of the Water-Soluble Fraction of Power-Plant Ash and Its Effect on the Process of Crystallization of Water, *Atmos. Environ. a-Gen.*, *27*(5), 655-660, doi: 10.1016/0960-1686(93)90183-Y.

Kaakinen, J. W., R. M. Jorden, M. H. Lawasani, and R. E. West (1975), Trace-Element Behavior in a Coal-Fired Power-Plant, *Environ. Sci. Technol. 9*(9), 862-869, doi: 10.1021/es60107a012.

Reicher, N., L. Segev, and Y. Rudich (2017), The Weizmann Supercooled Droplets Observation (WISDOM) on a Microarray and Application for Ambient Dust, *Atmos. Meas. Tech. Discuss.*, 1-25, doi: 10.5194/amt-2017-172.

Steenari, B. M., S. Schelander, and O. Lindqvist (1999), Chemical and leaching characteristics of ash from combustion of coal, peat and wood in a 12 MW CFB - a comparative study, *Fuel*, *78*(2), 249-258, doi: 10.1016/S0016-2361(98)00137-9.

Umo, N. S., B. J. Murray, M. T. Baeza-Romero, J. M. Jones, A. R. Lea-Langton, T. L. Malkin, D. O'Sullivan, L. Neve, J. M. C. Plane, and A. Williams (2015), Ice nucleation by combustion ash particles at conditions relevant to mixed-phase clouds, *Atmos. Chem. Phys.*, *15*(9), 5195-5210, doi: 10.5194/acp-15-5195-2015.

Cooperation

Darmstadt University of Technology, Darmstadt, Germany;
University of Leipzig, Leipzig, Germany;
Aarhus University, Aarhus, Denmark;
Leibniz Institute of Surface Engineering, Leipzig, Germany;
Helmholtz Centre for Environmental Research, Leipzig, Germany

Articles

The new turbulent Leipzig Aerosol Cloud Interaction Simulator (LACIS-T): A moist air wind tunnel for investigating cloud microphysics - turbulence interactions

Dennis Niedermeier[1], Jens Voigtländer[1], Silvio Schmalfuß[1], Raymond Shaw[2], Jörg Schumacher[3], Frank Stratmann[1]

[1] Leibniz Institute for Tropospheric Research (TROPOS), Leipzig, Germany

[2] Michigan Technological University, Houghton, MI, USA

[3] Technische Universität Ilmenau, Ilmenau, Germany

Mit Hilfe des neu errichteten turbulenten Feuchtluft-Windkanals LACIS-T (Turbulent Leipzig Aerosol Cloud Interaction Simulator) möchten wir das mechanistische Verständnis hinsichtlich Turbulenz-Wolkenmikrophysik-Wechselwirkungsprozesse verbessern. Die Anfangs-/ Randbedingungen hinsichtlich Temperatur und Wasserdampfkonzentration können definiert eingestellt werden. Die sich innerhalb des Windkanals etablierenden turbulenten Temperatur- und Feuchtigkeitsfelder führen u.a. zu Fluktuationen im Wasserdampfpartialdruck, deren Einflüsse auf wolkenmikrophysikalischen Prozesse wie z.B. die Wolkentropfenaktivierung und das Gefrieren von Wolkentropfen nun unter reproduzierbaren Laborbedingungen untersucht werden können. Das grundlegende Funktionsprinzip des Windkanals, sowie erste Ergebnisse zur Tropfenaktivierung und dem vorangehenden hygroskopischen Partikelwachstum werden hier vorgestellt.

Introduction

Atmospheric clouds are highly non-stationary, inhomogeneous, and intermittent, and embody an enormous range of spatial and temporal scales. Strong couplings across those scales between turbulent fluid dynamics and microphysical processes are integral to cloud evolution [*Bodenschatz et al.*, 2010].

Besides clouds being highly complex systems in themselves, they occur sporadically in locations usually hard to reach. Therefore, investigating atmospheric clouds in-situ is an ambitious, expensive and often impossible task. To make things even worse, measurements in atmospheric clouds suffer from a lack of reproducibility regarding initial and boundary conditions. Due to these issues, the examination of individual cloud processes in the laboratory is mandatory for increasing our understanding of cloud microphysical processes, and their interactions with turbulence [*Stratmann et al.*, 2009].

The newly built turbulent moist air wind tunnel LACIS-T (Turbulent Leipzig Aerosol Cloud Interaction Simulator) is an ideal facility for pursuing mechanistic understanding concerning these processes and interactions. Within the tunnel, under well-defined and reproducible laboratory conditions, we are able to adjust precisely controlled turbulent temperature and water vapour fields, so as to achieve supersaturation levels allowing for, e.g., the detailed investigation of aerosol particle activation to cloud droplets.

Turbulent Leipzig Aerosol Cloud Interaction Simulator

Figure 1 schematically shows the layout of the moist air wind tunnel LACIS-T. The tunnel is designed as a closed loop, in which the air circulates continuously with a total flow rate of up to 10.000 l/min. The actual measuring section (Fig. 1, right) of the channel is 2 m long, 80 cm wide and 20 cm deep. Cloud
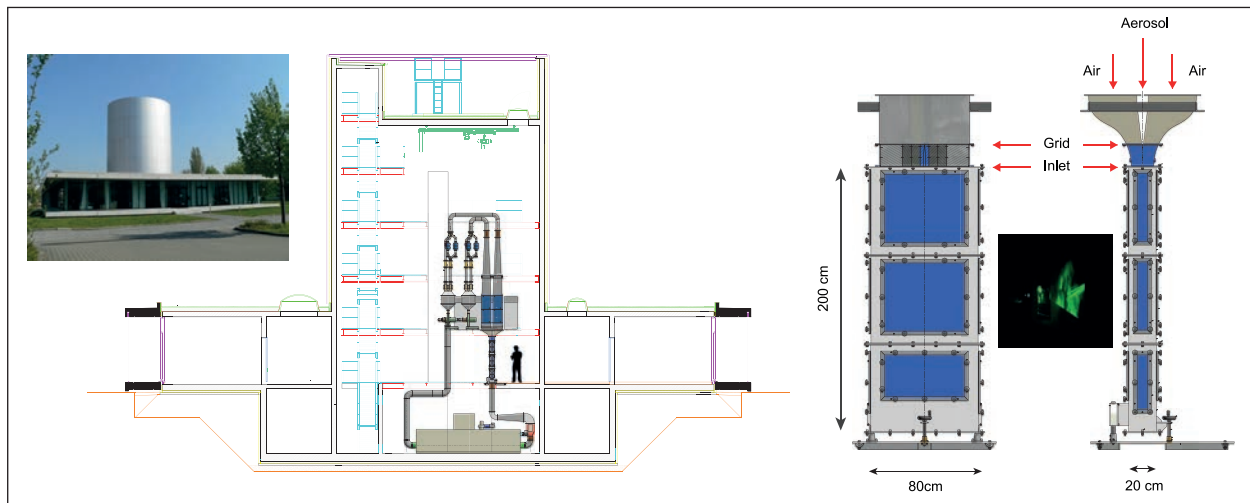
Fig. 1: Schematic of the wind tunnel inside the TROPOS cloud laboratory and photo of the cloud laboratory building. On the right hand side the measuring section is schematically shown giving an impression of its dimensions. The position of the particle injection is at the point where the particle-free air streams of both branches start to mix. The right photo shows a cloud which is visualized via a green laser light sheet.

formation (photo of the "cloud" in Fig. 1 (right) which is visualized via a green laser light sheet) occurs via turbulent mixing of three conditioned flows (i.e. two particle-free air streams, "Air" and one aerosol stream, "Aerosol"), and is initiated at the inlet of the measuring section. The turbulence required for mixing the flows is generated by two passive planar grids (mesh length of 19 mm, rod diameter of 5 mm and a blockage of 30%) in the air streams (approx. 5.000 l/min each). The air streams are humidified by Nafion humidifiers (Permapure Inc.) and tempered by two separate heat exchangers. The aerosol flow (approx. 3 l/min) is intro-duced into the mixing zone of the two air streams. In the measuring section, the characterization of the respective fluid and thermodynamic states, as well as the microphysical properties of the cloud formed (droplet size, number of droplets, etc.), is carried out. After passing through the measuring section, the entire flow is dried, split up again into two streams driven by blowers and cleaned by filters before humidi-fication takes place. For the investigations presented here, we placed a welas 2300 optical system (from Palas) inside LACIS-T to characterize the (cloud) particle size distributions.

First results

The first microphysical experiments carried out at LACIS-T are proof of principle that turbulence - cloud microphysical interaction processes can be studied in the wind tunnel. The results of two corresponding experiments are described in the following.

In the first experiment, investigations on the deliquescence and hygroscopic growth of NaCl particles with a diameter of 320 nm were carried out.

Thereto, the temperatures of both particle-free air streams were adjusted to 20°C. Different dew point temperatures were set, which resulted in different mean relative humidities (RH) inside the measuring section. The aerosol flow was introduced into the wind tunnel in two ways, i.e., dry and already humidified, i.e., measurements were performed on the deliques-cence and on the efflorescence branches of the hygroscopic growth curve, respectively. In Fig. 2a the resulting particle diameters are shown as a function of the mean RH. The blue solid line represents the corresponding Köhler curve (efflorescence branch). We observe deliquescence to take place at approx. 75% RH, which compares well to literature data (e.g., 75.7% measured at 25°C by *Tang et al.* [1976], and 75.3% derived from the thermodynamic properties of a saturated NaCl solution [*Robinson and Stokes*, 1970]). Note that the investigations were performed at a total flow rate of 10.000 l/min, which makes the accuracy of the results even more impressive. Looking in more detail, deliquescence is observed over a certain RH range, which might be an indication for an influence of the prevailing turbulent RH fluctua-tions. This will be investigated in more detail in future studies.

In the second experiment, results are shown in Fig. 2b, droplet activation was investigated utilizing size selected NaCl particles. A fixed maximum mean supersaturation was set and then the dry particle diameter was varied. Generally, it was observed, that the majority of the measured droplets feature sizes below the critical activation diameter (d_{crit} = 1.3 µm for 100 nm, to d_{crit} > 5 µm for 400 nm, respectively). However, for dry sizes of 100 nm and 200 nm, tails of the droplet size distributions are reaching into the
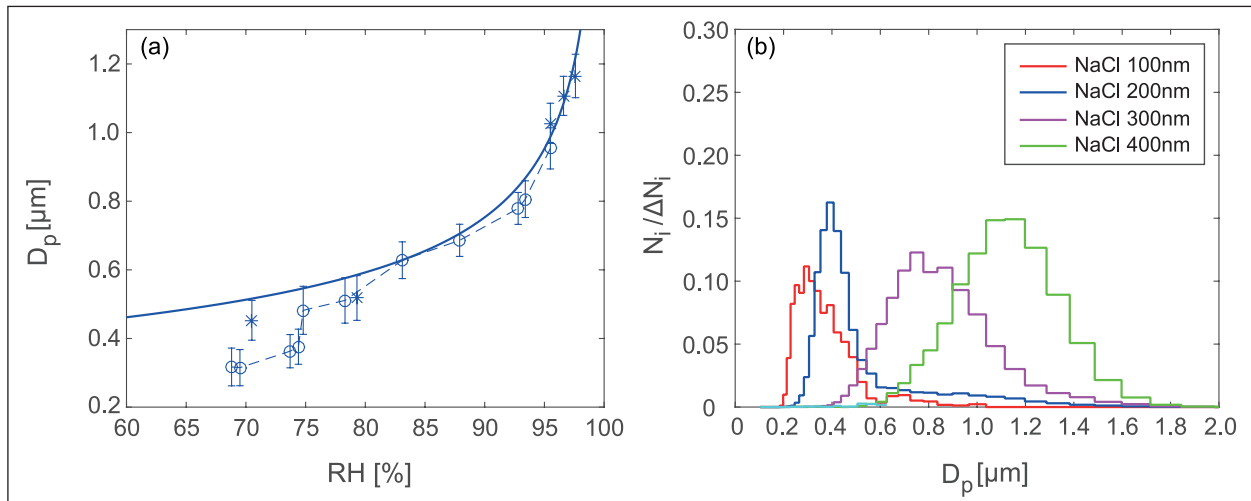
Fig. 2: a) Measured deliquescence (open circles) and efflorescence (asterisks) branches of the hygroscopic growth curve for NaCl particles with a dry diameter of 320 nm at T = 20°C. The theoretical Köhler curve (solid line) is shown for reference. b) Droplet activation: Measured size distributions (normalized) for a given set maximum mean supersaturation for four different dry particle diameters.

range above the critical diameters. This indicates that existing fluctuations in the supersaturation cause droplet activation of some of these particles.

Summary and Outlook

The first experiments carried out at LACIS-T clearly documented its feasibility for investigating cloud microphysical processes under turbulent conditions. We were able to accurately quantify the deliquescence and hygroscopic growth behaviour of sodium chloride particles, and thereby observed indications of possible influences of RH fluctuations on deliquescence. We also found first hints of turbulence influenced droplet activation. Overall, both wind-tunnel behaviour and found results are very promising and will be further investigated and quantified in the near future**.**

References

Bodenschatz, E., S. P. Malinowski, R. A. Shaw, and F. Stratmann (2010), Can we understand clouds without turbulence? *Science*, 327, 970-971.

Stratmann F., O. Möhler, R. Shaw, and H. Wex (2009), Laboratory Cloud Simulation: Capabilities and Future Directions, in *Clouds in the Perturbed Climate System*, MIT Press, Cambridge, MA, 149-172.

Tang, I. N., H. R. Munkelwitz, and J. G. Davis (1977), Aerosol growth studies - II. Preparation and growth measurements of monodisperse salt aerosols. *J. Aerosol Sci.*, 8(3), 149-159.

Robinson, R. A. and R. H. Stokes (1970), *Electrolyte Solutions*, 2nd revised edit., Butterworths, London.

Funding

Modeling mixed-phase microphysics of an arctic stratus using COSMO-SPECS

Martin Simmel, Oswald Knoth, Ina Tegen

Mit Hilfe des gekoppelten Modellsystems COSMO-SPECS wird ein idealisierter arktischer Stratus untersucht. Vergleiche mit anderen Modellstudien ergeben trotz einer Überschätzung des Flüssig-wasserpfads eine realistische Wiedergabe des Eisgehalts der Mischphasenwolke. Die Aufrechterhal-tung konstanter Eispartikelkonzentrationen erfordert aufgrund der Sedimentation der Eispartikel einen ständigen Nachschub neuer Eiskeime, der im vorliegenden Fall nicht durch dynamische Prozesse (z. B. Einmischen an der Oberkante der Wolke) geleistet werden kann. Eine Erklärung wäre eine zeitabhängige Bildung der Eispartikel.

Introduction

In the range above about -38 °C ice forma-tion in clouds typically is caused by heterogeneous freezing which means that a so-called ice nucleating particle (INP) is needed to trigger the primary freezing process. In the atmosphere, the most important INPs typically consist of biological or mineral material and are highly variable in type, time, and space. It is widely accepted that the immersion freezing process is the dominant freezing mode for most of the clouds in this temperature range. To avoid an overestimation of primary ice formation in modelling, the number of INP has to be treated prognostically.

Especially for long-living quasi-stationary clouds (e.g., Arctic stratus) the interaction between the liquid and the ice phase via the gas phase (Wege-ner-Bergeron-Findeisen process) and the balance between ice particle sinks (sedimentation) and sources (primary ice formation, e.g., by immersion freezing) determines ice fraction as well as cloud life time. This rises the question for the origin of the newly activated INPs (stochastic vs. deterministic approach, entrainment) and requires a detailed description of microphysics as well as dynamics.

The model system COSMO-SPECS

The model system COSMO-SPECS (formerly LM-SPECS, [*Grützun et al.*, 2008]) consists of the COSMO model (COnsortium for Small scale MOdeling) and the spectral microphysics model SPECS [*Simmel and Wurzler*, 2006; *Diehl et al.*, 2006]. SPECS was improved with respect to ice particle (IP) shapes and prognostic INP fields within the model version AK-SPECS [*Simmel et al.*, 2015] which was applied to simulate mixed-phase micro-physics of altocumulus clouds.

Test case: ISDAC Arctic Stratus

On 26 April 2008 an extended mixed-phase stratiform Arctic Stratus was observed during ISDAC (Indirect and Semi-Direct Aerosol Campaign). These observations were used to derive a case study for a comparison of 11 LES models [*Ovchinnikov et al.*, 2014, OV2014] using bulk or bin microphysics. Dynamics as well as certain ice microphysics and radiation parameterizations were prescribed very thor-oughly to pin down the remaining model uncertaini-ties. Three different setups were given with respect to IP concentration: 0 (ice0, warm run), 1 IP/l, and 4 IP/l (ice1 and ice4, mixed-phase runs). COSMO-SPECS was applied to these setups for comparison to the other models and to analyse primary ice formation when ice particle concentration is prescribed with a constant value. The model domain consists of 45 x 45 grid points in the horizontal direction with a resolu-tion of 50 m and 188 constant levels with a vertical resolution of 10 m. Horizontally periodic boundary conditions are applied. Comparison of different model domain sizes (25 x 25, 65 x 65) as well as resolution (100 m) shows little influence on the model results.
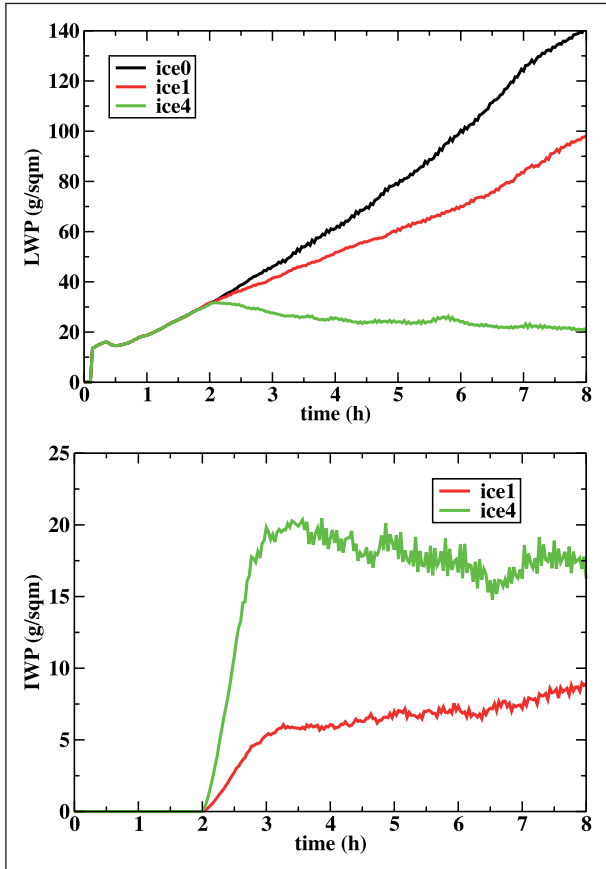
Fig. 1: LWP (top) and IWP (bottom) for the three ISDAC model runs (black: ice0, red: ice1, green: ice4).

Model Results and Discussion

Liquid and Ice Water Paths (LWP and IWP)
Time series of LWP (top) and IWP (bottom) are shown for the three model runs in Fig. 1. LWP steadily increases for ice0 and ice1, whereas for ice4 LWP remains almost constant after 2h model time when ice microphysics is switched on. IWP shows a sharp increase within the first hour; afterwards a relatively constant value is reached. Except for ice4, LWP is considerably higher than in OV2014 whereas IWP is comparable to the results of the models with bin microphysics.

Virtual INP concentrations The prognostic INP field within COSMO-SPECS was used to calculate a "virtual INP concentration" corresponding to the number of INP which had to be activated to reach the target ice particle concentration. Shortly after ice onset at 2 h, the virtual INP concentration corresponds to the actual ice particle concentration according to Fig. 2. However, over time the virtual INP concentration grows which means that higher INP concentrations would have been necessary to reach the prescribed ice particle concentrations and that these INP cannot be provided by entrainment. This

result supports the assumption of time-dependent ice formation being the INP source.

Size-resolved ice number mixing ratios OV2014 showed that the shape of the ice particle NSD (number size distribution) is crucial for the amount of ice produced via deposition as well as for sedimentation. Figure 3 shows a layer-averaged ice particle NSD for ice4 after 4 h. A typical NSD pattern evolves: Smallest ice particles are found at cloud top where nucleation takes place. When falling through the mixed-phase cloud, a rapid growth occurs reaching its maximum below cloud. Concentration variations are also caused by convergence/divergence effects due to turbulence as well as size-dependent terminal fall velocities. This illustrates that the assumption of a fixed NSD used by most of the bulk models is an oversimplification.
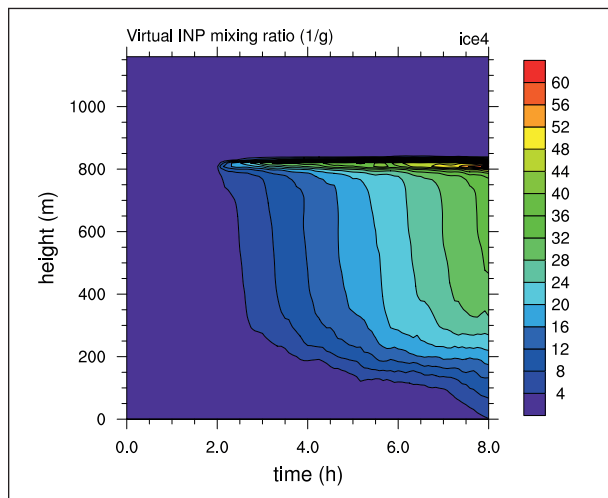
Fig. 2: Virtual INP concentration for case ice4.
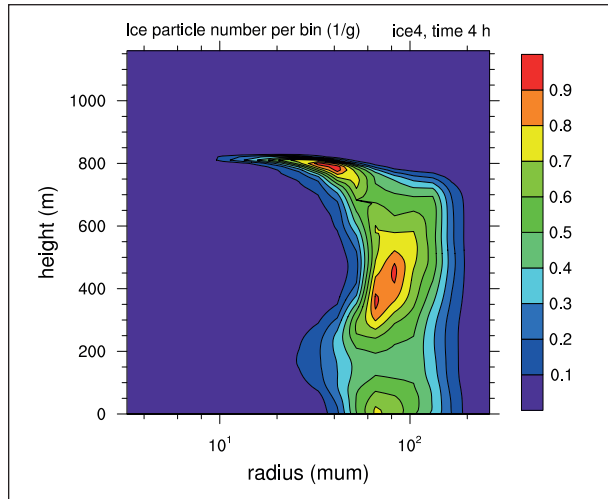
Fig. 3: Layer-averaged ice particle number size distribution for case ice4 after 4 h model time.

References

Diehl, K., M. Simmel, and S. Wurzler (2006), Numerical sensitivity studies on the impact of aerosol properties and drop freezing modes on the glaciation, microphysics, and dynamics of clouds, *J. Geophys. Res.*, 111, doi:10.1029/2005JD005884.

Grützun, V., O. Knoth, and M. Simmel (2008), Simulation of the influence of aerosol particle characteristics on clouds and precipitation with LM-SPECS: Model description and first results, *Atmos. Res.* 90, 233–242.

Ovchinnikov, M., A. S. Ackerman, A. Avramov, A. Chen4, J. Fan, A. M. Fridlind, S. Ghan, J. Harrington, C. Hoose, A. Korolev, G. M. McFarquhar, H. Morrison, M. Paukert, J. Savre, B. J. Shipway, M. D. Shupe, A. Solomon, and K. Sulia (2014), Intercomparison of large-eddy simulations of Arctic mixed-phase clouds: Importance of ice size distribution assumptions, J. Adv. Model. Earth Syst., 6, 223–248, doi:10.1002/2013MS000282.

Simmel, M. and S. Wurzler (2006), Condensation and activation in sectional cloud microphysical models, *Atmos. Res.*, 80, 218–236, doi:10.1016/j.atmosres.2005.08.002.

Simmel, M., J. Bühl, A. Ansmann, and I. Tegen (2015), Ice phase in altocumulus clouds over Leipzig: remote sensing observations and detailed modeling, *Atmos. Chem. Phys.*, 15, 10453–10470, doi:10.5194/acp-15-10453-2015.

Cooperation

Center for Information Services and High Performance Computing (ZIH), TU Dresden, Germany

Modelling black carbon aerosol transport to the Arctic

Jacob Schacht, Bernd Heinold, Ina Tegen

Die Arktis erwärmt sich deutlich schneller als der Rest der Erde. Der Ruß in der arktischen Atmosphäre trägt durch direkten Strahlungseinfluss zu dieser Erwärmung bei. Modelle weisen Probleme bei der Reproduzierung von Messungen auf. Hier werden Änderungen in der Rußbeladung der arktischen Atmosphäre bei Nutzung verschiedener Emissionsdatensätze untersucht. Es ergeben sich teilweise Änderungen von über 30 % in der zentralen Arktis.

Introduction

The Arctic is warming twice as fast as the rest of the planet [*Wendisch et al*., 2017]. Aerosol particles transported from different natural and anthropogenic sources affect the Arctic energy balance by direct interaction with solar and thermal radiation and by changing cloud properties as well as atmospheric dynamics. Aerosol, therefore, makes a potentially important contribution to the rapid change in Arctic climate. Global aerosol-climate models are particularly suited to study sources and transport pathways of the aerosols and their effects. Here, black carbon (BC) is of particular interest, as it is highly absorbing at solar wavelengths and tends to warm the atmosphere. When deposited on snow/ice it lowers the surface albedo and accelerates sea ice melting. However, models struggle to reproduce the seasonality and vertical distribution of Arctic aerosol. One key issue are uncertainties in the prescribed emissions of air pollutants [*Eckhardt et al*., 2015; *Arnold et al.*, 2016].

Method

The emission-related uncertainties in the model estimates of the distribution and effects of aerosol in the Arctic region are investigated with the aerosol-climate model ECHAM6.3-HAM2.3 using different state-of-the-art inventories of air pollutant emissions: (1) ACCMIP [van Vuuren et al. 2010] and (2) ECLIPSE v5a [*Klimont et al.*, 2017] (hereafter

as ECLIPSE). ACCMIP includes anthropogenic and biomass burning emissions and is fixed for year 2000. ECLIPSE comprises only anthropogenic sources, which however are more recent (years: 2005, 2010, 2015) and include gas flaring, an important source of BC in the Arctic. Current daily fire emissions are available from GFAS (Global Fire Assimilation System) [*Kaiser et al.*, 2012]. In addition, we use a new high-resolution emission database for BC over Russia [*Huang et al.,* 2015] (BCRUS, hereafter). The evaluation study comprises model runs with the following combinations of emission inventories: (i) ACCMIP, (ii) ACCMIP-GFAS, where the original fire emissions are replaced by GFAS, (iii) ECLIPSE-GFAS, and (iv) ECLIPSE-BCRUS-GFAS. ECHAM6.3-HAM2.3 is run at T63 horizontal resolution (~1.8°) with 47 vertical levels for 2008–2012. The runs are nudged to ERA-Interim reanalysis.

The modelling results are compared to measurements from the ACCESS aircraft campaign similar to *Schwarz et al.* [2017] for AeroCom Phase-II models. The campaign took place around Norway/Svalbard in July 2012.

Results and Discussion

Figure 1a shows the annual mean BC burden (years 2008–2012) from the ECLIPSE-BCRUS-GFAS run. Highest values of BC can be found in the main source regions of Central and Eastern Europe of up to 7.9 mg m^{-2}, China (17.4 mg m^{-2}) and central northern
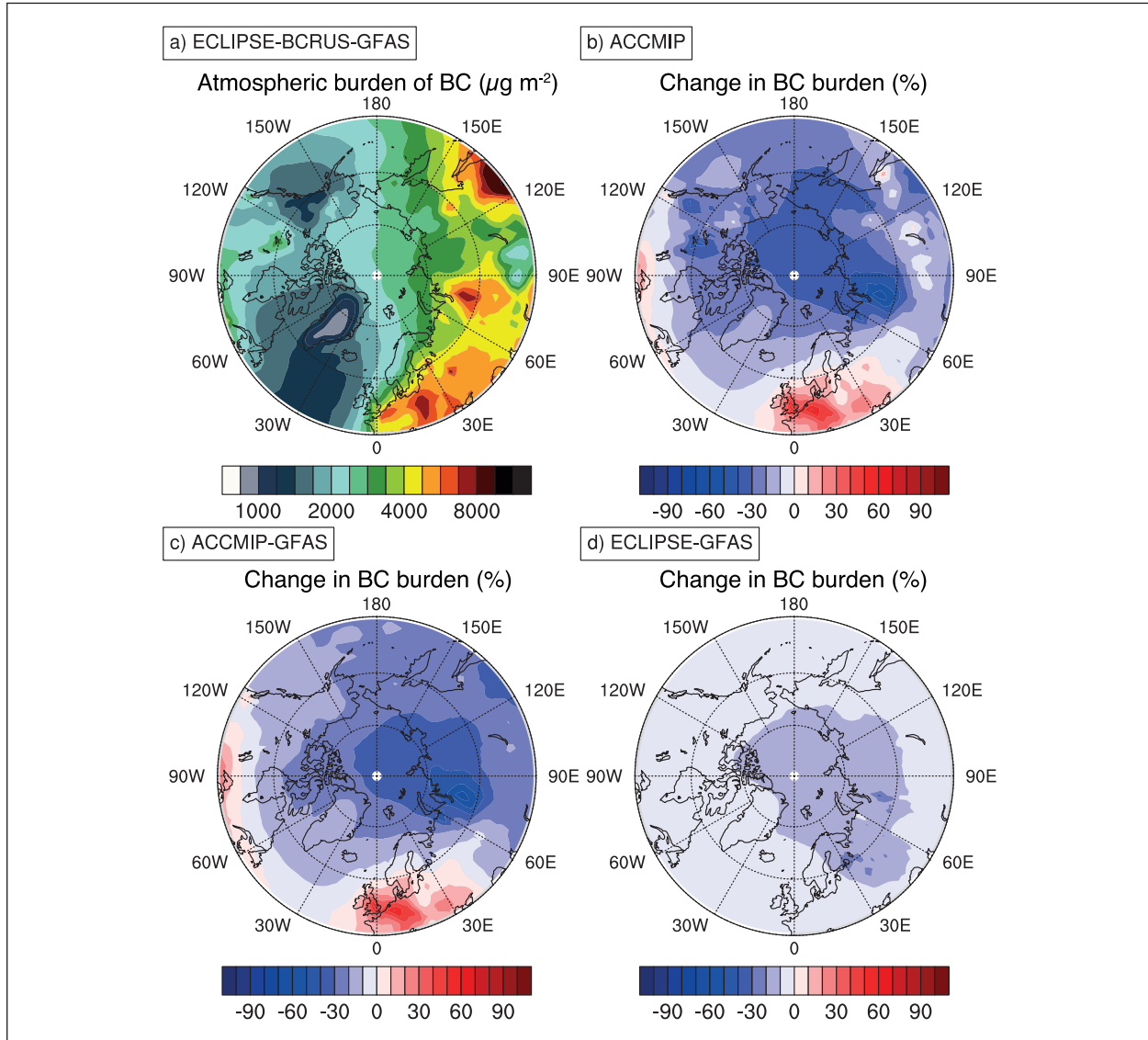
Fig. 1: (a) Annual averaged atmospheric burden of black carbon (BC) for the years 2008-2012 simulated with ECHAM-HAM using the ECLIPSE-BCRUS-GFAS emissions. Difference in BC burden between the run using ECLIPSE-BCRUS-GFAS and runs that utilized the (b) ACCMIP, (c) ACCMIP-GFAS and (d) ECLIPSE-GFAS emission data.

Russia (7.9 mg m^{-2}) (Fig. 1a). The differences in BC between the ECLIPSE-BCRUS-GFAS run and other runs are shown in Fig. 1b–1d, respectively.

The ACCMIP run produces a lower BC burden in most areas, with the largest discrepancies in the Russian region (up to 70 % less) where gas flaring is the dominant source of BC. The differences in eastern Siberia and North America are likely connected to the differing biomass burning representations. While the ECLIPSE-BCRUS-GFAS run uses real-time daily fire emissions, ACCMIP includes fixed values for the year 2000. This adds up to a difference in BC burden over the land free central Arctic of more than 30 % on annual average.

Both runs using ACCMIP show similar patterns, as they do not include gas flaring. When comparing

Fig. 1b and Fig. 1c, there is a more negative difference in southern Russia for ACCMIP-GFAS. This is likely because the ACCMIP fire emissions in this area are higher than provided by the GFAS dataset. The opposite effect is seen in eastern Russia and North America. The differences between ECLIPSE-BCRUS-GFAS and ACCMIP-GFAS in the central Arctic are still at about 30 % lower.

The differences in the BC burden between ECLIPSE-GFAS and ECLIPSE-BCRUS-GFAS (Fig. 1d) are not as remarkable, since only the anthropogenic BC emissions in Russia are different. In both runs the gas flaring emissions are included, but higher (locally up to 0.26 g m^{-2} year^{-1}) in the BCRUS emissions dataset. Because of their vicinity to the central Arctic, even slightly higher gas flaring emissions have

a large impact on the Arctic aerosol load. Applying the BCRUS inventory leads to a more than 10% higher BC burden over the central Arctic.

Figure 2 shows a relative comparison of modelled BC profiles with aircraft measurements from the ACCESS campaign. The model strongly overestimates the BC concentration near the ground, but especially the ECLIPSE and BCRUS runs reproduce the measurements quite well between 950 and 800 hPa. Above 800 hPa, the model overestimates the concentration by a factor of 2 to 4, with the ACCMIP run performing slightly better. This points towards issues with removal processes rather than with emissions.

In summary, this evaluation study shows the range of emission-related uncertainties in current model estimates of Arctic aerosol abundance. In a next step, the impact of these uncertainties on aerosol radiative properties and forcing will be further investigated. After thorough evaluation, the global ECHAM6.3-HAM2.3 simulations will be used to provide an up-to-date estimate of the budget and direct radiative forcing of aerosol in the Arctic.

Fig. 2: Vertical profiles of averaged model/measurement ratios of BC concentration. Compared are measurements from the aircraft campaign ACCESS (July 2012 in Norway/Svalbard) with ECHAM-HAM model results at the nearest grid point. The colours represent the different emission setups.

References

Arnold, S., K. Law, C. Brock, J. Thomas, S. Starkweather, K. von Salzen, A. Stohl, S. Sharma, M. Lund, M. Flanner, T. Petaja, H. Tanimoto, J. Gamble, J. Dibb, M. Melamed, N. Johnson, M. Fidel, V.-P. Tynkkynen, A. Baklanov, S. Eckhardt, S. Monks, J. Browse, and H. Bozem (2016), Arctic air pollution: Challenges and opportunities for the next decade, *Elem. Sci. Anth.*, *4*, doi: 10.12952/journal.elementa.000104.

Eckhardt, S., B. Quennehen, D. J. L. Olivié, T. K. Berntsen, R. Cherian, J. H. Christensen, W. Collins, S. Crepinsek, N. Daskalakis, M. Flanner, A. Herber, C. Heyes, Ø. Hodnebrog, L. Huang, M. Kanakidou, Z. Klimont, J. Langner, K. S. Law, M. T. Lund, R. Mahmood, A. Massling, S. Myriokefalitakis, I. E. Nielsen, J. K. Nøjgaard, J. Quaas, P. K. Quinn, J. C. Raut, S. T. Rumbold, M. Schulz, S. Sharma, R. B. Skeie, H. Skov, T. Uttal, K. von Salzen, and A. Stohl (2015), Current model capabilities for simulating black carbon and sulfate concentrations in the Arctic atmosphere: a multi-model evaluation using a comprehensive measurement data set, *Atmos. Chem. Phys.*, *15*(16), 9413-9433, doi: 10.5194/acp-15-9413-2015.

Huang, K., J. S. Fu, V. Y. Prikhodko, J. M. Storey, A. Romanov, E. L. Hodson, J. Cresko, I. Morozova, Y. Ignatieva, and J. Cabaniss (2015), Russian anthropogenic black carbon: Emission reconstruction and Arctic black carbon simulation, *J. Geophys. Res. - Atmos.*, *120*(21), 11,306-311,333, doi: 10.1002/2015JD023358.

Kaiser, J. W., A. Heil, M. O. Andreae, A. Benedetti, N. Chubarova, L. Jones, J. J. Morcrette, M. Razinger, M. G. Schultz, M. Suttie, and G. R. van der Werf (2012), Biomass burning emissions estimated with a global fire assimilation system based on observed fire radiative power, *Biogeosciences*, *9*(1), 527-554, doi: 10.5194/bg-9-527-2012.

Klimont, Z., K. Kupiainen, C. Heyes, P. Purohit, J. Cofala, P. Rafaj, J. Borken-Kleefeld, and W. Schöpp (2017), Global anthropogenic emissions of particulate matter including black carbon, *Atmos. Chem. Phys.*, *17*(14), 8681-8723, doi: 10.5194/acp-17-8681-2017.

Lund, M. T., T. K. Berntsen, and B. H. Samset (2017), Sensitivity of black carbon concentrations and climate impact to aging and scavenging in OsloCTM2–M7, *Atmos. Chem. Phys.*, *17*(9), 6003-6022, doi: 10.5194/acp-17-6003-2017.

van Vuuren, D. P., J. Edmonds, M. Kainuma, K. Riahi, A. Thomson, K. Hibbard, G. C. Hurtt, T. Kram, V. Krey, J.-F. Lamarque, T. Masui, M. Meinshausen, N. Nakicenovic, S. J. Smith, and S. K. Rose (2011), The representative concentration pathways: an overview, *Clim. Change*, *109*(1), 5, doi: 10.1007/s10584-011-0148-z.

Wendisch, M., M. Brückner, J. Burrows, S. Crewell, K. Dethloff, K. Ebell, C. Lüpkes, A. Macke, J. Notholt, J. Quaas, A. Rinke, and I. Tegen (2017), Understanding Causes and Effects of Rapid Warming in the Arctic, edited.

Funding
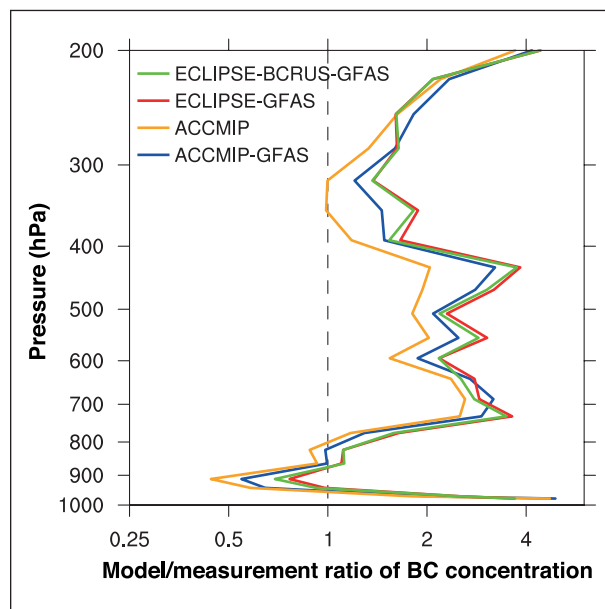
Impact of Saharan dust on atmospheric ice nucleation – the ML-CIRRUS case

Bernd Heinold, Michael Weger

Saharastaub ist ein wichtiger Faktor für Wetter und Klima im Mittelmeerraum und in Europa. Mittels interaktiver Staubmodellierung wird der Einfluss von Mineralstaub auf die Eisbildung in der Atmosphäre für einen bedeutenden Saharastaubausbruch Anfang April 2014 untersucht. Die Ergebnisse zeigen eine signifikante staubbedingte Zunahme des Eiswassergehalts im Bereich mittelhoher Mischphasenwolken sowie der Cirrus-Bewölkung. Die Berücksichtigung interaktiver Aerosol-Wolken-Mikrophysik führt damit zur Verbesserung der vom Modell sonst unterschätzten Bedeckung mit hohen Wolken.

Introduction

Saharan dust is an important factor impacting weather and climate in the Mediterranean and Europe. While the direct radiative effect of mineral dust has been studied elaborately in the past, large uncertainties remain concerning the dust impact on cloud properties, in particular on ice formation. Studies suggest that numerical weather forecasts tend to be biased during strong dust events, which is likely due to a missing interactive aerosol feedback on radiation and clouds [*Rieger et al.*, 2017].

Interactive dust modelling is used to study the role of mineral dust in ice nucleation. The question is investigated how considering dust-cloud interactions affects the model representation of clouds. A dense Saharan dust plume over Europe in early April 2014 associated with strong cloud development provides an interesting test case.

Methods

The regional model COSMO–MUSCAT (Consortium for Small-scale Modeling – MultiScale Chemistry Aerosol Transport) is used for the Saharan dust simulations. The model computes emission, transport, dry and wet deposition of desert dust [*Heinold et al.*, 2011]. Interactive runs consider the dust effect on radiation and clouds, and the related dynamic feedback.

The impact of Saharan dust on ice nucleation is studied by applying the two–moment cloud microphysics scheme by Seifert and Beheng [2006] using the new empirical INP parameterization by *Ullrich et al.* [2017]. Dust can act as CCN or INP depending on atmospheric conditions.

Dust emission and transport towards Europe are simulated on a domain with 14 km horizontal grid spacing covering Europe and northern Africa. The interactive simulations are performed on a one-way nested 2.8-km domain over central Germany (Fig. 1). The model experiments comprise runs with interactive dust feedback on clouds and radiation as well as runs using a climatological number of dust CCN/INPs.

The model is evaluated with data from the Leipzig Aerosol and Cloud Remote Observations System (LACROS) at Leipzig, satellite remote sensing and measurements from the HALO mission on Mid Latitude Cirrus (ML-CIRRUS) [*Voigt et al.*, 2016].

Results and Discussion

The study's subject is a major Saharan dust outbreak, which affected much of Europe during the first week of April 2014. The formation of a Mediterranean low had caused several dust emission events in Morocco and Algeria. The Saharan dust was lifted and transported northwards by strong southerly airflow on the west side of an upper ridge over northern
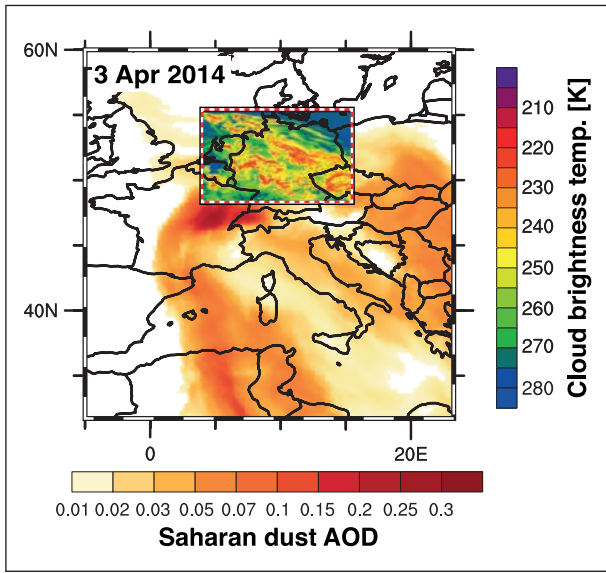
Fig. 1: Subset of the 14-km model domain (dashed line) and 2.8-km nest (dotted line) for the dust initialisation and dust-cloud interaction simulations with COSMO-MUSCAT, respectively. Map of Saharan desert dust aerosol optical depth (AOD) for 3 April 2014 computed with COSMO-MUSCAT (outer domain) and cloud-top brightness temperature derived from COSMO cloud properties (inner domain).

Africa and central Europe. The dust plume reached France on 2 and 3 April (Fig. 1). Over Germany, the maximum dust load occurred from 4 to 5 April. Within a second surge, Saharan dust was advected across Italy towards south-eastern Europe. While the main dust layers were located below 4–6 km height, a small fraction of dust also reached the upper troposphere.

For the 4 and 5 April, satellite imagery shows an extensive cloud cover, including widespread cirrus, over north-eastern France, Benelux and Germany, which was associated with an old frontal system, and a stationary cloud band along the Alps. Throughout the two days, the whole of Germany was influenced by high clouds with the large cirrus shield moving eastwards.

Spatial patterns and temporal evolution of the modelled dust plume qualitatively compare well with observations. Initially, a good quantitative agreement between model results and AERONET sun photometer measurements is found over southern and western Europe. Later, the comparison with AERONET data is hampered by cloudiness. Compared to lidar observations at Leipzig, however, the modelled dust extinction for 4 and 5 April is underestimated by a factor up to 10. The dust height in general is well reproduced. The interactive simulations are therefore initialised with a 10-fold increased dust concentration.

The experiments show that the impact of Saharan dust on warm cloud microphysics is minor. The cloud droplet number is only slightly increased

by additional CCNs due to dust. A significant effect, however, is found for mixed-phase clouds. As a result of efficient heterogeneous freezing, Saharan dust considerably increases the number of ice particles. In the model run with online dust-cloud interaction, the ice water content (IWC) is enhanced by up to 50 % compared to the run with a low prescribed climatological INP number (Fig. 2). At temperatures below homogeneous freezing level, the ice nucleation is also enhanced by mineral dust. In particular between 7 and 8 km, the IWC is much higher in the feedback run (Fig. 2), as heterogeneously freezing dust particles and homogeneous freezing contribute to the ice formation.

There is some evidence that the quality of numerical weather forecast in terms of cloud cover is significantly reduced in the presence of mineral dust in this and other cases [*Voigt et al.*, 2016; *Rieger et al.*, 2017]. Here, the COSMO considerably underestimates high-level clouds while mid-level clouds are captured reasonably well compared to satellite data (Fig 2). Considering interactive aerosol-cloud microphysics improves the cloud representation, although cirrus remains underestimated. In addition, including direct and semi-direct radiative effects of dust appears to have a large potential to improve the model performance. Further evaluation is needed to rule out other processes that might be missed or misrepresented.
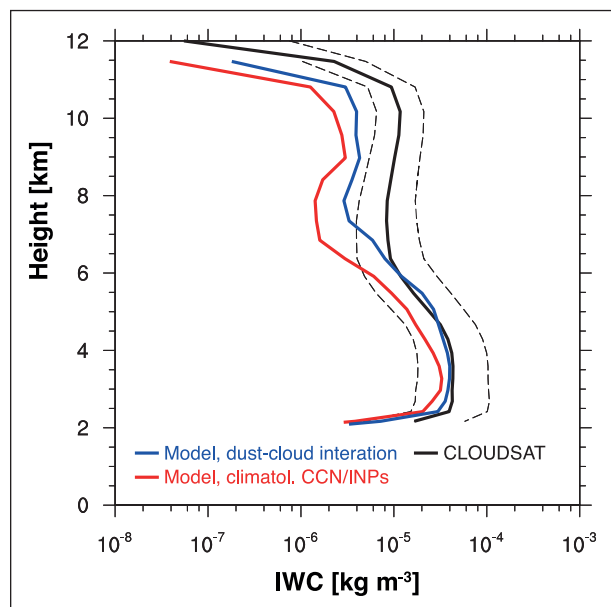
Fig. 2: Time-averaged vertical profiles of ice water content (IWC) along the CloudSat satellite overpass from 48.3°N, 0.6°E to 55.2°N, 7.4°E on 4 April 2014 at about 1230 UTC. Comparison of modelled profiles from simulations using climatological CCN/INP concentrations (red line) and interactive dust-cloud feedback (blue line) with the CloudSat radar observations (black line). The dashed lines show the variance of the CloudSat retrieval.

References

Heinold, B., I. Tegen, K. Schepanski, M. Tesche, M. Esselborn, V. Freudenthaler, S. Gross, K. Kandler, P. Knippertz, D. Müller, A. Schladitz, C. Toledano, B. Weinzierl, A. Ansmann, D. Althausen, T. Müller, A. Petzold, and A. Wiedensohler (2011), Regional modelling of Saharan dust and biomass-burning smoke Part 1: Model description and evaluation, *Tellus B*, 63(4), 781–799, doi:10.1111/j.1600-0889.2011.00570.x.

Rieger, D., A. Steiner, V. Bachmann, P. Gasch, J. Förstner, K. Deetz, B. Vogel, and H. Vogel (2017), Impact of the 4 April 2014 Saharan dust outbreak on the photovoltaic power generation in Germany, *Atmos. Chem. Phys.*, 17, 13391–13415, doi:10.5194/acp-17-13391-2017.

Seifert, A. and K. D. Beheng (2006), A two-moment cloud microphysics parameterization for mixed-phase clouds. Part 1: Model description, *Meteorol. Atmos. Phys.*, 92, 45–66, doi:10.1007/s00703-005-0112-4.

Ullrich, R., C. Hoose, O. Möhler, M. Niemand, R. Wagner, K. Höhler, N. Hiranuma, H. Saathoff, and T. Leisner (2017), A New Ice Nucleation Active Site Parameterization for Desert Dust and Soot, *J. Atmos. Sci.*, 74, 699–717, doi:10.1175/JAS-D-16-0074.1

Voigt, C., U. Schumann, A. Minikin, A. Abdelmonem, A. Afchine, S. Borrmann, M. Boettcher, B. Buchholz, L. Bugliaro, A. Costa, J. Curtius, M. Dollner, A. Dörnbrack, V. Dreiling, V. Ebert, A. Ehrlich, A. Fix, L. Forster, F. Frank, D. Fütterer, A. Giez, K. Graf, J. Grooß, S. Groß, K. Heimerl, B. Heinold, T. Hüneke, E. Järvinen, T. Jurkat, S. Kaufmann, M. Kenntner, M. Klingebiel, T. Klimach, R. Kohl, M. Krämer, T.C. Krisna, A. Luebke, B. Mayer, S. Mertes, S. Molleker, A. Petzold, K. Pfeilsticker, M. Port, M. Rapp, P. Reutter, C. Rolf, D. Rose, D. Sauer, A. Schäfler, R. Schlage, M. Schnaiter, J. Schneider, N. Spelten, P. Spichtinger, P. Stock, A. Walser, R. Weigel, B. Weinzierl, M. Wendisch, F. Werner, H. Wernli, M. Wirth, A. Zahn, H. Ziereis, and M. Zöger (2017), ML-CIRRUS: The Airborne Experiment on Natural Cirrus and Contrail Cirrus with the High-Altitude Long-Range Research Aircraft HALO, *Bull. Amer. Meteor. Soc.*, 98, 271–288, doi:10.1175/BAMS-D-15-00213.1.

Cooperation

Deutscher Wetterdienst (DWD), Offenbach, Germany;
Karlsruhe Institute of Technology (KIT), Institute for Meteorology and Climate Research, Karlsruhe, Germany;
Deutsches Zentrum für Luft- und Raumfahrt (DLR), Institute of Atmospheric Physics, Oberpfaffenhofen, Wessling, Germany

Regional modelling of SOA formation under consideration of HOMs

Kathrin Gatzsche[1], Yoshiteru Iinuma[2], Andreas Tilgner[1], Laurent Poulain[1], Torsten Berndt[1], Ralf Wolke[1], Wolfram Schröder[1], Marie Luttkus[1], Hartmut Herrmann[1], Ina Tegen[1]

[1] Leibniz Institute for Tropospheric Research (TROPOS), Leipzig, Germany
[2] now at: Okinawa Institute of Science and Technology Graduate University (OIST), Okinawa, Japan

Neue Laborstudien haben gezeigt, dass hochoxidierte, organische Oxidationsprodukte (HOMs) der Monoterpene, des Isoprens und der Sesquiterpene über eine geringe Volatilität verfügen. Aufgrund der damit einhergehenden effektiven Partitionierung in die Partikelphase, beeinflussen diese Oxidationsprodukte maßgeblich die Bildung von sekundärem organischem Aerosol (SOA). Um den Einfluss dieser Oxidationsprodukte auf die Bildung von SOA auf der regionalen Skala zu untersuchen, wurden der verwendete Gasphasen-Mechanismus und das bestehende SOA-Modul von COSMO-MUSCAT diesbezüglich erweitert. Die Modellergebnisse einer ersten Studie zeigen überwiegend einen Zuwachs des organischen Aerosols unter Berücksichtigung der HOMs.

Introduction

Secondary organic aerosol (SOA) is the major burden of the atmospheric organic particulate matter with 140-910 TgC yr^{-1} [*Hallquist et al.*, 2009]. SOA particles are formed via the oxidation of volatile organic carbons (VOCs), where the volatility of the VOCs is lowered. Accordingly, gaseous compounds can either nucleate to form new particles or condense on existing particles. The framework of SOA formation is very complex under natural conditions because there are a multitude of gas-phase precursors, atmospheric degradation processes, and products after oxidation. Up to now, numerical models tend to underestimate measured SOA mass [*Volkamer et al.*, 2006]. Thus, the present study aims at an improved understanding of SOA formation processes.

Here, the formation and immediate partitioning of highly oxygenated molecules (HOMs), which have been found in the gas phase during laboratory and field studies [*Berndt et al.*, 2016b; *Jokinen et al.*, 2015; *Mutzel et al.*, 2015] have been considered in the regional model COSMO-MUSCAT (COnsortium for Small-scale MOdelling and MUlti-Scale Chemistry Aerosol Transport). The regarded compounds are characterized by low volatility, which causes a fast partitioning into the particle phase, which is important for the early aerosol growth of SOA particles. Thus, the measured HOM yields have been incorporated in the utilized gas-phase chemistry mechanism [*Gatzsche et al.*, 2018]. Model results showing the impact of HOMs on the regional SOA formation are presented.

Model framework

In the present study the 3-D model COSMO-MUSCAT is utilized, which is qualified for process studies in local and regional areas. The model system consists of two online-coupled codes. The non-hydrostatic and compressible meteorological model COSMO [*Schättler et al.*, 2013], as meteorological driver, and the chemistry transport model MUSCAT [*Wolke et al.*, 2012], for atmospheric transport as well as chemical transformations of gas-phase and particle-phase species.

Within MUSCAT the biogenic VOC emissions are derived by the emission scheme of *Steinbrecher et al.* [2009]. The gas-phase chemistry mechanism is composed of RACM (Regional Atmospheric Chemistry Mechanism, *Stockwell et al.* [1997]) and MIM2 (Mainz Isoprene Mechanism 2, *Karl et al.*
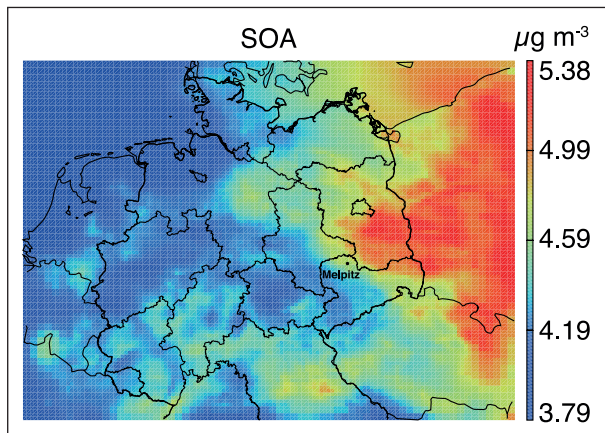
Fig. 1: Monthly average of the SOA mass concentration for May 2014 considering HOMs (surface layer).

[2006]). SOA formation is described by the SORGAM module (Secondary Organic Aerosol Model, *Schell et al.* [2001]), which has been implemented in the updated version of *Li et al.* [2013]. The HOM gas-phase formation yields have been incorporated in the existing gas-phase chemistry mechanism for α- and β-pinene, limonene, mycrene [*Berndt et*

al., 2016b; *Jokinen et al.*, 2015], for three sesquiterpenes (α-cedrene, β-caryophyllene, and α-humulene, *Richters et al.* [2016]), and isoprene [*Berndt et al.*, 2016a]. Model simulations have been performed for May 2014 for a simulation domain centred over north Germany and with a resolution of 8 km x 8 km. Furthermore, hourly field measurements of the TROPOS field site Melpitz are available from 07 to 27 May 2014.

Results and discussion

Figure 1 displays the monthly averaged SOA mass concentration for the simulation under consideration of HOMs in the period of May 2014. The maximum of the SOA mass concentrates over Poland and the East of Germany (mainly Brandenburg). Thus, Melpitz is located at the border of this area with high SOA mass concentrations (cf. Fig. 1).

The comparison of monthly averaged SOA mass concentrations for simulations with and without consideration of HOMs reveals that the addition of HOMs increases the SOA formation (cf. Fig. 2a). Furthermore, the main precursor sources
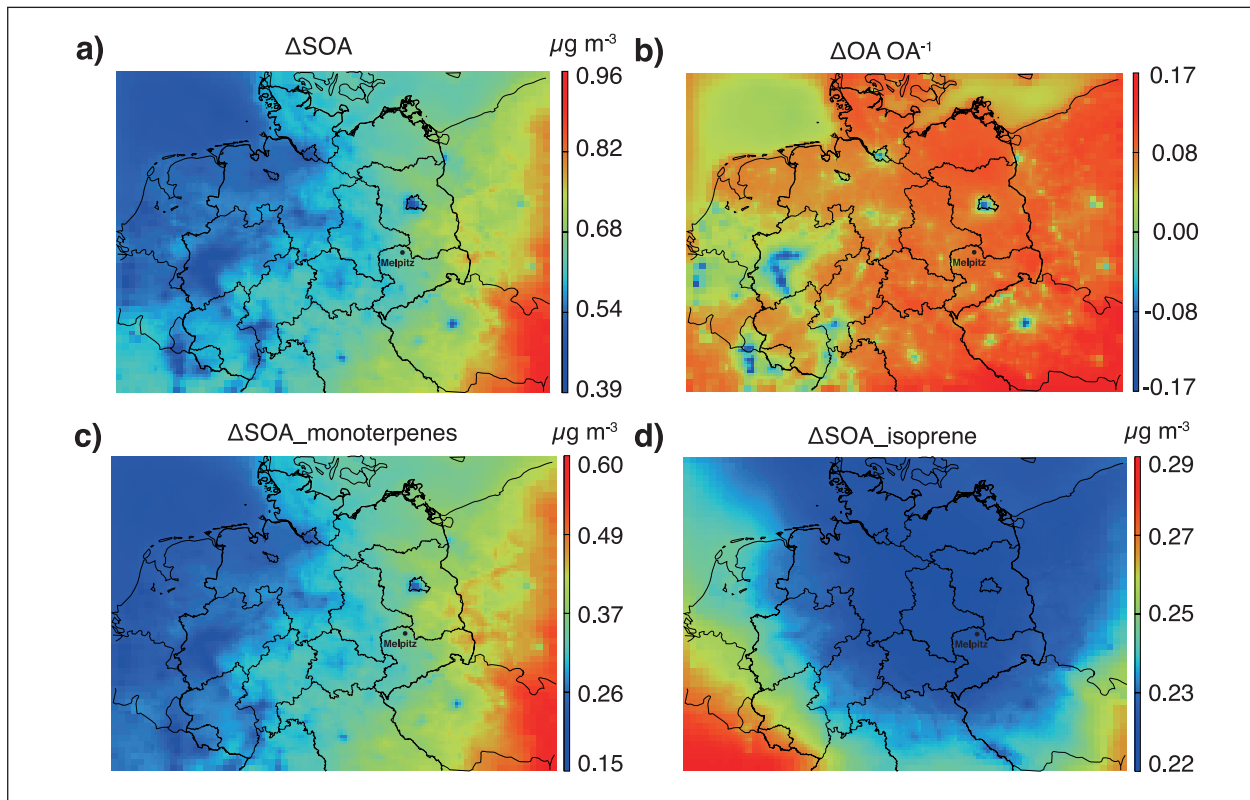
Fig. 2: (a) Absolute difference of monthly average of SOA mass concentration for May 2014 (SORGAM with HOMs minus SORGAM without HOMs), for the absolute value of SOA mass for the simulation with HOMs see Fig. 1; (b) Relative difference of monthly average of organic mass concentration (SORGAM with HOMs minus SORGAM without HOMs, ΔOA) related to the organic mass without consideration of HOMs (OA) for May 2014; (c) Absolute difference of monthly average of SOA mass concentration from monoterpenes for May 2014 (SORGAM with HOMs minus SORGAM without HOMs); (d) same as (c) for SOA mass from isoprene. All figures display the surface layer.
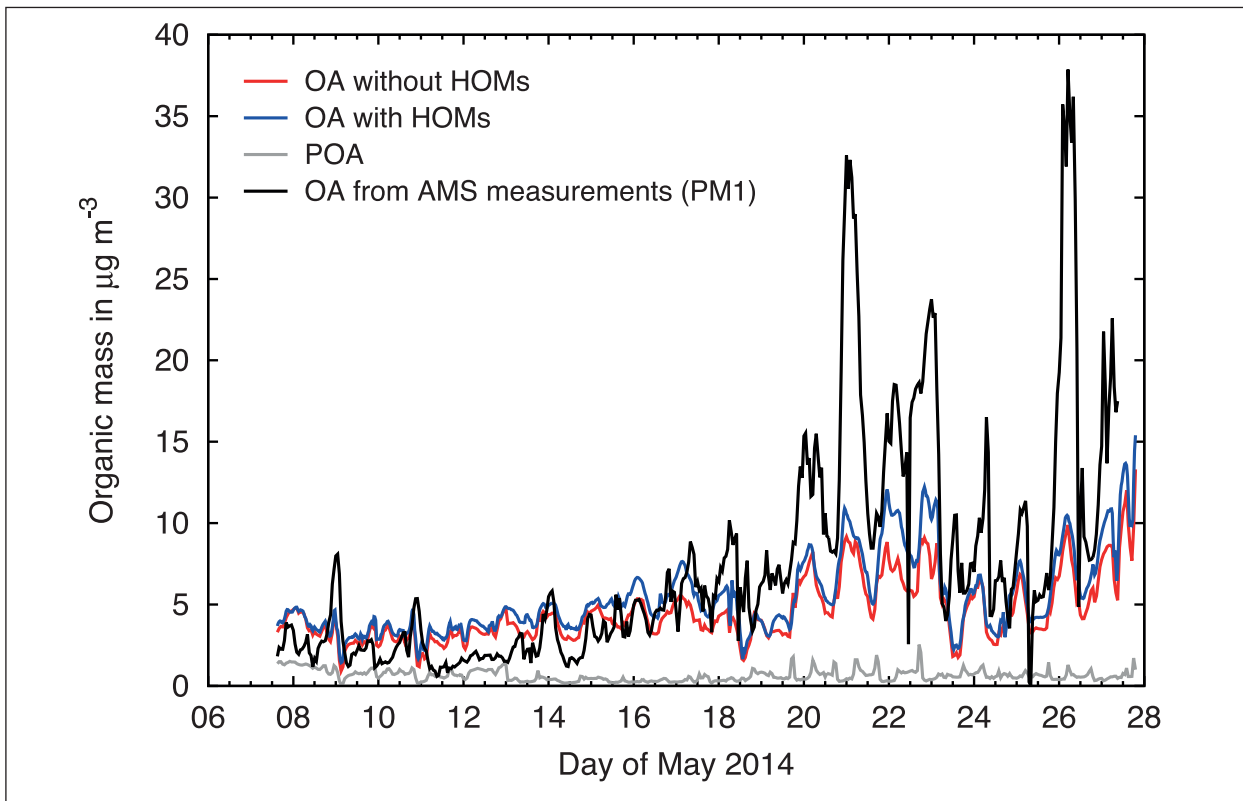
Fig. 3: Results of the 3-D model COSMO-MUSCAT for the TROPOS field site Melpitz (51° 32' N, 12° 54' E, 87 m asl); Hourly model results of organic mass calculated from SOA and POA with HOMs (blue line) and without HOMs (red line), simulated primary organic aerosol (POA, gray line) and hourly AMS measurements of organic mass (PM1, black line).

of the increased SOA mass have been investigated. Monoterpenes cause higher SOA mass concentrations especially in the east of the considered domain, whereby the maximum difference is observed over the west of Poland and Czech Republic (cf. Fig. 2c). The relative increase for monoterpene related SOA ranges between 11 % and 40 % in the domain. This circumstance is due to the high HOM yields of monoterpenes. Also isoprene causes a significant increase in the SOA mass, however the concentration differences can be only obtained in a rather small region in the East of France (cf. Fig. 2d). Nevertheless, the relative increase of the SOA mass from isoprene ranges between 74 % and 101 %. The local distribution of the SOA mass increase for both HOM classes are linked to the emissions of their associated precursors (not shown here). Consequently, the total SOA mass is increased by 17 % for the major part of the model domain, but reduced in some conurbations with predominant anthropogenic emissions (cf. Fig. 2d).

In Fig. 3, a comparison between the hourly measured and simulated organic aerosol mass concentrations at the TROPOS field site Melpitz

is shown with and without consideration of HOMs. Online measurements of the particle composition at Melpitz have been conducted with an Aerodyne High Resolution Time-of-Flight Aerosol Mass Spectrometer (HR-TOF-AMS, Aerodyne, Inc., *DeCarlo et al.* [2006]), to derive the organic aerosol mass (PM1.0). For comparison, simulated SOA and POA (primary organic aerosol) were added up to get the modelled organic mass concentration (OA). POA contributes only to a minor amount of the simulated organic mass (14 %/17 % with HOMs/without HOMs). The temporal trend of the simulated and the measured organic aerosol mass is in good agreement. However, the model does not capture some characteristic concentration peaks of the organic mass. Overall, the simulation considering HOMs results in more organic mass as the base case (about 17.5 % at Melpitz) and, therefore, is more consistent with the AMS measurements. Furthermore, it can be seen from Fig. 3 that the measured OA mass of the AMS is from 18 to 28 May often higher than the modelled OA, demonstrating the still incomplete SOA formation description in the present model.

References

Berndt, T., H. Herrmann, M. Sipilä, and M. Kulmala (2016), Highly Oxidized Second-Generation Products from the Gas-Phase Reaction of OH Radicals with Isoprene, *J. Phys. Chem. A*, 120(51), 10150-10159.

Berndt, T., et al. (2016), Hydroxyl radical-induced formation of highly oxidized organic compounds, *Nat. Commun.*, 7(13677).

DeCarlo, P. F., et al. (2006), Field-Deployable, High-Resolution, Time-of-Flight Aerosol Mass Spectrometer, *Anal. Chem.*, 78(24), 8281-8289.

Gatzsche, K., Y. Iinuma, A. Mutzel, T. Berndt, L. Poulain, A. Tilgner, and R. Wolke (2018), In: Air Pollution Modeling and its Application XXV, edited, Springer International Publishing.

Hallquist, M., et al. (2009), The formation, properties and impact of secondary organic aerosol: current and emerging issues, *Atmos. Chem. Phys.*, 9(14), 5155-5236.

Jokinen, T., et al. (2015), Production of extremely low volatile organic compounds from biogenic emissions: Measured yields and atmospheric implications, *Proc. Nat. Acad. Sci.*, 112(23), 7123-7128.

Karl, M., H. P. Dorn, F. Holland, R. Koppmann, D. Poppe, L. Rupp, A. Schaub, and A. Wahner (2006), Product study of the reaction of OH radicals with isoprene in the atmosphere simulation chamber SAPHIR, *J. Atmos. Chem.*, 55(2), 167-187.

Li, Y. P., H. Elbern, K. D. Lu, E. Friese, A. Kiendler-Scharr, T. F. Mentel, X. S. Wang, A. Wahner, and Y. H. Zhang (2013), Updated aerosol module and its application to simulate secondary organic aerosols during IMPACT campaign May 2008, *Atmos. Chem. Phys.*, 13(13), 6289-6304.

Mutzel, A., et al. (2015), Highly Oxidized Multifunctional Organic Compounds Observed in Tropospheric Particles: A Field and Laboratory Study, *Environ. Sci. Technol.*, 49(13), 7754-7761.

Richters, S., H. Herrmann, and T. Berndt (2016), Highly Oxidized RO_2 Radicals and Consecutive Products from the Ozonolysis of Three Sesquiterpenes, *Environ. Sci. Technol.*, 50(5), 2354-2362.

Schättler, U., G. Doms, and C. Schraff (2013), A description of the nonhydrostatic regional COSMO-Model. Part VII: User's guide. Deutscher Wetterdienst, Offenbach, edited.

Schell, B., I. J. Ackermann, H. Hass, F. S. Binkowski, and A. Ebel (2001), Modeling the formation of secondary organic aerosol within a comprehensive air quality model system, *J. Geophys. Res. - Atmos.*, 106(D22), 28275-28293.

Steinbrecher, R., G. Smiatek, R. Koeble, G. Seufert, J. Theloke, K. Hauff, P. Ciccioli, R. Vautard, and G. Curci (2009), Intra- and inter-annual variability of VOC emissions from natural and semi-natural vegetation in Europe and neighbouring countries, *Atmos. Environ.*, 43(7), 1380-1391.

Stockwell, W. R., F. Kirchner, M. Kuhn, and S. Seefeld (1997), A new mechanism for regional atmospheric chemistry modeling, Journal of Geophysical Research: Atmospheres, 102(D22), 25847-25879.

Volkamer, R., J. L. Jimenez, F. San Martini, K. Dzepina, Q. Zhang, D. Salcedo, L. T. Molina, D. R. Worsnop, and M. J. Molina (2006), Secondary organic aerosol formation from anthropogenic air pollution: Rapid and higher than expected, *Geophys. Res. Lett.*, 33(17), 1944-8007.

Wolke, R., W. Schröder, R. Schrödner, and E. Renner (2012), Influence of grid resolution and meteorological forcing on simulated European air quality: A sensitivity study with the modeling system COSMO-MUSCAT, *Atmos. Environ.*, 53, 110-130.

AtCSol – An experimental environment for the simulation of large chemical multiphase mechanisms

Willi Schimmel, Oswald Knoth

Zum besseren Verständnis und Vorhersagbarkeit luftchemischer Prozesse in der Gas-, Partikel- und Flüssigphase werden derzeit immer umfassendere chemische Reaktionssysteme entwickelt, welche mit der Berücksichtigung längerkettiger organischer Verbindungen schnell exponentiell in der Anzahl der chemischen Reaktanten und Reaktionen wachsen. Um derartige komplexe chemische Systeme effizient zu lösen, müssen angepasste numerische Verfahren verwendet werden. Ein wesentlicher Bestandteil bei der numerischen Lösung ist die Generierung großer schwachbesetzter Matrizen und das Lösen linearer Gleichungssysteme mit diesen Matrizen. Im Falle der Kopplung von Gas- und Partikelphase erhöht sich der Aufwand weiter. Die experimentelle Simulationsumgebung AtCSol ermöglicht die effiziente Lösung großer kinetischer Systeme und dient gleichzeitig als Experimentierumgebung zum Test neuer numerischer Verfahren im Anwendungsbereich Atmosphärenchemie.

Introduction

The simulation and analysis of comprehensive chemical reaction mechanisms require the development of efficient algorithms for the application of very large chemical kinetics systems. The software package **AtCSol** (Atmospheric Chemistry Solver), written in modern Fortran, was developed as an experimental environment for the simulation of large atmospheric chemistry mechanisms. AtCSol has the purpose to investigate the behaviour of different mathematical techniques applied to large chemistry problems. Several software packages have been developed to analyse these systems, e.g., KPP [*Sandu et al.*, 2006], ChemKin [*Kee et al.*, 1996], and SPACCIM [*Wolke et al.*, 2005] currently used at TROPOS. In contrast to KPP, where a fixed Fortran code, for every new chemical mechanism has to be generated, then compiled and then executed, AtCSol, reads a reaction system containing n_R reactions, generates a set of n_S stiff ordinary differential equations (ODEs) and solves it directly. With given model scenarios one can simulate the evolution of species in a box-model framework over a user defined time interval.

AtCSol can handle very large and complex multiphase mechanisms, e.g. MCM (Master Chemical Mechanism) [*Bloss et al.*, 2005] coupled with CAPRAM (Chemical Aqueous Phase RAdical

Mechanism) [*Tilgner et al.*, 2014] with more than 10,000 species and 23,000 reactions, in a comparatively short time. Reasons are a very efficient implementation for the calculation of reaction rates and a comprehensive suite of stiff numerical integrators, where efficiency is obtained by carefully exploiting the sparsity structures of the Jacobian. The Fortran code is also fully modularized and does not require the use of additional 3rd party software.

Generation of ODEs

In the beginning, AtCSol reads the reaction system and generates sparse matrices from the stoichiometric coefficients of the reaction system. The difference between product and educt matrix,

$v = v^p - v^e$, multiplied with the reaction rates r generates the right-hand side of an ordinary differential equation describing the evolution of the kinetical system. Note that the stoichiometric matrix v is usually very sparse. The system can then be represented in a very short manner as a matrix vector product:

$dc/dt = v^T r + c^{emis}$, where the change in concentration is equal to the matrix-vector product plus time dependent emissions rates and possibly other processes like deposition and dilution.

In order to compute the reaction rates r, all reaction rate constants are calculated in an efficient

form such that only a minimum number of queries is necessary. Besides simple temperature dependent reactions (e.g.: Arrhenius), AtCSol is able to evaluate the constants of a wide range of reaction types, e.g. pressure-dependent reactions (e.g.: Lind, Troe), photolytic reactions, fast equilibrium reactions (e.g.: dissociation) and also phase transitions. The interchange between the gas and liquid phase is specified according to the Schwartz approach [*Schwartz*, 1986].

Numeric Solver

From the numerical point of view, atmospheric chemistry is challenging due to the coexistence of very stable (e.g., CH_4) and very reactive (e.g., $O(^1D)$) species. In mathematics, this phenomenon is better known as *stiffness*. Rosenbrock methods are chosen to solve these stiff ordinary differential equations. Because of its excellent stability properties, larger time steps can be made within the simulation. In addition, a step size control is implemented, via embedded formula, to modify the size of the time step according to its local error. The cost of using Rosenbrock methods is the need to calculate the solution of s linear equation systems, where s is the number of stages in the Rosenbrock method. This requires additionally the calculation of the Jacobian of the ODE system, the sparse matrix product $J = v^T D_r v^e D_c^{-1}$, where D_r and D_c are in addition diagonal matrices containing the rates and the concentrations on its main diagonal. For larger systems, this product can be computationally very expensive. Finally, in the standard scheme the following sparse linear equation set has to be solved

$$\left(I - \triangle t\, \gamma J\right) u_i = \triangle t \left(v^T r_i + c^{emis}\right) + \sum_{j=1}^{i-1} d_{ij} u_j,$$

$$c^{new} = c^{old} + \sum_{j=1}^{s} m_j u_j$$

The system is solved with a direct sparse LU factorization based on a symmetric ordering scheme (minimum degree) [*Markowitz*, 1957]. Our own experiments show that this ordering is superior to other ordering strategies. A second approach which skips the calculation of the Jacobian J and also simplifies the computation of the right-hand side is compared to the standard approach. To avoid the sparse matrix products the linear system from above is expanded to the larger, block structured linear system

$$\begin{bmatrix} D_r^{-1} & \gamma v^e \\ v^T & \frac{1}{\triangle t} D_c \end{bmatrix} \begin{bmatrix} x \\ \tilde{u}_i \end{bmatrix} = \begin{bmatrix} -D_r^{-1} r_i \\ c^{emis} \end{bmatrix} + \frac{1}{\triangle t} \sum_{j=1}^{i-1} d_{ij} \begin{bmatrix} 0 \\ D_c \tilde{u}_j \end{bmatrix},$$

$$c^{new} = c^{old} + D_c \sum_{j=1}^{s} m_j \tilde{u}_j$$

The advantages of the extended system are that only the main diagonal has to be updated and the calculation of the right-hand side reduces to a component wise vector-vector multiplication. Using again the same sparse solver as for the standard approach leads to a stable solution procedure without any other provisions for stability. Since the standard approach can be seen as a special type of LU-factorization of the extended form the number of operations is usually decreased. Figure 1 and 2 show the nonzero structures of the two linear systems and their corresponding LU-decomposition for the large
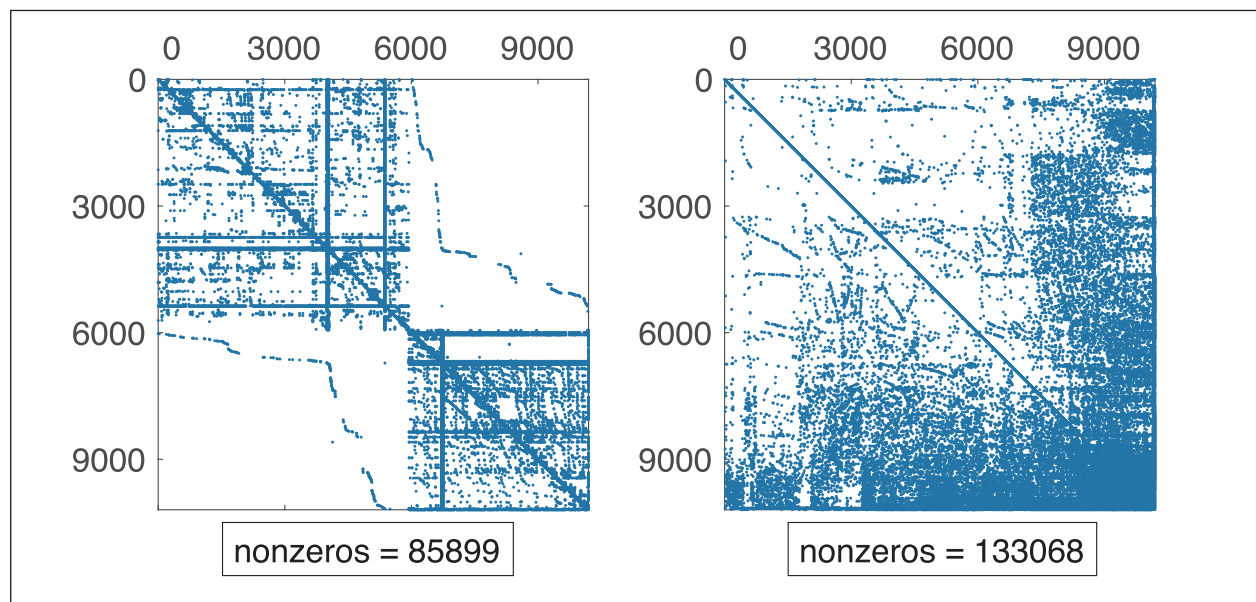
Fig. 1: Matrix sparsity pattern Jacobian (left) and LU decomposition (right).
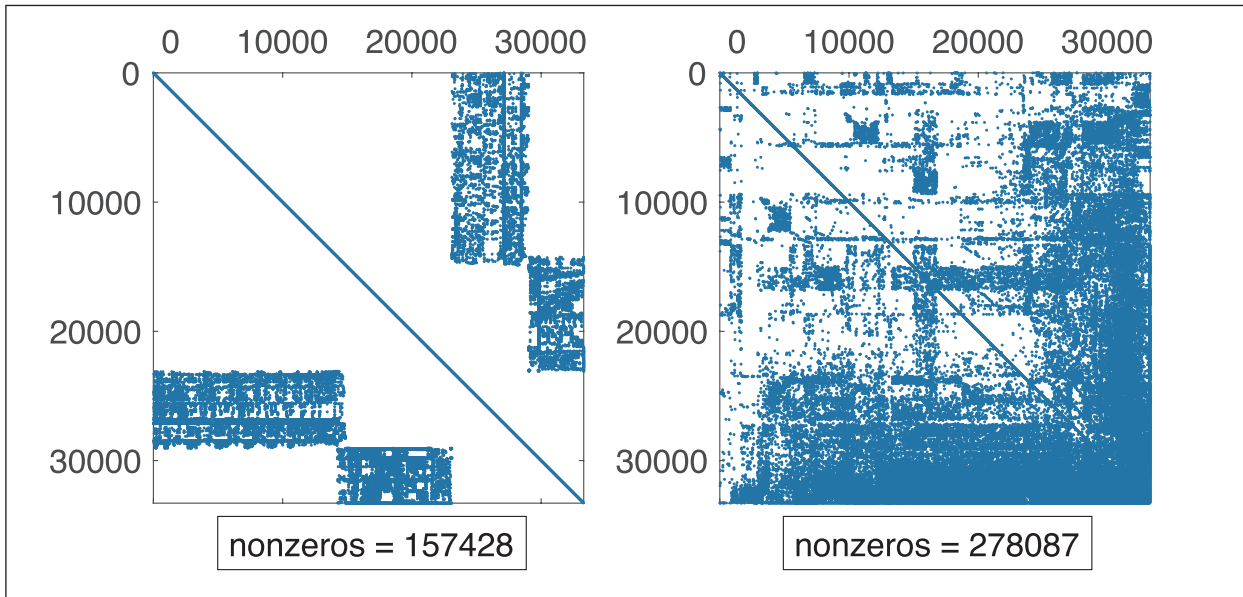
Fig. 2: Matrix sparsity pattern extended block matrix system (left) and LU decomposition (right).

coupled mechanism MCM3.1+CAPRAM4.0. Note that the matrix dimension in Fig. 2 is much larger than the standard form in Fig. 1, also the number of non-zeros is larger. Nevertheless, a 3-day simulation for the

coupled mechanism MCM3.1+CAPRAM4.0 shows that integration time is 20[sec] using the extended block system compared to 25[sec] using the standard approach.

References

Sandu, A. and Sander, R. (2006), Technical note: Simulating chemical systems in Fortran90 and Matlab with the Kinetic PreProcessor KPP-2.1, *Atmos. Chem. Phys.*, 6, 187-195

Kee R. J., Rupley F. M., Meeks E., and Miller J. A. (1996), Chemkin-III: A Fortran Chemical Kinetics Package for the Analysis of Gas-Phase Chemical and Plasma Kinetics, Sandia National Laboratories Report SAND96-8216

Wolke, R., Sehili, A. M., Simmel, M., Knoth, O., Tilgner, A., Herrmann, H. (2005), SPACCIM: A parcel model with detailed microphysics and complex multiphase chemistry, *Atmos. Environ.*, 39, 4375-4388

Bloss, C., Wagner, V., Jenkin, M. E., Volkamer, R., Bloss, W. J., Lee, J. D., Heard, D. E., Wirtz, K., Martin-Reviejo, M., Rea, G., Wenger, J. C., Pilling, M. J. (2005), Development of a detailed chemical mechanism (MCMv3.1) for the atmospheric oxidation of aromatic hydrocarbons, *Atmos. Chem. Phys.*, 5, 641-664

Tilgner, A., Bräuer, P., Wolke, R., Herrmann, H. (2014), Multiphase chemical processing by clouds: Modelling the HCCT-2010 hill cap cloud experiment with SPACCIM/CAPRAM4.0α, EGU General Assembly 2014

Schwartz, S. (1986), Mass transport considerations pertinent to aqueous phase reactions of gases in liquid water clouds, Jaeschke, W. (Ed.), Chemistry of Multiphase Atmospheric Systems, NATO ASI Series. Springer, Berlin, 415–471

Markowitz, H. (1957), The Elimination form of the Inverse and its Application to Linear Programming, *Manage. Sci.*, 3, 255-269

Characterization of humic-like substances in particles with 2D-chromatography and ultra-high resolution mass spectrometry

Tobias Spranger[1], Dominik van Pinxteren[1], Oliver Lechtenfeld[2], Thorsten Reemtsma[2], Hartmut Herrmann[1]

[1] Leibniz Institute for Tropospheric Research (TROPOS), Leipzig, Germany

[2] Helmholtz Centre for Environmental Research (UFZ), Leipzig, Germany

Organischer Kohlenstoff ist eine der Hauptkomponenten von atmosphärischen Aerosolpartikeln und spielt eine wichtige Rolle für die Wolkenbildung und den Strahlungshaushalt der Erde. Die genaue Zusammensetzung ist jedoch weitgehend unbekannt, weshalb ein Großteil der organischen Verbindungen unter dem Begriff der humin-ähnliche Substanzen zusammengefasst wird. Um diese hochkomplexe Mischung besser zu analysieren und zu charakterisieren, wurde eine Fraktionierungsmethode mittels 2D-Flüssigchromatografie entwickelt. Mit Hilfe dieser wurden deutliche Unterschiede in der Zusammensetzung der humin-ähnlichen Substanzen zwischen Sommer und Winter sowie verschiedenen Luftströmungen für die Messstation Melpitz offenbart. Des Weiteren wurden durch die Kombination der 2D-Methode und ultrahochauflösender Massenspektrometrie neue Erkenntnisse über die genaue molekulare Zusammensetzung gewonnen.

Introduction

Organic carbon (OC) contributes up to 70 % to the total particle mass of atmospheric aerosol particles [*Kanakidou et al.*, 2005] and plays an important role for cloud formation and the earth radiative budget, as it alters microphysical properties and the ability of particles to serve as cloud condensation nuclei [*Kristensen et al.*, 2012]. Moreover, it is expected to be involved in a wide range of human health issues [*Mauderly and Chow*, 2008] and can have an impact on ecosystems [*Fuzzi et al.*, 2006]. Despite its importance, only a small fraction has been identified on a molecular level, due to the high complexity with thousands of substances. OC is dominated by a class of substances often referred as humic-like substances (HULIS), which contributes up to 80 % to the water-soluble organic carbon [*Zheng et al.*, 2013]. Elucidating its composition is therefore crucial to understand aerosol properties and its role e.g. in the cloud formation process. At the same time, the high complexity of the chemically unresolved mixture is challenging. Thus, there is a strong need for chromatographic techniques to at least fractionate the complex mixture to reduce the complexity of HULIS and get a better understanding of its composition. How-ever, routinely applied methods like one-dimensional reversed-phase liquid chromatography (RP-HPLC) with a linear gradient or size exclusion chromatography (SEC) lead to unresolved broad bands with only some individual peaks on top.

Result and Discussion

In the Framework of the DFG-project HuCar (Classification of HULIS carbon from different atmospheric environments via a 2D-offline chromatography), an offline two-dimensional chromatographic method was developed, combining SEC and RP-HPLC, for a detailed fractionation of aerosol particle extracts. The particle extracts are separated via optimized SEC into five fractions in molar mass ranges between 160-900 g/mol. Each fraction is than reconcentrated and separated further into eleven RP-HPLC fractions with calculated octanol/water partition coefficients of 0.2-3.3, utilizing a newly developed "spiked gradient" method [*Spranger et al.*, 2017]. Heat maps of the UV-absorption at 254 nm illustrate the distribution of HULIS in the two-dimensional size-vs-polarity space (Fig. 1). The distribution differs strongly depending on season and air mass input for a set of samples from Melpitz, a background station near Leipzig, Germany.
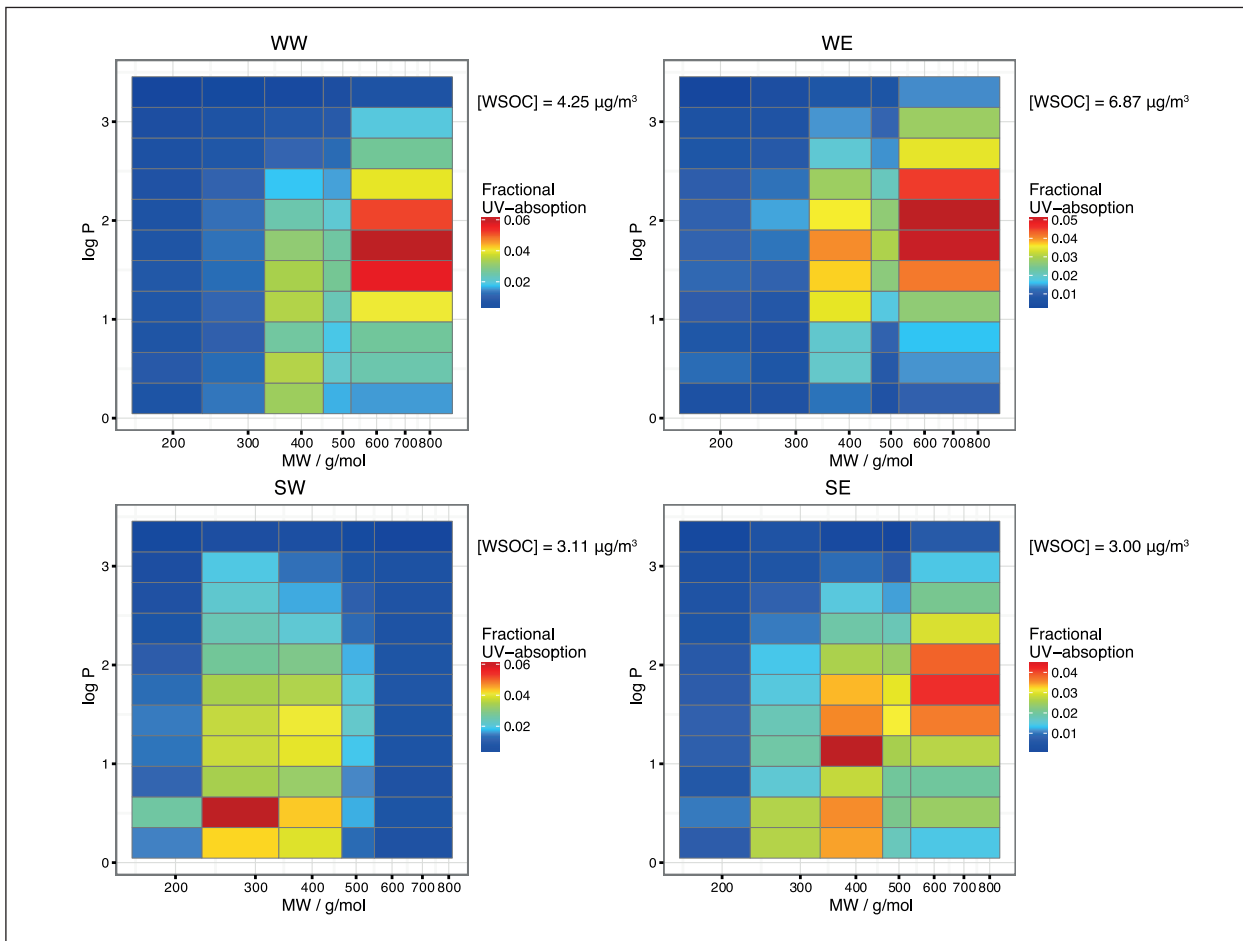
Fig. 1: 2D heat maps of Melpitz PM10 fractionated extracts for two seasons and air mass inflow regimes, i.e. winter west (WW), winter east (WE), summer west (SW), and summer east (SE).

In winter, the largest molecules with a relatively low polarity dominate the absorption properties. This is even more distinct for easterly winds, were long-range transport from Eastern Europe plays a major role. In summer, the smaller more polar molecules dominate the absorption, likely due to stronger biogenic influences. Also in summer, there are differences between the different air mass influences, as the largest molecules are more present with easterly winds, similar to the winter samples.

Additionally to the UV-absorption measurements, the individual fractions of one filter sample were analysed by direct infusion ultra-high resolution electrospray ionisation Fourier transform ion cyclotron mass spectrometry (12T SolariX XR, Bruker Daltronics). The number of identified, unique molecular formulas increased by a factor of ~2.3 for the fractionated sample as compared to a single measurement of the bulk sample extract, likely due to a reduction of ion suppression in the electrospray ionisation and hence sensitivity enhancement of low concentration HULIS compounds [*Noziere et al.*, 2015]. So-called Van Krevelen diagrams (Fig. 2) can illustrate the signals distri-
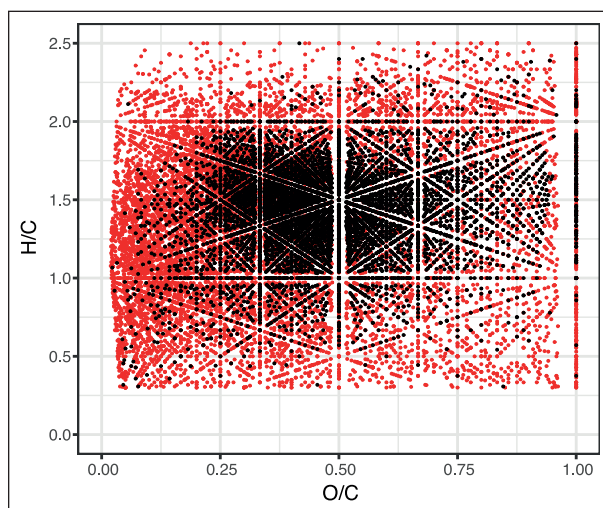
Fig. 2: Van Krevelen diagram of bulk (black) and molecular formulas newly found in fractionated sample (red).

butions of the newly found molecular formulas in comparison to the bulk sample. While the bulk signals are clustered in the centre, the new signals are spread over the whole area of possible formulas with the ma-

jority of signals being at lower oxygen-to-carbon ratios. One can expect a lower ionisation efficiency with lower oxygen content, thus these compounds can only be measured in the fractionated sample. Within the newly found molecular formulas were also many aromatic compounds, which have not been measured before in the aqueous phase. Further, detailed information about the chemical composition are gained for each fraction. For later eluting HPLC fractions, the hydrogen-to-carbon ratio increases, while the oxygen- and nitrogen-to-carbon ratios, as well as the carbon oxidation state, decreases. The results also show a high amount of poly-aromatic compounds and a high nitrogen-to-carbon ratio for the SEC fractions containing the largest molecules (>520 g/mol), possibly explaining the high absorption of these mainly anthropogenic associated fractions.

References

Fuzzi, S., M. O. Andreae, B. J. Huebert, M. Kulmala, T. C. Bond, M. Boy, S. J. Doherty, A. Guenther, M. Kanakidou, K. Kawamura, V. M. Kerminen, U. Lohmann, L. M. Russell, and U. Poschl (2006), Critical assessment of the current state of scientific knowledge, terminology, and research needs concerning the role of organic aerosols in the atmosphere, climate, and global change, *Atmos. Chem. Phys.*, *6*, 2017-2038.

Kanakidou, M., J. H. Seinfeld, S. N. Pandis, I. Barnes, F. J. Dentener, M. C. Facchini, R. Van Dingenen, B. Ervens, A. Nenes, C. J. Nielsen, E. Swietlicki, J. P. Putaud, Y. Balkanski, S. Fuzzi, J. Horth, G. K. Moortgat, R. Winterhalter, C. E. L. Myhre, K. Tsigaridis, E. Vignati, E. G. Stephanou, and J. Wilson (2005), Organic aerosol and global climate modelling: a review, *Atmos. Chem. Phys.*, *5*, 1053-1123.

Kristensen, T. B., H. Wex, B. Nekat, J. K. Nojgaard, D. van Pinxteren, D. H. Lowenthal, L. R. Mazzoleni, K. Dieckmann, C. B. Koch, T. F. Mentel, H. Herrmann, A. G. Hallar, F. Stratmann, and M. Bilde (2012), Hygroscopic growth and CCN activity of HULIS from different environments, *J. Geophys. Res. - Atmos.*, *117*(D22203), doi: Artn D22203Doi 10.1029/2012jd018249.

Mauderly, J. L., and J. C. Chow (2008), Health effects of organic aerosols, *Inhal. Toxicol.*, *20*(3), 257-288, doi: 10.1080/08958370701866008.

Noziere, B., M. Kaberer, M. Claeys, J. Allan, B. D'Anna, S. Decesari, E. Finessi, M. Glasius, I. Grgic, J. F. Hamilton, T. Hoffmann, Y. Iinuma, M. Jaoui, A. Kahno, C. J. Kampf, I. Kourtchev, W. Maenhaut, N. Marsden, S. Saarikoski, J. Schnelle-Kreis, J. D. Surratt, S. Szidat, R. Szmigielski, and A. Wisthaler (2015), The Molecular Identification of Organic Compounds in the Atmosphere: State of the Art and Challenges, *Chem. Rev.*, *115*(10), 3919-3983, doi: 10.1021/cr5003485.

Spranger, T., D. van Pinxteren, and H. Herrmann (2017), Two-Dimensional Offline Chromatographic Fractionation for the Characterization of Humic-Like Substances in Atmospheric Aerosol Particles, *Environ. Sci. Technol.*, doi: 10.1021/acs. est.7b00077.

Zheng, G. J., K. B. He, F. K. Duan, Y. Cheng, and Y. L. Ma (2013), Measurement of humic-like substances in aerosols: A review, *Environ. Pollut.*, *181*, 301-314, doi: DOI 10.1016/j. envpol.2013.05.055.

Articles

Direct probing of Criegee intermediates from gas-phase ozonolysis using chemical ionization mass spectrometry

Torsten Berndt[1], Hartmut Herrmann[1], Theo Kurtén[2]

[1] Leibniz Institute for Tropospheric Research (TROPOS), Leipzig, Germany

[2] Department of Chemistry, University of Helsinki, Helsinki, Finland

Criegee Intermediate (CIs), welche hauptsächlich über die Gasphasenozonolyse von Alkenen gebildet werden, stellen ein Oxidationsmittel in der Atmosphäre dar. Der direkte CI Nachweis wird dringend zur Beurteilung der atmosphärischen CI Prozesse benötigt. Es wurde erstmalig eine Methode des CI Direktnachweises mittels Massenspektrometrie gefunden, welche den CI Nachweis von 10^4 - 10^5 Molekülen cm^{-3} erlaubt.

Das einfachste CI, CH_2OO, ist als Addukt mit protonierten Ethern, bevorzugt protoniertes Tetrahydrofuran, detektierbar. Kinetische Messungen ergaben k(CH_2OO + SO_2) = (3.3 $\pm$ 0.9) $\times$ 10^{-11} und k(CH_2OO + Essigsäure) = (1.25 $\pm$ 0.30) $\times$ 10^{-10} cm^3 Molekül^{-1} s^{-1} bei T = 295 $\pm$ 2 K in sehr guter Übereinstimmung mit derzeit akzeptierten Literaturwerten.

Die CIs aus der Ozonolyse von Cyclohexen wurden als protonierte Spezies (CI)H$^+$ verfolgt, welche mittels protonierter Amine als Protonenüberträger erzeugt wurden. Kinetische Messungen deuten auf eine veränderte Reaktivität der CIs des Cyclohexens verglichen mit der des CH_2OO hin.

Introduction

The gas-phase ozonolysis of alkenes in the atmosphere forms chemically activated Criegee intermediates, which can be stabilized by bath-gas collisions to form thermalized Criegee intermediates (CIs). These can further react via unimolecular steps or bimolecular reactions with water vapor and trace gases. CIs are believed to play a significant role as atmospheric oxidants, especially for the oxidation of SO_2 forming H_2SO_4 [*Cox and Penkett*, 1971]. Due to the complexity of the ozonolysis reaction, the determination of reaction parameters, such as CI formation yields and rate coefficients, is very challenging. Kinetic measurements based on indirect methods lead to rate coefficients of CI reactions, which are in most cases affected with high uncertainty [*Calvert et al.*, 2000].

A breakthrough in the kinetic measurements has been achieved by using diiodomethane photolysis for CH_2OO generation coupled with direct CI probing by means of synchrotron photoionization mass spectrometry. For CH_2OO + SO_2, a rate coefficient of (3.9 $\pm$ 0.7) $\times$ 10^{-11} cm^3 molecule^{-1} s^{-1} at 293 K was obtained being orders of magnitude higher than reported before [*Welz et al.*, 2012]. The diiodoalkane photolysis technique has been successfully applied for CH_3CHOO and $(CH_3)_2COO$ studies as well. However, it remains questionable whether this approach will be applicable for a wide range of CIs due to the limited availability of the corresponding diiodoalkanes.

Here a direct and sensitive CI measurement technique based on atmospheric pressure - chemical ionization mass spectrometry is described that meets the requirements to probe CIs from atmospherically relevant ozonolysis reactions. Selected kinetic measurements were carried out to demonstrate the usability of this technique. Quantum-chemical calculations provided the needed proton affinities for a series of compounds and information on cluster stabilities [*Berndt et al.*, 2017].

Experimental

The experiments have been conducted in a free-jet flow system at a pressure of 1 bar purified air and a temperature of 295 ± 2 K [*Berndt et al.*, 2015]. The reaction time was 7.9 s in all experiments. This set-up allows the investigation of oxidation reaction for atmospheric conditions in absence of wall effects. CI detection was carried out using a CI-APi-TOF mass spectrometer (chemical ionization - atmospheric pressure interface - time-of-flight) sampling the centre flow from the flow system. Used reagent ions XH^+ were protonated ethers, i.e. $X \equiv$ tetrahydrofuran or diethylether, or protonated amines, $X \equiv$ n- or tert.-butylamine or diethylamine.

Results

CH_2OO. Beginning with CH_2OO, the primary idea was to detect the CI as protonated species $(CH_2OO)H^+$ formed via $XH^+ + CH_2OO \rightarrow (CH_2OO)H^+ + X$. Due to CH_2OO´s relatively high proton affinity (PA) of 850 - 855 kJ/mol a reagent ion precursors X with an accordingly high PA can be applied to ensure a selective ionization process. Tetrahydrofuran, PA = 822 - 826 kJ/mol, was found to form the reagent ion $XH^+ \equiv (THF)H^+$ with good purity under our reaction conditions. The experiments revealed that the reaction $(THF)H^+ + CH_2OO$ predominantly yielded the adduct $(CH_2OO)(THF)H^+$. The formation of this adduct and of the protonation product $(CH_2OO)H^+$ with a ratio of ~45 strictly followed the expected CH_2OO generation and was not influenced by adding propane as OH radical scavenger, see Fig. 1.
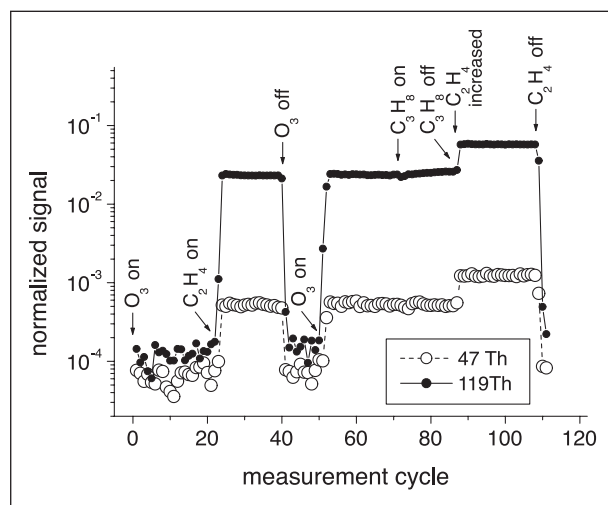
Fig. 1: Measured ion traces at the nominal mass of 47 Th, $(CH_2OO)H^+$, and at 119 Th, $(CH_2OO)(THF)H^+$, as a function of different reactant conditions.
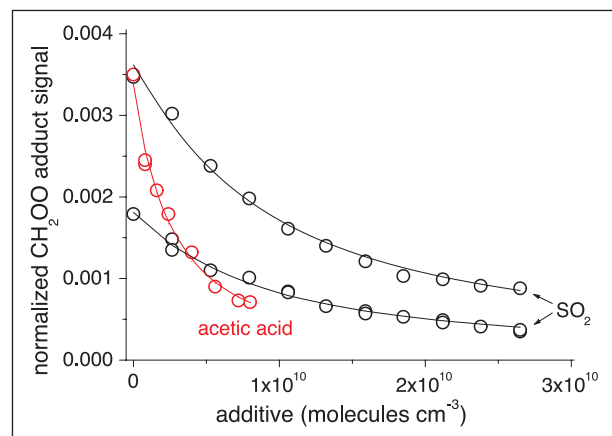
Fig. 2: Kinetic measurements: $(CH_2OO)(THF)H^+$ adduct signal as a functions of added SO_2 or acetic acid. The lines represent the best-fit results of data analysis.

The CH_2OO adduct signal with $(THF)H^+$, $(CH_2OO)(THF)H^+$, was measured as a function of reacted ethylene by varying either ethylene for a constant ozone concentration or vice versa. For an ethylene conversion < 10^8 molecules cm^{-3}, both measurement series gave a joint straight line indicating the absence of significant bimolecular steps for CH_2OO consumption. Based on that, a CH_2OO detection limit of better than 10^5 molecules cm^{-3} can be stated for a 10-minute integration time considering a measureable change of the normalized CH_2OO adduct signal of about 10^{-5}. Furthermore, the rate coefficient of the ion-molecule reaction, $(THF)H^+ + CH_2OO$, k = (7.6 - 12.4) × 10^{-10} cm^3 molecule^{-1} s^{-1} has been calculated.

Kinetic measurements of the reactions of CH_2OO with SO_2 and acetic acid have been conducted under conditions of an ethylene conversion < 10^8 molecules cm^{-3}, i.e. in absence of unwanted bimolecular CH_2OO steps, see Fig. 2. Hence, the CH_2OO consumption was governed by the unimolecular CH_2OO decomposition and the reaction with the additive. The reaction of CH_2OO with the additives was followed by monitoring the CH_2OO adduct signal, $(CH_2OO)(THF)H^+$. The obtained rate coefficient k($CH_2OO + SO_2$) = (3.3 ± 0.9) × 10^{-11} cm^3 molecule^{-1} s^{-1} is in good agreement with the result of the direct CH_2OO detection method using diiodomethane photolysis for CH_2OO generation as given by *Welz et al.* [2012]. For the reaction with acetic acid we measured k(CH_2OO + acetic acid) = (1.25 ± 0.30) × 10^{-10} cm^3 molecule^{-1} s^{-1} being again in very good agreement with the literature data of (1.2 ± 0.1) × 10^{-10} or (1.3 ± 0.1) × 10^{-10} cm^3 molecule^{-1} s^{-1} [*Welz et al.*, 2014].

C_6-Criegee intermediates from the ozonolysis of cyclohexene. Next, the detection of CIs arising from cyclic alkenes, such as from the terpenes α-pinene and limonene, was carried out selecting
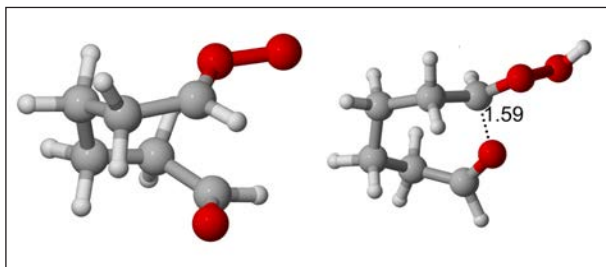
Fig. 3: Lowest-energy structures of the neutral (left) and protonated (right) anti-OHC(CH$_2$)$_4$CHOO Criegee intermediate. The distance between the aldehyde-group oxygen and the Criegee-group carbon is given in Ångström.

cyclohexene as the simplest surrogate. The idea was again to probe the CIs as protonated species (CI)H$^+$, XH$^+$ + CI $\rightarrow$ (CI)H$^+$ + X. Expected CIs from cyclohexene ozonolysis are the syn- and anti-conformers OHC(CH$_2$)$_4$CHOO with a calculated PA of 970.5 and 987.1 kJ/mol, respectively. A series of amines with PAs in the range of 921 - 952 kJ/mol appeared to be well-suited precursors for the reagent ions XH$^+$.

The exceptionally high proton affinity of OHC(CH$_2$)$_4$CHOO is related to strong electrostatic interactions between the aldehyde-group oxygen and the Criegee-group carbon in the OHC(CH$_2$)$_4$CHOOH$^+$ cation, as illustrated in Fig. 3. This 7-membered ring stabilizes the cationic form by several tens of kJ/mol.

A linearly rising signal with increasing cyclohexene conversion was observed at nominal 131 Th for protonated CIs, (CI)H$^+$, using the corresponding aminium cations XH$^+$ generated from of the chosen amines. Almost identical signal strengths emerged for n- and tert.-butylammonium while for diethylammonium the signals were substantially weaker. It can be speculated that in the latter case merely a fraction of the CIs, maybe the anti-conformer only, was efficiently protonated due to the relatively high PA of diethylamine. For n- and tert.-butylammonium, however, the good agreement of the signal intensities points to an overall probing of both conformers by each amine. Isobaric C$_6$H$_{10}$O$_3$ products like the aldehyde group containing acid (OHC(CH$_2$)$_4$COOH), the dioxirane, possible secondary ozonides or vinyl hydroperoxides cannot influence the (CI)H$^+$ signal due to their relatively low PAs, which do not enable protonation under the chosen conditions.

Kinetic experiments have been conducted for syn- and anti-OHC(CH$_2$)$_4$CHOO in total measuring the disappearance of the (CI)H$^+$ signal in presence of SO$_2$, acetone and acetic acid. The deduced C$_6$-CI reactivity is clearly different compared with that of CH$_2$OO. At the moment it is hard to give a justifiable explanation for this discrepancy. It is supposed that the aldehyde group significantly influences the CI reactivity of the cyclohexene derived CIs.

References

Berndt, T., et al., Direct probing of Criegee intermediates from gas-phase ozonolysis using chemical ionization mass spectrometry. *J. Am. Chem. Soc.* **139**, 13387-13392 (2017).

Berndt, T., et al., Gas-Phase Ozonolysis of Cycloalkenes: Formation of Highly Oxidized RO$_2$ Radicals and Their Reactions with NO, NO$_2$, SO$_2$, and Other RO$_2$ Radicals. *J. Phys. Chem. A* **119**, 10336-10348 (2015).

Calvert, J. G., et al., The Mechanisms of Atmospheric Oxidation of the Alkenes, Oxford University Press, Oxford, 2000.

Cox, R. A. and Penkett, S. A., Oxidation of Atmospheric SO$_2$ by Products of the Ozone–Olefin Reaction. *Nature* **230**, 321-322 (1971).

Welz, O., et al., Direct Kinetic Measurements of Criegee Intermediate (CH$_2$OO) Formed by Reaction of CH$_2$I with O$_2$. *Science* **335**, 204-207 (2012).

Welz, O., et al., Rate Coefficients of C$_1$ and C$_2$ Criegee Intermediate Reactions with Formic and Acetic Acid Near the Collision Limit: Direct Kinetics Measurements and Atmospheric Implications. *Angew. Chem. Int. Ed.* **126**, 4635-4638 (2014).

Cooperation
University of Helsinki, Helsinki, Finland

Radical-Driven Oxidation of Isoprene-Derived Oxidation Products in the Aqueous Phase

Tobias Otto, Bastian Stieger, Thomas Schaefer, Peter Mettke, Hartmut Herrmann

Die Dihydroxycarbonyle, 3,4-Dihydroxy-2-butanon (DHBO) und 2,3-Dihydroxy-2-methylpropanal (DHMP), sind Produkte der Isoprenoxidation dritter Generation unter unbelasteten Bedingung. Aufgrund ihrer Wasserlöslichkeit sind sie potentielle Vorläuferverbindungen für die Bildung von in der Flüssigphase gebildetem sekundären organischen Aerosol (aqSOA). In der vorliegenden Arbeit wurde die Reaktionskinetik mit Hydroxyl- (OH), Nitrat- (NO$_3$) und Sulfatradikalen (SO$_4^-$), sowie die Produktverteilung der radikalischen Oxidation mit OH-Radikalen in wässriger Phase untersucht. Die erhaltenen Reaktionsgeschwindigkeitskonstanten belegen einen raschen Abbau beider Verbindungen in der wässrigen Phase. In den Produktstudien konnten erstmals zur Oxidation mit OH-Radikalen dieser Verbindungen potentielle aqSOA-Vorläuferverbindungen nachgewiesen werden.

Introduction

The dihydroxycarbonyls 3,4-dihydroxy-2-bu-tanone (DHBO) and 2,3-dihydroxy-2-methylpropanal (DHMP) are formed from isoprene oxidation products in the atmospheric gas phase under rural conditions (cf. Fig. 1) [*Bates et al.*, 2016]. Both compounds are supposed to be well water soluble by their Henry's Law constants $H^{cp}_{(DHBO)} \approx 2666$ mol L^{-1} atm^{-1} and $H^{cp}_{(DHMP)} \approx 1466$ mol L^{-1} atm^{-1}. Hence, further aqueous-phase oxidations can potentially lead to the formation of aqueous secondary organic aerosol (aqSOA) precursor.

Consequently, the present study aims at the investigation of the aqueous-phase oxidation kinetics driven by hydroxyl (OH), nitrate (NO$_3$) and sulfate (SO$_4^-$) radicals, and product distributions to assess the impact of these processes on the aqSOA precursor budget.

Experiments

Second order rate constants of the radical-driven oxidation reactions were obtained using a laser flash photolysis–laser long path absorption (LFP-LLPA) setup, similar to setups used in former studies [*Herr-*

mann, 2003; *Hoffmann et al.*, 2009; *Schaefer et al.*, 2012].

The product studies were performed in a 300 mL temperature controlled aqueous-phase photoreactor. The reactor is equipped with a quartz glass window to irradiate the sample solution with a Xe arc light source. As hydroxyl radical source, hydrogen peroxide was photolyzed in the OH-driven oxidation experi-
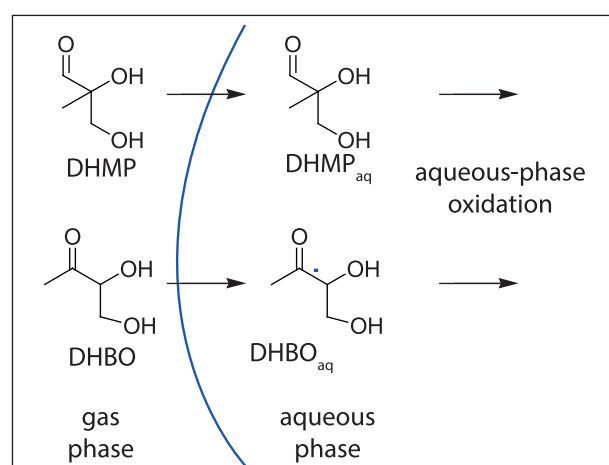
Fig. 1: Schematic depiction of the partitioning and aqueous-phase processing of DHBO and DHMP.

Tab. 1: *Determined temperature-dependent second order rate constants for DHBO and DHMP with OH, SO_4^- and NO_3.*

Entry	DHBO	DHMP
OH / $M^{-1} s^{-1}$	$k_{2nd} (T) = (5.2 \pm 0.3) \times 10^9 \times e^{\left(\frac{-4.2 \pm 2.7}{1000 \times RT}\right)}$	$k_{2nd} (T) = (4.4 \pm 0.2) \times 10^9 \times e^{\left(\frac{-3.2 \pm 2.2}{1000 \times RT}\right)}$
NO_3 / $M^{-1} s^{-1}$	$k_{2nd} (T) = (1.1 \pm 0.1) \times 10^{11} \times e^{\left(\frac{-26.4 \pm 6.3}{1000 \times RT}\right)}$	$k_{2nd} (T) = (3.0 \pm 0.3) \times 10^{12} \times e^{\left(\frac{-32.0 \pm 7.9}{1000 \times RT}\right)}$
SO_4^- / $M^{-1} s^{-1}$	$k_{2nd} (T) = (3.1 \pm 0.1) \times 10^9 \times e^{\left(\frac{-12.1 \pm 1.4}{1000 \times RT}\right)}$	$k_{2nd} (T) = (2.4 \pm 0.2) \times 10^9 \times e^{\left(\frac{-10.5 \pm 3.8}{1000 \times RT}\right)}$

ments. To avoid chemistry triggered by deep ultra violet light and mimic the actinic spectrum, glass filters (5 mm WG 295 and 5 mm WG305) were applied to absorb light below 290 nm efficiently. The experiments were performed using concentrations of 5×10^{-3} mol L^{-1} hydrogen peroxide and 1×10^{-4} mol L^{-1} of the organic compound. The initial pH was 6.0 ± 0.1 and not buffered yielding lower pH during the experiment time. Samples were taken at intervals of 15 min for 3 h and 30 min for additional 3 h. Afterwards the samples were treated using a detailed protocol as explained in *Otto et al.* [2017].

Results and Discussion

Kinetics. The radical-driven oxidation kinetics of OH, NO_3 and SO_4^- radicals with DHBO and DHMP were investigated in the aqueous phase for the first time. Table 1 shows the temperature dependent rate constant expressions. The expressions show for the

OH radical reaction rate constants a negligibly small temperature-dependence and consequently low activation energies E_A, 4.2 ± 2.7 kJ mol^{-1} and 3.2 ± 2.2 kJ mol^{-1}. Comparing these activation energies and the Arrhenius pre-exponential factor as well, the obtained results are in good agreement with previous reported values of structurally similar α-hydroxycarbonyl compounds, such as hydroxyacetone, 2-hydroxy-3-butanone (cf. [*Gligorovski*, 2005; *Hesper*, 2003]). The activation energies for the reactions of SO_4^- and NO_3 radicals are a factor 3 to one order of magnitude higher compared to OH, with a general trend of the activation energies from OH < SO_4^- < NO_3.

Product studies. Besides the kinetics, also the products formed by these radical reactions are important to clarify possible ongoing subsequent oxidation processes.

Figure 2 shows the molar fraction of the single products for the OH-driven oxidation of DHBO as function of experiment time. The error bars repre-
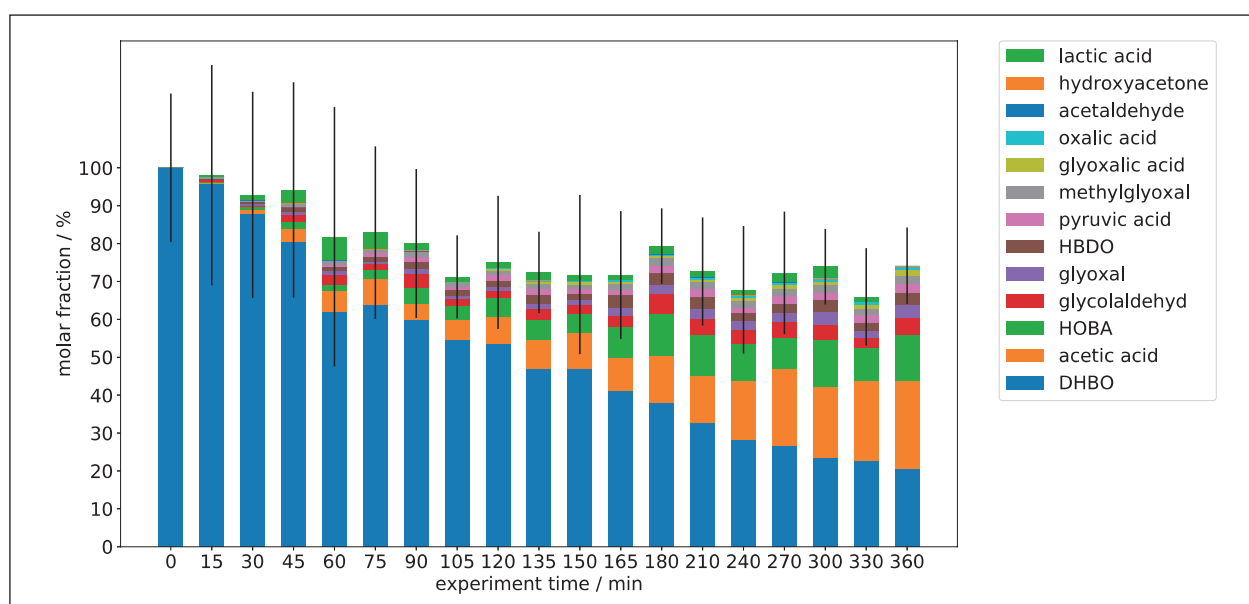
Fig. 2: *Time-dependent percentage turnovers of the OH-driven oxidation of DHBO.*
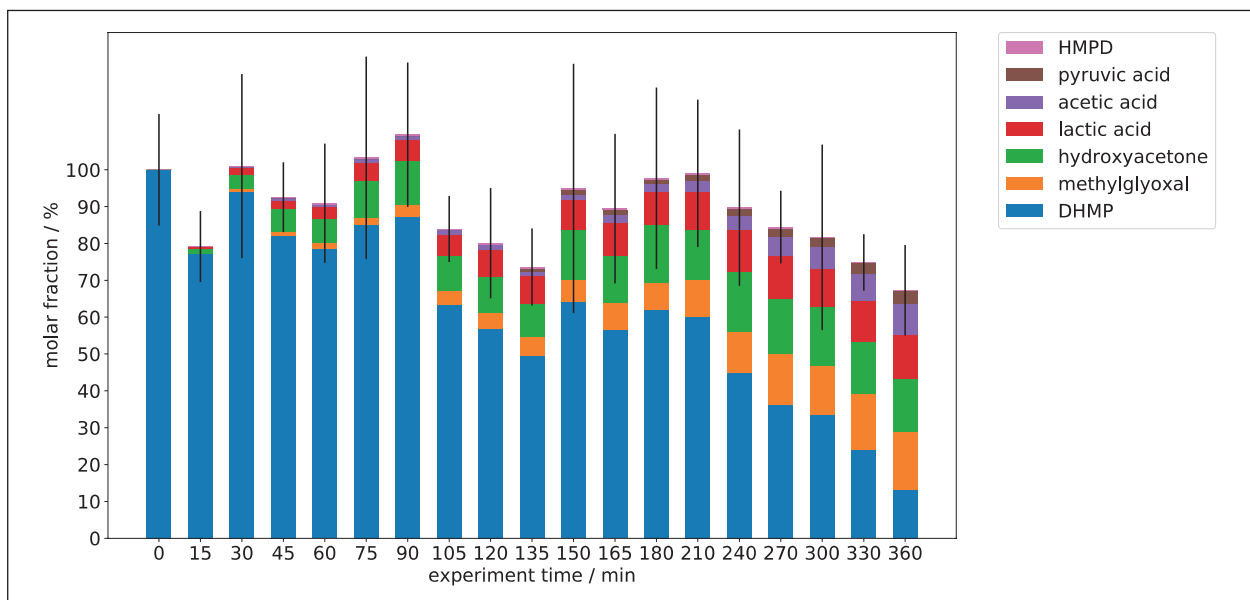
Fig. 3: Time-dependent percentage turnovers of the OH-driven oxidation of DHMP.

sent the sum of the single errors (2σ, n = 2) of each fraction. For these experiments, the modeled steady state hydroxyl radical concentration is about 1 × 10^{-13} mol L^{-1} which is in the range of atmospheric OH concentration to ensure that only atmospheric relevant oxidation pathways are triggered. Both observed products, 2-hydroxy-3-oxobutanal (HOBA) and 1-hydroxy-2,3-butadione (HBDO) proof the theoretical expectation of them as first generation oxidation products. Moreover, they show approximately a constant ratio of 4 to 1 as also expected by calculations using the structure activity relationship method by Monod and Doussin [*Doussin and Monod*, 2013; *Monod and Doussin*, 2008]. Over the whole experimental time hydroxyacetone is observed with a maximum yield of 1%. However, based on thermochemistry calculation it is a possible second-generation oxidation product. An explanation of this small yield is the relatively high reactivity of hydroxyacetone towards OH radicals. In agreement with that, methylglyoxal and lactic acid are observed with yields up to 2 and 6%, respectively, that can partly be seen as subsequent oxidation products of hydroxyacetone. The further oxidation of methylglyoxal and lactic acid will yield in a major fraction of pyruvic acid (maximum yield of 2.5%). Pyruvic acid is thought to be an accumulating species in this oxidation scheme, but it is not. Due to the experimentally caused high hydrogen peroxide concentrations pyruvic acid is oxidized by H_2O_2 to acetic acid, which shows an outstanding yield of approximately 23% that partly stand for converted pyruvic acid. Overall, a total carbon balance of 75% was achieved for the oxidation of DHBO. The minor fractions of glycolaldehyde, glyoxal, glyoxalic acid, oxalic acid are caused by the

direct photochemistry of DHBO, proven in additional experiments. Nevertheless, this pathway is largely suppressed by the chosen experimental conditions (occurrence less than 5%, due to the predominant absorption of H_2O_2).

Figure 3 shows the molar fraction of the single products of the second investigated OH-driven oxidation of DHMP as function of experiment time. The error bars represent the sum of the single errors (2σ, n = 2) of each fraction. The observed 2-hydroxy-2-methylpropandial (HMPD) is expected to be a first generation oxidation product of DHMP, with a yield of only 0.4%. Besides this, also 2,3-dihydroxy-2-methylpropanoic acid is qualitatively detected and is supposed to be a first generation oxidation product of DHMP as well. Both pathways lead to the proved formation of hydroxyacetone (maximum yield of approximately 15%, cf. Fig. 3). Hydroxyacetone reacts in a ketol-endiol tautomerism to lactaldehyde as well. These intermediates are further oxidized to the observed products lactic acid, with a yield of approximately 13%, and methyglyoxal (approximated yield of 15%). As described above for the oxidation of DHBO, pyruvic acid is formed via the oxidation of lactic acid and hydroxyacetone. Consequently, pyruvic acid is oxidized to acetic acid by virtue of high concentrations of hydrogen peroxide during the performed experiments. In total, a carbon balance of 67% is obtained for the oxidation of DHMP. The experiments on the OH-driven oxidation of DHMP are not influenced by the direct photochemistry of the precursor.

In conclusion, the aqueous-phase oxidation of DHBO and DHMP were investigated for the first

time in this study and show by their second order rate constants an efficient processing in the aqueous phase. The product studies revealed polyfunctionalized carbonyl compounds and carboxylic acids as products, as well as smaller dicarbonyls, carbonyls and carboxylic acids — altogether common analytes in atmospheric particles and cloud water or rain — which influence the aqSOA precursor budget and may contribute to the aqSOA formation.

References

Bates, K. H., T. B. Nguyen, A. P. Teng, J. D. Crounse, H. G. Kjaergaard, B. M. Stoltz, J. H. Seinfeld, and P. O. Wennberg (2016), Production and Fate of C-4 Dihydroxycarbonyl Compounds from Isoprene Oxidation, *J. Phys. Chem. A*, 120(1), 106-117, doi: 10.1021/acs.jpca.5b10335.

Doussin, J. F., and A. Monod (2013), Structure–Activity Relationship for the Estimation of OH-Oxidation Rate Constants of Carbonyl Compounds in the Aqueous Phase, *Atmos. Chem. Phys.*, 13(23), 11625-11641, doi: 10.5194/acp-13-11625-2013.

Gligorovski, S. (2005), Laser Based Studies of OH Radical Reactions in Aqueous Solution, Universität Leipzig Leipzig.

Herrmann, H. (2003), Kinetics of Aqueous Phase Reactions Relevant for Atmospheric Chemistry, *Chem. Rev.*, 103(12), 4691-4716, doi: 10.1021/cr020658q.

Hesper, J. (2003), Spektroskopische und Kinetische Untersuchungen von Reaktionen der Radikale O2- und OH in Wässriger Phase, Universität Leipzig Leipzig.

Hoffmann, D., B. Weigert, P. Barzaghi, and H. Herrmann (2009), Reactivity of Poly-Alcohols towards OH, NO3 and SO4– in Aqueous Solution, *Phys. Chem. Chem. Phys.*, 11(41), 9351-9363.

Monod, A., and J. F. Doussin (2008), Structure-Activity Relationship for the Estimation of OH-Oxidation Rate Constants of Aliphatic Organic Compounds in the Aqueous Phase: Alkanes, Alcohols, Organic Acids and Bases, *Atmos. Environ.*, 42(33), 7611-7622, doi: https://doi.org/10.1016/j.atmosenv.2008.06.005.

Otto, T., B. Stieger, P. Mettke, and H. Herrmann (2017), Tropospheric Aqueous-Phase Oxidation of Isoprene-Derived Dihydroxycarbonyl Compounds, *J. Phys. Chem. A*, 121(34), 6460-6470, doi: 10.1021/acs.jpca.7b05879.

Schaefer, T., J. Schindelka, D. Hoffmann, and H. Herrmann (2012), Laboratory Kinetic and Mechanistic Studies on the OH-Initiated Oxidation of Acetone in Aqueous Solution, *J. Phys. Chem. A*, 116(24), 6317-6326, doi: 10.1021/jp2120753.

Modelling of tropospheric non-radical aqueous-phase oxidations of organic compounds

Andreas Tilgner, Erik Hans Hoffmann, Ralf Wolke, Hartmut Herrmann

Oxidationen von organischen Verbindungen in der troposphärischen Flüssigphase sind von großer Bedeutung, da sie zur Bildung und Prozessierung von sekundärer organischer Aerosolmasse beitragen können. Neben wichtigen Oxidationen durch radikalische Oxidantien werden auch Oxidationsreaktionen von nicht-radikalischen Oxidantien wie O_3 und H_2O_2 als wichtig erachtet. Jedoch sind diese für organische Verbindungen in derzeitigen Modellen kaum berücksichtigt. Daher war das Ziel dieser Studie, die Entwicklung eines komplexen Multiphasenchemiemoduls zur Beschreibung von nicht-radikalischen Reaktionsprozessen sowie dessen Anwendung im Chemieprozessmodell SPACCIM. Mit dem entwickelten Reaktionsmodul (103 Multiphasenprozesse) wurden Modellsimulationen für kontinentale Umweltbedingungen durchgeführt. Die Studien haben gezeigt, dass nicht-radikalische Oxidantien bedeutsam für die Prozessierung oxidierter organischer Verbindungen d.h. für deren Systemkonzentration und ihren Beitrag zur organischen aqSOA Bildung sein können. Die Simulationen zeigten, dass Ozonolysen in der Flüssigphase für oxidierte ungesättigte organische Verbindungen und Reaktionen von H_2O_2 insbesondere für substituierte organische Säuren substantiell zur Oxidation beitragen können.

Introduction

Tropospheric cloud droplets and deliquesced aerosol particles comprise a complex aqueous oxidative environment with simultaneously occurring chemical transformations of both radical and non-radical oxidants. Since several years, it is known that soluble organic compounds may undergo also various chemical aqueous-phase oxidative and non-oxidative processes [*Ervens et al.*, 2011; *Herrmann et al.*, 2015] leading to aqSOA (aqueous Secondary Organic Aerosol). In the recent past, kinetic investigations of non-radical aqueous phase oxidation reactions by H_2O_2 and O_3 gained increasing attention in atmospheric chemistry. Several kinetic and product laboratory studies have been performed during the last years (see [*Herrmann et al.*, 2015] and references therein). Kinetic comparison studies, e.g., by *Tilgner and Herrmann* [2010] and, *Schöne and Herrmann* [2014] have clearly concluded that aqueous-phase non-radical oxidation reactions by H_2O_2 and O_3 should be important pathways for the tropospheric fate of organic compounds besides the well-known radical oxidation processes [*Tilgner and Herrmann*, 2010] and therefore needs to be considered in multiphase models. Unfortunately, the majority of the available kinetic and mechanistic non-radical oxidation data are not yet considered in current atmospheric chemistry mechanisms and models. In order to improve the still limited understanding of non-radical aqueous-phase oxidations, detailed model studies

have been performed in the present study applying a newly developed reaction module.

Mechanism development and multiphase modelling

In order to improve the still limited understanding of non-radical aqueous-phase chemical processes, detailed model studies at TROPOS have been recently performed applying a newly developed reaction module within the SPectral Aerosol Cloud Chemistry Interaction Model (SPACCIM, [*Wolke et al.*, 2005]). The new reaction module has been developed mainly based on recent literature data (e.g., [*Schöne and Herrmann*, 2014; *Schöne et al.*, 2014]) and has been coupled to the MCMv3.2/CAPRAM4.0 mechanism with 21328 multiphase processes. The new module contains 103 additional reactions of organic carbonyl compounds and acids such as methacrolein (MACR), methyl vinyl ketone (MVK), acrylic acid (AA), meth-

acrylic acid (MAA), pyruvic acid (PYRAC), glyoxylic acid (GLYAC), for example. Besides 22 updated OH and NO_3 reactions, further SO_4^- radical reactions and firstly non-radical oxidations by H_2O_2 and O_3 were considered with 53 new reactions. SPACCIM model simulations have been carried out for remote environmental conditions using a non-permanent meteorological scenario (see *Tilgner et al.* [2013] for details). The model analyses are focused on multiphase reactions of organic compounds and particularly the role of non-radical oxidation pathways compared to radical oxidation under both cloud and deliquesced particle conditions. To examine the influence of various chemical subsystems on multiphase aqSOA processing different sensitivity runs were performed. Investigations of important organic compounds are done by detailed time-resolved reaction flux analyses. Such detailed flux analyses were used to determine the most important oxidants and help to understand the time evolution of their concentrations.
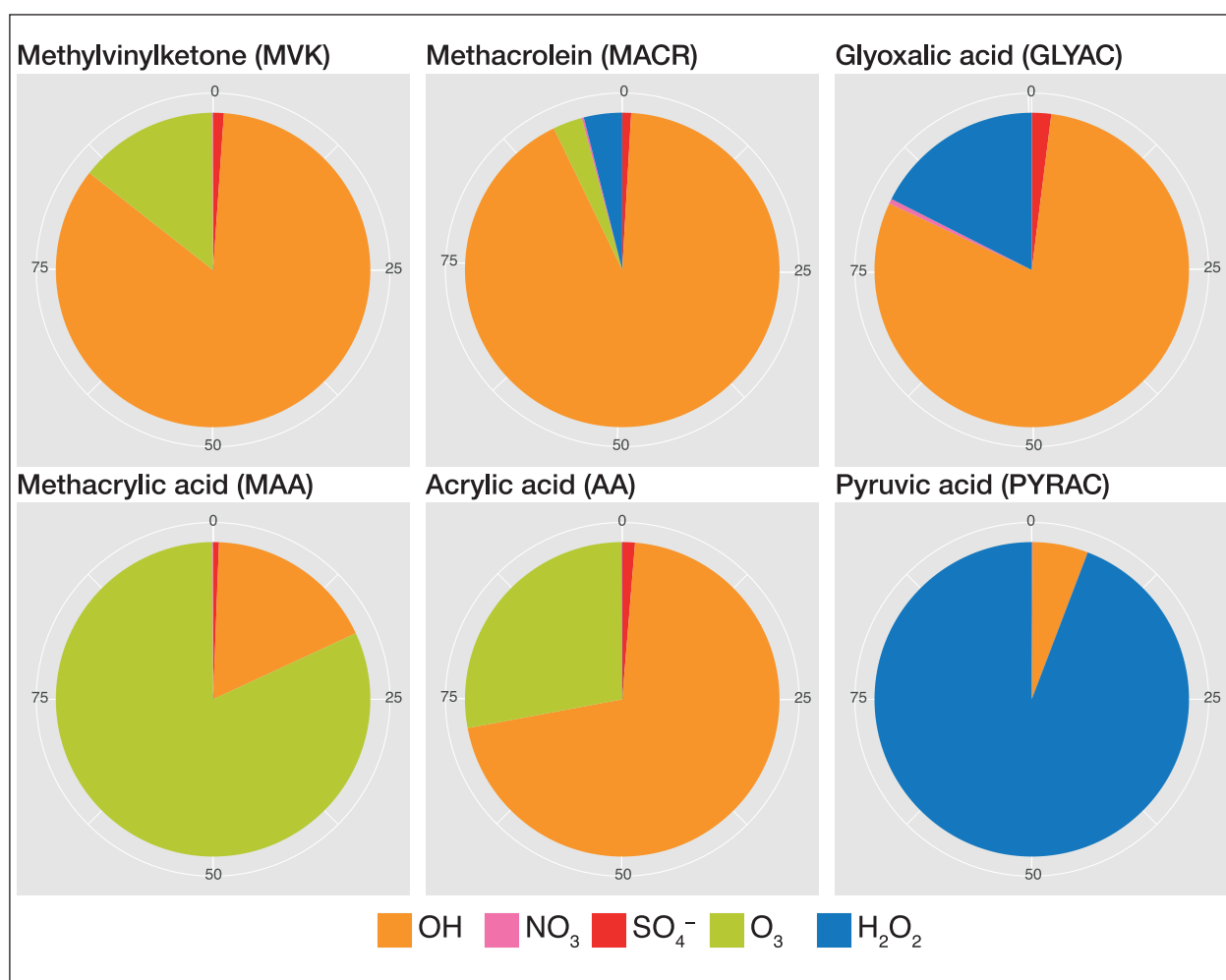
Fig.1: Depiction of the relative contributions [%] of different radical and non-radical oxidants to the aqueous-phase oxidation of selected OVOCs under remote environmental conditions modelled with MCM3.2/CAPRAM4.0 and an additional reaction module considering non-radical oxidation reactions (contributions calculated using the modelled oxidation fluxes of the whole model run of about 108h).
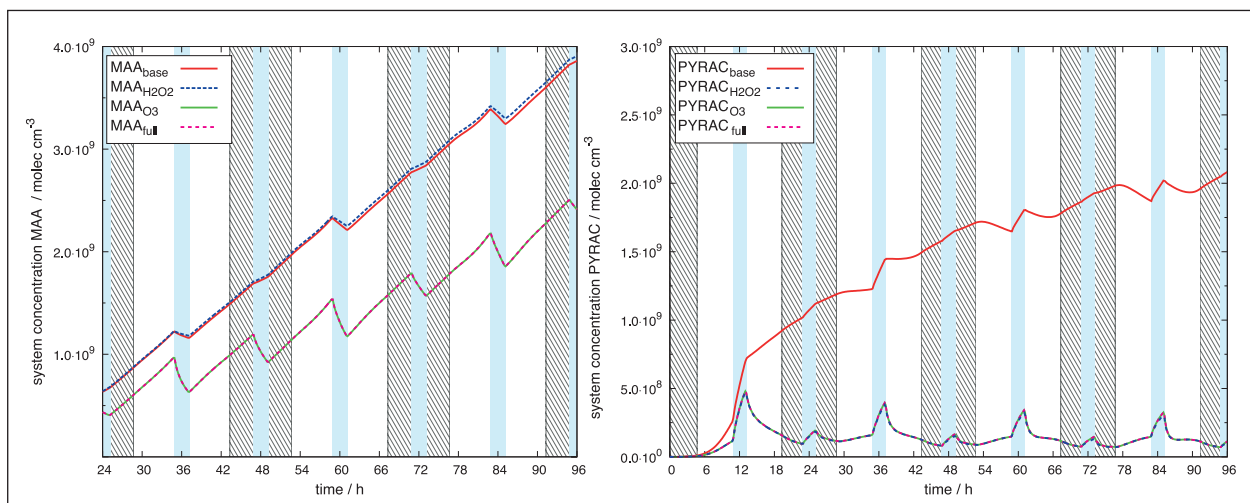
Fig.2: Modelled system concentration (sum of gas + aqueous phase concentration) of methacrylic acid (MAA, left) and pyruvic acid (PYRAC, right) during the 2nd - 4th simulation day and the different remote mechanism runs.

Model results

The performed model studies have shown that non-radical oxidations by O_3 and H_2O_2 can play an important role in the aqueous oxidation of organic compounds besides key radical oxidants such as OH. The simulations demonstrated that O_3 can be important for quite soluble unsaturated organic compounds such as MAA and AA particularly under remote cloud conditions. For MAA, the studies have shown that O_3 can be even more important than OH, with a contribution of about 82 % to the overall aqueous-phase oxidation flux under remote environmental conditions (see Fig. 1). The added non-radical oxidation processes by ozone leads to reduced system concentrations of soluble unsaturated organic compounds such as MAA (see Fig. 2) and AA. Moreover, the considered ozonolysis reactions contributes only slightly to the overall aqSOA formation.

Furthermore, the present model runs have shown that H_2O_2 can be an important oxidant particularly for substituted organic acids under both cloud and deliquesced particle conditions. For example, 94 % of the pyruvic acid (PYRAC) degradation fluxes under remote conditions (see Fig. 1) are caused by aqueous H_2O_2 leading to substantially lowered production fluxes of its typical OH oxidation products, keto-malonic acid and oxalic acid. The consideration of the aqueous-phase H_2O_2 reactions with PYRAC leads to substantially reduced system concentrations (see Fig. 2) and consequently to the formation of

acetic acid. Therefore, added non-radical oxidation processes by H_2O_2 can decrease the overall aqSOA formation flux as in the case of PYRAC. However, it should be mentioned that in case of other unsaturated organic compounds, H_2O_2 reactions might also be able to contribute to increased SOA formation fluxes and formation of more oxygenated organic compounds due to the conversion of double bonds into diol functionalities. Thus, from this study a comprehensive conclusion regarding the importance of H_2O_2 reactions for aqSOA formation and the overall aqueous-phase processing of organic aerosol constituents cannot yet be drawn because of the limited degree of coverage of the H_2O_2 chemistry with organic constituents in currently available mechanisms and models. Further kinetic and mechanistic laboratory investigations and consequent model applications are definitely needed to more comprehensively investigate the role of non-radical oxidations of organic compounds by H_2O_2 and O_3 in detail.

Summary

Overall, the simulations imply that non-radical oxidation pathways by both H_2O_2 and O_3 needs also to be considered in multiphase chemistry models for certain organic compound classes besides important radical oxidations for an advanced modelling of the tropospheric aqSOA processing in deliquesced particles and cloud droplets.

References

Ervens, B., B. J. Turpin, and R. J. Weber (2011), Secondary organic aerosol formation in cloud droplets and aqueous particles (aqSOA): a review of laboratory, field and model studies, *Atmos. Chem. Phys.*, *11*(21), 11069-11102, doi: 10.5194/acp-11-11069-2011.

Herrmann, H., T. Schaefer, A. Tilgner, S. A. Styler, C. Weller, M. Teich, and T. Otto (2015), Tropospheric aqueous-phase chemistry: Kinetics, mechanisms, and its coupling to a changing gas phase, *Chem. Rev.*, *115*(10), 4259-4334.

Schöne, L., and H. Herrmann (2014), Kinetic measurements on the reactivity of hydrogen peroxide and ozone towards small atmospherically relevant aldehydes, ketones and organic acids in aqueous solution, *Atmos. Chem. Phys.*, *14*, 4503-4514, doi: doi:10.5194/acp-14-4503-2014, 2014.

Schöne, L., J. Schindelka, E. Szeremeta, T. Schaefer, D. Hoffmann, K. J. Rudzinski, R. Szmigielski, and H. Herrmann (2014), Atmospheric aqueous phase radical chemistry of the isoprene oxidation products methacrolein, methyl vinyl ketone, methacrylic acid and acrylic acid - kinetics and product studies, *Phys. Chem. Chem. Phys.*, *16*(13), 6257-6272, doi: 10.1039/C3CP54859G.

Tilgner, A., and H. Herrmann (2010), Radical-driven carbonyl-to-acid conversion and acid degradation in tropospheric aqueous systems studied by CAPRAM, *Atmos. Environ.*, *44*(40), 5415-5422, doi: 10.1016/j.atmosenv.2010.07.050.

Tilgner, A., P. Bräuer, R. Wolke, and H. Herrmann (2013), Modelling multiphase chemistry in deliquescent aerosols and clouds using CAPRAM3. 0i, *J. Atmos. Chem.*, *70*(3), 221-256.

Wolke, R., A. M. Sehili, M. Simmel, O. Knoth, A. Tilgner, and H. Herrmann (2005), SPACCIM: A parcel model with detailed microphysics and complex multiphase chemistry, *Atmos. Environ.*, *39*(23-24), 4375-4388.

Daytime AtmospheRic chemistry of Key compounds provoKed by NIGHTtime atmospheric chemistry (DARK KNIGHT)

Anke Mutzel, Olaf Böge, Hartmut Herrmann

Flüchtige organische Verbindungen (VOC) werden in großen Mengen (1300 TgC Jahr^{-1}) von biogenen und anthropogenen Quellen in die Atmosphäre emittiert. Die Oxidation solcher Verbindungen führt zur Bildung von semivolatilen Produkten, welche in die Partikelphase übergehen können und somit zur Bildung von sekundärem organischem Aerosol (SOA) beitragen. Die globale SOA Produktion anthropogenen Ursprungs beläuft sich auf 0,05 – 9,7 Tg pro Jahr. Hingegen wird die biogene SOA Produktion mit bis zu 910 Tg pro Jahr beziffert, was einem Umsatz von 70% der emittierten biogenen VOCs entspricht. Ein solcher Umsatz ist unvereinbar mit den vergleichsweise niedrigen SOA Ausbeuten aus Aerosolkammerexperimenten. Die Ursache für diese Diskrepanz liegt vermutlich an zusätzlichen SOA Bildungswegen wie der Weiterreaktion von VOC Oxidationsprodukten, welche von den Umgebungsbedingungen wie dem Oxidationsmittel, der relativen Feuchte und der Art der vorhandenen Partikel abhängt. Somit sind zwar Tag- und Nachtchemie grundverschieden, allerdings auch eng miteinander verbunden, denn die Produkte der Nachtchemie werden durch die darauffolgende Tagchemie weiterprozessiert und umgekehrt. Dadurch wird das Partitionierungsverhalten der Produkte und somit die SOA Bildung stark beeinflusst. Daher wird im Rahmen des Projektes Dark Knight der Einfluss der Tagchemie auf die Nachtchemie und umgekehrt untersucht.

Introduction

The fate of VOCs and the subsequent chemistry of their oxidation products are strongly influenced by the environmental conditions such as the available oxidants, the presence of trace gases such NO_x and SO_2, temperature, relative humidity and the properties of pre-existing particles. Consequently, the partitioning behavior of formed products and thus the SOA formation processes as well are strongly dependent of the mentioned parameters.

The chemistry that takes place during the daytime influences the subsequent nighttime chemistry and vice versa. Compounds that are emitted during the daytime are continuously oxidized by OH radicals or ozone to form semi-volatile organic compounds. In the evening when the OH radical production drops down, the VOCs and their oxidation products that remain in the atmosphere are subjected to the nighttime chemistry in which the NO_3 radicals and ozone are most important. Equally, the daytime chemistry processes VOCs and their oxidation products that are emitted or formed during the nighttime. Therefore, daytime and nighttime chemistry cannot be considered separately but strongly influence each other. So far, laboratory SOA formation studies have focused on either daytime chemistry or nighttime chemistry, and the knowledge about the interaction between daytime and nighttime chemistry and their influences on the fate of VOCs, semi-volatile oxidation products and SOA formation are generally missing.
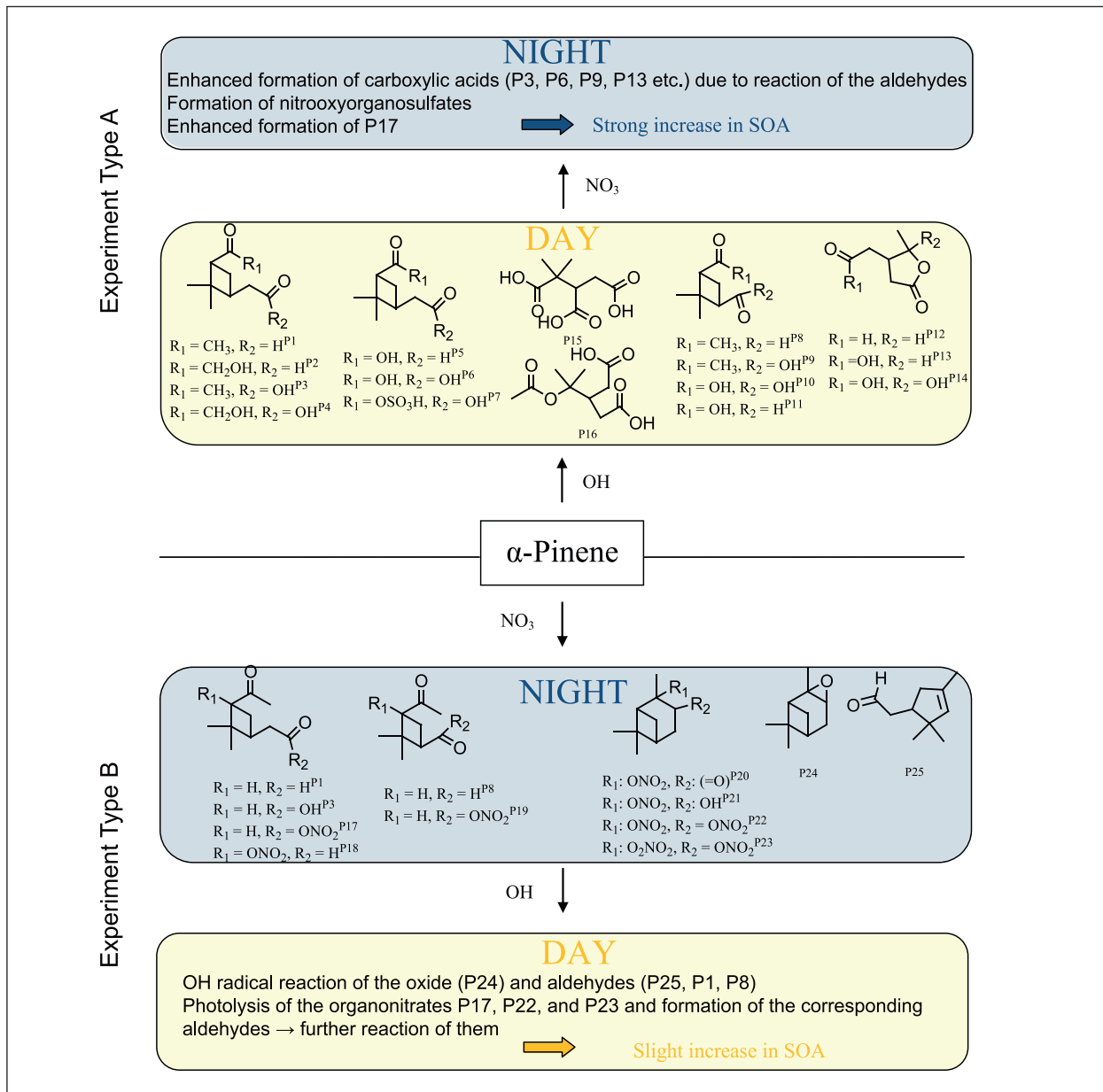
Fig. 1: Reaction scheme of the oxidation of α-pinene during daytime with subsequent nighttime chemistry (Experiments type A, upper part) and during nighttime with subsequent daytime chemistry (Experiments type B, lower part).

Method

The aerosol chamber LEAK is used to examine the interconnection of day- and nighttime chemistry. In the first set of experiments the oxidation of key biogenic and anthropogenic hydrocarbons (α-pinene, limonene and *m*-cresol) by OH or NO_3 radicals and the subsequent chemical analysis for the identification of gaseous and particulate products originated by the selected oxidant was conducted. The second set is focused on performing both day- and nighttime chemistry in a single smog chamber experiment. Experiment type A starts with daytime chemistry (OH radical) followed by nighttime chemistry (NO_3 radical)

and the experiments type B start with nighttime chemistry (NO_3 radical) with a subsequent daytime chemistry (OH radical).

Results and Discussion

From the first set of experiments it was found that all precursor compounds produce SOA with OH radicals as well as with NO_3 radicals, except the oxidation of cresol with NO_3 radicals. The chemical composition of organic mass produced by OH radicals differs from that obtained from NO_3 radical oxidation, e.g. the oxidation of α-pinene with NO_3 leads mainly to the formation of pinonic acid whereby the oxidation

with OH radicals yields terpenylic acid and pinic acid. These two are often related to early particle growth and might cause the higher SOA mass obtained from OH radical induced oxidation [*Mutzel et al.*, 2016].

The second set of experiments indicated that the experiment sequence (day/night or night/day) is decisive for the formation of secondary organic aerosol. For the experiments type A (day/night) the formation of particulate organic mass stopped by switching from OH to NO$_3$ radicals, whereas the increase of particle mass during experiments of type B (NO$_3$/OH) still continuous when changing NO$_3$ to OH. This result indicates that the formation of condensable products mainly proceeds via oxidation with OH radicals. Furthermore, first indications were obtained that also the chemical composition changes. Filter samples collected from cresol oxidation show a yellow color after experiments of type B. Contrary experiments of type A do not show any color change. This might indicate that solely the oxidation with NO$_3$ radicals with a subsequent processing with OH radicals leads to the formation of brown carbon. This is very interesting in terms of the optical properties of particles as brown carbon absorbs light within the UV range [*Shapiro et al.*, 2009]. Potential candidates for brown carbon are nitrophenols and imidazoles [*Teich et al.*, 2016]. In

the case of cresol the yellow color is mainly caused by the presence of nitrophenols, such as methyl-nitrocatechol with was successfully detected from LC/MS analysis. Methyl-nitrocatechol was identified from field measurements as important tracer for biomass burning [*Iinuma et al.*, 2010]. The presence of this compound in smog chamber generated SOA underlines the suitability of LEAK to form and investigate atmospheric relevant SOA material. Besides particulate products also a change of the gas-phase product distribution was observed. Aside highly oxidized multifunctional compounds [*Mutzel et al.*, 2015; HOMs] also organonitrates were detected by chemical ionization atmospheric pressure interface time of flight mass spectrometer. Many of the detected HOMs start the increase during the OH radical reaction and by changing to the NO$_3$ system the signals start to decrease which is mainly caused by further reaction of HOMs in the gas phase.

In conclusion, the on-going project Dark Knight connects day- and time chemistry within one chamber experiment. This is the first time that this kind of experiment is performed. From the results is can be shown that the oxidation sequence drastically changes the product distribution, the particle growth as well as the optical properties.

References

Iinuma, Y., O. Böge, R. Graefe, and H. Herrmann (2010), Methyl-Nitrocatechols: Atmospheric Tracer Compounds for Biomass Burning Secondary Organic Aerosols, *Environ. Sci. Technol.*, *44*(22), 8453-8459, doi: 10.1021/es102938a.

Mutzel, A., M. Rodigast, Y. Iinuma, O. Böge, and H. Herrmann (2016), Monoterpene SOA – Contribution of first-generation oxidation products to formation and chemical composition, *Atmos. Environ.*, *130*, 136-144, doi: doi:10.1016/j.atmosenv.2015.10.080.

Mutzel, A., L. Poulain, T. Berndt, Y. Iinuma, M. Rodigast, O. Böge, S. Richters, G. Spindler, M. Sipilä, T. Jokinen, M. Kulmala, and H. Herrmann (2015), Highly oxidized multifunctional organic compounds observed in tropospheric particles: A field and laboratory study, *Environ. Sci. Technol.*, *49*(13), 7754-7761, doi: doi:10.1021/acs.est.5b00885.

Shapiro, E. L., J. Szprengiel, N. Sareen, C. N. Jen, M. R. Giordano, and V. F. McNeill (2009), Light-absorbing secondary organic material formed by glyoxal in aqueous aerosol mimics, *Atmos. Chem. Phys.*, *9*(7), 2289-2300, doi: 10.5194/acp-9-2289-2009.

Teich, M., D. van Pinxteren, and H. Herrmann (2014), Determination of nitrophenolic compounds from atmospheric particles using hollow-fiber liquid-phase microextraction and capillary electrophoresis/mass spectrometry analysis, *Electrophoresis*, *35*(9), 1353-1361, doi: doi:10.1002/elps.201300448.

Teich, M., D. van Pinxteren, S. Kecorius, Z. Wang, and H. Herrmann (2016), First quantification of imidazoles in ambient aerosol particles: Potential photosensitizers, brown carbon constituents and hazardous components, *Environ. Sci. Technol.*, *50*, 1166-1173, doi: 10.1021/acs.est.5b05474.

Appendices

Publications

Publication statistics

	2016	2017
Total number of publications	**298**	**256**
Books (author, editor)	4	2
Book sections	2	6
Conference proceedings	3	2
Publications, peer-reviewed	121	79
Publications, other	4	12
Lectures, invited	11	14
Conference contributions / Lectures, other	153	141

Publications

2016

Achatz, U., Ribstein, B., **Senf, F.** and Klein, R. 2016. The interaction between synoptic-scale balanced flow and a finite-amplitude mesoscale wave field throughout all atmospheric layers : Weak and moderately strong stratification. Q. J. Roy. Meteor. Soc., **143**, 342-361.

Alastuey, A., Querol, X., Aas, W., Lucareli, F., Pérez, N., Moreno, T., Cavalli, F., Areskoug, H., Balan, V., Catrambone, M., Cebumis, D., Cerro, J. C., Conil, S., Gevorgyan, L., Hueglin, C., Imre, K., Jaffrezo, J.-L., Leeson, S. R., Mihalopoulos, N., Mitosinkova, M., O'Dowd, C. D., Pey, J., Putaud, J.-P., Riffault, V., Ripoll, A., Sciare, J., Sellegri, K., **Spindler, G.** and Yttri, K. E. 2016. Geochemistry of PM_{10} over Europe during the EMEP intensive measurement periods in summer 2012 and winter 2013. Atmos. Chem. Phys., **16**, 6107-6129. doi:10.5194/acp-16-6107-2016.

Augustin-Bauditz, S., **Wex, H.**, **Denjean, C.**, **Hartmann, S.**, Schneider, J., Schmidt, S., Ebert, M. and **Stratmann, F.** 2016. Laboratory-generated mixtures of mineral dust particles with biological substances: Characterization of the particle mixing state and immersion freezing behavior. Atmos. Chem. Phys., **16**, 5531-5543. doi:10.5194/acp-16-5531-2016.

Baars, H., **Kanitz, T.**, **Engelmann, R.**, **Althausen, D.**, **Heese, B.**, Komppula, M., Preißler, J., Tesche, M., **Ansmann, A.**, **Wandinger, U.**, Lim, J.-H., Ahn, J. Y., Stachlewska, I. S., Amiridis, V., Marinou, E., **Seifert, P.**, **Hofer, J.**, **Skupin, A.**, **Schneider, F.**, **Bohlmann, S.**, **Foth, A.**, **Bley, S.**, Pfüller, A., Giannakaki, E., Lihavainen, H., Viisanen, Y., Hooda, R. K., Pereira, S., Bortoli, D., Wagner, F., Mattis, I., Janicka, L., Markowicz, K. M., Achert, P., Artaxo, P., Pauliquevis, T., Souza, R. A. F., Sharma, V. P., van Zyl, P. G., Beukes, J. P., Sun, J. Y., Rohwer, E. G., Deng, R., Mamouri, R. E. and Zamorano, F. 2016. An overview of the first decade of Polly[NET]: An emerging network of automated Raman-polarization lidars for continuous aerosol profiling. Atmos. Chem. Phys., **16**, 5111-5137. doi:10.5194/acp-16-5111-2016.

Babkovskaia, N., Rannik, U., Phillips, V., **Siebert, H.**, **Wehner, B.** and Boy, M. 2016. A DNS study of aerosol and small-scale cloud turbulence interaction Atmos. Chem. Phys., **16**, 7889-7898. doi:10.5194/acp-16-7889-2016.

Barlakas, V., **Macke, A.** and Wendisch, M. 2016. SPARTA - Solver for Polarized Atmospheric Radiative Transfer Applications: Introduction and application to Saharan dust fields. J. Quant. Spectrosc. Radiat. Transfer, **178**, 77-92. doi:10.1016/j.jqsrt.2016.02.019.

Appendices: Publications

Basart, S., Dulac, F., Baldasano, J. M., Nabat, P., Mallet, M., Solmon, F., Laurent, B., Vincent, J., Menut, L., El Amraoui, L., Sic, B., Chaboureau, J.-P., Léon, J.-F., **Schepanski, K.**, Renard, J.-B., Ravetta, F., Pelon, J., Di Biagio, C., Formenti, P., Chiapello, I., Roujean, J.-L., Ceamanos, X., Carrer, D., Sicard, M., Delbarre, H., Roberts, G., Jungermann, W. and Attié, J.-L. 2016. Extensive comparison between a set of European dust regional models and observations in the Western Mediterranean for the summer 2012 Pre-ChArMEx/ TRANQA campaign. *In: D. G. Steyn and N. Chaumerliac (Eds.), Air pollution modeling and its application XXIV : Proceedings of the 34th International Technical Meeting on Air Pollution Modelling and Its Application (Montpellier, France, 4-8 May 2015)*. Springer International Publishing, Switzerland, p. 79-83 (Chapter 13). doi:10.1007/978-3-319-24478-5. (Springer Proceedings in Complexity).

Berndt, T., **Herrmann, H.**, Sipilä, M. and Kulmala, M. 2016. Highly oxidized second-generation products from the gas-phase reaction of OH radicals with isoprene. J. Phys. Chem. A, **120**, 10150-10159. doi:10.1021/ acs.jpca.6b10987.

Berndt, T., **Richters, S.**, Jokinen, T., Hyttinen, N., Kurtén, T., Otkjær, R. V., Kjaergaard, H. G., **Stratmann, F.**, **Herrmann, H.**, Sipilä, M., Kulmala, M. and Ehn, M. 2016. Hydroxyl radical-induced formation of highly oxidized organic compounds. Nat. Commun., **7:13677**, 8 pp. doi:10.1038/ncomms13677.

Birmili, W., **Weinhold, K.**, **Rasch, F.**, **Sonntag, A.**, **Sun, J.**, **Merkel, M.**, **Wiedensohler, A.**, Bastian, S., Schladitz, A., Löschau, G., Cyrys, J., Pitz, M., Gu, J., Kusch, T., Flentje, H., Quass, U., Kaminski, H., Kuhlbusch, T. A. J., Meinhardt, F., Schwerin, A., Bath, O., Ries, L., Gerwig, H., Wirtz, K. and Fiebig, M. 2016. Long-term observations of tropospheric particle number size distributions and equivalent black carbon mass concentrations in the German Ultrafine Aerosol Network (GUAN). Earth Syst. Sci. Data, **8**, 355-382. doi:10.5194/essd-8-355-2016.

Bley, S., **Deneke, H.** and **Senf, F.** 2016. Meteosat-based chracterization of the spatiotemporal evolution of warm convective cloud fields over Central Europe. J. Appl. Meteorol. Clim., **55**, 2181-2195.

Bravo-Aranda, J. A., Belegante, L., Freudenthaler, V., Alados-Arboledas, A., Nicolae, D., Granados-Muñoz, M. J., Guerrero-Rascado, J. L., Amodeo, A., D'Amico, G., **Engelmann, R.**, Pappalardo, G., Kokkalis, P., Mamouri, R., Papayannis, A., Navas-Guzmán, F., Olmo, F. J., **Wandinger, U.**, Amato, F. and Haeffelin, M. 2016. Assessment of lidar depolarization uncertainty by means of a polarimetric lidar simulator. Atmos. Meas. Tech., **9**, 4935-4953. doi:10.5194/amt-9-4935-2016.

Brock, C. A., Wagner, N. L., Anderson, B. E., Attwood, A. R., Beyersdorf, A., Campuzano-Jost, P., Carlton, A. G., Day, D. A., Diskin, G. S., Gordon, T. D., Jimenez, J. L., Lack, D. A., Liao, J., Markovic, M. Z., Middlebrook, A. M., Ng, N. L., Perring, A. E., Richardson, M. S., Schwarz, J. P., Washenfelder, R. A., **Welti, A.**, Xu, L., Ziemba, L. D. and Murphy, D. M. 2016. Aerosol optical properties in the southeastern United States in summer - Part 1: Hygroscopic growth. Atmos. Chem. Phys., **16**, 4987-5007. doi:10.5194/acp-16-4987-2016.

Brock, C. A., Wagner, N. L., Anderson, B. E., Beyersdorf, A., Campuzano-Jost, P., Day, D. A., Diskin, G. S., Gordon, T. D., Jimenez, J. L., Lack, D. A., Liao, J., Markovic, M. Z., Middlebrook, A. M., Perring, A. E., Richardson, M. S., Schwarz, J. P., **Welti, A.**, Ziemba, L. D. and Murphy, D. M. 2016. Aerosol optical properties in the southeastern United States in summer – Part 2: Sensitivity of aerosol optical depth to relative humidity and aerosol parameters. Atmos. Chem. Phys., **16**, 5009-5019. doi:10.5194/acp-16-5009-2016.

Bühl, J., **Seifert, P.**, **Myagkov, A.** and **Ansmann, A.** 2016. Measuring ice- and liquid-water properties in mixed-phase cloud layers at the Leipzig Cloudnet station. Atmos. Chem. Phys., **16**, 10609-10620. doi:10.5194/ acp-16-10609-2016.

Cavalli, F., Alastuey, A., Areskoug, H., Ceburnis, D., Čech, J., Genberg, J., Harrison, R. M., Jaffrezo, J. L., Kiss, G., Laj, P., Mihalopoulos, N., Perez, N., Quincey, P., Schwarz, J., Sellegri, K., **Spindler, G.**, Swietlicki, E., Theodosi, C., Yttri, K. E., Aas, W. and Putaud, J. P. 2016. A European aerosol phenomenology 4: Harmonized concentrations of carbonaceous aerosol at 10 regional background sites across Europe. Atmos. Environ., **144**, 133-145. doi:10.1016/j.atmosenv.2016.07.050.

Chaboureau, J.-P., Flamant, C., Dauhut, T., Kocha, C., Lafore, J.-P., Lavaysse, C., Marnas, F., Mokhtari, M., Pelon, J., Reinares Martínez, I., **Schepanski, K.** and Tulet, P. 2016. Fennec dust forecast intercomparison over the Sahara in June 2011. Atmos. Chem. Phys., **16**, 6977-6995. doi:10.5194/acp-16-6977-2016.

Chaikovsky, A., Dubovik, O., Holben, B., Bril, A., Goloub, P., Tanré, D., Pappalardo, G., **Wandinger, U.**, Chaikovskaya, L., Denisov, S., Grudo, J., Lopatin, A., Karol, Y., Lapyonok, T., Amiridis, V., **Ansmann, A.**, Apituley, A., Allados-Arboledas, L., Binietoglou, I., Boselli, A., D'Amico, G., Freudenthaler, V., Giles, D., Granados-Muñoz, M. J., Kokkalis, P., Nicolae, D., Oshchepkov, S., Papayannis, A., Perrone, M. R., Pietruczuk, A., Rocadenbosch, F., Sicard, M., Slutsker, I., Talianu, C., De Tomasi, F., Tsekeri, A., Wagner, J.

and Wang, X. 2016. Lidar-Radiometer Inversion Code (LIRIC) for the retrieval of vertical aerosol properties from combined lidar/radiometer data: development and distribution in EARLINET. Atmos. Meas. Tech., **9**, 1181-1205. doi:10.5194/amt-9-1181-2016.

Chandrakar, K. K., Cantrell, W., Chang, K., Ciochetto, D., **Niedermeier, D.**, Ovchinnikov, M., Shaw, R. A. and Yang, F. 2016. Aerosol indirect effect from turbulence-induced broadening of cloud-droplet size distributions. Proc. Nat. Acad. Sci. (PNAS), **113**, 14243–14248. doi:10.1073/pnas.1612686113.

Chang, K., Bench, J., Brege, M., Cantrell, W., Chandrakar, K., Ciochetto, D., Mazzoleni, C., Mazzoleni, L. R., **Niedermeier, D.** and Shaw, R. A. 2016. A laboratory facility to study gas–aerosol–cloud interactions in a turbulent environment: The Π Chamber. Bull. Amer. Meteor. Soc., **97**, 2343-2358. doi:10.1175/BAMS-D-15-00203.1.

Chen, Y., Cheng, Y., **Ma, N.**, **Wolke, R.**, Nordmann, S., **Schüttauf, S.**, Ran, L., **Wehner, B.**, **Birmili, W.**, Denier van der Gon, H. A. C., Mu, Q., **Barthel, S.**, **Spindler, G.**, **Stieger, B.**, **Müller, K.**, Zheng, G.-J., Pöschl, U., Su, H. and **Wiedensohler, A.** 2016. Sea salt emission, transport and influence on size-segregated nitrate simulation: A case study in northwestern Europe by WRF-Chem. Atmos. Chem. Phys., 12081–12097. doi:10.5194/acp-16-12081-2016.

Chen, Y., Cheng, Y.-F., Nordmann, S., **Birmili, W.**, Denier van der Gon, H. A. C., **Ma, N.**, **Wolke, R.**, **Wehner, B.**, **Sun, J.**, **Spindler, G.**, Mu, Q., Pöschl, U., Su, H. and **Wiedensohler, A.** 2016. Evaluation of the size segregation of elemental carbon (EC) emission in Europe: Influence on the simulation of EC long-range transportation. Atmos. Chem. Phys., **16**, 1823-1835. doi:10.5194/acp-16-1823-2016.

Chouza, F., Reitebuch, O., **Jähn, M.**, Rahm, S. and Weinzierl, B. 2016. Vertical wind retrieved by airborne lidar and analysis of island induced gravity waves in combination with numerical models and in situ particle measurements. Atmos. Chem. Phys., **16**, 4675-4692. doi:10.5194/acp-16-4675-2016.

Daellenbach, K. R., Bozzetti, C., Křepelová, A., Canonaco, F., Wolf, R., Zotter, P., Fermo, P., Crippa, M., Slowik, J. G., Sosedova, Y., Zhang, Y., Huang, R.-J., **Poulain, L.**, Szidat, S., Baltensperger, U., El Haddad, I. and Prévôt, A. S. H. 2016. Characterization and source apportionment of organic aerosol using offline aerosol mass spectrometry. Atmos. Meas. Tech., **9**, 23-39. doi:10.5194/amt-9-23-2016.

Denjean, C., Cassola, F., Mazzino, A., Triquet, S., Chevaillier, S., Grand, N., Bourrianne, T., Momboisse, G., Sellegri, K., Schwarzenbock, A., Freney, E., Mallet, M. and Formenti, P. 2016. Size distribution and optical properties of mineral dust aerosols transported in the western Mediterranean. Atmos. Chem. Phys., **16**, 1081-1104. doi:10.5194/acp-16-1081-2016.

Engelmann, R., **Kanitz, T.**, **Baars, H.**, **Heese, B.**, **Althausen, D.**, **Skupin, A.**, **Wandinger, U.**, Komppula, M., Stachlewska, I. S., Amiridis, V., Marinou, E., Mattis, I., Linné, H. and **Ansmann, A.** 2016. The automated multiwavelength Raman polarization and water-vapor lidar Polly[XT]: The neXT generation. Atmos. Meas. Tech., **9**, 1767-1784. doi:10.5194/amt-9-1767-2016.

Feistel, R., Wielgosz, R., Bell, S. A., Camões, M. F., Cooper, J. R., Dexter, P., Dickson, A. G., Fisicaro, P., Harvey, A. H., Heinonen, M., **Hellmuth, O.**, Kretzschmar, H.-J., Lovell-Smith, J. W., McDougall, T. J., Pawlowicz, R., Ridout, P., Seitz, S., Spitzer, P., Stoica, D. and Wolf, H. 2016. Metrological challenges for measurements of key climatological observables: Oceanic salinity and pH, and atmospheric humidity. Part 1: Overview. Metrologia, **53**, R1-R11. doi:10.1088/0026-1394/53/1/R1.

Feistel, R., Wielgosz, R., Bell, S. A., Camões, M. F., Cooper, J. R., Dexter, P., Dickson, A. G., Fisicaro, P., Harvey, A. H., Heinonen, M., **Hellmuth, O.**, Kretzschmar, H.-J., Lovell-Smith, J. W., McDougall, T. J., Pawlowicz, R., Ridout, P., Seitz, S., Spitzer, P., Stoica, D. and Wolf, H. 2016. Digital Supplement of the article "Metrological challenges for measurements of key climatological observables: Oceanic salinity and pH, and atmospheric humidity. Part 1: Overview". Metrologia, **53**, R1-R11 (23 p.). doi:10.1088/0026-1394/53/1/R1.

Fiedler, S., Knippertz, P., Woodward, S., Martin, G., Bellouin, N., Ross, A. N., **Heinold, B.**, **Schepanski, K.**, Birch, C. E. and **Tegen, I.** 2016. A process-based evaluation of dust-emitting winds in the CMIP5 simulation of HadGEM2-ES. Clim. Dyn., **46**, 1107-1130. doi:10.1007/s00382-015-2635-9.

Field, P. R., Lawson, R. P., Brown, P. R. A., Lloyd, G., Westbrook, C., Moisseev, D., Miltenberger, A., Nenes, A., Blyth, A., Choularton, T., Connolly, P., **Bühl, J.**, Crosier, J., Cui, Z., Dearden, C., DeMott, P., Flossmann, A., Heymsfield, A., Huang, Y., **Kalesse, H.**, Kanji, Z. A., Korolev, A., Kirchgaessner, A., Lasher-Trapp, S., Leisner, T., McFarquhar, G., Phillips, V., Stith, J. and Sullivan, S. 2016. Secondary ice production - current state of the science and recommendations for the future (Chapter 7). *In: Ice formation and evolution in clouds and precipitation : Measurement and modeling challenges*. AMS, p. 7.1-7.20 (Online first 28 November 2016). doi:10.1175/AMSMONOGRAPHS-D-16-0014.1. (AMS Meteorological Monographs).

Appendices: Publications

Forkel, R., Brunner, D., Baklanov, A., Balzarini, A., Hirtl, M., Honzak, L., Jiménez-Guerrero, P., Jorba, O., Pérez, J. L., San José, R., **Schröder, W.**, Tsegas, G., Werhahn, J., **Wolke, R.** and Žabkar, R. 2016. A multi-model case study on aerosol feedbacks in online coupled chemistry-meteorology models within the COST Action ES1004 EuMetChem. *In: D. G. Steyn and N. Chaumerliac (Eds.), Air pollution modeling and its application XXIV : Proceedings of the 34th International Technical Meeting on Air Pollution Modelling and Its Application (Montpellier, France, 4-8 May 2015).* Springer International Publishing, Switzerland, p. 23-28 (Chapter 4). doi:10.1007/978-3-319-24478-5. (Springer Proceedings in Complexity).

Fountoukis, C., Megaritis, A. G., Skyllakou, K., Charalampidis, P. E., Denier van der Gon, H. A. C., Crippa, M., Prévôt, A. S. H., Fachinger, F., **Wiedensohler, A.**, Pilinis, C. and Pandis, S. N. 2016. Simulating the formation of carbonaceous aerosol in a European Megacity (Paris) during the MEGAPOLI summer and winter campaigns. Atmos. Chem. Phys., **16**, 3727-3741. doi:10.5194/acp-16-3727-2016.

Garimella, S., **Kristensen, T. B.**, **Ignatius, K.**, **Welti, A.**, **Voigtländer, J.**, Kulkarni, G. R., Sagan, F., Kok, G. L., Dorsey, J., Nichman, L., Rothenberg, D. A., Rösch, M., Kirchgäßner, A. C. R., Ladkin, R., **Wex, H.**, Wilson, T. W., Ladino, L. A., Abbatt, J. P. D., Stetzer, O., Lohmann, U., **Stratmann, F.** and Cziczo, D. J. 2016. The SPectrometer for Ice Nuclei (SPIN): An instrument to investigate ice nucleation. Atmos. Meas. Tech., **9**, 2781–2795. doi:10.5194/amt-9-2781-2016.

George, C., Beeldens, A., Barmpas, F., Doussin, J.-F., Manganelli, G., **Herrmann, H.**, Kleffmann, J. and Mellouki, A. 2016. Impact of photocatalytic remediation of pollutants on urban air quality. Front. Environ. Sci. Eng., **10**, 11. doi:10.1007/s11783-016-0834-1.

Granados-Muñoz, M. J., Navas-Guzman, F., Guerrero-Rascado, J. L., Bravo-Aranda, J. A., Binietoglou, I., Pereira, S. N., Basart, S., Baldasano, J. M., Belegante, L., Chaikovsky, A., Comeron, A., D'Amico, G., Dubovik, O., Ilic, L., Kokkalis, P., Muñoz-Porcar, C., Nickovic, S., Nicolae, D., Olmo, F. J., Papayannis, A., Pappalardo, G., Rodriguez, A., **Schepanski, K.**, Sicard, M., Vukovic, A., **Wandinger, U.**, Dulac, F. and Alados-Arboledas, L. 2016. Profiling aerosol microphysical properties at several EARLINET/AERONET sites during July 2012 ChArMEx/EMEP campaign. Atmos. Chem. Phys., **16**, 7043-7066. doi:10.5194/acp-16-7043-2016.

Grawe, S., **Augustin-Bauditz, S.**, **Hartmann, S.**, **Hellner, L.**, Pettersson, J. B. C., Prager, A., **Stratmann, F.** and **Wex, H.** 2016. The immersion freezing behavior of ash particles from wood and brown coal burning. Atmos. Chem. Phys., **16**, 13911-13928. doi:10.5194/acp-16-13911-2016.

Grayson, J. W., Zhang, Y., **Mutzel, A.**, Renbaum-Wolff, L., **Böge, O.**, Kamal, S., **Herrmann, H.**, Martin, S. T. and Bertram, A. K. 2016. Effect of varying experimental conditions on the viscosity of α-pinene derived secondary organic material. Atmos. Chem. Phys., **16**, 6027-6040. doi:10.5194/acp-16-6027-2016.

Groß, S., Gasteiger, J., Freudenthaler, V., **Müller, T.**, Sauer, D., Toledano, C. and **Ansmann, A.** 2016. Saharan dust contribution to the Caribbean summertime boundary layer – a lidar study during SALTRACE. Atmos. Chem. Phys., **16**, 11535-11546. doi:10.5194/acp-16-11535-2016.

Haarig, M., **Althausen, D.**, **Ansmann, A.**, **Klepel, A.**, **Baars, H.**, **Engelmann, R.**, Groß, S. and Freudenthaler, V. 2016. Measurement of the linear depolarization ratio of aged dust at three wavelengths (355, 532 and 1064 nm) simultaneously over Barbados. EPJ Web of Conferences, **119 [The 27th International Laser Radar Conference (ILRC 27) New York City, USA, July 5-10, 2015]**, Article Number 18009 (4 p.). doi:10.1051/epjconf/201611918009.

Haarig, M., **Engelmann, R.**, **Ansmann, A.**, Veselovskii, I., Whiteman, D. N. and **Althausen, D.** 2016. 1064 nm rotational Raman lidar for particle extinction and lidar-ratio profiling: Cirrus case study. Atmos. Meas. Tech., **9**, 4269-4278. doi:10.5194/amt-9-4269-2016.

Hande, L. B., **Engler, C.**, Hoose, C. and **Tegen, I.** 2016. Parameterizing cloud condensation nuclei concentrations during HOPE. Atmos. Chem. Phys., **16**, 12059-12079. doi:10.5194/acp-16-12059-2016.

Hartmann, S., **Wex, H.**, **Clauss, T.**, **Augustin-Bauditz, S.**, **Niedermeier, D.**, **Rösch, M.** and **Stratmann, F.** 2016. Immersion freezing of kaolinite: Scaling with particle surface area. J. Atmos. Sci., **73**, 263-278. doi:10.1175/JAS-D-15-0057.1.

Heinold, B., **Tegen, I.**, **Schepanski, K.** and **Banks, J. R.** 2016. New developments in the representation of Saharan dust sources in the aerosol-climate model ECHAM6-HAM2. Geosci. Model Dev., **9**, 765-777. doi:10.5194/gmd-9-765-2016.

Heintzenberg, J., Cereceda-Balic, F., Vidal, V. and Leck, C. 2016. Scavenging of black carbon in Chilean coastal fogs. Sci. Total Environ., **541**, 341-347. doi:10.1016/j.scitotenv.2015.09.057.

Heinze, R., Dipankar, A., Carbajal Henken, C., Moseley, C., Sourdeval, O., Trömel, S., Xie, X., Adamidis, P., Ament, F., **Baars, H.**, Barthlott, C., Behrendt, A., Blahak, U., **Bley, S.**, Brdar, S., Brueck, M., Crewell, S., **Deneke, H.**, Di Girolamo, P., Evaristo, R., Fischer, J., Frank, C., Friederichs, P., Göcke, T., Gorges, K.,

Hande, L., Hanke, M., Hansen, A., Hege, H.-C., Hoose, C., Jahns, T., Kalthoff, N., Klocke, D., Kneifel, S., Knippertz, P., Kuhn, A., Laar, T., **Macke, A.**, Maurer, V., Mayer, B., Meyer, C. I., Muppa, S. K., Neggers, R. A. J., Orlandi, E., Pantillon, F., Pospichal, B., Röber, N., Scheck, L., Seifert, A., **Seifert, P.**, **Senf, F.**, Siligam, P., Simmer, C., Steinke, S., Stevens, B., Wapler, K., Weniger, M., Wulfmeyer, V., Zängl, G., Zhang, D. and Quaas, J. 2016. Large-eddy simulations over Germany using ICON : A comprehensive evaluation. Q. J. Roy. Meteor. Soc., **143**, 69-100. doi:10.1002/qj.2947.

Hellmuth, O. 2016. Selected aspects of new particle formation in the earth atmosphere: Organic aerosol formation and pre-nucleation molecular clustering. Joint Institute for Nuclear Research (JINR), Dubna, 456 pp. (Nucleation theory and applications : Special issues. Review series on selected topics of atmospheric sol formation ; Vol. 3).

Hellmuth, O. 2016. Selected aspects of new particle formation in the earth atmosphere: Phenomenology and mechanistic description. Joint Institute for Nuclear Research (JINR), Dubna, vi, 495 pp. (Nucleation theory and applications : Special issues. Review series on selected topics of atmospheric sol formation ; Vol. 2).

Hermann, M., Weigelt, A., **Assmann, D.**, **Pfeifer, S.**, **Müller, T.**, **Conrath, T.**, **Voigtländer, J.**, **Heintzenberg, J.**, **Wiedensohler, A.**, Martinsson, B. G., Deshler, T., Brenninkmeijer, C. A. M. and Zahn, A. 2016. An optical particle size spectrometer for aircraft-borne measurements in IAGOS-CARIBIC. Atmos. Meas. Tech., **9**, 2179-2194. doi:10.5194/amt-9-2179-2016.

Hofer, J., **Althausen, D.**, Abdullaev, S. F., **Engelmann, R.** and **Baars, H.** 2016. Central Asian Dust Experiment (CADEX): Multiwavelength polarization Raman lidar observations in Tajikistan. EPJ Web of Conferences, **119 [The 27th International Laser Radar Conference (ILRC 27) New York City, USA, July 5-10, 2015]**, Article Number 18006 (4 p.). doi:10.1051/epjconf/201611918006.

Hoffmann, E. H., **Tilgner, A.**, **Schrödner, R.**, **Bräuer, P.**, **Wolke, R.** and **Herrmann, H.** 2016. An advanced modeling study on the impacts and atmospheric implications of multiphase dimethyl sulfide chemistry. Proc. Nat. Acad. Sci. (PNAS), **113**, 11776–11781. doi:10.1073/pnas.1606320113.

Hoyle, C. R., Fuchs, C., Järvinen, E., Saathoff, H., Dias, A., El Haddad, I., Gysel, M., Coburn, S. C., Tröstl, J., Bernhammer, A.-K., Bianchi, F., Breitenlechner, M., Corbin, J. C., Craven, J., Donahue, N. M., Duplissy, J., Ehrhart, S., Frege, C., Gordon, H., Höppel, N., Heinritzi, M., **Kristensen, T. B.**, Molteni, U., Nichman, L., Pinterich, T., Prévôt, A. S. H., Simon, M., Slowik, J. G., Steiner, G., Tomé, A., Vogel, A. L., Volkamer, R., Wagner, A. C., Wagner, R., Wexler, A. S., Williamson, C., Winkler, P. M., Yan, C., Amorim, A., Dommen, J., Curtius, J., Gallagher, M. W., Flagan, R. C., Hansel, A., Kirkby, J., Kulmala, M., Möhler, O., **Stratmann, F.**, Worsnop, D. and Baltensperger, U. 2016. Aqueous phase oxidation of sulphur dioxide by ozone in cloud droplets. Atmos. Chem. Phys., **16**, 1693-1712. doi:10.5194/acp-16-1693-2016.

Iinuma, Y., Keywood, M. and **Herrmann, H.** 2016. Characterization of primary and secondary organic aerosols in Melbourne airshed: The influence of biogenic emissions, wood smoke and bushfires. Atmos. Environ., **130**, 54-63. doi:10.1016/j.atmosenv.2015.12.014.

Jähn, M., Muñoz-Esparza, D., Chouza, F., O., R., **Knoth, O.**, **Haarig, M.** and **Ansmann, A.** 2016. Investigations of boundary layer structure, cloud characteristics and vertical mixing of aerosols at Barbados with large eddy simulations. Atmos. Chem. Phys., **16**, 651-674. doi:10.5194/acp-16-651-2016.

Järvinen, E., **Ignatius, K.**, Nichman, L., **Kristensen, T. B.**, Fuchs, C., Hoyle, C. R., Höppel, N., Corbin, J. C., Craven, J., Duplissy, J., Ehrhart, S., El Haddad, I., Frege, C., Gordon, H., Jokinen, T., Kallinger, P., Kirkby, J., Kiselev, A., Naumann, K.-H., Petäjä, T., Pinterich, T., Prevot, A. S. H., Saathoff, H., Schiebel, T., Sengupta, K., Simon, M., Slowik, J. G., Tröstl, J., Virtanen, A., Vochezer, P., Vogt, S., Wagner, A. C., Wagner, R., Williamson, C., Winkler, P. M., Yan, C., Baltensperger, U., Donahue, N. M., Flagan, R. C., Gallagher, M., Hansel, A., Kulmala, M., **Stratmann, F.**, Worsnop, D. R., Möhler, O., Leisner, T. and Schnaiter, M. 2016. Observation of viscosity transition in α-pinene secondary organic aerosol. Atmos. Chem. Phys., **16**, 4423-4438. doi:10.5194/acp-16-4423-2016.

Kalesse, H., de Boer, G., Solomon, A., Oue, M., Ahlgrimm, M., Zhang, D., Shupe, M. D., Luke, E. and Protat, A. 2016. Understanding rapid changes in phase partitioning between cloud liquid and ice in stratiform mixed-phase clouds: An Arctic case study. Mon. Wea. Rev., **144**, 4805-4826. doi:10.1175/MWR-D-16-0155.1.

Kalesse, H., Szyrmer, W., Kneifel, S., Kollias, P. and Luke, E. 2016. Fingerprints of a riming event on cloud radar Doppler spectra: Observations and modeling. Atmos. Chem. Phys., **16**, 2997-3012. doi:10.5194/acp-16-2997-2016.

Kaufmann, L., Marcolli, C., **Hofer, J.**, Pinti, V., Hoyle, C. R. and Peter, T. 2016. Ice nucleation efficiency of natural dust samples in the immersion mode. Atmos. Chem. Phys., **16**, 11177-11206. doi:10.5194/acp-16-11177-2016.

Appendices: Publications

Kecorius, S., Kivekäs, N., Kristensson, A., **Tuch, T.**, Covert, D. S., **Birmili, W.**, Lihavainen, H., Hyvärinen, A.-P., Martinsson, J., Sporre, M. K., Swietlicki, E., **Wiedensohler, A.** and Ulevicius, V. 2016. Significant increase of aerosol number concentrations in air masses crossing a densely trafficked sea area. Oceanologia, **58**, 1-12. doi:10.1016/j.oceano.2015.08.001.

Kienast-Sjögren, E., Rolf, C., **Seifert, P.**, Krieger, U. K., Luo, B. P., Krämer, M. and Peter, T. 2016. Climatological and radiative properties of midlatitude cirrus clouds derived by automatic evaluation of lidar measurements. Atmos. Chem. Phys., **16**, 7605-7621. doi:10.5194/acp-16-7605-2016.

Kiendler-Scharr, A., Mensah, A. A., Friese, E., Topping, D., Nemitz, E., Prevot, A. S. H., Äijälä, M., Allan, J., Canonaco, F., Canagaratna, M., Carbone, S., Crippa, M., Dall Osto, M., Day, D. A., De Carlo, P., Di Marco, C. F., Elbern, H., Eriksson, A., Freney, E., Hao, L., **Herrmann, H.**, Hildebrandt, L., Hillamo, R., Jimenez, J. L., Laaksonen, A., McFiggans, G., Mohr, C., O'Dowd, C., Otjes, R., Ovadnevaite, J., Pandis, S. N., **Poulain, L.**, Schlag, P., Sellegri, K., Swietlicki, E., Titta, P., Vermeulen, A., Wahner, A., Worsnop, D. and Wu, H.-C. 2016. Ubiquity of organic nitrates from nighttime chemistry in the European submicron aerosol. Geophys. Res. Lett., **43**, 7735-7744. doi:10.1002/20165GL069239.

Kioutsioukis, I., Im, U., Solazzo, E., Bianconi, R., Badia, A., Balzarini, A., Baró, R., Bellasio, R., Brunner, D., Chemel, C., Curci, G., Denier van der Gon, H., Flemming, J., Forkel, R., Giordano, L., Jiménez-Guerrero, P., Hirtl, M., Jorba, O., Manders-Groot, A., Neal, L., Pérez, J. L., Pirovano, G., San Jose, R., Savage, N., **Schroder, W.**, Sokhi, R. S., Syrakov, D., Tuccella, P., Werhahn, J., **Wolke, R.**, Hogrefe, C. and Galmarini, S. 2016. Insights into the deterministic skill of air quality ensembles from the analysis of AQMEII data. Atmos. Chem. Phys., **16**, 15629-15652. doi:10.5194/acp-16-15629-2016.

Kneifel, S., Kollias, P., Battaglia, A., Leinonen, J., Maahn, M., **Kalesse, H.** and Tridon, F. 2016. First observations of triple-frequency radar Doppler spectra in snowfall: Interpretation and applications. Geophys. Res. Lett., **43**, Online first. doi:10.1002/2015GL067618.

Kremser, S., Thomason, L. W., von Hobe, M., **Hermann, M.**, Deshler, T., Timmreck, C., Toohey, M., Stenke, A., Schwarz, J. P., Weigel, R., Fueglistaler, S., Prata, F. J., Vernier, J.-P., Schlager, H., Barnes, J. E., Antuña-Marrero, J.-C., Fairlie, D., Palm, M., Mahieu, E., Notholt, J., Rex, M., Bingen, C., Vanhellemont, F., Bourassa, A., Plane, J. M. C., Klocke, D., Carn, S. A., Clarisse, L., Trickl, T., Neely, R., James, A. D., Rieger, L., Wilson, J. C. and Meland, B. 2016. Stratospheric aerosol - Observations, processes, and impact on climate. Rev. Geophys., **54**, 1-58. doi:10.1002/2015RG000511.

Kristensen, T. B., **Müller, T.**, Kandler, K., Benker, N., Hartmann, M., Prospero, J. M., **Wiedensohler, A.** and **Stratmann, F.** 2016. Properties of cloud condensation nuclei (CCN) in the trade wind marine boundary layer of the western North Atlantic. Atmos. Chem. Phys., **16**, 2675-2688. doi:10.5194/acp-16-2675-2016.

Kuang, Y., Zhao, C. S., **Ma, N.**, Liu, H. J., Bian, Y. X., Tao, J. C. and Hu, M. 2016. Deliquescent phenomena of ambient aerosols on the North China Plain. Geophys. Res. Lett., **43**, 8744-8750. doi:10.1002/2016GL070273.

Kumar, P., **Wiedensohler, A.**, Birmili, W., Quincey, P. and Hallquist, M. 2016. Ultrafine particles pollution and measurements. *In: M. de la Guardia and S. Armenta (Eds.), Comprehensive analytical chemistry*. Elsevier, Amsterdam, p. 369-390 (Chapter 15). doi:10.1016/bs.coac.2016.04.004.

Kupiszewski, P., Zanatta, M., **Mertes, S.**, Vochezer, P., Lloyd, G., Schneider, J., Schenk, L., Schnaiter, M., Baltensperger, U., Weingartner, E. and Gysel, M. 2016. Ice residual properties in mixed-phase clouds at the high-alpine Jungfraujoch site. J. Geophys. Res. - Atmos., **121**, 12343-12362. doi:10.1002/2016JD024894.

Li, X., Chen, M., **Le, H. P.**, Wang, F., Guo, Z., **Iinuma, Y.**, Chen, J. and **Herrmann, H.** 2016. Atmospheric outflow of PM2.5 saccharides from megacity Shanghai to East China Sea: Impact of biological and biomass burning sources. Atmos. Environ., **143**, 1-14. doi:10.1016/j.atmosenv.2016.08.039.

Li, X., Jiang, L., **Hoa, L. P.**, Lyu, Y., Xu, T., Yang, X., **Iinuma, Y.**, Chen, J. and **Herrmann, H.** 2016. Size distribution of particle-phase sugar and nitrophenol tracers during severe urban haze episodes in Shanghai. Atmos. Environ., **145**, 115-127. doi:10.1016/j.atmosenv.2016.09.030.

Lovell-Smith, J. W., Feistel, R., Harvey, A. H., **Hellmuth, O.**, Bell, S. A., Heinonen, M. and Cooper, J. R. 2016. Metrological challenges for measurements of key climatological observables. Part 4: Atmospheric relative humidity. Metrologia, **53**, R40-R59. doi:10.1088/0026-1394/53/1/R40.

Lv, Y., Li, X., Xu, T. T., Cheng, T. T., Yang, X., Chen, J. M., **Iinuma, Y.** and **Herrmann, H.** 2016. Size distributions of polycyclic aromatic hydrocarbons in urban atmosphere: Sorption mechanism and source contributions to respiratory deposition. Atmos. Chem. Phys., **16**, 2971–2983. doi:10.5194/acp-16-2971-2016.

Ma, N., Zhao, C., Tao, J., Wu, Z., **Kecorius, S.**, **Wang, Z.**, **Größ, J.**, Liu, H., Bian, Y., Kuang, Y., **Teich, M.**, **Spindler, G.**, **Müller, K.**, **van Pinxteren, D.**, **Herrmann, H.**, Hu, M. and **Wiedensohler, A.** 2016. Variation of CCN activity during new particle formation events in the North China Plain. Atmos. Chem. Phys., **16**,

8593-8607. doi:10.5194/acp-16-8593-2016.

Macke, A. and Mishchenko, M. I. 2016. Electromagnetic and light scattering by nonspherical particles XV: Celebrating 150 years of Maxwell's electromagnetics. J. Quant. Spectrosc. Radiat. Transfer, **178**, 1-4. doi:10.1016/j.jqsrt.2015.12.001.

Madhavan, B. L., Kalisch, J. and **Macke, A.** 2016. Shortwave surface radiation network for observing small-scale cloud inhomogeneity fields. Atmos. Meas. Tech., **9**, 1153-1166. doi:10.5194/amt-9-1153-2016.

Mallet, M., Dulac, F., Formenti, P., Nabat, P., Sciare, J., Roberts, G., Pelon, J., Ancellet, G., Tanré, D., Parol, F., Denjean, C., Brogniez, G., di Sarra, A., Alados-Arboledas, L., Arndt, J., Auriol, F., Blarel, L., Bourrianne, T., Chazette, P., Chevaillier, S., Claeys, M., D'Anna, B., Derimian, Y., Desboeufs, K., Di Iorio, T., Doussin, J.-F., Durand, P., Féron, A., Freney, E., Gaimoz, C., Goloub, P., Gómez-Amo, J. L., Granados Muñoz, M. J., Grand, N., Hamonou, E., Jankowiak, I., Jeannot, M., Léon, J.-F., Maillé, M., Mailler, S., Meloni, D., Menut, L., Momboisse, G., Nicolas, J., Podvin, T., Pont, V., Rea, G., Renard, J.-B., Roblou, L., **Schepanski, K.**, Schwarzenboeck, A., Sellegri, K., Sicard, M., Solmon, F., Somot, S., Torres, B., Totems, J., Triquet, S., Verdier, N., Verwaerde, C., Waquet, F., Wenger, J. and Zapf, P. 2016. Overview of the Chemistry-Aerosol Mediterranean Experiment/Aerosol Direct Radiative Forcing on the Mediterranean Climate (ChArMEx/ADRIMED) summer 2013 campaign. Atmos. Chem. Phys., **16**, 455-504. doi:10.5194/acp-16-455-2016.

Mamouri, R. and **Ansmann, A.** 2016. Potential of polarization lidar to provide profiles of CCN- and INP-relevant aerosol parameters. Atmos. Chem. Phys., **16**, 5905-5931. doi:10.5194/acp-16-5905-2016.

Mamouri, R.-E., **Ansmann, A.**, Nisantzi, A., Solomos, S., Kallos, G. and Hadjimitsis, D. G. 2016. Extreme dust storm over the eastern Mediterranean in September 2015: Satellite, lidar, and surface observations in the Cyprus region. Atmos. Chem. Phys., **16**, 13711-13724. doi:10.5194/acp-16-13711-2016.

Mattis, I., D'Amico, G., **Baars, H.**, Amodeo, A., Madonna, F. and Iarlori, M. 2016. EARLINET Single Calculus Chain – technical – Part 2: Calculation of optical products. Atmos. Meas. Tech., **9**, 3009-3029. doi:10.5194/amt-9-3009-2016.

Merk, D., **Deneke, H.**, Pospichal, B. and **Seifert, P.** 2016. Investigation of the adiabatic assumption for estimating cloud micro- and macrophysical properties from satellite and ground observations. Atmos. Chem. Phys., **16**, 933-952. doi:10.5194/acp-16-933-2016.

Mothes, F., **Böge, O.** and **Herrmann, H.** 2016. A chamber study on the reactions of O_3, NO, NO_2 and selected VOCs with a photocatalytically active cementitious coating material. Environ. Sci. Pollut. Res., **23**, 15250-15261. doi:10.1007/s11356-016-6612-6.

Mutzel, A., **Rodigast, M.**, **Iinuma, Y.**, **Böge, O.** and **Herrmann, H.** 2016. Monoterpene SOA – Contribution of first-generation oxidation products to formation and chemical composition. Atmos. Environ., **130**, 136-144. doi:10.1016/j.atmosenv.2015.10.080.

Myagkov, A., **Seifert, P.**, Bauer-Pfundstein, M. and **Wandinger, U.** 2016. Cloud radar with hybrid mode towards estimation of shape and orientation of ice crystals. Atmos. Meas. Tech., **9**, 469-489. doi:10.5194/amt-9-469-2016.

Myagkov, A., **Seifert, P.**, **Wandinger, U.**, **Bühl, J.** and **Engelmann, R.** 2016. Relationship between temperature and apparent shape of pristine ice crystals derived from polarimetric cloud radar observations during the ACCEPT campaign. Atmos. Meas. Tech., **9**, 3739-3754. doi:10.5194/amt-9-3739-2016.

Nehr, S., Gladtke, D., Hellack, B., **Herrmann, H.**, Hoffmann, B., Kuhlbusch, T. A. J., Schins, R. P. F., Wiesen, P. and Zellner, R. 2016. Tropospheric aerosols - Current research and future air quality policy. Gefahrst. Reinhalt. L., **76**, 231-237.

Nehr, S., **Herrmann, H.**, Theloke, J. and Wiesen, P. 2016. NMVOCs, NO_x, O_3, and the EU thematic strategy on air pollution (NMVOCs, NO_x, O_3, und die Thematische Strategie der EU zur Luftreinhaltung). Gefahrst. Reinhalt. L., **76**, 7-13.

Nguyen, Q. T., Glasius, M., Sørensen, L. L., Jensen, B., Skov, H., **Birmili, W.**, **Wiedensohler, A.**, Kristensson, A., Nøjgaard, J. K. and Massling, A. 2016. Seasonal variation of atmospheric particle number concentrations, new particle formation and atmospheric oxidation capacity at the high Arctic site Villum Research Station, Station Nord. Atmos. Chem. Phys., **16**, 11319-11336. doi:10.5194/acp-16-11319-2016.

Nichman, L., Fuchs, C., Järvinen, E., **Ignatius, K.**, Höppel, N. F., Dias, A., Heinritzi, M., Simon, M., Tröstl, J., Wagner, A. C., Wagner, R., Williamson, C., Yan, C., Connolly, P. J., Dorsey, J. R., Duplissy, J., Ehrhart, S., Frege, C., Gordon, H., Hoyle, C. R., **Kristensen, T. B.**, Steiner, G., Donahue, N. M., Flagan, R., Gallagher, M. W., Kirkby, J., Möhler, O., Saathoff, H., Schnaiter, M., **Stratmann, F.** and Tomé, A. 2016. Phase transition observations and discrimination of small cloud particles by light polarization in expansion chamber experiments. Atmos. Chem. Phys., **16**, 3651-3664. doi:10.5194/acp-16-3651-2016.

Appendices: Publications

Papagiannopoulos, N., Mona, L., Alados-Arboledas, L., Amiridis, V., **Baars, H.**, Binietoglou, I., Bortoli, D., D'Amico, G., Giunta, A., Guerrero-Rascado, J. L., **Schwarz, A.**, Pereira, S., Spinelli, N., **Wandinger, U.**, Wang, X. and Pappalardo, G. 2016. CALIPSO climatological products: Evaluation and suggestions from EARLINET. Atmos. Chem. Phys., **16**, 2341-2357. doi:10.5194/acp-16-2341-2016.

Pfeifer, S., **Müller, T.**, **Weinhold, K.**, Zikova, N., dos Santos, S. M., Marinoni, A., Bischof, O. F., Kykal, C., Ries, L., Meinhardt, F., Aalto, P., Mihalopoulos, N. and **Wiedensohler, A.** 2016. Intercomparison of 15 aerodynamic particle size spectrometers (APS 3321): Uncertainties in particle sizing and number size distribution. Atmos. Meas. Tech., **9**, 1545-1551. doi:10.5194/amt-9-1545-2016.

Platis, A., Altstädter, B., **Wehner, B.**, Wildmann, N., Lampert, A., **Hermann, M.**, **Birmili, W.** and Bange, J. 2016. An observational case study on the influence of atmospheric boundary-layer dynamics on new particle formation. Bound.-Lay. Meteorol., **158**, 67-92. doi:10.1007/s10546-015-0084-y.

Rauthe-Schöch, A., Baker, A. K., Schuck, T. J., Brenninkmeijer, C. A. M., Zahn, A., **Hermann, M.**, Stratmann, G., Ziereis, H., van Velthoven, P. F. J. and Lelieveld, J. 2016. Trapping, chemistry, and export of trace gases in the South Asian summer monsoon observed during CARIBIC flights in 2008. Atmos. Chem. Phys., **16**, 3609-3629. doi:10.5194/acp-16-3609-2016.

Richters, S., **Herrmann, H.** and **Berndt, T.** 2016. Highly oxidized RO_2 radicals and consecutive products from the ozonolysis of three sesquiterpenes. Environ. Sci. Technol., **50**, 2354-2362. doi:10.1021/acs.est.5b05321.

Richters, S., **Herrmann, H.** and **Berndt, T.** 2016. Different pathways of the formation of highly oxidized multifunctional organic compounds (HOMs) from the gas-phase ozonolysis of β-caryophyllene. Atmos. Chem. Phys., **16**, 9831-9845. doi:10.5194/acp-16-9831-2016.

Rodigast, M., **Mutzel, A.**, **Schindelka, J.** and **Herrmann, H.** 2016. A new source of methylglyoxal in the aqueous phase. Atmos. Chem. Phys., **16**, 2689–2702. doi:10.5194/acp-16-2689-2016.

Rosati, B., Gysel, M., **Rubach, F.**, Mentel, T. F., Goger, B., **Poulain, L.**, Schlag, P., Miettinen, P., Pajunoja, A., Virtanen, A., Klein Baltink, H., Henzing, J. S. B., **Größ, J.**, Gobbi, G. P., **Wiedensohler, A.**, Kiendler-Scharr, A., Decesari, S., Facchini, M. C., Weingartner, E. and Baltensperger, U. 2016. Vertical profiling of aerosol hygroscopic properties in the planetary boundary layer during the PEGASOS campaigns. Atmos. Chem. Phys., **16**, 7295-7315. doi:10.5194/acp-16-7295-2016.

Rosati, B., Herrmann, E., Bucci, S., Fierli, F., Cairo, F., Gysel, M., Tillmann, R., **Größ, J.**, Gobbi, G. P., Di Liberto, L., Di Donfrancesco, G., **Wiedensohler, A.**, Weingartner, E., Virtanen, A., Mentel, T. F. and Baltensperger, U. 2016. Studying the vertical aerosol extinction coefficient by comparing in situ airborne data and elastic backscatter lidar. Atmos. Chem. Phys., **16**, 4539-4554. doi:10.5194/acp-16-4539-2016.

Roth, A., Schneider, J., Klimach, T., **Mertes, S.**, **van Pinxteren, D.**, **Herrmann, H.** and Borrmann, S. 2016. Aerosol properties, source identification, and cloud processing in orographic clouds measured by single particle mass spectrometry on a Central European mountain site during HCCT-2010. Atmos. Chem. Phys., **16**, 505-524. doi:10.5194/acp-16-505-2016.

Rusumdar, A. J., **Wolke, R.**, **Tilgner, A.** and **Herrmann, H.** 2016. Treatment of non-ideality in the SPACCIM multiphase model – Part 1: Model development. Geosci. Model Dev., **9**, 247-281. doi:10.5194/gmd-9-247-2016.

Sahyoun, M., **Wex, H.**, Gosewinkel, U. K., Šantl-Temkiv, T., Nielsen, N. W., Finster, K., Sørensen, J. H., **Stratmann, F.** and Korsholm, U. S. 2016. On the usage of classical nucleation theory in quantification of the impact of bacterial INP on weather and climate. Atmos. Environ., **139**, 230–240. doi:10.1016/j.atmosenv.2016.05.034.

Sandrini, S., **van Pinxteren, D.**, Giulianelli, L., **Herrmann, H.**, **Poulain, L.**, Facchini, M. C., Gilardoni, S., Rinaldi, M., Paglione, M., Turpin, B. J., Pollini, F., Bucci, S., Zanca, N. and Decesari, S. 2016. Size-resolved aerosol composition at an urban and a rural site in the Po Valley in summertime: Implications for secondary aerosol formation. Atmos. Chem. Phys., **16**, 10879-10897. doi:10.5194/acp-16-10879-2016.

Schepanski, K., Mallet, M., **Heinold, B.** and **Ulrich, M.** 2016. North African dust transport toward the western Mediterranean basin: Atmospheric controls on dust source activation and transport pathways during June-July 2013. Atmos. Chem. Phys., **16**, 14147-14168. doi:10.5194/acp-16-14147-2016.

Schmale, J., **Henning, S.**, Henzing, J. S., Keskinen, H., Sellegri, K., Ovadnevaite, J., Bougiatioti, A., Kalivitis, N., Stavroulas, I., Jefferson, A., Park, M., Schlag, P., Kristensson, A., Ivamoto, Y., Pringle, K., Reddington, C., Aalto, P., Äijälä, M., Baltensperger, U., Bialek, J., **Birmili, W.**, Bukowiecki, N., Ehn, M., Fjæraa, A. M., Fiebig, M., Frank, G., Fröhlich, R., Frumau, A., Furuya, M., Hammer, E., Heikkinen, L., Herrmann, E., Holzinger, R., Hyono, H., Kanakidou, M., Kiendler-Scharr, A., Kinochi, K., Kos, G., Kulmala, M., Mihalopoulos, N., Nenes, A., O'Dowd, C., Paramonov, M., Petäjä, T., Picard, D., **Poulain, L.**, Prévôt, A. S. H., Slowik, J., **Sonntag,**

A., Swietlicki, E., Svenningsson, B., Tsurumaru, H., **Wiedensohler, A.**, Wittbom, C., Ogren, J., Matsuki, A., Yum, S. S., Myhre, C. L., Carslaw, K., **Stratmann, F.** and Gysel, M. 2016. Collocated observations of cloud condensation nuclei, particle size distributions, and chemical composition. Sci. Data, **4:170003**, 26 pp. doi:10.1038/sdata.2017.3.

Schmelzer, J. W. P. and **Hellmuth, O.** (Eds.) 2016. Review series on selected topics of atmospheric sol formation: Volume 2 : Selected aspects of new particle formation in the earth atmosphere: Phenomenology and mechanistic description, vi, 495 pp., Joint Institute for Nuclear Research (JINR), Dubna. (Nucleation theory and applications : Special issues).

Schmelzer, J. W. P. and **Hellmuth, O.** (Eds.) 2016. Review series on selected topics of atmospheric sol formation: Volume 3 : Selected aspects of new particle formation in the earth atmosphere: Organic aerosol formation and pre-nucleation molecular clustering, viii, 456 pp., Joint Institute for Nuclear Research (JINR), Dubna. (Nucleation theory and applications : Special issues).

Siebert, H. and Shaw, R. A. 2016. Supersaturation fluctuations during the early stage of cumulus formation. J. Atmos. Sci., **74**, 975-988. doi: 10.1175/JAS-D-16-0115.1.

Sipilä, M., Sarnela, N., Jokinen, T., Henschel, H., Junninen, H., Kontkanen, J., **Richters, S.**, Kangasluoma, J., Franchin, A., Peräkylä, O., Rissanen, M. P., Ehn, M., Vehkamäki, H., Kurten, T., **Berndt, T.**, Petäjä, T., Worsnop, D., Cebumis, D., Kerminen, V.-M., Kulmala, M. and O'Dowd, C. 2016. Molecular-scale evidence of aerosol particle formation via sequential addition of HIO_3. Nature, Online first. doi:10.1038/nature19314.

Skupin, A., **Ansmann, A.**, **Engelmann, R.**, **Seifert, P.** and **Müller, T.** 2016. Four-year long-path monitoring of ambient aerosol extinction at a central European urban site: Dependence on relative humidity. Atmos. Chem. Phys., **16**, 1863-1876. doi:10.5194/acp-16-1863-2016.

Slemr, F., Weigelt, A., Ebinghaus, R., Kock, H. H., Bödewadt, J., Brenninkmeijer, C. A. M., Rauthe-Schöch, A., Weber, S., **Hermann, M.**, Becker, J., Zahn, A. and Martinsson, B. 2016. Atmospheric mercury measurements onboard the CARIBIC passenger aircraft. Atmos. Meas. Tech., **9**, 2291-2302. doi:10.5194/amt-9-2291-2016.

Su, H., Cheng, Y., **Ma, N.**, Wang, Z., Wang, X., Pöhlker, M. L., Nillius, B., **Wiedensohler, A.** and Pöschl, U. 2016. A broad supersaturation scanning (BS2) approach for rapid measurement of aerosol particle hygroscopicity and cloud condensation nuclei activity. Atmos. Meas. Tech., **9**, 5183-5192. doi:10.5194/amt-9-5183-2016.

Sullivan, A. P., Hodas, N., Turpin, B. J., Skog, K., Keutsch, F. N., Gilardoni, S., Paglione, M., Rinaldi, M., Decesari, S., Facchini, M. C., **<u>Poulain, L.</u>**, **Herrmann, H.**, **Wiedensohler, A.**, Nemitz, E., Twigg, M. M. and Collett Jr., J. L. 2016. Evidence for ambient dark aqueous SOA formation in the Po Valley, Italy. Atmos. Chem. Phys., **16**, 8095-8108. doi:10.5194/acp-16-8095-2016.

Teich, M., **van Pinxteren, D.**, **Kecorius, S.**, **Wang, Z.** and **Herrmann, H.** 2016. First quantification of imidazoles in ambient aerosol particles: Potential photosensitizers, brown carbon constituents and hazardous components. Environ. Sci. Technol., **50**, 1166-1173. doi:10.1021/acs.est.5b05474.

Tham, Y. J., Wang, Z., Li, Q., Yun, H., Wang, W., Wang, X., Xue, L., Lu, K. D., **Ma, N.**, Bohn, B., Li, X., **Kecorius, S.**, **Größ, J.**, Shao, M., **Wiedensohler, A.**, Zhang, Y. and Wang, T. 2016. Significant concentrations of nitryl chloride sustained in the morning: Investigations of the causes and impacts on ozone production in a polluted region of northern China. Atmos. Chem. Phys., **16**, 14959-14977. doi:10.5194/acp-16-14959-2016.

Tuch, T., **Weinhold, K.**, **Merkel, M.**, Nowak, A., Klein, T., Quincey, P., Stolzenburg, M. and **Wiedensohler, A.** 2016. Dependence of CPC cut-off diameter on particle morphology and other factors. Aerosol Sci. Technol., **50**, 331-338. doi:10.1080/02786826.2016.1152351.

van Pinxteren, D., **Fomba, K. W.**, **Mertes, S.**, **Müller, K.**, **Spindler, G.**, Schneider, J., Lee, T., Collett, J. L. and **Herrmann, H.** 2016. Cloud water composition during HCCT-2010: Scavenging efficiencies, solute concentrations, and droplet size dependence of inorganic ions and dissolved organic carbon. Atmos. Chem. Phys., **16**, 3185–3205. doi:10.5194/acp-16-3185-2016.

van Pinxteren, D., **Fomba, K. W.**, **Spindler, G.**, **Müller, K.**, **Poulain, L.**, **Iinuma, Y.**, Löschau, G., Hausmann, A. and **Herrmann, H.** 2016. Regional air quality in Leipzig, Germany: Detailed source apportionment of size-resolved aerosol particles and comparison with the year 2000. Faraday Discuss., **189**, 291-315. doi:10.1039/C5FD00228A.

Van Zadelhoff, G. J., Donovan, D., **Wandinger, U.**, Daou, D., **Horn, S.**, **Hünerbein, A.**, Fischer, J., von Bismarck, J., Filipitsch, F., Docter, N., Eisinger, M., Lajas, D. and Wehr, T. 2016. Overview of the Earthcare L2 lidar retrieval chain. EPJ Web of Conferences, **119 [The 27th International Laser Radar Conference (ILRC 27) New York City, USA, July 5-10, 2015]**, Article Number 01003 (4 p.). doi:10.1051/epjconf/201611901003

Appendices: Publications

Voigt, C., Schumann, U., Minikin, A., Abdelmonem, A., Afchine, A., Borrmann, S., Boettcher, M., Buchholz, B., Bugliaro, L., Costa, A., Curtius, J., Dollner, M., Dörnbrack, A., Dreiling, V., Ebert , V., Ehrlich, A., Fix, A., Forster, L., Frank, F., Fütterer, D., Giez, A., Graf, K., Grooß, J.-U., Groß, S., Heimerl, K., **Heinold, B.**, Hüneke, T., Järvinen, E., Jurkat, T., Kaufmann, S., Kenntner, M., Klingebiel, M., Klimach, T., Kohl, R., Krämer, M., Krisna, T. C., Luebke, A., Mayer, B., **Mertes, S.**, Molleker, S., Petzold, A., Pfeilsticker, K., Port, M., Schlage, R., Schnaiter, M., Schneider, J., Spelten, N., Spichtinger, P., Stock, P., Walser, A., Weigel, R., Weinzierl, B., Wendisch, M., Werner, F., Wernli, H., Wirth, M., Zahn, A., Ziereis, H. and Zöger, M. 2016. ML-CIRRUS - The airborne experiment on natural cirrus and contrail cirrus with the high-altitude long-range research aircraft HALO. Bull. Amer. Meteor. Soc., **98**, 271-288. doi:10.1175/BAMS-D-15-00213.1.

Wagner, R., **Schepanski, K.**, **Heinold, B.** and **Tegen, I.** 2016. Interannual variability in the Saharan dust source activation - Toward understanding the differences between 2007 and 2008. J. Geophys. Res. - Atmos., Online first. doi:10.1002/2015JD024302.

Wandinger, U., **Baars, H.**, Engelmann, R., **Hünerbein, A.**, **Horn, S.**, Kanitz, T., Donovan, D., Van Zadelhoff, G. J., Daou, D., Fischer, J., von Bismarck, J., Filipitsch, F., Docter, N., Eisinger, M., Lajas, D. and Wehr, T. 2016. HETEAC: The aerosol classification model for EarthCARE. EPJ Web of Conferences, **119 [The 27th International Laser Radar Conference (ILRC 27) New York City, USA, July 5-10, 2015]**, Article Number 01004 (4 p.). doi:10.1051/epjconf/201611901004

Wandinger, U., Freudenthaler, V., **Baars, H.**, Amodeo, A., **Engelmann, R.**, **Mattis, I.**, Groß, S., Pappalardo, G., Giunta, A., D'Amico, G., Chaikovsky, A., Osipenko, F., Slesar, A., Nicolae, D., Belegante, L., Talianu, C., Serikov, I., Linné, H., Jansen, F., Apituley, A., Wilson, K. M., de Graaf, M., Trickl, T., Giehl, H., Adam, M., Comerón, A., Muñoz-Porcar, C., Rocadenbosch, F., Sicard, M., Tomás, S., Lange, D., Kumar, D., Pujadas, M., Molero, F., Fernández, A. J., Alados-Arboledas, L., Bravo-Aranda, J. A., Navas-Guzmán, F., Guerrero-Rascado, J. L., Granados-Muñoz, M. J., Preißler, J., Wagner, F., Gausa, M., Grigorov, I., Stoyanov, D., Iarlori, M., Rizi, V., Spinelli, N., Boselli, A., Wang, X., Lo Feudo, T., Perrone, M. R., De Tomasi, F. and Burlizzi, P. 2016. EARLINET instrument intercomparison campaigns: Overview on strategy and results. Atmos. Meas. Tech., **9**, 1001-1023. doi:10.5194/amt-9-1001-2016.

Wendisch, M., Pöschl, U., Andreae, M. O., Machado, L. A. T., Albrecht, R., Schlager, H., Rosenfeld, D., Martin, S. T., Abdelmonem, A., Afchine, A., Araùjo, A., Artaxo, P., Aufmhoff, H., Barbosa, H. M. J., Borrmann, S., Braga, R., Buchholz, B., Cecchini, M. A., Costa, A., Curtius, J., Dollner, M., Dorf, M., Dreiling, V., Ebert, V., Ehrlich, A., Ewald, F., Fisch, G., Fix, A., Frank, F., Fütterer, D., Heckl, C., Heidelberg, F., Hüneke, T., Jäkel, E., Järvinen, E., Jurkat, T., Kanter, S., **Kästner, U.**, Kenntner, M., Kesselmeier, J., Klimach, T., Knecht, M., Kohl, R., Kölling, T., Krämer, M., Krüger, M., Krisna, T. C., Lavric, J. V., Longo, K., Mahnke, C., Manzi, A. O., Mayer, B., **Mertes, S.**, Minikin, A., Molleker, S., Münch, S., Nilius, B., Pfeilsticker, K., Pöhlker, C., Roiger, A., Rose, D., Rosenow, D., Sauer, D., Schnaiter, M., Schneider, J., Schulz, C., de Souza, R. A. F., Spanu, A., Stock, P., Vila, D., Voigt, C., Walser, A., Walter, D., Weigel, R., Weinzierl, B., Werner, F., Yamasoe, M. A., Ziereis, H., Zinner, T. and Zöger, M. 2016. Introduction of the ACRIDICON–CHUVA campaign studying tropical deep convective clouds and precipitation over Amazonia using the new German research aircraft HALO. Bull. Amer. Meteor. Soc., **97**, 1885-1908. doi:10.1175/BAMS-D-14-00255.1.

Wex, H., **Dieckmann, K.**, Roberts, G. C., **Conrath, T.**, Izaguirre, M. A., **Hartmann, S.**, **Herenz, P.**, **Schäfer, M.**, **Ditas, F.**, **Schmeissner, T.**, **Henning, S.**, **Wehner, B.**, **Siebert, H.** and **Stratmann, F.** 2016. Aerosol arriving on the Caribbean island of Barbados: Physical properties and origin. Atmos. Chem. Phys., **16**, 14107-14130. doi:10.5194/acp-16-14107-2016.

Wolke, R., **Tilgner, A.**, **Schrödner, R.**, Nielsen, C. and **Herrmann, H.** 2016. Regional scale dispersion modelling of amines from industrial CCS processes with COSMO-MUSCAT. *In: D. G. Steyn and N. Chaumerliac (Eds.), Air pollution modeling and its application XXIV : Proceedings of the 34th International Technical Meeting on Air Pollution Modelling and Its Application (Montpellier, France, 4-8 May 2015)*. Springer International Publishing, Switzerland, p. 259-263 (Chapter 42). doi:10.1007/978-3-319-24478-5. (Springer Proceedings in Complexity).

Wu, Z. J., Zheng, J., Shang, D. J., Du, Z. F., Wu, Y. S., Zeng, L. M., **Wiedensohler, A.** and Hu, M. 2016. Particle hygroscopicity and its link to chemical composition in the urban atmosphere of Beijing, China, during summertime. Atmos. Chem. Phys., **16**, 1123–1138. doi:10.5194/acp-16-1123-2016.

Zanatta, M., Gysel, M., Bukowiecki, N., **Müller, T.**, Weingartner, E., Areskoug, H., Fiebig, M., Yttri, K. E., Mihalopoulos, N., Kouvarakis, G., Beddows, D., Harrison, R. M., Cavalli, F., Putaud, J. P., **Spindler, G.**, **Wiedensohler, A.**, Alastuey, A., Pandolfi, M., Sellegri, K., Swietlicki, E., Jaffrezo, J. L., Baltensperger, U. and Laj, P. 2016. A European aerosol phenomenology 5: Climatology of black carbon optical properties at 9 regional

background sites across Europe. Atmos. Environ., **145**, 346-364. doi:10.1016/j.atmosenv.2016.09.035.

Zellner, R., **Herrmann, H.**, Wiesen, P. and Nehr, S. 2016. New and emerging technologies of societal relevance: Impact on air quality and climate. Chem. Ing. Tech., **88**, 1257-1258. doi:10.1002/cite.201650083.

Zhang, N., Geronimo, I., Paneth, P., **Schindelka, J.**, **Schaefer, T.**, **Herrmann, H.**, Vogt, C. and Richnow, H. H. 2016. Analyzing sites of OH radical attack (ring vs. side chain) in oxidation of substituted benzenes via dual stable isotope analysis ($\delta^{13}C$ and δ^2H). Sci. Total Environ., **542 (A)**, 484-494. doi:10.1016/j.scitotenv.2015.10.075.

Zhang, S. L., **Ma, N.**, **Kecorius, S.**, Wang, P. C., Hu, M., **Wang, Z. B.**, **Größ, J.**, Wu, Z. J. and **Wiedensohler, A.** 2016. Mixing state of atmospheric particles over the North China Plain. Atmos. Environ., **125**, 152-164. doi:10.1016/j.atmosenv.2015.10.053.

Zhang, Y., Wang, X., Wen, S., **Herrmann, H.**, Weiqiang, Y., Huang, X., Zhang, Z., Huang, Z., He, Q. and George, C. 2016. On-road vehicle emissions of glyoxal and methylglyoxal from tunnel tests in urban Guangzhou, China. Atmos. Environ., **127**, 55-60. doi:10.1016/j.atmosenv.2015.12.017.

Zhang, Y., Zhang, Q., Cheng, Y., Su, H., **Kecorius, S.**, **Wang, Z.**, **Wu, Z.**, Hu, M., Zhu, T., **Wiedensohler, A.** and He, K. 2016. Measuring the morphology and density of internally mixed black carbon with SP2 and VTDMA: New insight into the absorption enhancement of black carbon in the atmosphere. Atmos. Meas. Tech., **9**, 1833-1843. doi:10.5194/amt-9-1833-2016.

2017

Ansmann, A., **Rittmeister, F.**, **Engelmann, R.**, Basart, S., Benedetti, A., Spyrou, C., Remy, S., **Skupin, A.**, **Baars, H.**, **Seifert, P.**, **Senf, F.** and Kanitz, T. 2017. Profiling of Saharan dust from the Caribbean to West Africa – Part 2: Shipborne lidar measurements versus forecasts. Atmos. Chem. Phys., **17**, 14987-15006. doi:10.5194/acp-17-14987-2017.

Baars, H., **Seifert, P.**, **Engelmann, R.** and **Wandinger, U.** 2017. Target categorization of aerosol and clouds by continuous multiwavelength-polarization lidar measurements. Atmos. Meas. Tech., **10**, 3175-3201. doi:10.5194/amt-10-3175-2017.

Banks, J. R., Brindley, H. E., Stenchikov, G. and **Schepanski, K.** 2017. Satellite retrievals of dust aerosol over the Red Sea and the Persian Gulf (2005-2015). Atmos. Chem. Phys., **17**, 3987-4003. doi:10.5194/acp-17-3987-2017.

Barahona, D., Molod, A. and **Kalesse, H.** 2017. Direct estimation of the global distribution of vertical velocity within cirrus clouds. Sci. Rep., **7:6840**, 11. doi:10.1038/s41598-017-07038-6.

Baró, R., Palacios-Peña, L., Baklanov, A., Balzarini, A., Brunner, D., Forkel, R., Hirtl, M., Honzak, L., Pérez, J. L., Pirovano, G., San José, R., **Schröder, W.**, Werhahn, J., **Wolke, R.**, Zabkar, R. and Jiménez-Guerrero, P. 2017. Regional effects of atmospheric aerosols on temperature: An evaluation of an ensemble of online coupled models. Atmos. Chem. Phys. Discuss., **17**, 9677-9696. doi:10.5194/acp-17-9677-2017.

Berndt, T., **Herrmann, H.** and Kurten, T. 2017. Direct probing of Criegee intermediates from gas-phase ozonolysis using chemical ionization mass spectrometry. J. Amer. Chem. Soc., **139**, 13387-13392. doi:10.1021/jacs.7b05849.

Bley, S., **Deneke, H.**, **Senf, F.** and Scheck, L. 2017. Metrics for the evaluation of warm convective cloud fields in a large-eddy simulation with Meteosat images. Q. J. Roy. Meteor. Soc., **143**, 2050-2060. doi:10.1002/qj.3067.

Bozzetti, C., El Haddad, I., Salameh, D., Daellenbach, K. R., Fermo, P., Gonzalez, R., Minguillón, M. C., **Iinuma, Y.**, **Poulain, L.**, Elser, M., Müller, E., Slowik, J. G., Jaffrezo, J.-L., Baltensperger, U., Marchand, N. and Prévôt, A. S. H. 2017. Organic aerosol source apportionment by offline-AMS over a full year in Marseille. Atmos. Chem. Phys., **17**, 8247-8268. doi:10.5194/acp-17-8247-2017.

Brüggemann, M., **Poulain, L.**, Held, A., Stelzer, T., Zuth, C., **Richters, S.**, **Mutzel, A.**, **van Pinxteren, D.**, **Iinuma, Y.**, Katkevica, S., **Rabe, R.**, **Herrmann, H.** and Hoffmann, T. 2017. Real-time detection of highly oxidized organosulfates and BSOA marker compounds during the F–BEACh 2014 field study. Atmos. Chem. Phys., **17**, 1453-1469. doi:10.5194/acp-17-1453-2017.

Bühl, J., Alexander, S., Crewell, S., Heymsfield, A., **Kalesse, H.**, Khain, A., Maahn, M., van Tricht, K. and Wendisch, M. 2017. Chapter 10: Remote sensing. *In: Ice formation and evolution in clouds and precipitation : Measurement and modeling challenges*. AMS, p. 10.1-10.21 (Online: 4 April 2017). doi:10.1175/AMSMONOGRAPHS-D-16-0015.1. (AMS Meteorological Monographs).

Appendices: Publications

Burkert-Kohn, M., **Wex, H.**, **Welti, A.**, **Hartmann, S.**, **Grawe, S.**, **Hellner, L.**, **Herenz, P.**, Atkinson, J. D., **Stratmann, F.** and Kanji, Z. A. 2017. Leipzig ice nucleation chamber comparison (LINC): Intercomparison of ofur online ice nucleation counters. Atmos. Chem. Phys., **17**, 11683-11705. doi:10.5194/acp-17-11683-2017.

Burkholder, J. B., Abbatt, J. P. D., Barnes, I., Roberts, J. M., Melamed, M. L., Ammann, M., Bertram, A. K., Cappa, C. D., Carlton, A. G., Carpenter, L. J., Crowley, J. N., Dubowski, Y., Gerorge, C., Heard, D. E., **Herrmann, H.**, Keutsch, F. N., Kroll, J. H., McNeill, V. F., Ng, N. L., Nizkorodov, S. A., Orlando, J. J., Percival, C. J., Picquet-Varrault, B., Rudich, Y., Seakins, P. W., Surratt, J. D., Tanimoto, H., Thornton, J. A., Tong, Z., Tyndall, G. S., Wahner, A., Weschler, C. J., Wilson, K. R. and Ziemann, P. J. 2017. The essential role for laboratory studies in atmospheric chemistry. Environ. Sci. Technol., **51**, 2519-2528. doi:10.1021/acs.est.6b04947.

Chiloane, E. K., Beukes, J. P., van Zyl, P. G., Maritz, P., Vakkari, V., Josipovic, M., Venter, A. D., Jaars, K., Tiitta, P., Kulmala, M., **Wiedensohler, A.**, Liousse, C., Mkhatshwa, G. V., Ramandh, A. and Laakso, L. 2017. Spatial, temporal and source contribution assessments of black carbon over the northern interior of South Africa. Atmos. Chem. Phys., **17**, 6177-6196. doi:10.5194/acp-17-6177-2017.

Ciarelli, G., Aksoyoglu, S., El Haddad, I., Bruns, E. A., Crippa, M., **Poulain, L.**, Äijälä, M., Carbone, S., Freney, E., O'Dowd, C., Baltensperger, U. and Prévôt, A. S. H. 2017. Modelling winter organic aerosol at the European scale with CAMx: Evaluation and source apportionment with a VBS parameterization based on novel wood burning smog chamber experiments. Atmos. Chem. Phys., **17**, 7653-7669. doi:10.5194/acp-17-7653-2017.

Coluzza, I., Creamean, J., Rossi, M. J., **Wex, H.**, Alpert, P. A., Bianco, V., Boose, Y., Dellago, C., Felgitsch, L., Fröhlich-Nowoisky, J., **Herrmann, H.**, Jungblut, S., Kanji, Z. A., Menzl, G., Moffett, B., Moritz, C., **Mutzel, A.**, Pöschl, U., Schauperl, M., Scheel, J., Stopelli, E., **Stratmann, F.**, Grothe, H. and Schmale III, D. G. 2017. Perspectives on the future of ice nucleation research: Research needs and unanswered questions identified from two international workshops. Atmosphere, **8**, 28. doi:10.3390/atmos8080138.

Costa, A., Meyer, J., Afchine, M., Luebke, A., Günther, G., Dorsey, J. R., Gallagher, M. W., Ehrlich, A., Wendisch, M., Baumgardner, D., **Wex, H.** and Krämer, M. 2017. Classification of Arctic, mid-latitude and tropical clouds in the mixed-phase temperature regime. Atmos. Chem. Phys., **17**, 12219–12238. doi:10.5194/acp-17-12219-2017.

Costabile, F., **Alas, H.**, Aufderheide, M., Avino, P., Amato, F., Argentini, S., Barnaba, F., Berico, M., Bernardoni, V., Biondi, R., Calzolai, G., Canepari, S., Casasanta, G., Ciampichetti, S., Conidi, A., Cordelli, E., Di Ianni, A., Di Liberto, L., Facchini, M. C., Facci, A., Frasca, D., Gilardoni, S., Grollino, M. G., Gualtieri, M., Lucarelli, F., Malaguti, A., Manigrasso, M., Montagnoli, M., Nava, S., Padoan, E., Perrino, C., Petralia, E., Petenko, I., Querol, X., Simonetti, G., Tranfo, G., Ubertini, S., Valli, G., Valentini, S., Vecchi, R., Volpi, F., **Weinhold, K.**, **Wiedensohler, A.**, Zanini, G. and Gobbi, G. P. 2017. First results of the "Carbonaceous aerosol in Rome and environs (CARE)" experiment: Beyond current standards for PM_{10}. Atmosphere, **8**, 249 (41 pp.). doi:10.3390/atmos8120249.

Cziczo, D. J., Ladino, L., Boose, Y., Kanji, Z. A., Kupiszewski, P., Lance, S., **Mertes, S.** and **Wex, H.** 2017. Chapter 8: Measurements of ice nucleating particles and ice residuals. *In: Ice formation and evolution in clouds and precipitation : Measurement and modeling challenges*. AMS, p. 8.1-8.13. doi:10.1175/AMSMONOGRAPHS-D-16-0008.1. (AMS Meteorological Monographs ; 58).

Dipu, S., Quaas, J., **Wolke, R.**, **Stoll, J.**, Mühlbauer, A., Sourdeval, O., Salzmann, M., **Heinold, B.** and **Tegen, I.** 2017. Implementation of aerosol-cloud interactions in the regional atmosphere-aerosol model COSMO-MUSCAT(5.0) and evaluation using satellite data. Geosci. Model Dev., **10**, 2231-2246. doi:10.5194/gmd-10-2231-2017.

Ehn, M., **Berndt, T.**, Wildt, J. and Mentel, T. 2017. Highly osygenated molecules from atmospheric autoxidation of hydrocarbons: A prominent challenge for chemical kinetics studies. Int. J. Chem. Kinet., **49**, 821-831. doi:10.1002/kin.21130.

Engel, A., Bange, H. W., Cunliffe, M., Burrows, S. M., Friedrichs, G., Galgani, L., **Herrmann, H.**, Hertkorn, N., Johnson, M., Liss, P. S., Quinn, P. K., Schartau, M., Soloviev, A., Stolle, C., Upstill-Goddard, R., **van Pinxteren, M.** and Zäncker, B. 2017. The ocean's vital skin: Toward an integrated understanding of the sea surface microlayer. Front. Mar. Sci., **4**, 14. doi: 10.3389/fmars.2017.00165.

Falge, E., Köck, K., **Gatzsche, K.**, Voß, L., Schäfer, A., Berger, M., Dlugi, R., Pyles, R. D., Paw, U. K. T., Raabe, A. and Foken, T. 2017. Modelling of energy and matter exchange. *In: T. Foken (Ed.) Energy and matter fluxes of a spruce forest ecosystem*. Springer, Berlin, Heidelberg, p. 379-414. doi:10.1007/978-3-319-49389-3. (Ecological Studies (Analysis and Synthesis) ; 229).

Feuerstein, S. and **Schepanski, K.** 2017. Geomorphological and meteorological controls on the temporal

variability in dust source activation at Saharan dust-hot-spots. J. Geophys. Res. - Atmos., under review.

Field, P. R., Lawson, R. P., Brown, P. R. A., Lloyd, G., Westbrook, C., Moisseev, D., Miltenberger, A., Nenes, A., Blyth, A., Choularton, T., Connolly, P., **Buehl, J.**, Crosier, J., Cui, Z., Dearden, C., DeMott, P., Flossmann, A., Heymsfield, A., Huang, Y., **Kalesse, H.**, Kanji, Z. A., Korolev, A., Kirchgaessner, A., Lasher-Trapp, S., Leisner, T., McFarquhar, G., Phillips, V., Stith, J. and Sullivan, S. 2017. Chapter 7: Secondary ice production: Current state of the science and recommendations for the future. *In: Ice formation and evolution in clouds and precipitation : Measurement and modeling challenges.* AMS, p. 7.1-7.20 (Online: 6 April 2017). doi:10.1175/ AMSMONOGRAPHS-D-16-0014.1. (AMS Meteorological Monographs).

Filioglou, M., Nikandrova, A., Niemelä, S., **Baars, H.**, Mielonen, T., Leskinen, A., Brus, D., Romakkaniemi, S., Giannakaki, E. and Komppula, M. 2017. Profiling water vapor mixing ratios in Finland by means of a Raman lidar, a satellite and a model. Atmos. Meas. Tech., **10**, 4303-4316. doi:10.5194/amt-10-4303-2017.

Fomba, K. W., **van Pinxteren, D.**, **Müller, K.**, **Spindler, G.** and **Herrmann, H.** 2017. Assessment of trace metal levels in size-resolved particulate matter in the area of Leipzig. Atmos. Environ., **in press**, 26 pp.

Gatzsche, K., **Iinuma, Y.**, **Tilgner, A.**, **Mutzel, A.**, **Berndt, T.** and **Wolke, R.** 2017. Kinetic modeling studies of SOA formation from α-pinene ozonolysis. Atmos. Chem. Phys., **17**, 13187-13211. doi:10.5194/acp-2017-275.

Gouveia, D. A., Barja, B., Barbosa, H. M. J., **Seifert, P.**, **Baars, H.**, Pauliquevis, T. and Artaxo, P. 2017. Optical and geometrical properties of cirrus clouds in Amazonia derived from 1 year of ground-based lidar measurements. Atmos. Chem. Phys., **17**, 3619-3636. doi:10.5194/acp-17-3619-2017.

Gunsch, M. J., Kirpes, R. M., Kolesar, K. R., Barrett, T. E., China, S., Sheesley, R. J., Laskin, A., **Wiedensohler, A.**, **Tuch, T.** and Pratt, K. A. 2017. Contributions of transported Prudhoe Bay oil field emissions to the aerosol population in Utqiagvik, Alaska. Atmos. Chem. Phys., **17**, 10879-10892. doi:10.5194/acp-17-10879-2017.

Haapanala, P., Räisänen, P., McFarquhar, G. M., Tiira, J., **Macke, A.**, Kahnert, M., DeVore, J. and Nousiainen, T. 2017. Disk and circumsolar radiances in the presence of ice clouds. Atmos. Chem. Phys., **17**, 6865-6882. doi:10.5194/acp-17-6865-2017.

Haarig, M., **Ansmann, A.**, **Althausen, D.**, **Klepel, A.**, Groß, S., Freudenthaler, V., Toledano, C., Mamouri, R.-E., Farrell, D. A., Prescod, D. A., Marinou, E., Burton, S. P., Gasteiger, J., **Engelmann, R.** and **Baars, H.** 2017. Triple-wavelength depolarization-ratio profiling of Saharan dust over Barbados during SALTRACE in 2013 and 2014. Atmos. Chem. Phys., **17**, 10767-10794. doi:10.5194/acp-17-10767-2017.

Haarig, M., **Ansmann, A.**, Gasteiger, J., Kandler, K., **Althausen, D.**, **Baars, H.**, **Radenz, M.** and Farrell, D. A. 2017. Dry versus wet marine particle optical properties: RH dependence of depolarization ratio, backscatter, and extinction from multiwavelength lidar measurements during SALTRACE. Atmos. Chem. Phys., **17**, 14199-14217. doi:10.5194/acp-17-14199-2017.

Hama, S. M. L., **Ma, N.**, Cordell, R. L., Kos, G. P. A., **Wiedensohler, A.** and Monks, P. S. 2017. Lung deposited surface area in Leicester urban background site/UK: Sources and contribution of new particle formation. Atmos. Environ., **151**, 94-107. doi:10.1016/j.atmosenv.2016.12.002.

Heese, B., **Baars, H.**, **Bohlmann, S.**, **Althausen, D.** and Deng, R. 2017. Continuous vertical aerosol profiling with a multi-wavelength Raman polarization lidar over the Pearl River Delta, China. Atmos. Chem. Phys., **17**, 6679-6691. doi:10.5194/acp-17-6679-2017.

Heese, B., Böhm, C. and **Seifert, P.** 2017. *Automatic ceilometer-based backscatter coefficient retrieval - Improving network capabilities by combining ceilometer networks and AERONET.* EMS (European Meteorological Society) Annual Meetings, Dublin, Ireland, 4-8 September 2017. Adv. Sci. Res.

Heese, B., **Hofer, J.**, **Baars, H.**, **Engelmann, R.**, **Althausen, D.** and Schechner, Y. Y. 2017. *Wild fire aerosol optical properties measured by lidar at Haifa, Israel.* 28th International Laser Radar Conference (ILRC), Bucharest, Romania, 25-30 June 2017. EPJ Web of Conferences.

Heintzenberg, J., Tunved, P., Gali, M. and Leck, C. 2017. New particle formation in the Svalbard region 2006-2015. Atmos. Chem. Phys., **17**, 6153-6175. doi:10.5194/acp-17-6153-2017.

Hellmuth, O. 2017. Selected aspects of new particle formation in the earth atmosphere: Ion-mediated aerosol formation. Joint Institute for Nuclear Research (JINR), Dubna, 513 pp. (Nucleation theory and applications : Special issues. Review series on selected topics of atmospheric sol formation ; Vol. 4).

Hofer, J., **Althausen, D.**, Abdullaev, S. F., Makhmudov, A. N., Nazarov, B. I., Schettler, G., **Engelmann, R.**, **Baars, H.**, **Fomba, K. W.**, **Müller, K.**, **Heinold, B.**, Kandler, K. and **Ansmann, A.** 2017. Long-term profiling of mineral dust and pollution aerosol with multiwavelength polarization Raman lidar at the Central Asian site of Dushanbe, Tajikistan : Case studies. Atmos. Chem. Phys., **17**, 14559-14577. doi:10.5194/acp-17-14559-2017.

Appendices: Publications

Horváth, Á., Hautecoeur, A., Borde, R., **Deneke, H.** and Buehler, S. A. 2017. Evaluation of the EUMETSAT global AVHRR wind product. J. Appl. Meteorol. Clim., **56**, 2353-2376. doi:0.1175/JAMC-D-17-0059.1.

Huang, S., <u>Poulain, L.</u>, **van Pinxteren, D.**, **van Pinxteren, M.**, **Wu, Z.**, **Herrmann, H.** and **Wiedensohler, A.** 2017. Latitudinal and seasonal distribution of particulate MSA over the Atlantic using a validated quantification method with HR-ToF-AMS. Environ. Sci. Technol., **51**, 418-426. doi:10.1021/acs.est.6b03186.

Janicka, L., Stachlewska, I. S., Veselovskii, I. and **Baars, H.** 2017. Temporal variations in optical and microphysical properties of mineral dust and biomass burning aerosol derived from daytime Raman lidar observations over Warsaw, Poland. Atmos. Environ., **169**, 162-174. doi:10.1016/j.atmosenv.2017.09.022.

Kanji, Z. A., Ladino, L. A., **Wex, H.**, Boose, Y., Burkert-Kohn, M., Cziczo, D. J. and Krämer, M. 2017. Chapter 1: Overview of ice nucleating particles. *In: Ice formation and evolution in clouds and precipitation: Measurement and modeling challenges*. AMS, Boston, p. 1.1-1.33. doi:10.1175/AMSMONOGRAPHS-D-16-0006.1. (AMS Meteorological Monographs ; 58).

Kecorius, S., **Ma, N.**, **Teich, M.**, **van Pinxteren, D.**, Zhang, S., **Größ, J.**, **Spindler, G.**, **Müller, K.**, **Iinuma, Y.**, Hu, M., **Herrmann, H.** and **Wiedensohler, A.** 2017. Influence of biomass burning on mixing state of sub-micron aerosol particles in the North China Plain. Atmos. Environ., **164**, 259-269. doi:10.1016/j.atmosenv.2017.05.023.

Kecorius, S., Madueño, L., Vallar, E., **Alas, H.**, Betito, G., **Birmili, W.**, Cambaliza, M. O., Catipay, G., Gonzaga-Cayetano, M., Galvez, M. C., Lorenzo, G., **Müller, T.**, Simpas, J. B., Tamayo, E. G. and **Wiedensohler, A.** 2017. Aerosol particle mixing state, refractory particle number size distributions and emission factors in a polluted urban environment: Case study of Metro Manila, Philippines. Atmos. Environ., **170**, 169-183. doi:10.1016/j.atmosenv.2017.09.037.

Knippertz, P., Hamza, I., Kassimou, A., Laurent, B., Orji, B. N., Osika, D. P., **Schepanski, K.**, **Tegen, I.** and Fink, A. 2017. Dust. *In: D. J. Parker and M. Diop-Kane (Eds.), Meteorology of tropical West Africa: The forecasters' handbook*. John Wiley & Sons, Hoboken, p. 175-203. doi:10.1002/9781118391297.

Kolesar, K. R., Cellini, J., Peterson, P. K., Jefferson, A., **Tuch, T.**, **Birmili, W.**, **Wiedensohler, A.** and Pratt, K. A. 2017. Effect of Prudhoe Bay emissions on atmospheric aerosol growth events observed in Utqiaġvik (Barrow), Alaska. Atmos. Environ., **152**, 146-155. doi:10.1016/j.atmosenv.2016.12.019.

Kuang, Y., Zhao, C., Tao, J., Bian, Y., **Ma, N.** and Zhao, G. 2017. A novel method for deriving the aerosol hygroscopicity parameter based only on measurements from a humidified nephelometer system. Atmos. Chem. Phys., **17**, 6651-6662. doi:10.5194/acp-17-6651-2017.

Li, J., Wang, X., Chen, J., Zhu, C., Li, W., Li, C., Liu, L., Xu, C., Wen, L., Xue, L., Wang, W., Ding, A. and **Herrmann, H.** 2017. Chemical composition and droplet size distribution of cloud at the summit of Mount Tai, China. Atmos. Chem. Phys., **17**, 9885-9896. doi:10.5194/acp-17-9885-2017.

Macke, A., **Seifert, P.**, **Baars, H.**, Barthlott, C., Beekmans, C., Behrendt, A., Bohn, B., Brueck, M., **Bühl, J.**, Crewell, S., Damian, T., **Deneke, H.**, **Düsing, S.**, Foth, A., Di Girolamo, P., Hammann, E., Heinze, R., Hirsikko, A., **Kalisch, J.**, Kalthoff, N., Kinne, S., Kohler, M., Löhnert, U., **Madhavan, B. L.**, Maurer, V., Muppa, S. K., Schween, J., Serikov, I., **Siebert, H.**, Simmer, C., Späth, F., Steinke, S., Träumner, K., Trömel, S., **Wehner, B.**, Wieser, A., Wulfmeyer, V. and Xie, X. 2017. The HD(CP)[2] Observational Prototype Experiment HOPE – An Overview. Atmos. Chem. Phys., **17**, 4887-4914. doi:10.5194/acp-17-4887-2017.

Madhavan, B. L., **Deneke, H.**, **Witthuhn, J.** and **Macke, A.** 2017. Multiresolution analysis of the spatiotemporal variability in global radiation observed by a dense network of 99 pyranometers. Atmos. Chem. Phys., **17**, 3317-3338. doi:10.5194/acp-17-3317-2017.

Marinou, E., Amiridis, V., Binietoglou, I., Tsikerdekis, A., Solomos, S., Proestakis, E., Konsta, D., Papagiannopoulos, N., Tsekeri, A., Viastou, G., Zanis, P., Balis, D., **Wandinger, U.** and **Ansmann, A.** 2017. Three-dimensional evolution of Saharan dust transport towards Europe based on a 9-year EARLINET-optimized CALIPSO dataset. Atmos. Chem. Phys., **17**, 5893-5919. doi:10.5194/acp-17-5893-2017.

Martinsson, B. G., Friberg, J., Sandvik, O. S., **Hermann, M.**, van Velthoven, P. J. F. and Zahn, A. 2017. Particulate sulfur in the upper troposphere and lowermost stratosphere - sources and climate forcing. Atmos. Chem. Phys., **17**, 10937-10953. doi:10.5194/acp-17-10937-2017.

Mu, Q., Lammel, G., Gencarelli, C. N., Hedgecock, I. M., **Chen, Y.**, Přibylová, P., **Teich, M.**, Zhang, Y., Zheng, G., **van Pinxteren, D.**, Zhang, Q., **Herrmann, H.**, Shiraiwa, M., Spichtinger, P., Su, H., Pöschl, U. and Cheng, Y. 2017. Regional modelling of polycyclic aromatic hydrocarbons: WRF-Chem-PAH model development and East Asia case studies. Atmos. Chem. Phys., **17**, 12253-12267. doi:10.5194/acp-17-12253-2017.

Nehr, S., Borowiak, A., **Herrmann, H.**, Wiesen, P. and Zellner, R. 2017. New and emerging technologies of societal

relevance: Impact on air quality and climate: 3rd VDI/DECHEMA/GDCh Expert Forum on Atmospheric Chemistry (EFAC 3). Gefahrst. Reinhalt. L., **77**, 15-18.

Ng, N. L., Brown, S. S., Archibald, A. T., Atlas, E., Cohen, R. C., Crowley, J. N., Day, D. A., Donahue, N. M., Fry, J. L., Fuchs, H., Griffin, R. J., Guzman, M. I., **Herrmann, H.**, Hodzic, A., **Iinuma, Y.**, Jimenez, J. L., Kiendler-Scharr, A., Lee, B. H., Luecken, D. J., Mao, J., McLaren, R., **Mutzel, A.**, Osthoff, H. D., Ouyang, B., Picquet-Varrault, B., Platt, U., Pye, H. O. T., Rudich, Y., Schwantes, R. H., Shiraiwa, M., Stutz, J., Thornton, J. A., **Tilgner, A.**, Williams, B. J. and Zaveri, R. A. 2017. Nitrate radicals and biogenic volatile organic compounds: Oxidation, mechanisms, and organic aerosol. Atmos. Chem. Phys., **17**, 2103-2162. doi:10.5194/acp-17-2103-2017.

Ortiz-Amezcua, P., Guerrero-Rascado, J. L., Granados Muñoz, M. J., Benavent-Oltra, J. A., Böckmann, C., Samaras, S., Stachlewska, I. S., Janicka, L., **Baars, H.**, **Bohlmann, S.** and Alados-Arboledas, L. 2017. Microphysical characterization of long-range transported biomass burning particles from North America at three EARLINET stations. Atmos. Chem. Phys., **17**, 5931-5946. doi:10.5194/acp-17-5931-2017.

Otto, T., **Stieger, B.**, **Mettke, P.** and **Herrmann, H.** 2017. Tropospheric aqueous-phase oxidation of isoprene-derived dihydroxycarbonyl compounds. J. Phys. Chem. A, **121**, 6460-6470. doi:10.1021/acs.jpca.7b05879.

Paukert, M., Hoose, C. and **Simmel, M.** 2017. Redistribution of ice nuclei between cloud and rain droplets: Parameterization and application to deep convective clouds. J. Adv. Model. Earth Syst., **9**, 514-535. doi:10.1002/2016MS000841.

Reddington, C. L., Carslaw, K. S., Stier, P., Schutgens, N., Coe, H., Liu, D., Allan, J., Browse, J., Pringle, K. J., Lee, L. A., Yoshioka, K., Johnson, J. S., Regayre, L. A., Spracklen, D. V., Mann, G. W., Clarke, A., **Hermann, M.**, **Henning, S.**, **Wex, H.**, **Kristensen, T.**, Leaitch, R., Pöschl, U., Rose, D., Andreae, M. O., Schmale, J., Kondo, Y., Oshima, N., Schwarz, J. P., Nenes, A., Anderson, B., Roberts, G. C., Snider, J. R., Leck, C., Quinn, P. K., Chi, X., Ding, A., Jimenez, J. L. and Zhang, Q. 2017. The Global Aerosol Synthesis and Science Project (GASSP): Measurements and modelling to reduce uncertainty. Bull. Amer. Meteor. Soc., **98**, 1857-1877. doi:10.1175/BAMS-D-15-00317.1.

Rempel, M., **Senf, F.** and **Deneke, H.** 2017. Object-based metrics for forecast verification of convective development with geostationary satellite data. Mon. Wea. Rev., **145**, 3161-3178.

Richters, S., Pfeifle, M., Olzmann, M. and **Berndt, T.** 2017. *endo*-Cyclization of unsaturated RO_2 radicals from the gas-phase ozonolysis of cyclohexadienes. Chem. Commun., **53**, 4132-4135. doi:10.1039/c7cc01350g.

Rittmeister, F., **Ansmann, A.**, **Engelmann, R.**, **Skupin, A.**, **Baars, H.**, Kanitz, T. and Kinne, S. 2017. Profiling of Saharan dust from the Caribbean to western Africa – Part 1: Layering structures and optical properties from shipborne polarization/Raman lidar observations. Atmos. Chem. Phys., **17**, 12963-12983. doi:10.5194/acp-17-12963-2017.

Rodigast, M., **Mutzel, A.** and **Herrmann, H.** 2017. A quantification method for heat-decomposable methylglyoxal oligomers and its application on 1,3,5-trimethylbenzene SOA. Atmos. Chem. Phys., **17**, 3929-3943. doi:10.5194/acp-17-3929-2017.

Rose, C., Sellegri, K., Moreno, I., Velarde, F., Ramonet, M., **Weinhold, K.**, Krejci, R., Andrade, M., **Wiedensohler, A.**, Ginot, P. and Laj, P. 2017. CCN production by new particle formation in the free troposphere. Atmos. Chem. Phys., **17**, 1529-1541. doi:10.5194/acp-17-1529-2017.

Schepanski, K., **Heinold, B.** and **Tegen, I.** 2017. Harmattan, Saharan heat low and West African Monsoon circulation: Modulations on the Saharan dust outflow towards the North Atlantic. Atmos. Chem. Phys., **17**, 10223-10243. doi:10.5194/acp-17-10223-2017.

Schmelzer, J. W. P. and **Hellmuth, O.** (Eds.) 2017. Review series on selected topics of atmospheric sol formation: Volume 4 : Selected aspects of new particle formation in the earth atmosphere: Ion-mediated aerosol formation, viii, 456 pp., Joint Institute for Nuclear Research (JINR), Dubna. (Nucleation theory and applications : Special issues).

Schmidt, S., Schneider, J., Klimach, T., **Mertes, S.**, **Schenk, L. P.**, Kupiszewski, P., Curtius, J. and Borrmann, S. 2017. Online single particle analysis of ice particle residuals from mountain-top mixed-phase clouds using laboratory derived particle type assignment. Atmos. Chem. Phys., **17**, 575-594. doi:10.5194/acp-17-575-2017.

Schneider, J., **Mertes, S.**, **van Pinxteren, D.**, **Herrmann, H.** and Borrmann, S. 2017. Uptake of nitric acid, ammonia, and organics in orographic clouds: Mass spectrometric analyses of droplet residual and interstitial aerosol particles. Atmos. Chem. Phys., **17**, 1571-1593. doi:10.5194/acp-17-1571-2017.

Appendices: Publications

Schrod, J., Weber, D., Drücke, J., Keleshis, C., Pikridas, M., Ebert, M., Cvetkovic, B., Nickovic, S., Marinou, E., **Baars, H.**, **Ansmann, A.**, Vrekoussis, M., Mihalopoulos, N., Sciare, J., Curtius, J. and Bingemer, H. G. 2017. Ice nucleating particles over the Eastern Mediterranean measured by unmanned aircraft systems. Atmos. Chem. Phys., **17**, 4817-4835. doi:10.5194/acp-17-4817-2017.

Senf, F. and **Deneke, H.** 2017. Uncertainties in synthetic Meteosat SEVIRI infrared brightness temperatures in the presence of cirrus clouds and implications for evaluation of cloud microphysics. Atmos. Res., **183**, 113-129. doi:10.1016/j.atmosres.2016.08.012.

Senf, F. and **Deneke, H.** 2017. Satellite-based characterization of convective growth and glaciation properties in relation to precipitation formation over Central Europe. J. Appl. Meteorol. Clim., **56**, 1827-1845.

Soleimani, B., **Knoth, O.** and Weiner, R. 2017. IMEX peer methods for fast-wave-slow-wave problems. Appl. Numer. Math., **118**, 221-237. 10.1016/j.apnum.2017.02.016.

Spranger, T., **van Pinxteren, D.** and **Herrmann, H.** 2017. Two-dimensional offline chromatographic fractionation for the characterization of humic-like substances in atmospheric aerosol particles. Environ. Sci. Technol., 5061-5070. doi:10.1021/acs.est.7b00077.

Stachlewska, I. S., Zawadsza, O. and **Engelmann, R.** 2017. Effect of heat wave conditions on aerosol optical properties derived from satellite and ground-based remote sensing over Poland. Remote Sens., **9**, 1199. doi:10.3390/rs9111199.

Stieger, B., **Spindler, G.**, Fahlbusch, B., **Müller, K.**, **Grüner, A.**, **Poulain, L.**, Thöni, L., Seitler, E., Wallasch, M. and **Herrmann, H.** 2017. Measurements of PM_{10} ions and trace gases with the online system MARGA at the research station Melpitz in Germany: A five-year study. J. Atmos. Chem., 38 pp. doi:10.1007/s10874-017-9361-0.

Teich, M., **van Pinxteren, D.**, Wang, M., **Kecorius, S.**, **Wang, Z.**, **Müller, T.**, Močnik, G. and **Herrmann, H.** 2017. Contributions of nitrated aromatic compounds to the light absorption of water-soluble and particulate brown carbon in different atmospheric environments in Germany and China. Atmos. Chem. Phys., **17**, 1653-1672. doi:10.5194/acp-17-1653-2017.

Thorenz, U. R., Baker, A. K., Leedham Elvidge, E. C., Sauvage, C., Riede, H., van Velthoven, P. F. J., **Hermann, M.**, **Weigelt, A.**, Oram, D. E., Brenninkmeijer, C. A. M., Zahn, A. and Williams, J. 2017. Investigating African trace gas sources, vertical transport, and oxidation using IAGOS-CARIBIC measurements between Germany and South Africa between 2009 and 2011. Atmos. Environ., **158**, 11-26. doi:10.1016/j.atmosenv.2017.03.021.

Tsekeri, A., Lopatin, A., Amiridis, V., Marinou, E., **Igloffstein, J.**, Siomos, N., Solomos, S., Kokkalis, P., **Engelmann, R.**, **Baars, H.**, Gratsea, M., Raptis, P. I., Binietoglou, I., Mihalopoulos, N., Kalivitis, N., Kouvarakis, G., Bartsotas, N., Kallos, G., Basart, S., Schuettemeyer, D., **Wandinger, U.**, **Ansmann, A.**, Chaikovsky, A. P. and Dubovik, O. 2017. GARRLiC and LIRIC: Strengths and limitations for the characterization of dust and marine particles along with their mixtures. Atmos. Meas. Tech., **10**, 4995-5016. doi:10.5194/amt-10-4995-2017.

van Pinxteren, M., **Barthel, S.**, **Fomba, K. W.**, **Müller, K.**, von Tümpling, W. and **Herrmann, H.** 2017. The influence of environmental drivers on the enrichment of organic carbon in the sea surface microlayer and in submicron aerosol particles - measurements from the Atlantic Ocean. Elem. Sci. Anth., **5**, 21. doi:10.1525/elementa.225.

Wang, S., Wu, R., **Berndt, T.**, Ehn, M. and Wang, L. 2017. Formation of highly oxidized radicals and multifunctional products from the atmospheric oxidation of alkylbenzenes. Environ. Sci. Technol., **51**, 8442-8449. doi:0.1021/acs.est.7b02374.

Wang, Z., **Birmili, W.**, **Hamed, A.**, **Wehner, B.**, **Spindler, G.**, Pei, X., Wu, Z., Cheng, Y., Su, H. and **Wiedensohler, A.** 2017. Contributions of volatile and nonvolatile compounds (at 300°C) to condensational growth of atmospheric nanoparticles: An assessment based on 8.5 years of observations at the Central Europe background site Melpitz. J. Geophys. Res. - Atmos., **122**, 485-497. doi:10.1002/2016JD025581.

Weinzierl, B., **Ansmann, A.**, Prospero, J. M., **Althausen, D.**, Benker, N., Chouza, F., Dollner, M., Farrell, D., **Fomba, K. W.**, Freudenthaler, V., Gasteiger, J., Groß, S., **Haarig, M.**, **Heinold, B.**, Kandler, K., Kristensen, T. B., Mayol-Bracero, O. L., **Müller, T.**, Reitebuch, O., Sauer, D., Schäfler, A., **Schepanski, K.**, Spanu, A., **Tegen, I.**, Toledano, C. and Walser, A. 2017. The Saharan aerosol long-range transport and aerosol-cloud-interaction experiment: Overview and selected highlights. Bull. Amer. Meteor. Soc., **98**, 1427-1451. doi:10.1175/BAMS-D-15-00142.1.

Wendisch, M., Brückner, M., Burrows, J. P., Crewell, S., Dethloff, K., Ebell, K., Lüpkes, C., **Macke, A.**, Notholt, J., Quaas, J., Rinke, A. and **Tegen, I.** 2017. Understanding causes and effects of rapid warming in the Arctic. Eos, **98**, doi:10.1029/2017EO064803.

Wiedensohler, A., **Wiesner, A.**, **Weinhold, K.**, **Birmili, W.**, **Hermann, M.**, **Merkel, M.**, **Müller, T.**, **Pfeifer, S.**, **Schmidt, A.**, **Tuch, T.**, **Velarde, F.**, Quincey, P., Seeger, S. and Nowak, A. 2017. Mobility particle size spectrometers : Calibration procedures and measurement uncertainties. Aerosol Sci. Technol., Online first: 11 October 2017 (19 p.). doi:10.1080/02786826.2017.1387229.

Witthuhn, J., **Deneke, H.**, **Macke, A.** and Bernhard, G. 2017. Algorithms and uncertainties for the determination of multispectral irradiance components and aerosol optical depth from a shipborne rotating shadowband radiometer. Atmos. Meas. Tech., **10**, 709-730. doi:10.5194/amt-10-709-2017.

Wu, Z. J., **Ma, N.**, **Größ, J.**, **Kecorius, S.**, Lu, K. D., Shang, D. J., Wang, Y., Wu, Y. S., Zeng, L. M., Hu, M., **Wiedensohler, A.** and Zhang, Y. H. 2017. Thermodynamic properties of nanoparticles during new particle formation events in the atmosphere of North China Plain. Atmos. Res., **188**, 55-63. doi:10.1016/j.atmosres.2017.01.007.

Zerefos, C. S., Eleftheratos, K., Kapsomenakis, J., Solomos, S., Inness, A., Balis, D., Redondas, A., Eskes, H., Allaart, M., Amiridis, V., Dahlback, A., De Bock, V., Diémoz, H., **Engelmann, R.**, Eriksen, P., Fioletov, V., Gröbner, J., Heikkilä, A., Petropavlovskikh, I., Jarosławski, J., Josefsson, W., Karppinen, T., Köhler, U., Meleti, C., Repapis, C., Rimmer, J., Savinykh, V., Shirotov, V., Siani, A. M., Smedley, A. R. D., Stanek, M. and Stübi, R. 2017. Detecting volcanic sulfur dioxide plumes in the Northern Hemisphere using the Brewer spectrophotometers, other networks, and satellite observations. Atmos. Chem. Phys., **11**, 551-574. doi:10.5194/acp-17-551-2017.

Zielhofer, C., von Suchodoletz, H., Fletcher, W., Schneider, B., Dietze, E., Schlegel, M., **Schepanski, K.**, Weninger, B., Mischke, S. and Mikdad, A. 2017. Millennial-scale fluctuations in Saharan dust supply across the decline of the African Humid Period. Quat. Sci. Rev., **171**, 119-135. doi:10.1016/j.quascirev.2017.07.010.

Appendices: University courses

University courses

Lecturer	Course	WS 2015/ 2016	SS 2016	WS 2016/ 2017	SS 2017	WS 2017/ 2018
Ansmann, A. Althausen, D. Seifert, P. Engelmann, R.	Active Remote Measurement in Atmospheric Research (2sh) Seminar Active Remote Sensing (2 sh)	x x		x x		
Fomba, K. W.	Atmospheric and Marine Sciences Summer School, UniCv, Cape Verde, October 16-18, 2017					x
Herrmann, H.	Basic Atmospheric Chemistry + Exercises (3 sh) Atmospheric Chemistry + Exercises (3 sh) Atmospheric Chemistry Seminar (1 sh) Atmospheric Chemistry Lab course (1 sh)	x x x x	x x x	x x x x	x x x	x x x x
	The Third Sino-European School on Atmospheric Chemistry (SESAC), November 21-30, 2017	x				x
	Atmospheric and Marine Sciences Summer School, Praia, Cape Verdes, October 16-18, 2017				x	
Kalesse, H. Haarig, M.	NoSoaT-Training School (North South Atlantic Training Transect), on board Polarstern Expedition PS102, November 16 - December 13, 2016			x		
Macke, A.	Atmospheric Radiation (1 sh)		x		x	
Macke, A. Deneke, H.	Satellite Remote Sensing + Exercises (2 sh)		x			
Macke, A. Stratmann, F.	Cloud Physics + Exercises (3 sh)		x			
Mutzel, A.	Advanced study Analytics and Spektroscopy		x		x	
Schepanski, K.	Dust in the Atmosphere (2sh) Dust in the Atmosphere Seminar (1sh)			x x		x x
	Identification and characterisation of dust sources using satellite observations and model simulations (EuMetTrain EnviWeek)		x			
Siebert, H.	Advanced Training Module of the Leipzig Graduate School on Clouds, Aerosols and Radiation (LGS-CAR) "Cloud droplet concentration", October 17-18, 2016, title: "In situ observations"			x		

Lecturer	Course	WS 2015/ 2016	SS 2016	WS 2016/ 2017	SS 2017	WS 2017/ 2018
Stratmann, F.	Advanced Training Module of the Leipzig Graduate School on Clouds, Aerosols and Radiation (LGS-CAR) "Cloud microphysics measurements", February 24-25, 2017			x		
Tegen, I.	Modeling of Atmospheric Trace Substances (2 sh) Seminar Modeling of Atmospheric Trace Substances (1 sh)	x x	x	x x		x x
	Modelling of the Atmosphere (2sh)		x		x	
	Basics of Mesoscale Model Simulations + Exercises (3 sh)		x		x	
	Contribution to Module SQ15 'Energy and Environment', University of Leipzig: "Transport of atmospheric pollutants"			x		x
Wandinger, U.	Scattering and Atmospheric Optics (2 sh) Seminar Applied Scattering Theory (1 sh)		x x			
Wiedensohler, A. Stratmann, F. Hermann, M. Müller, T.	Atmospheric Aerosols (2 sh) Master Seminar Atmospheric Aerosols (1 sh)	x x		x x		x x
	Atmospheric Aerosols (2 sh) Bachelor Seminar Atmospheric Aerosols (1 sh)		x x			
Wiedensohler, A.	12th Summer School on Atmospheric Aerosol Physics, Measurement, and Sampling Hyytiälä, Finland, May 20 - 27, 2016		x		x	
	12th Summer School on Atmospheric Aerosol Physics, Measurement, and Sampling Chennai, India, February 14 - 25, 2016	x				
	12th Summer School on Atmospheric Aerosol Physics, Measurement, and Sampling Schneefernerhaus, Germany, April 03 - 08, 2016		x			x
van Pinxteren, M.	Guest lecture: Analysis and Spectroscopy: Gas Chromatography, Lecture in an one week course			x		x
Wex, H.	Advanced Training Module of the Leipzig Graduate School on Clouds, Aerosols and Radiation (LGS-CAR) "Cloud droplet concentration", October 17-18, 2016, title: "Köhler theory, droplet activation and lab studies"			x		

Appendices: Academic degrees

Academic degrees

Completed academic qualifications 2016/2017

Academic degree*	Name	Title	Faculty	Year
Ph. D.	Barlakas, V.	A new three-dimensional vector radiative transfer model and applications to Saharan dust fields	University of Leipzig, Faculty of Physics and Earth Sciences	2016
	Barthel, S.	Regionale Modellstudien zur Untersuchung von Emissionsparametrisierungen des primären marinen Aerosols	University of Leipzig, Faculty of Physics and Earth Sciences	2016
	Bauditz S.	Immersion freezing experiments of biological, mineral dust and dust-bio-mixed particles with the Leipzig Aerosol Cloud Interaction Simulator	University of Leipzig, Faculty of Physics and Earth Sciences	2017
	Bley, S.	Investigation of warm convective cloud fields with Meteosat observations and high resolution models	University of Leipzig, Faculty of Physics and Earth Sciences	2017
	Chen, Y.	Evaluation and improvement of particle number / mass size distribution modelling in WRF-Cem over Europe	University of Leipzig, Faculty of Physics and Earth Sciences	2017
	Foth, A.	Optimal estimation of water vapour profiles using a combination of Raman lidar and microwave radiometer	University of Leipzig, Faculty of Physics and Earth Sciences	2017
	Huang, S.	Chemical composition of the submicrometer aerosol over the Atlantic Ocean	University of Leipzig, Faculty of Physics and Earth Sciences	2016
	Jähn, M.	Large eddy simulation studies of Island effects in the Caribbean trade wind region	University of Leipzig, Faculty of Physics and Earth Sciences	2016
	Merk, D.	Uncertainties in the quantification of aerosol-cloud interactions	University of Leipzig, Faculty of Physics and Earth Sciences	2017
	Mothes, F.	Labor- und Felduntersuchungen zu den Auswirkungen photokatalytisch aktiver Materialien auf die urbane Luftqualität	University of Leipzig, Faculty of Chemistry and Mineralogy	2017
	Myagkov, A.	Shape-temperature relationship of ice crystals in mixed-phase clouds based on observations with polarimetric cloud radar	University of Leipzig, Faculty of Physics and Earth Sciences	2016

Academic degree*	Name	Title	Faculty	Year
Ph. D.	Richters, S.	A kinetic and mechanistic investigation of the gas-phasee ozonolysis of four sesquiterpenes	University of Leipzig, Faculty of Chemistry and Mineralogy	2016
	Rodigast, M.	The role of methylglyoxal from aromatics oxidation in aqSOA formation	University of Leipzig, Faculty of Chemistry and Mineralogy	2016
	Schindelka, J.	Aerosolkammer- und Flüssigphasenuntersuchungen zur Oxidation von Isopren im troposphärischen Multiphasensystem	University of Leipzig, Faculty of Chemistry and Mineralogy	2016
	Schrödner, R.	Modeling the tropospheric multiphase aerosol-cloud processing using the 3-D chemistry transport model COSMO-MUSCAT	University of Leipzig, Faculty of Physics and Earth Sciences	2016
	Schwarz, A.	Aerosol typing over Europe and its benefits for the CALIPSO and EarthCARE missions : Statistical analysis based on multiwavelength aerosol lidar measurements from ground-based EARLINET stations and comparison to spaceborne CALIPSO data	University of Leipzig, Faculty of Physics and Earth Sciences	2016
	Teich, M.	Imidazoles and nitrated aromatic compounds as constituents of light-absorbing brown carbon in atmospheric particles: Analytical developments, ambient concentrations and impact on particle optical properties	University of Leipzig, Faculty of Chemistry and Mineralogy	2017
M.Sc.	Bergmann, D.	Über den Einfluss von Konvektion auf die bodennahe Größenverteilung von Aerosolpartikeln in Deutschland	Technical University Dresden, Institute of Geography	2017
	Bohlmann, S.	Aerosol profiling with lidar over the Atlantic Ocean during meridional Polarstern cruises	University of Leipzig, Faculty of Physics and Earth Sciences	2017
	Faust, M.	Entwicklung eines Lagrangeschen Partikeldispersionsmodells zur Identifizierung von Geruchsquellen im Erzgebirge	University of Leipzig, Faculty of Physics and Earth Sciences	2017
	Felber, T.	Kinetische Untersuchungen von Imidazolen in der troposphärischen Flüssigphasenchemie	University of Leipzig, Faculty of Chemistry and Mineralogy	2016

Appendices: Academic degrees

Academic degree*	Name	Title	Faculty	Year
M.Sc.	Griesche, H.	Evaluation of the effect of mineral dust aerosol on the forecast skill of numerical weather prediction models based on remote sensing observations	University of Leipzig, Faculty of Physics and Earth Sciences	2016
	Kaduk, C.	Characterization of the optical properties of complex aerosol mixtures observed with a multiwavelength-Raman-polarization lidar during the 6-weeks BACCUS campaign in Cyprus in spring 2015	University of Leipzig, Faculty of Physics and Earth Sciences	2017
	Luttkus, M. L.	Einfluss biogener Emissionen auf die Bildung von sekundärem organischem Aerosol (SOA)	University of Leipzig, Faculty of Physics and Earth Sciences	2017
	Müller, M.	Optimierung von verallgemeinerten Split-Explizit-Runge-Kutta-Verfahren für die numerische Wettervorhersage	University of Engineering, Economics and Culture in Leipzig, Fakulty for Computer Sciences, Mathematics and Natural Sciences	2016
	Radenz, M.	Observation of in-cloud vertical air motion with a combination of Doppler lidar, cloud radar and radar wind profiler - Results of the COLRAWI campaign	University of Leipzig, Faculty of Physics and Earth Sciences	2017
	Rörup, B.	Analysis of airborne black carbon measurements with the micro-Aethalometer AE51	University of Leipzig, Faculty of Physics and Earth Sciences	2017
	Schimmel, W.	Numerische Simulation auf die Bildung von sekundärem organischem Aerosol (SOA)	University of Engineering, Economics and Culture in Leipzig, Fakulty for Computer Sciences, Mathematics and Natural Sciences	2017
	Tatzelt, Ch.	Characerication of weather states over Germany using cloud-typing and textural features from satellite remote sensing	University of Leipzig, Faculty of Physics and Earth Sciences	2017
	Ulrich, M.	Interactions of mineral Dust and tropical Storms on the North Atlantic	University of Leipzig, Faculty of Physics and Earth Sciences	2017
	Villanueva Ortiz, D.	Atmospheric spreading of infectious diseases: Legionnaires' disease outbreaks within Europe, atmospheric-dispersion models and mesoscale circulation systems	University of Leipzig, Faculty of Physics and Earth Sciences	2017

Academic degree*	Name	Title	Faculty	Year
B.Sc.	Enderich, L.	Comparison of measurement techniques to determine the particle absorption coefficient during a field campaign on Cyprus	University of Leipzig, Faculty of Physics and Earth Sciences	2017
	Urbanneck, C.	Berücksichtigung von Eisflächen in LES-Modellen zur Simulation arktischer Grenzschichten	University of Leipzig, Faculty of Physics and Earth Sciences	2016

* Habil.: Habilitation, Ph. D.: Doctoral theses, Dipl.: Diploma, M.Sc.: Master of Science, B.Sc.: Bachelor of Science

Summary of completed academic qualifications

Academical degrees	Number		Total
	2016	**2017**	
Habilitation	0	0	0
Doctoral theses	10	7	17
Master of Science	3	11	14
Bachelor of science	1	1	2

Awards

Name	Prize	Awarding institution	Comments/Description
A. Wiedensohler	Highly Cited Researcher 2016	Thomsen Reuters	Highly Cited Researchers represents the world's leading scientific minds. Over three thousand researchers earned the distinction by writing the greatest numbers of reports officially designated by Essential Science Indicators[SM] as Highly Cited Papers
J. Hofer	6. Best Student Papers at the OSA Light, Energy and the Environment Congress in Leipzig, Germany, 2016	The Optical Society (OSA), Energy Congress 2016	Title: "Lidars in Dust and Aerosol Observation, Optical Instrumentation for Energy & Environmental Applications"

Appendices: Awards

Name	Prize	Awarding institution	Comments/Description
M. Haarig	The ILCR 28th Prize for the Best Student Oral Presentation 2017	ILRC 28 (International Coordination-group for Laser Atmospheric Studies, Bucharest, 25-30 June 2017	Title: "Triple wave-lenghts lidar observations of the linear depolarization ratio of dried marine particles"
S. Grawe	Best Oral Student Presentation in the ICNAA 2017 conference	20th International Conference on Nucleation and Atmospheric Aerosols, Helsinki, 25-30 June 2017	Title: "Immersion freezing induced by different kinds of coal fly ash"
D. Althausen	Science Slam "Competition of Cooperation Projects" in the framework of the BMBF „Ländertag Zentralasien", 2017	German Federal Ministry for Education and Research (BMBF)	Science Slam on the topic central asian dust (CADEX project)
A. Wiedensohler	Highly Cited Researcher 2017	Thomsen Reuters	Highly Cited Researchers represents the world's leading scientific minds. Over three thousand researchers earned the distinction by writing the greatest numbers of reports officially designated by Essential Science Indicators[SM] as Highly Cited Papers
D. Assmann	Outstanding Student Poster and PICO (OSPP) Awards 2017 Atmospheric Sciences	European Geosciences Union	Title: "Spatio-temporal aerosol particle distributions in the Upper Troposphere/Lowermost Stratosphere measured by the IAGOS-CARIBIC Observatory" (Assmann, D.; Hermann, M.; Weigelt, A.; Martinsson, B.; Brenninkmeijer, C.; Rauthe-Schöch, A.; van Velthoven, P.; Bönisch, H.; Zahn, A.)
T. Spranger	Poster Award ICCE 2017	Norwegian Chemical Society, International conference on Chemistry and the Environment (ICCE) 2017 June 18-22, 2017	Best poster, title: "Elucidating the composition of humic-like substances in atmospheric aerosol particles via 2D liquid chromatographic fractionation and ultra-high resolution mass spectrometry"

Name	Prize	Awarding institution	Comments/Description
K. Gatzsche	Poster Award EAC 2017	European Aerosol Conference (EAC) 2017, Zurich, Switzerland, August 27 - September 1, 2017	Best poster: title: "Regional SOA modelling under consideration of HOMs"
R. Wagner	Poster Award EAC 2017	European Aerosol Conference (EAC) 2017, Zurich, Switzerland, August 27 - September 1, 2017	Best poster: title: "Relevance of wildfires on dust emissions via interaction with near-surface wind pattern"

Editorships

Name	Journal
Ansmann, A.	Guest Editor "Atmospheric Measurement Techniques"
	Guest Editor "Atmospherics, Chemistry and Physics"
Deneke, H.	Editorial Board Member EBM Remote Sensing, Section Atmospheric Remote Sensing
Herrmann, H.	Editorial Board Member "Atmospheric Measurement Techniques"
	Editorial Board Member "Atmospheric Pollution Research"
	Atmospheric Chemistry and Physics, Special Issue Editor (HCCT-2010)
	Editorial Board Member Aerosol and Air Quality Research (AAQR)
Macke, A.	Editorial Board Member "Atmospheric Measurement Techniques"
	Member of the Editorial Committee "promet"
Schepanski, K.	Associate Editor, Aeolian Research
Tegen, I.	Associate Editor, Journal of Geophysical Research, Atmospheres
Wandinger, U.	Editorial Board Member "Atmospheric Measurement Techniques"
Wiedensohler, A.	Editorial Chief in "Atmospheric Chemistry and Physics"
	Editorial Board Member "Atmospheric Measurement Techniques"
	Chief Editor Atmospheric Environment

Appendices: Reviews / Memberships

Reviews

Reviews	Number	
	2016	**2017**
Journals	160	150
Projects	32	19
Others	5	6
Total	197	175

Memberships

Name	Board
Althausen, D.	Commission on Air Pollution Prevention of VDI and DIN - Standards Committee KRdL NA 134-02-01-22 UA "Ground-based remote sensing of meteorological parameters" Department II Environmental Meteorology
Deneke, H.	Member of the Steering Committee of the BMWi Research Network MetPVNet
	Member of the International Radiation Comission
Hellmuth, O.	Membership in the International Association for the Properties of Water and Steam (IAPWS), Working Group Thermophysical Properties of Water and Steam (TPWS)
	Leibniz-Sozietät der Wissenschaften zu Berlin e. V.
Hermann, M.	Scientific Steering Committee (WLA) HALO
	Member of the "Stratospheric Sulfur and its Role in Climate" (SSiRC), SPARC initiative planning committee
Herrmann, H.	Chairman of the working group "Atmospheric Chemistry" in the GDCh-division "Environmental Chemistry and Ecotoxicology (AKAC)"
	DECHEMA/GDCh/ (Bunsengesellschaft Bunsen Society); Gemeinschaftsausschuss „Chemie der Atmosphäre" (Community Committee "Chemistry of the Atmosphere")
	DECHEMA/GDCh/KRdL Division Particulate Matter - Co-Chair
	IUPAC Task Group on Atmospheric Chemical Kinetic Data Evaluation
	Advisory Board Member of ProcessNet-Fachgemeinschaft (Specialist Community) SuPER
	Fellow of International Union of Pure and Applied Chemistry
	Co-Representative "International Surface Ocean - Lower Atmosphere Study" Projekt (SOLAS)

Name	Board
Herrmann, H.	Membership of the Royal Society of Chemistry (RSC)
	Membership of the American Chemical Society (AMC)
	Member of the Second International Indian Ocean Expedition (IIOE-2)
	Concurrent Professor for Environmental Sciences and Engineering at Fudan University, Shanghai, China
Macke, A.	Member of the Scientific Advisory Board „Meteorologische Zeitschrift"
	Member of the International Radiation Comission
	Member of the HALO Science Steering Comitee
	Member of the HALO Board of Trusties
	Member of the DFG Senate Commission Oceanography
	Member of the EU Steering Committee of the Leibniz Association
	Member of the DFG Topical Board 313 "Atmosphere and Ocean Research"
	Deputy Chair of Section E of the Leibniz Association
	Member of the Steering Committee of the Leibniz-Research Network "Crisis in a globalized World"
	Member of the Steering Committee of the BMBF Research Network HD(CP)2
	Member of the Steering Committee Collaborative Research Cluster TR 172 "Arctic Amplification"
Mertes, S.	Member of the DFG-Collaborative Research Centres TR172 "Arctic Amplification: Climate Relevant Atmospheric and SurfaCe Processes, and Feedback Mechanisms (AC)³"
	Member of the Science Team of CIRRUS-HL: The airborne experiment on CIRRUS in High Latitudes with the highaltitude long-range research aircraft HALO
Müller, Ke.	Member of the "German Library Association (dbv)"
	Member of the "Professional Association Information Library (BIB)"
Müller, Ko.	VDI and DIN - Standards Committee KRdL, member of the working group "Measurement of aerosol particles in the outdoor air"
	Member of the KRdL working group „Spiegelgremium zu CEN/TC 264/WG 35 EC/OC in PM"
Poulain, L.	Management Committee Member for COST-COLOSSAL

Appendices: Memberships

Name	Board
Schepanski, K.	Member of Executive Commitee Leibniz Research Alliance "INFECTIONS'21"
	Board member of the International Society for Aeolian Research (ISAR)
	Steering Commitee member of the Leibniz Research Alliance "INFECTIONS'21"
Spindler, G.	VDI and DIN - Standards Committee KRdL, member of the working group "Measurement of aerosol particles in the outdoor air"
	Member of the KRdL working group „Spiegelgremium zu CEN/TC 264/WG 35 EC/OC in PM"
Stratmann, F.	Work Package (WP) Leader EU-Projekt EUROCHAMP 2
	Member of the EUROCHAMP 2 User Selection Panel (USP)
	Board member of the International Comission on Clouds and Precipitation (ICCP)
Tegen, I.	"SDS-WAS" (WMO Sand and Dust Storm Warning Advisory and Assessment System), Member of Steering Committee
	Member of Scientific Advisory Committe "Science Europe"
	HAMMOZ Steering Comittee member
van Pinxteren, D.	Member of the European working group CEN/TC 264/WG 44 "Source apportionment"
	Member of the KRdl National Mirror Committee of CEN/TC 264/WG 44 "Source apportionment"
Wandinger, U.	Member of the ESA-JAXA EarthCARE Joint Mission Advisory Group
	Member of the EARLINET Council
	Member Scientific Steering Committee and Work Package Leader EU Project ACTRIS-2
	Member of Executive Board of ACTRIS Prepatory Phase Project and WP Leader
Wehner, B.	Board member of the Leipzig Branche of DMG (German Meteorological Society)
	Chair of the Working Group "Atmospheric Aerosols" within the EAA (European Aerosol Assembly)
	Speaker of the Working Group Chairs within the EAA (European Aerosol Assembly)
	Member of the Board of GAeF (Gesellschaft für Aerosolforschung)
Wex, H.	Board-Member of the International Comission on Clouds and Precipitation (ICCP)
Wiedensohler, A.	"Scientific Advisory Group" for aerosols within the "Global Atmosphere Watch"-program of the Meteorological Organization

Name	Board
Wiedensohler, A.	VDI-Commission "Particle Counting in the Atmosphere"
	Scientific Steering Committee member (SSC) and Work Package (WP) leader of the EU project ACTRIS
	Guest Professor at the "Peking University", Department of Environmental Science, China
	Head of the World Calibration Center WMO-GAW
	Head of the European Center for Aerosol Calibration (ECAC)
	Member of the Comité Européen de Normalisation, working group "CEN/TC 264/WG 32 Air quality - Determination of the particle number concentration"
	Member of the International Organization for Standardization (ISO), working group "ISO/TC 24/SC 4 Particle characterization"

Guest scientists

Name	Period of stay	Institution
Leng, C.	07.04.15 - 31.03.16	Fudan University, Shanghai, China
Sun, X.	01.08.15 - 31.01.16	Fudan University, Shanghai, China
Zhang, Y.	01.08.15 - 30.01.16	Jinan University, Guangzhou, China
Venables, D.	24.08.15 - 30.06.16	University College Cork, Ireland
Khedidji, S.	01.10.15 - 31.08.16	Université de Bouria, Algeria
Balderama, V.	01.10.15 - 30.09.16	Universidad Mayor de San Andres, La Paz, Bolivia
Kroflic, A.	01.11.15 - 31.10.16	National Institute of Chemistry Hajdrihova, Ljubljana, Slovenia
Lei, T.	04.01. - 04.02.16	Max-Planck-Institut für Chemie, Mainz, Germany
Wang, X.	04.01. - 04.02.16	Max-Planck-Institut für Chemie, Mainz, Germany
Zhao, J.	11.01. - 01.02.16	East China University of Science and Technology, Shanghai, China
Donaldson, J.	26.01. - 31.01.16	University of Toronto, Canada
Baergen, A.	28.02. - 12.03.16	University of Toronto, Canada
Shen, X.	29.02. - 15.03.16	Chinese Academy of Meteorological Schience, Peking, China

Appendices: Guest scientists

Name	Period of stay	Institution
Sun, J.	29.02. - 15.03.16	Chinese Academy of Meteorological Schience, Peking, China
Wang, X.	29.02. - 15.03.16	Chinese Academy of Meteorological Schience, Peking, China
Kubelova, L.	01.03. - 31.05.16	Czech Academy of Sciences, Prag, Czech Republic
Shaw, R.	04.03. - 21.04.16	Michigan Technological University, Houghton, USA
Lei, T.	09.03. - 08.04.16	Max Planck Institute for Chemistry, Mainz, Germany
Wang, X.	09.03. - 08.04.16	Max Planck Institute for Chemistry, Mainz, Germany
Catipay, G.	01.04. - 30.04.16	Manila Observatory, Diliman, Philippines
Ogren, J.	13.04. - 07.05.16	National Organic and Atmospheric Administration, Washington, USA
Cordoba, C.	01.06. - 31.08.16	National Institute of Aerospace Technology, Madrid, Spain
Morozov, I.	28.07. - 28.08.16	Russian Academy of Sciences, Moskau, Russia
Syromyatnikov, A.	28.07. - 28.08.16	Russian Academy of Sciences, Moskau, Russia
Gouveia, D.	01.08. - 15.10.16	University of Sao Paulo, Sao Paulo, Brazil
Zhu, Y.	01.09.16 - 31.08.17	Environmental Research Institute, Shandong Univeristy, China
Kalapov, I.	25.09. - 03.10.16	Bulgarian Academy of Sciences, Sofia, Bulgaria
Apaza, F.	01.10. - 31.12.16	Universidad Mayor de San Andres, La Paz, Bolivia
Quinones, V.	01.10. - 29.12.16	Venezuelan Institute for Scientific Research, Caracas, Venezuela
Zhang, C.	24.10. - 31.12.16	Xi'an Jiantong University, Xi'an, China
Clemen, H.	27.10. - 18.11.16	Max Planck Institute for Chemistry, Mainz, Germany
Eriksen, S.	27.10. - 18.11.16	Max Planck Institute for Chemistry, Mainz, Germany
Schneider, J.	27.10. - 18.11.16	Max Planck Institute for Chemistry, Mainz, Germany
Scholz, W.	17.01. - 27.01.17	Universität Innsbruck, Austria
Mentler, B.	17.01. - 27.01.17	Universität Innsbruck, Austria
Fischer, L.	17.01. - 27.01.17	Universität Innsbruck, Austria
Willink, D.	30.01. - 03.02.17	Leibniz Institute for Agricultural Engineering Potsdam-Bornim, Germany
Chen, J.	05.02. - 05.03.17	Peking University, China

Appendices: Guest scientists / Visits of TROPOS scientists

Name	Period of stay	Institution
Desai, N.	12.02. - 04.03.17	Michigan Technological University, Houghton, USA
Shaw, R.	21.02. - 02.03.17	Michigan Technological University, Houghton, USA
Wang, L.	28.04. - 31.10.17	East China University, Shanghai, China
Scholz, W.	08.05. - 09.06.17	University of Innsbruck, Austria
Mentler, B.	08.05. - 09.06.17	University of Innsbruck, Austria
Fischer, L.	08.05. - 09.06.17	University of Innsbruck, Austria
Brown, A.	26.05. - 06.08.17	Tulane University, New Orleans, USA
Mazzoleni, C.	19.06. - 31.08.17	Michigan Technological University, Houghton, USA
Schum, S.	19.06. - 31.08.17	Michigan Technological University, Houghton, USA
Gouveia, D.	01.07. - 30.09.17	University of Sao Paulo, Sao Paulo, Brazil
Madueno, L.	17.07.17 - 16.07.18	Ateneo de Manila University, Manila, Phillipines
Hussein, T.	01.08. - 31.08.17	University of Jordan, Amman, Jordan
Tamayo, E.	09.09. - 30.11.17	University of the Philppines Diliman, Quezon City, Philippines
He, L.	01.11.17 - 31.12.18	Environmental Research Institute, Shandong University, China
Manzi, M.	20.11.17 - 23.03.18	University of Buenos Aires, Buenos Aires, Argentina
Wenwen, S.	01.12.17 - 30.03.18	Environmental Research Institute, Shandong University, China

Visits of TROPOS scientists

Name	Period of stay	Institution
Althausen, D.	11.01. - 15.01.16	Technion University, Haifa, Israel
Baars, H.	11.01. - 15.01.16	Technion University, Haifa, Israel
Wiedensohler, A.	30.01. - 04.02.16	Manila Observatory, Philippines
Wiedensohler, A.	15.02. - 24.02.16	Indian Institute of Technology Madras, Chennai, India
van Pinxteren, M.	06.03. - 11.03.16	Plymouth University, UK
Kalesse, H.	09.06. - 17.06.16	Uni Boulder/NOAA, Boulder, USA

Appendices: Visits of TROPOS scientists

Name	Period of stay	Institution
Spindler, G.	26.06. - 01.07.16	Sino-German Science Center, (Peking University), China
Kalesse, H.	18.07. - 08.08.16	McGill University, Montreal, Canada
Althausen, D.	23.07. - 30.07.16	Technion University, Haifa, Israel
Hofer, J.	23.07. - 30.07.16	Technion University, Haifa, Israel
Bühl, J.	05.09. - 09.09.16	Met Office, Exeter, UK
Heese, B.	28.11. - 03.12.16	Technion University, Haifa, Israel
Hofer, J.	28.11. - 03.12.16	Technion University, Haifa, Israel
Bühl, J.	11.12. - 31.12.16	Cyprus University of Technology, Limassol, Cyprus
Ansmann, A.	25.12.16 - 05.01.17	Tel Aviv University, Tel Aviv, Israel
Engelmann, R.	15.03. - 25.03.17	NOA Finokalia, Crete, Greece
Althausen, D.	20.03. - 31.03.17	Technion University, Haifa, Israel
Heese, B.	20.03. - 31.03.17	Technion University, Haifa, Israel
Herrmann, H.	01.04. - 10.04.17	Fudan Universität, Shanghai, China
Engelmann, R.	26.07. - 02.08.17	CUT Limassol, Cyprus
Mettke, P.	01.10. - 30.10.17	University Mohammed V de Rabat, Marocco
Tegen, I.	16.10. - 20.10.17	University Wien, Austria
Otto, T.	01.11. - 21.12.17	Ionicon Analytik Ges.m.b.H., Innsbruck, Austria
Althausen, D.	06.11. - 11.11.17	Baengnyeong Island Atmospheric Research Centre, South Korea
Mettke, P.	20.11. - 19.12.17	Fudan University, Shanghai, China
Althausen, D.	04.12. - 09.12.17	Technion University, Haifa, Israel

Meetings

Meetings	Date	National/international	Number of participants
ACTRIS-D Meeting, TROPOS, Leipzig	04.04. - 05.04.16	national	21
Asian-Dust Session at DUST 2016, 2nd International Conference on Atmospheric Dust, Castellaneta Marina	16.06.16	international	50
MarParCloud Kick-off Meeting, Grimma	17.06.16	national	20
7th Conference of the Society of Environmental Toxicology and Chemistry – Europe (SETAC) – German Language Branch (GLB) e.V., Tübingen	05.09. - 08.09.16	national	220
Leipzig Graduate School / Advanced Training Module (ATM) "Cloud Droplet Number Concentration", Leipzig	17.10. - 18.10.16	national	20
GEODUST 2016, 1st meeting of the GEODUST International Focus Group of the INQUA TERPRO Commission, Leipzig	22.11.16	international	20
3. Leipziger Staubtag, Leipzig	23.11.16	international	60
3rd VDI Expert Forum on Atmospheric Chemistry (EFAC 3), Frankfurt (Main)	05.12. - 06.12.16	national	60
Leipzig Graduate School / Advanced Training Module (ATM) "Cloud Microphysical Measurements", Leipzig	23.02. - 24.02.17	international	15
Workshop on Cloud Microphysics - Turbulence Interaction, Leipzig	28.02. - 01.03.17	international	21
Cloudnet School Cyprus, Limassol	27.03. - 31.03.17	international	30
MarParCloud Status Meeting, Leipzig	04.05.17	national	20
Leipzig Graduate School / Advanced Training Module (ATM) "Polar Mid-Latitude Interactions", Leipzig	04.10. - 05.10.17	international	30
Atmospheric and Marine Sciences Summer School, UniCv, Cape Verde	16.10. - 18.10.17	international	55
GEODUST 2017, 2nd meeting of the GEODUST International Focus Group of the INQUA TERPRO Commission, Namibia	22.10. - 27.10.17	international	12
PM-Ost Final Workshop, Leipzig	02.11.17	international	30
4th Dust Day, Bremen	21.11. - 23.11.17	international	40

Appendices: International and national field campaigns

International and national field campaigns

Campaign	Project partner
(AC)³ PS102 and PS106 (PASCAL, SIPCA) DFG SFB-TR 172 "Arctic Amplification" TROPOS: all departments	University Leipzig, Leipzig Institute for Meteorology; University of Bremen; Alfred-Wegener-Institute Helmholtz Center for Polar and Marine Research; University of Cologne, Germany
ACLOUD Arctic CLoud Observations Using airborne measurements during polar Day DFG CRC-TR 172 "Arctic Amplification" TROPOS: ExAWoMp Dept.˙, Modelling Dept.	Max Planck Institute for Chemistry, Mainz; Alfred Wegener Institute, Bremerhaven; University of Leipzig, Leipzig Institute for Meteorology; Karlsruhe Institute for Technology; Johannes Gutenberg University Mainz; University of Cologne, Germany; University of Clermont-Ferrand, France
AEROCLO-sA/ALLDUST-SA Walvisbay (Namibia) TROPOS: Modelling Dept.	Laboratoire Interuniversitaire des Systèmes Atmosphériques, Créteil, Laboratoire ATmosphères, Milieux, Observations Spatiales, Paris; Laboratoire d'Optique Atmosphérique, Lille, France
Aerosol measurements at the Atlas mountains, Ifrane, Morocco TROPOS: Chemistry Dept.	Mohammed V University in Rabat, Morocco; ICARE, France; IRCELYON, France
Acores 2017 Azores Stratocumulus measurements of Radiation, Turbulence and Aerosols TROPOS: ExAWoMp Dept.	Max Planck Institute for Chemistry, Mainz; University Leipzig, Leipzig Institute for Meteorology, Germany; Michigan Technology University, USA; University of Warsaw, Poland
ACTRIS Summer Flux Campaign, Kosetice TROPOS: Remote Sensing Dept.	no partners
Aerosol Measurements on the research vessel Polarstern TROPOS: ExAWoMp Dept., Chemistry Dept.	no partners
A-LIVE Absorbing aerosol layers in a changing climate: aging, lifetime and dynamics TROPOS: ExAWoMp Dept.	Germany, Austria, UK, Spain
Bacchus TROPOS: Remote Sensing Dept.	Germany, Cyprus
CADEX Central Asian Dust EXperiment TROPOS: Remote Sensing Dept., Modelling Dept.	S.U. Umarov Physical-Technical Institute of Academy of Sciences of the Republic of Tajikistan; Helmholtz Centre Potsdam - GFZ German Research Centre for Geosciences, Germany
CARE Carbonaceous Aerosol in Rome and Environs Experiment TROPOS: ExAWoMp Dept.	Germany, Italy, Spain

Appendices: International and national field campaigns

Campaign	Project partner
Chacaltaya permanent field experiment Bolivia TROPOS: ExAWoMp Dept.	Universidad Mayor de San Andrés, La Paz, Bolivia
CLOUDNET (permanent experiment) Cloud Measurement Network Leipzig, Germany TROPOS: Remote Sensing Dept.	CLOUDNET Consortium
Colrawi TROPOS: Remote Sensing Dept.	Germany
EARLINET (permanent experiment) European Aerosol Research Lidar Network Leipzig, Germany TROPOS: Remote Sensing Dept.	EARLINET Consortium
Gif-Projekt: 3D-Widefield Sky Scatterer Tomography by Lidar Anchor TROPOS: Remote Sensing Dept.	Technion University, Haifa, Israel
GUAN German Ultrafine Aerosol Network TROPOS: ExAWoMp Dept., Chemistry Dept.	German Federal Environmental Agency, Langen; German Research Center for Environmental Health, Munich; Saxon State Ministry of the Environment and Agriculture, Dresden; Institute of Energy and Environmental Technology e.V. (IUTA), Duisburg; German Weather Service (DWD), Hohenpeißenberg, Germany; ISSEP, Liège, Belgium
Hera4Halo Developments concerning the physical and chemical characterization of ice nucleating aerosol particles with HALO TROPOS: Chemistry Dept.	HALO Consortium
IAGOS-CARIBIC Monthly intercontinental measurement flights Civil Aircraft for Remote Sensing and In situ measurement in Tropospheric and Lower Stratosphere based on the Instrumentation Container Concept TROPOS: ExAWoMp Dept.	CARIBIC Consortium
INUIT-Jungfraujoch-2017 Ice Nuclei Research Unit TROPOS: ExAWoMp Dept.	Max Planck Institute for Chemistry, Mainz; Goethe University Frankfurt (Main); Karlsruhe Institute for Technology; TU Darmstadt, Germany; ETH Zürich, Switzerland; Paul Scherrer Institut, Switzerland; University of Manchester, UK
INUIT-LACIS-Campaign Ice Nuclei Research Unit - LACIS TROPOS: ExAWoMp Dept.	Max Planck Institute for Chemistry, Mainz; Goethe University Frankfurt (Main); TU Darmstadt, Germany; ETH, Zürich, Switzerland
INUIT-LACIS-Campaign "Fly-Ashes" TROPOS: ExAWoMp Dept.	Max Planck Institute for Chemistry, Mainz; TU Darmstadt, Germany

Appendices: International and national field campaigns

Campaign	Project partner
INUIT-LACIS-Campaign "PCVI-coupling" Ice Nuclei Research Unit - LACIS TROPOS: ExAWoMp Dept.	Max Planck Institute for Chemistry, Mainz; Goethe University Frankfurt (Main); TU Darmstadt, Germany
INUIT-Cyprus-2016-Campaign Ice Nuclei Research Unit - TROPOS: ExAWoMp Dept.	Max Planck Institute for Chemistry, Mainz; Goethe University Frankfurt (Main); Karlsruhe Institute for Technology; TU Darmstadt, Germany
ISOSOA Isoprene-derived secondary organic aerosol TROPOS: Chemistry Dept.	no partners
MarParCloud Laboratory campaign TROPOS: Chemistry Dept., ExAWoMp Dept.	Leibniz Center for Tropical Marine Ecology; Leibniz Institute for Baltic Research, Warnemünde; University of Oldenburg, University of Hamburg, Germany
MarParCloud Field campaign at CVAO TROPOS: Chemistry Dept., ExAWoMp Dept.	Leibniz Center for Tropical Marine Ecology; Leibniz Institute for Baltic Research, Warnemünde; University of Oldenburg; University of Hamburg, Germany
Melpitz Winter campaign Charaterization of aerosol particles and their properties in the column above the research station Melpitz TROPOS: all departments	TU Braunschweig; University Tübingen; Saxon State Ministry of the Environment and Agriculture, Dresden; University Bayreuth; Fachhochschule Düsseldorf; TU Darmstadt; German Weather Service, Offenbach, Germany; Paul-Scherrer-Institute, Villigen, Switzerland
PASCAL Physical feedback of Arctic PBL, Sea ice, Cloud And AerosoL, Polarstern cruise leg PS106.1 und PS106.2 DFG SFB-TR 172 "Arctic Amplification" TROPOS: all departments	University Leipzig, Leipzig Institute for Meteorology; University of Bremen; Alfred Wegener Institute Helmholtz Center for Polar and Marine Research; University of Cologne; Free University Berlin (FUB), Germany
PollyNet (Permanent experiment) Network of institutions with a PollyXT TROPOS: Remote Sensing Dept.	PollyNet Consortium
Schmücke kompakt Summer-time aerosol and cloud water TROPOS: Chemistry Dept.	no partners
Low Emission Zone Leipzig TROPOS: ExAWoMp Dept.	Saxon State Ministry of the Environment and Agriculture, Dresden, Germany
Scientific and technical support During an international CEN-fieldcampaign at UBA-EMEP[1] station Waldhof TROPOS: Cemistry Dept.	Umweltbundesamt, Germany
Whiteface Mountain NY, US, pilot study TROPOS: Cemistry Dept.	USA, Germany

* Experimental Aerosol and Cloud Microphysics Department
[1] EMEP: Co-operative Programme for Monitoring and Evaluation of the Long-Range Transmission of Air Pollutants in Europe

Cooperations

International cooperations

Research project	Cooperation partners
3D Widefield Sky Scatterer Tomography by Lidar Anchor	Technion Universität, Haifa, Israel
ACRIDICON-CHUVA Aerosol, Cloud, Precipitation, and Radiation Interactions and Dynamics of Convective Cloud System - Cloud processes of the main precipitation systems in Brazil	23 partners from Germany, USA, Brazil
ACCEPT Analysis of the Composition of Clouds with Extended Polarization Techniques	Ludwig Maximilian University Munich, Germany; University of Technology, Delft, Royal Meteorological Institute of the Netherlands (KNMI), The Netherlands, Metek GmbH, Elmshorn, Germany
ACoMa Advanced Chemical process Modelling of aqSOA	LISA, Universite Paris Est Creteil et Universite Paris Diderot, Creteil, France; University of York, Wolfson Atmospheric Chemistry Laboratories, Department of Chemistry, UK
ACTOS Airborne Cloud Turbulence Observation System - Interaction between turbulent mixing processes and cloud micro-physical characteristics in stratiform boundary layer clouds	Michigan Technological University, Department of Physics, Houghton, USA
ACTRIS Aerosols, Clouds, and Trace gases Research InfraStructure Network	more than 100 partners from 21 European countries
ACTRIS measurement station Melpitz Cooperation partners involved in research projects at the TROPOS Research Station Melpitz	Norway, United Kingdom, Italy, Switzerland, Czech Republic, Hungary, Ireland, Finland, Austria, Sweden, Bulgaria, Belgium, France, Greece, The Netherlands, Spain, Denmark, Latvia, Poland, Portugal
AEROCLO-SA (Aerosol RadiatiOn and CLOuds in Southern Africa)	Institut de Recherches sur la Catalyse et l'Environnement de Lyon; Laboratoire Atmosphères, Milieux, Observations spatiales; LA Laboratoire d'Aérologie; UNIV LILLE1, Laboratoire d'Optique Atmosphérique; Laboratoire Interuniversitaire des Systèmes Atmosphériques, France
AERONET Aerosol Robotic Network, federation of ground-based remote sensing aerosol networks	Germany, Czech Republic, Denmark, Italy, France, Norway, UK, Spain, Slovenia, Sweden, Hungary, Greece, Switzerland
AIE Atmospheric Environmental Impacts of Aerosol in East Asia	30 partners

Appendices: Cooperations

Research project	Cooperation partners
A-LIFE (ERC starting grant project) Absorbing aerosol layers in a changing climate: aging, lifetime and dynamics	University Vienna, Austria; German Aerospace Center; Ludwig Maximilian University Munich, Germany
Anthropogenic influence of Asian aerosol on tropical cirrus clouds	National Center for Atmospheric Research (NCAR), Boulder, Colorado, USA
APRIL Atmospheric Products from Imager and Lidar	Royal Netherlands Meteorological Institute (KNMI), The Netherlands; Institute for Space Science, Free University of Berlin (FUB), Germany
AQMEII Air Quality Model Evaluation International Initiative	Austria, Australia, Belgium, Canada, Switzerland, Cyprus, Germany, Denmark, Finland, France, Greece, Italy, Luxembourg, Malta, The Netherlands, Norway, Poland, Portugal, Sweden, UK, USA
ATTO (Amazonian Tall Tower Observatory)	Instituto Nacional de Pesquisas da Amazônia INPA, Manaus; Universidade do Estado de Amazonas, Manaus, Brazil; Max Planck Institute for Chemistry, Mainz, Germany
Azores 2017 Measurements on clouds, aerosols, and radiation at the Azores	University Leipzig, Leipzig Institute for Meteorology; Max Planck Institute for Chemistry, Mainz, Germany; Michigan Technological University, Department of Physics, Houghton; Brookhaven National Laboratory, Upton, NY, USA; University of Warsaw, Poland
BACCHUS Impact of Biogenic versus Anthropogenic emissions on Clouds and Climate: towards a Holistic UnderStanding	20 partners from Switzerland, Finland, Germany, UK, Norway, Greece, Italy, Ireland, Bulgaria, Israel, France, Cyprus
CADEX Central Asian Dust Experiment	S.U. Umarov Physical-Technical Institute, Dushanbe, Republic of Tajikistan
COST Action COLOSSAL "Chemical On-Line cOmpoSition and Source Apportionment of fine aerosoL" CA16109	partners from 24 European countries, USA
CAREBeijing-North China Plain Air Quality Research in Beijing	China, France, UK, USA, Germany
CARIBIC/IAGOS Civil Aircraft for Remote Sensing and In situ measurement in Tropospheric and Lower Stratosphere based on the Instrumentation Container Concept	Germany, UK, France, The Netherlands, Switzerland, Sweden
CARRIBA Cloud, Aerosol, Radiation, and tuRbulence in the trade wInd regime over Barbados	Caribbean Institute for Meteorology and Hydrology, Barbados, Meteo France, France; Max Planck Institute for Meteorology; University Leipzig, Leipzig Institute for Meteorology, Germany

Research project	Cooperation partners
Central European Air Quality Cooperation - Harmonization of aerosol sampling and measurement; exchange of measurement data; comparison of PM transport models	Poland, Czech Republic
ChArMEx / ADRIMED Chemistry-Aerosol Mediterranean Experiment / Aerosol Direct Radiative Impact on the regional climate in the Mediterranean region	France, Italy, Germany
CLOUD – motion Cosmics leaving OUtdoor Droplets - International Training Network	Germany, Switzerland, Finland, Austria, UK
CLOUD Cosmics Leaving OUtdoor Droplets	16 partners from Germany, Switzerland, Finland, Austria, Portugal, Russia, UK, USA
COMPoSE Characterization of phase-partitioning in mixed-phase clouds	Brookhaven National Laboratory (BNL), Upton, NY, USA; McGill University, Montréal, QC, Canada
COST Chemistry transport model intercomparison	Germany, Denmark, Finland, France, Bulgaria, Estonia, Italy, Malta, Spain, The Netherlands, Norway, Poland, Switzerland, UK, Greece, Israel
CyCare Cyprus Clouds, Aerosols, and Rain Experiment	Cyprus University of Technology, Limassol, Cyprus
Development and evaluation of methods for the quantification of trace compounds produced by biomass burning	Academy of Science of Taipei, Taiwan
EARLINET European Aerosol Research Network	Germany, Italy, Spain, Greece, Switzerland, Sweden, Portugal, Poland, Belarus, France, Bulgaria, Romania, Norway, The Netherlands, Finland, Ireland, Cyprus
EMPIR-BC European Metrology Programme for Innovation and Research - Black Carbon	Germany, France, UK, Finland, Greece, Switzerland
ESA-ADM European Space Agency, Atmospheric Dynamics Mission	European Space Research and Technology Center (ESTEC), The Netherlands
ESA-EarthCARE European Space Agency, Earth Clouds, Aerosol and Radiation Explorer	European Space Research and Technology Center (ESTEC), The Netherlands; Japan Aerospace Exploration Agency
EUROCHAMP-2020 Integration of European Simulation Chambers for Investigating Atmospheric Processes – Towards 2020 and beyond	Germany, France, Switzerland, Spain, Ireland, Finland, Greece, Italy, Romania, UK

Appendices: Cooperations

Research project	Cooperation partners
HCCT 2010 Hill Cap Cloud Thuringia 2010	Germany, UK, France, USA, Switzerland
Heterogeneous ice and salt crystallisation in aqueous electrolyte and polymeric solutions	State University St. Petersburg, Russia; University of Rostock; Leibniz Institute for Baltic Sea Research (IOW), Warnemünde, Germany; Institute of Thermomechanics AS, Czech Republic; University of Odessa; Kharkov Institute of Technology, Ukraine
IAGOS Integration of routine Aircraft measurements into a Global Observing System	Germany, UK, France
ICON-HAMMOZ Development Model development	Max Planck Institute for Meteorologie, Hamburg, Germany; ETH Zurich, Institute for Atmospheric and Climate Science, Zurich, Switzerland
IGAS IAGOS for the GMES Atmospheric Service, EU project	Germany, UK, France, Netherlands, Hungary, Switzerland (WMO)
Intercomparison of Satellite Derived Wind Observations	EUMETSAT, Darmstadt, Germany
ITARS - ITN Initial Training for Atmospheric Remote Sensing - Marie Curie Initial Training Network	Germany, Spain, Italy, UK, The Netherlands, Romania, France
Laboratory investigations in the field of liquid phase chemistry	National Institute of Chemistry Ljubljana, Slovenia; Université de Lyon; Université de Marseilles, France; Semenov Institute of Chemical Physics, Moscow, Russia
LACCT Leipzig Aerosol Cloud Turbulence Tunnel	Ilmenau University of Technology, Germany; Michigan Technological University, Houghton, USA
LACIS Leipzig Aerosol Cloud Interaction Simulator	USA, UK, Denmark, Germany, Finland, Austria, Switzerland
LACIS-T Leipzig Aerosol Cloud Turbulence Tunnel	Ilmenau University of Technology, Germany; Michigan Technological University, Houghton; University of Utah, Salt Lake City, USA
Lagrangian turbulence in clouds	Max Planck Institute for Dynamics and Self-Organization, Göttingen; Ilmenau University of Technology, Germany; Michigan Technological University, USA; University of Warsaw, Poland
LEAK Leipziger Aerosolkammer	University of British Columbia, Dept. of Chemistry, Canada; University College Cork, Ireland; Institute of Chemistry, Slovenia

Research project	Cooperation partners
LIVAS Lidar Climatology of Vertical Aerosol Structure for Space-Based Lidar Simulation Studies	Institute for Space Applications and Remote Sensing, National Observatory of Athens, Greece; Institute of Methodologies for Environmental Analysis of the National Research Council of Italy (IMAA-CNR), Potenza, Italy
MACE Manila Aerosol Characterization Experiment	De La Salle University, Manila, Philippines
MARSU Marine Atmospheric Science Unravelled: Analytical and Mass Spectrometric Techniques Development and Application	8 partners from Marocco, Kap Verde, France, Austria, Argentina, China
MelCol Charaterization of aerosol particles and their properties in the column above the research station Melpitz	Germany, Switzerland, Greece
Mobile Landstation Determining aerosol and cloud microphysical processes at distinct land-based sites	Lindenberg Meteorological Observatory; University of Cologne, Germany; Delft University of Technology, Delft, The Netherlands
Mobile Seestation Autonomous measurement platform for the determination of the material and energy exchanges between ocean and atmosphere	Helmholtz Centre for Ocean Research, Kiel; Alfred Wegener Institute Helmholtz Center for Polar and Marine Research, Bremerhaven; University Leipzig, Leipzig Institute for Meteorology; Max Planck Institute for Meteorology, Hamburg; University of Hamburg, Germany; National Observatory Athens, Greece,
Ocean Science Center Mindelo (OSCM)	Instituto Nacional de Desenvolvimento das Pescas, Mindelo, S. Vicente, Republic of Cape Verde; Helmholtz Centre for Ozean Research Kiel, Germany
OdCom Objektivierung der Geruchsbeschwerden im Erzgebirgskreis und Bezirk Ústí	7 partners from Germany and Czech Republic
PAREST PArtikel-REduktions-STrategien	Germany, The Netherlands
Pollynet Development and application of Polly systems	Finnish Meteorological Institute, Kuopio, Finland; Department of Applied Environmental Science, Stockholm University, Sweden; Institute of Geophysics, University of Warsaw, Poland; Universidade de Évora, Centro de Geofísica de Évora, Portugal; National Institute of Environmental Research, Air Quality Research Division, Korea; National Observatory of Athens, Greece
PRADACS Puerto Rico African Dust And Cloud Study	Germany, Puerto Rico, USA, Switzerland, Mexico, Brazil

Appendices: Cooperations

Research project	Cooperation partners
Properties and impacts of Secondary Organic Aerosols composed of highly oxidized multifunctional organic compounds (HOMs SOA)	Weizmann Institute, Rehovot, Israel
Regional modelling of the marine multiphase chemistry	Centre for Environmental and Climate Research, Lund University, Sweden
Relations between directly emitted wood burning emissions and ambient particle concentration in the Melbourne region	Commonwealth Scientific and Industrial Research Organization, Melbourne, Australia
Replicator measurements	National Centre for Atmospheric Research, Boulder, CO, USA
SOPRAN Surface Ocean Processes in the Anthropocene Cape Verde	Instituto Nacional de Desenvolvimento das Pescas, National Institute for Meteorology and Geophysics, Mindelo, S. Vicente, Republic of Cape Verde; University of York, UK; Hebrew University of Jerusalem, Israel
Theory of Ice and Salt Crystallization in Aqueous Electrolyte and Polymeric Solutions	Georgia Institute of Technology, Atlanta, Georgia, USA; IAWPS International Association for the Properties of Water and Steam; Institute for Thermal Physics, Ekaterinburg; Joint Institute for Nuclear Research Dubna; St. Petersburg State University, Saint Petersburg, Russia; SUNY at Buffalo, Buffalo, NY, USA
WCCAP World Calibration Center for Aerosol Physics	Anmyeon, Republic of Korea; Malaysian Meteorological Service, Danum Valley, Malaysia; Bulgarian Academy of Sciences, BEO-Moussala, Bulgaria

National cooperations

Research project	cooperation partners
Absorption efficiency of Black Carbon: determining representative atmospheric values and implications for radiative transfer	Max Planck Institute for Chemistry, Mainz
(AC)³ DFG-SFB/Transregio 172 Modelling of aerosols and aerosol cloud interactions in the Arctic	University Leipzig, Leipzig Institute for Meteorology; University of Bremen; University of Cologne; Alfred Wegener Institute Helmholtz Centre for Polar and Marine Research, Bremerhaven/Potsdam
(AC)³ projekt A-01, DFG-SFB/Transregio 172 Model–based quantification of aerosol and cloud processes and their effects in the Arctic	University Leipzig, Leipzig Institute for Meteorology; Alfred Wegener Institute Helmholtz Centre for Polar and Marine Research, Bremerhaven/Potsdam

Research project	cooperation partners
(AC)³ projekt D-02, DFG-SFB/Transregio 172 Model–based quantification of aerosol and cloud processes and their effects in the Arctic	University Leipzig, Leipzig Institute for Meteorology; Alfred Wegener Institute Helmholtz Centre for Polar and Marine Research, Bremerhaven/Potsdam
(AC)³ project A-02, DFG-SFB/Transregio 172 Tethered balloon-borne energy budget measurements in the cloudy central Arctic	University Leipzig, Leipzig Institute for Meteorology; Alfred Wegener Institute Helmholtz Centre for Polar and Marine Research, Bremerhaven/Potsdam
(AC)³ project B-03, DFG-CRC/Transregio 172 Characterization of Arctic mixed-phase clouds by airborne in-situ measurements and remote sensing	University Leipzig, Leipzig Institute for Meteorology; University of Cologne
ACRIDICON Aerosol, Cloud, Precipitation, and Radiation Interactions and Dynamics of Convective Cloud System	11 partners
ACTRIS-D Aerosols, Clouds, and Trace gases Research InfraStructure Network	13 project partners
AirShield (BMBF joint project) Airborne remote sensing for hazard inspection by network enabled lightweight drones	8 partners
ALADINA Investigating the Small-Scale Vertical and Horizontal Variability of the Atmospheric Boundary Layer Aerosol using Unmanned Aerial Vehicles	TU Baunschweig; University of Tübingen
Aging of the emissions in a smog chamber	Helmholtz Centre - German Research Center for Environmental Health; Cooperation Group of Comprehensive Molecular Analytics
PM-OST Source appointment of PM10 and estimation of contribution from trans-boundary air pollution	Senate Department for Urban Development and Housing, Berlin; Saxon State Agency for Environment, Agriculture and Geology, Dresden; Ministry of Rural Development, Environment and Agriculture of the Federal State of Brandenburg; Ministry of Rural Development, Protection of Nature and Geology, State of Mecklenburg-Western Pomerania
Azores 2017 Measurements on clouds, aerosols, and radiation at the Azores	University Leipzig, Leipzig Institute for Meteorology; Max-Planck-Institute for Chemistry, Mainz
CARIBIC-AMS An Automated Aerosol Mass Spectrometer for the Regular Chemical Characterization of Aerosol Particles in the Upper Troposphere and Lowermost Stratosphere	Max Planck Institute for Chemistry, Mainz

Appendices: Cooperations

Research project	cooperation partners
CLOUD-16	Goethe University Frankfurt (Main)
Colrawi Combined Observations with Lidar RAdar and WInd profiler	German Weather Service (DWD), Lindenberg
DWD-Raman-Lidar	German Weather Service (DWD), Offenbach; Meteorological Observatory Lindenberg; Loritus GmbH, Munich
Extramural Research Programme Improved Nowcasting of Convective Initiation with METEOSAT SEVIRI (INCITES)	German Weather Service (DWD), Offenbach
GUAN German Ultrafine Aerosol Network	Federal Environmental Agency, Dessau-Roßlau, Langen, Garmisch-Partenkirchen, Hofsgrund; German Weather Service (DWD), Hohenpeißenberg; IUTA Duisburg e. V.; Helmholtz Centre Munich - German Research Center for Environmental Health
HD(CP)2 (BMBF) High definition clouds and precipitation for advancing climate prediction	16 partners
High-resolution modelling of clouds and gravity wavelengths: scale analysis, numerics, validation (Leibniz competition project)	Leibniz Institute of Atmospheric Physics, Rostock; Potsdam Institute for Climate Impact Research (PIK), Potsdam
IAGOS-D In-situ Aircraft for a Global Observing System	Research Center Jülich; Karlsruhe Institute of Technology; Max Planck Institutes for Chemistry and Biogeochemistry, Jena; German Aerospace Center; University of Heidelberg
INFECTIONS'21 Transmission Control of Infections in the 21st Century, Leibniz Research Cluster	14 partners
INUIT Ice Nuclei Research Unit, DFG Research Unit	Max Planck Institute for Chemistry, Mainz; Goethe University Frankfurt (Main), TU Darmstadt; Johannes Gutenberg University Mainz; Bielefeld University; Karlsruhe Institute for Technology
Isotope analysis of stable oxdiation products induced by radical reactions in the aqueous phase	Helmholtz Centre for Environmental Research
HuCAR Classification of HULIS carbon from different atmospheric environments via a 2-D-Off-line chromatography (HuCar)	Helmholtz Centre for Environmental Research

Research project	cooperation partners
KLENOS Influence of a change of energy policy and climate on air quality as well as consequences for the compliance with limit values and examining further emissions	Federal Environmental Agency, Dessau-Roßlau; TU Dresden, Institute of Hydrology and Meteorology
MMS Leibniz Network "Mathematical Modeling and SImulation (MMS)"	24 partners
MARGA Physico-chemical characterization of the dynamic behaviour of ammonium salt in particulate matter aerosol particles - testing a new high-resolutions measurement method at EMEP[1]-Level 3-Station Melpitz	Federal Environmental Agency, Dessau-Roßlau
MarParCloud Marine biological production, organic aerosol particles and marine clouds: a Process Chain (Leibniz competition project)	Leibniz Center for Tropical Marine Ecology; Leibniz Institute for Baltic Research, Warnemünde; University of Oldenburg; University of Hamburg
MARSU: Marine Atmospheric Science Unravelled: Analytical and Mass Spectrometric Techniques Development and Application	8 partners
MetPVNet Development of innovative satellite-based methods for improved forecasts of PV-yield	11 partners
ML-CIRRUS Mid-Latitude Cirrus	10 partners
PalMod From the Last Interglacial to the Anthropocene: Modeling a Complete Glacial Cycle	17 partners
Parallel coupling framework and modern time integration methods for detailed cloud processes in atmospheric models	TU Dresden, Centre for Information Services and High Performance Computing, Desden; Martin Luther University Halle-Wittenberg
PollyNet Network of institutions with a PollyXT	German Weather Service (DWD), Hohenpeißenberg
Replicatorsonde observations of ice crystals	German Weather Service (DWD), Lindenberg
Influence of soot on air quality and climate (pilot study)	Saxon State Agency for Environment, Agriculture and Geology, Dresden

Appendices: Cooperations

Research project	cooperation partners
SALTRACE Saharan Aerosol Long-range Transport and Aerosol-Cloud-Interaction Experiment	DLR Oberpfaffenhofen; Ludwig Maximilian University of Munich; TU Darmstadt
SOARiAL Spread of Antibiotic Resistance in an Agrarian Landscape	Leibniz Institute DSMZ - German Collection of Microorganisms and Cell Cultures Braunschweig; Leibniz Centre for Agricultural Landscape Research Müncheberg; Leibniz Institute for Agriculture and Bioeconomy Potsdam, Free University of Berlin (FUB)
SOPRAN Surface Ocean Processes in the Anthropocene	8 partners
Statistical modelling of aerosol particle size distribution in urban and rural environment	TU Braunschweig, Section of climatology and environmental meteorology
Theory of ice and salt crystallisation in aqueous electrolyte and polymeric solutions	Polymer Physics, University of Rostock; Leibnitz Institute for Baltic Sea Research, Warnemünde
Low Emission Zone Deep analysis to verify the effectiveness of the Leipzig Low Emission Zone	Saxon State Agency for Environment, Agriculture and Geology, Dresden
Improvement of data quality for the measurement of ultrafine particles in the outdoor air	Saxon State Agency for Environment, Agriculture and Geology, Dresden

[1] EMEP: Co-operative Programme for Monitoring and Evaluation of the Long-Range Transmission of Air Pollutants in Europe

Boards

Boards of trustees

| Name	Institution
RORin C. Liebner	Saxon State Ministery for Science and the Arts
Prof. Dr. R. Haak	Federal Ministry of Education and Research
Prof. Dr. A. Wahner	Forschungszentrum Jülich GmbH, Institute for Energy and Climate Research, IEK-8: Troposphere

Scientific advisory board

Name	Institution
Prof. Dr. K. H. Schlünzen **(Chairperson)**	University of Hamburg, Meteorological Institute
Dr. C. George	IRCELYON - Institut de Recherches sur la Catalyse et l'Environnement de Lyon, University Claud Bernard
Prof. Dr. C. Hoose	Karlsruhe Institute of Technology (KIT), Institute of Meteorology and Climate Research (IMK)
Prof. Dr. T. Koop	Bielefeld University, Faculty of Chemistry
Prof. Dr. M. Kulmala	University of Helsinki, Department of Physics
Prof. Dr. J. Quaas	University Leipzig, Leipzig Institute for Meteorology (LIM)
Prof. Dr. M. Rapp	German Aerospace Center, Institute of Atmospheric Physics
Prof. Dr. R. Shaw	Michigan Technological University, Department of Physics

Appendices: Boards

Members of the TROPOS association

Name	Institution
Prof. Dr. C. Jacobi **(Chairman)**	Leipzig University, Leipzig Institute for Meteorology (LIM)
RORin C. Liebner	Saxon State Ministery for Science and the Arts
Prof. Dr. R. Haak	Federal Ministry of Education and Research
Prof. Dr. B. Abel	Leibniz Institute of Surface Engineering (IOM)
Prof. Dr. B. Brümmer	University of Hamburg, Meteorological Institute
Prof. Dr. W. Engewald	Leipzig University, Faculty for Chemistry and Mineralogy
Prof. Dr. J. Quaas	Leipzig University, Leipzig Institute for Meteorology (LIM)
Dr. H.-H. Richnow	Helmholtz Centre for Environmental Research (UFZ)
Prof. Dr. C. Simmer	Rhineland Friedrich Wilhelm University Bonn, Institute for Meteorology
Prof. Dr. P. Warneck	Professor emeritus
Prof. Dr. E. Renner, honorary member	Professor emeritus
Prof. Dr. J. Heintzenberg, honorary member	Professor emeritus